



UNIVERSIDADE ESTADUAL DE CAMPINAS

Faculdade de Engenharia Química

LETÍCIA MARIA SAMPAIO BARROS

IONIC LIQUID CRYSTAL FOR Li-O₂ BATTERIES

LÍQUIDO IÔNICO CRISTALINO PARA BATERIAS DE Li-O₂

CAMPINAS

2022

LETÍCIA MARIA SAMPAIO BARROS

IONIC LIQUID CRYSTAL FOR Li-O₂ BATTERIES

LÍQUIDO IÔNICO CRISTALINO PARA BATERIAS DE Li-O₂

Dissertation presented to the Faculty of Chemical Engineering of the University of Campinas in partial fulfilment of the requirements for the degree of Master in Chemical Engineering.

Dissertação apresentada à Faculdade de Engenharia Química da Universidade Estadual de Campinas como parte dos requisitos exigidos para a obtenção do título de Mestra em Engenharia Química.

Supervisor/Orientador: Prof. Dr. Rubens Maciel Filho

Co-Supervisor/Coorientador: Prof. Dr. Gustavo Doubek

ESTE TRABALHO CORRESPONDE À VERSÃO
FINAL DA DISSERTAÇÃO DEFENDIDA PELA ALUNA
LETÍCIA MARIA SAMPAIO BARROS, ORIENTADA
PELO PROF. DR. RUBENS MACIEL FILHO.

CAMPINAS

2022

Ficha catalográfica
Universidade Estadual de Campinas
Biblioteca da Área de Engenharia e Arquitetura
Rose Meire da Silva - CRB 8/5974

B278i Barros, Letícia Maria Sampaio, 1994-
Ionic liquid crystal for Li-O₂ batteries / Letícia Maria Sampaio Barros. –
Campinas, SP : [s.n.], 2022.

Orientador: Rubens Maciel Filho.

Coorientador: Gustavo Doubek.

Dissertação (mestrado) – Universidade Estadual de Campinas, Faculdade de Engenharia Química.

1. Baterias de lítio. 2. Líquidos iônicos. 3. Oxirredução. 4. Solventes orgânicos. 5. Aditivos. 6. Eletrólitos. I. Maciel Filho, Rubens, 1958-. II. Doubek, Gustavo, 1984-. III. Universidade Estadual de Campinas. Faculdade de Engenharia Química. IV. Título.

Informações Complementares

Título em outro idioma: Líquido iônico cristalino para baterias de Li-O₂

Palavras-chave em inglês:

Lithium batteries

Ionic liquids

Redox

Organic solvents

Additives

Electrolytes

Área de concentração: Engenharia Química

Titulação: Mestra em Engenharia Química

Banca examinadora:

Rubens Maciel Filho [Orientador]

Cristiane Barbieri Rodella

Hudson Giovani Zanin

Data de defesa: 25-02-2022

Programa de Pós-Graduação: Engenharia Química

Identificação e informações acadêmicas do(a) aluno(a)

- ORCID do autor: <https://orcid.org/0000-0002-9786-8783>

- Currículo Lattes do autor: <http://lattes.cnpq.br/0061299261432106>

FOLHA DE APROVAÇÃO

Dissertação de mestrado defendida por Letícia Maria Sampaio Barros e aprovada em 25 de fevereiro de 2022 pela Comissão Examinadora constituída pelos professores doutores:

Prof. Dr. Rubens Maciel Filho - Presidente e orientador
Faculdade de Engenharia Química – FEQ/UNICAMP
Videoconferência

Prof. Dr. Hudson Giovani Zanin
Faculdade de Engenharia Elétrica e Computação – FEEC/UNICAMP
Videoconferência

Dra. Cristiane Barbieri Rodella
Centro Nacional de Pesquisa em Energia e Materiais – CNPEM
Videoconferência

A Ata de Defesa, assinada pelos membros da Comissão Examinadora, consta no SIGA/Sistema de Fluxo de Dissertação/Tese e na Secretaria do Programa da Unidade.

AGRADECIMENTOS

Agradeço à Deus, por sempre estar ao meu lado e me dar forças para alcançar meus objetivos e superar todos os obstáculos.

Agradeço aos meus pais, Alexsandra e Marcelo, e ao meu irmão Gabriel, por me apoiarem em todas as minhas escolhas, acompanharem todos os meus passos e serem minha fonte de amor e cuidado.

Agradeço aos meus avós, Nonato e Salete, por sempre rezarem por mim e por todo o carinho e cuidado do mundo.

Em memória de minha avó, Maria Tereza, meu anjo de luz, que me ensinou sobre empoderamento e resiliência.

Agradeço à tia Inha, minha segunda mãe, e às minhas priminhas Karol e Nicolle, que amo de todo meu coração.

Agradeço aos meus tios Fátima, Andréia Karla, Eduardo, Wagner, Stênio, Junior, Eduardo e Andrea. E aos meus primos Arthur, Arnon, Manu e Sarah.

Agradeço à Mari e à Wedja, por acompanharem toda minha trajetória do mestrado, dividindo angústias e alegrias. Obrigada por todo o apoio e paciência.

Agradeço aos meus amigos de Maceió e Campinas, que sempre torceram por mim e apoiaram minhas escolhas. Ester, Thaylane, Laura, Carol, Guga, Thaís, Fafá, Paulinha, Jess, Ádila, Maria Clara, Babi, Amanda, Bianca.

Agradeço aos meus amigos e colegas de laboratório, por me ajudarem e tornarem meus dias mais leves, em especial à Lorrane, Júlia, Bruno e Martim, eu não teria chegado aqui sem vocês.

Agradeço à Chayene que, além da amizade, me proporcionou todo suporte desde o princípio, acompanhando de perto a evolução do trabalho e ajudando com o direcionamento da pesquisa.

Agradeço à Thayane pelo carinho e dedicação, pelas ideias, correções de trabalho e ajuda com os textos.

Agradeço ao meu orientador Professor Rubens Maciel e ao meu co-orientador Professor Gustavo Doubek, pela oportunidade e confiança em poder trabalhar com um projeto tão interessante e desafiador.

Agradeço à Unicamp e à Faculdade de Engenharia Química. Toda a equipe técnica, funcionários e professores.

Agradeço à banca por avaliar e contribuir com a dissertação.

O presente trabalho foi realizado com apoio da Coordenação de Aperfeiçoamento de Pessoal de Nível Superior – Brasil (CAPES) – Código de financiamento 001.

RESUMO

Na última década, o interesse pela substituição de combustíveis fósseis por alternativas de energia limpa aumentou substancialmente devido à considerável diminuição das reservas de petróleo, oscilação de preços e adoção de políticas públicas de incentivo às tecnologias limpas. No setor de transportes, a introdução da eletroquímica é bastante atrativa, principalmente o uso de baterias metal-ar que possuem uma grande capacidade energética. Nesse aspecto, a bateria Li-O₂ é uma das tecnologias mais promissoras, devido à sua impressionante densidade energética próxima à da gasolina. No entanto, esta bateria ainda não está disponível comercialmente, e a fabricação de um sistema com alta eficiência, ciclabilidade, estabilidade térmica e química, com todos os componentes compatíveis entre si é um grande desafio. A elaboração de um eletrólito ideal seria capaz de atender muitas dessas questões, se destacando o uso de aditivos em eletrólitos apróticos, os quais conseguem melhorar a estabilidade do sistema. Recentemente, o uso de eletrólitos à base de líquidos iônicos (LIs) tem se destacado por suas características únicas como ampla janela eletroquímica, baixa volatilidade e capacidade de dissolver muitos compostos orgânicos e inorgânicos. No entanto, os altos sobrepotenciais necessários para o funcionamento da bateria podem danificar o eletrólito e seus eletrodos, limitando sua ciclabilidade e reduzindo sua eficiência. Para evitar esses problemas, os mediadores redox (MRs) estão sendo bastante utilizados como catalisadores solúveis, dissolvendo-se uniformemente no eletrólito e reduzindo os sobrepotenciais de carga. Mesmo assim, o uso de LIs e MRs ainda está em seu estágio inicial, e a combinação de ambos é encontrada em poucos trabalhos, necessitando de maiores investigações. Portanto, visando atender parte dessas limitações, este projeto focou no desenvolvendo de baterias de Li-O₂ compostas de um cristal líquido iônico [C₁₆mim][Br] como aditivo para eletrólitos de DMSO/LiClO₄. O cátion [C₁₆mim]⁺ possui longa cadeia alquila, conferindo propriedades de cristal líquido ao material, enquanto o [Br]⁻ é um contra-íon utilizado como mediador redox. As propriedades eletroquímicas, estruturais e de transporte do eletrólito foram investigadas, sendo observado que o uso do aditivo melhorou a estabilidade eletroquímica do sistema, bem como aumentou sua condutividade iônica até concentrações de 1.456 M [C₁₆mim][Br], acima disso, as altas viscosidades atrapalharam a condutividade. Foi observado que o aditivo é capaz de formar agregados quando dissolvido em DMSO, os quais se reorganizam em nanoestruturas bem definidas a partir de 1.456 M. Essa função estrutural impacta na condutividade e também influencia no desempenho da bateria de Li-O₂, podendo ou não ser benéfico a depender da concentração de [C₁₆mim][Br] utilizado. Já o ânion [Br]⁻ foi um importante mediador que permitiu a ciclagem da bateria em potenciais de carga abaixo de 4.2 V. Por fim, definiu-se que o sistema diluído 0.050 M [C₁₆mim][Br] seria a concentração ótima, seguido pela concentração 1.456 M [C₁₆mim][Br].

Palavras-chave: Bateria de Li-O₂, líquidos iônicos, mediadores redox, líquido iônico cristalino.

ABSTRACT

In the last decade, the interest for replacing fossil fuels by clean energy alternatives has increased substantially due to the considerable decrease of oil reserves, price oscillation and adoption of public policies to encourage clean technologies. In the transport sector, the introduction of electrochemistry is quite attractive, especially the use of metal-air batteries that have a great energy capacity. In this aspect, the Li-O₂ battery is one of the most promising technologies, due to its impressive energy density close to gasoline. However, this battery is not yet commercially available, and the fabrication of a system with high efficiency, cyclability, thermal and chemical stability, with all components compatible with each other is a major challenge. The elaboration of an ideal electrolyte would be capable of attending many of those issues, highlighting the use of additives in aprotic electrolytes, which can improve the stability of the system. Recently, the use of electrolytes based on ionic liquids (ILs) has stood out because of their unique features such as wide electrochemical window, low volatility and the ability to dissolve many organic and inorganic compounds. However, the high overpotentials required for the battery operation can damage the electrolyte and the cell's electrodes, limiting its cyclability and reducing its efficiency. In order to avoid this inconvenience, redox mediators (RMs) are being increasingly used as soluble catalysts, dissolving evenly in the electrolyte and reducing the charge overpotentials. Even so, the use of ILs and RMs is still at its initial state, and the combination of both species is found just in a few papers, requiring further investigation. Therefore, in order to attend part of these issues, this project focused on the development of Li-O₂ batteries composed of the ionic liquid crystal [C₁₆mim][Br] as an additive for DMSO/LiClO₄ electrolytes, where the [C₁₆mim]⁺ cation has a long alkyl chain, conferring liquid crystal properties to the material, while [Br]⁻ is a counterion used as redox mediator. The electrochemical, structural and transport properties of the electrolyte were investigated, and it was observed that the additive use improved the electrochemical stability of the system, as well as increased its ionic conductivity for concentrations up to 1.456 M [C₁₆mim][Br], above that, the high viscosities interfered with conductivity. Furthermore, it was observed that the additive is able to form aggregates when dissolved in DMSO, which reorganize into well-defined nanostructures for concentrations above 1.456 M. This structural property impacts the conductivity and also influences the performance of the Li-O₂ battery, which may be beneficial or harmful to the system depending on the concentration of [C₁₆mim][Br] used. The anion [Br]⁻ was an important mediator that allowed the battery to cycle at charge potentials below 4.2 V. Finally, it was found that the diluted 0.050 M [C₁₆mim][Br] was the optimal concentration, followed by 1.456 M [C₁₆mim][Br].

Keywords: Li-O₂ cell, ionic liquids, redox mediator, ionic liquid crystal

LIST OF ABBREVIATIONS AND ACRONYMS

CNT	Carbon Nanotubes
CV	Cyclic Voltammetry
DSSC	Dye-sensitized Solar Cell
EIS	Electrochemical Impedance Spectroscopy
EV	Electric Vehicle
FESEM	Field Emission Scanning Electron Microscopy
FTIR	Fourier Transform Infrared Spectroscopy
GDL	Gas Diffusion Layer
[C ₁₆ mim ⁺]	1-hexadecyl-3-methylimidazolium
ICE	Internal Combustion Engine
IL	Ionic Liquid
ILC	Ionic Liquid Crystal
KB	Ketjen Black
LIB	Lithium Ion Battery
OCV	Open Circuit Voltage
OER	Oxygen Evolution Reaction
ORR	Oxygen Reduction Reaction
RM	Redox Mediator
SEI	Solid Electrolyte Interface
XPS	X-ray photoelectron spectroscopy
XRD	X-ray Diffraction

LIST OF SYMBOLS

σ	Ionic Conductivity
ΔV	Small Potential
A	Membrane Area
I	Current
I_0	Initial Current
I_{ss}	Steady Current
η_{dis}	Charge Overpotential
η_{dis}	Discharge Overpotential
Q_{charge}	Charge Capacity
$Q_{discharge}$	Discharge Capacity
R	Bulk Resistance
R_0	Interfacial Resistance
R_{ss}	Resistance After Polarization
t	Membrane Thickness
T_{Li^+}	Lithium Ion Transference Number
V	Potential

SUMMARY

1.	Introduction	12
1.1.	Objectives.....	15
1.1.1.	General Objectives:	15
1.1.2.	Specific Objectives:.....	15
1.2.	Dissertation Outline.....	15
1.3.	Main Contributions of This Work.....	16
2.	Literature Review and Fundamental Concepts	18
2.1.	Historical Context – Development of Batteries	18
2.2.	Configuration and Operation of Li-O ₂ Batteries	21
2.3.	Lithium Anode	23
2.4.	Oxygen Cathode.....	25
2.5.	Electrolytes.....	27
2.5.1.	DMSO Solvent for Non-aqueous Electrolyte.....	31
2.6.	Ionic Liquids	32
2.6.1.	General Properties of Ionic Liquids	32
2.6.2.	Ionic Liquids Crystals	34
2.7.	Cell Overpotential	36
2.8.	Redox Mediators	38
2.9.	Final Comments	40
3.	Methodology and Procedures.....	42
3.1.	Preparation of Electrolytes	42
3.2.	Preparation of Catalytic Ink for the Cathode.....	42
3.3.	Evaluation of the Electrolyte Properties.....	43
3.4.	Electrochemical Tests	43
3.5.	Chemical and Morphological Characterization.....	45
3.6.	Table of Nominal and Real Values	46
4.	Results and Discussion.....	47
4.1.	Investigation of the Electrolyte Properties	48
	Appendix A – Supplementary Information	82
4.2.	Investigation of the Ionic Liquid Crystal-Based Electrolyte in the Performance of Li-O ₂ Batteries.....	105
	Appendix B – Supplementary Information	129
4.3.	General Discussion.....	136
5.	Conclusions	140
6.	Future Work and Perspectives.....	141
7.	Scientific Production.....	142

Appendix C – Patent Request	143
References	147

Chapter 1

Introduction

The world economy is currently facing a serious energy crisis due to the unbridled growth in population and demand for energy (SALVUCCI & TATTINI, 2019). The transport sector alone accounts for approximately one-third of the total energy consumption. Furthermore, the predominant use of fossil fuels in vehicles with internal combustion engines (ICEs) contributes to the greenhouse effect, being responsible for ~25% of the total CO₂ emission to atmosphere. To revert this scenario, public policies play a key role in motivating the use of renewable and clean resources for energy and fuels. In this respect, the electrification of the worldwide energetic matrix promises to reduce its dependence on fossil fuels and improve the air quality (YOSHIO, M.; BRODD, R. J.; & KOZAWA, A., 2009), if energy is properly generated.

Investments in electric vehicles (EVs) are increasing substantially, and are estimated to reach ~30% of the transport market by 2030 (INTERNATIONAL ENERGY AGENCY, 2019). EVs are formed by a battery system with a cathode, an anode and an electrolyte. The currently available Li-ion battery (LIB) is the most commercialized worldwide, being used in personal electronic devices (*e.g.* cell phones, tablets, etc), and being the choice of EVs (ETACHERI *et al.*, 2011). However, their practical energy density is far from gasoline (150 Wh/Kg vs 1,700 Wh/Kg, respectively), indicating LIBs have insufficient energy capacity to fully attend the global demand and, hence, EVs cannot travel long distances (GIRISHKUMAR *et al.*, 2010a). To overcome these issues, studies led to a recent arrangement known as Li-O₂ or Li-air battery (YU; LIU; FENG, 2021).

Li-O₂ cell has stood out as the electrochemical device with the greatest theoretical gravimetric capacity (~3,500 Wh/Kg) (WANG, Chengyi; XIE; ZHOU, 2019), being an advantage for the energy sector. The cell arrangement is composed by a lithium metal anode and an oxygen (or air) cathode, which are separated by a membrane wetted with a liquid electrolyte or a solid membrane electrolyte. At the cathode occurs the oxygen reduction reaction (ORR) and evolution reaction (OER), which enable the cell operation. In addition, oxygen is widely available in atmosphere, reducing the device price, while lithium is a light material which could reduce the cell weight. However, this battery is not yet commercially

available and many challenges should be faced to enable its complete development (BALAISH; KRAYTSBERG; EIN-ELI, 2014).

The configuration of a Li-O₂ cell is based on the kind of electrolyte used, which can be liquid, divided into aqueous, non-aqueous (aprotic/organic solvents) and hybrid (mixed aqueous/aprotic electrolyte), or all-solid-state electrolytes (BALAISH; KRAYTSBERG; & EIN-ELI, 2014). Liquid electrolytes usually have higher ionic conductivity than the solid system, however, they have unstable electrochemical performance, can leak from the battery and cause a fire if that liquid is a flammable component (DENG, 2015). Furthermore, the solid system is safer and less prone to form lithium dendrites over the anode, but the high resistance between the interfaces of the electrodes with the electrolyte hinder the charge-discharge reactions, limiting the cell cyclability, and they deliver low ionic conductivity, which compromises the battery performance (YAO *et al.*, 2019).

Despite the advantages and disadvantages of each cell configuration, aprotic electrolytes are the most reported in literature and will be the focus of this project. Therefore, to overcome the hurdles related to the liquid electrolyte, investigations have led to the use of additives, such as ionic liquids (ILs) (SIMONETTI *et al.*, 2017) and Redox Mediators (RMs) (LIM *et al.*, 2016).

ILs are salts in room temperature and are considered green solvents because they are usually produced from renewable sources (HARJANI *et al.*, 2009). They have as advantages good ionic conductivity, wide electrochemical window, low vapour pressure, and improved cyclability compared to various organic or solid electrolytes. Different cationic groups, such as imidazolium, pyridinium and pyrrolidinium, are known from literature (SINGH, Geetanjali; KUMAR, 2008), being the imidazolium group the most studied in the battery field, due to its high stability and low toxicity (OLIVIER-BOURBIGOU; MAGNA; MORVAN, 2010). In general, ionic liquids with smaller cationic groups are studied due to their lower viscosity. However, there is a particular and underexplored property of ILs which have long alkyl chains that could be interesting for the battery application. When the size of the alkyl chain connected to the imidazolium ring is superior to 11 carbons, they have a liquid crystalline behaviour, receiving the denomination of ionic liquid crystals (ILCs) (YAMANAKA *et al.*, 2005). ILCs are ionic liquids with liquid crystal properties, which means they are able to form organised structures when dissolved in a solvent at a certain concentration and create preferential pathways for the ionic transport. Therefore, ILCs could deliver high ionic conductivity (YUAN; YANG; *et al.*, 2019).

As for Redox Mediators (RMs), their use has increased in the last few years. They are soluble catalysts which can be homogeneously dissolved in the electrolyte. Conventionally, in the absence of RMs, Li-O₂ cells face some instability during their operation (ZHOU *et al.*, 2019). On discharge, Li⁺ ions from the anodic side react with oxygen reduced (ORR) on the cathode at potentials close to 2.7 V, forming lithium oxides on the cathode side as reaction products (BRUCE *et al.*, 2012). On charge mode, potentials usually close to 4.5 V are necessary to evolve oxygen (OER) and decompose these discharge products. However, these high charge overpotentials can degrade the electrodes and the electrolyte, if the latter is unstable in a reactive medium, implying in poor cell cyclability and electrical efficiency (KUNDU *et al.*, 2015). Therefore, RMs are important because they are stable under oxidative environment and act in the cell cyclability, decomposing the lithium oxides formed on discharge, and lowering the charge overpotentials (KWAK, Jin *et al.*, 2016). Different classes of RMs are found in literature, in this work we focus on bromide anion, since halides are simple redox materials which act effectively in the cell rechargeability at potentials below 4 V (PARK *et al.*, 2018).

In this sense, combining ILs with RMs seems like an interesting approach to enhance the electrolyte stability. The combination of both materials is still very recent (ZHENG; DING; WANG, 2019), and the lack of information in literature brings a new path of possibilities in the battery studies. Therefore, the goal of this project is to overcome part of the instability issues mentioned earlier by introducing, for the first time, a multi-functional ionic liquid crystal (ILC), [C₁₆mim][Br], as additive for non-aqueous DMSO/LiClO₄ electrolyte for Li-O₂ batteries. The cation [C₁₆mim]⁺ belongs to the imidazolium IL group, which has structural properties due to its 16 carbons in the alkyl chain. These properties confer to the electrolyte higher electrochemical stability and ionic conductivity. In addition, the anion [Br]⁻ has redox properties which will be necessary for the cell rechargeability. Therefore, different properties can be reached in the unique [C₁₆mim][Br] material. In this work, we investigated the influence of the ILC into the electrolyte properties and how it affects the performance of Li-O₂ cell.

1.1. Objectives

1.1.1. General Objectives:

The main objective of this project was to develop a non-aqueous electrolyte containing an ionic liquid crystal with redox properties, $[C_{16}mim]^+[Br]^-$, as additive for Li-O₂ batteries, aiming at improving the electrolyte stability and enhancing the cell cyclability. This project used the ILC $[C_{16}mim][Br]$ combined with DMSO solvent and LiClO₄ salt. The electrochemical, transport and structural properties of the electrolyte were investigated, as well as the redox mediator function and the additive use were evaluated in the performance of the Li-O₂ battery.

1.1.2. Specific Objectives:

- Evaluate how different concentrations of $[C_{16}mim][Br]$ additive affect the physicochemical (viscosity, density and ionic conductivity) and structural (molecular and ionic arrangement) properties of the DMSO/LiClO₄ electrolyte;
- Investigate the electrochemical stability of the system due to ILC use;
- Evaluate the role of the bromide anion as a redox mediator for the battery cell;
- Perform deep discharge and cycling tests to evaluate the energetic capacity and cyclability;
- Characterize the electrolyte and the discharge products formed at the cathode via Raman Spectroscopy;
- Observe the discharge products and the changes in the cathode morphology via FESEM technique.

1.2. Dissertation Outline

This project is structured into chapters, as follows:

Chapter 1 introduces the importance and challenges of developing Li-O₂ batteries, focusing on the electrolyte limitations and the use of ionic liquid and redox mediator as additives to overcome the main issues. This chapter also presents the general and specific objectives of this dissertation, its structure and discusses the main results and contributions of this work.

Chapter 2 is a literature review of the Li-O₂ batteries, introducing the fundamental concepts of electrochemistry, presenting the cell components and its configuration, as well as the main limitations of the system and how to suppress them. The use of ionic liquids and redox mediators is also deeply discussed in this chapter.

Chapter 3 presents the methodology and procedures necessary for the development of this project.

Chapter 4 is divided into three sections and discusses the results obtained experimentally and via simulation, the latter developed in a partnership with the group of Prof Juarez Da Silva, from the Chemistry Department of the University of São Paulo (USP). **Section 1** is the first scientific paper, submitted to the Journal of Materials Chemistry A, which discusses the use of the ILC additive into the electrolyte properties. **Section 2** is the second paper, which is in writing process, discussing the electrolyte use in the performance of Li-O₂ batteries. **Section 3** is a general discussion and correlation of the two scientific papers developed during this dissertation project.

Chapter 5 presents the main conclusions of this work based on the results obtained.

Chapter 6 suggests future works and perspectives to complement the results obtained and contribute to the scientific community.

Chapter 7 shows the scientific production developed during this project.

1.3. Main Contributions of This Work

This is a pioneer study of an ionic liquid crystal (ILC) with redox mediator properties as additive for Li-O₂ batteries. In other words, the chosen material, [C₁₆mim][Br], can be considered as a multi-functional additive, which is an advantage to the system since different properties can be reached in a single component. The ILC [C₁₆mim][Br] is a solid at ambient temperature, which belongs to the imidazolium ionic liquid group. It has a liquid crystal character due to the long alkyl chain connected to the imidazolium ring, assuming a structural function. As for its anionic side, [Br]⁻ is a redox mediator that facilitates the cell cyclability and reduces the charge overpotentials.

It was found that the [C₁₆mim][Br] addition can improve the electrolyte electrochemical stability and ionic conductivity. Besides, the anion [Br]⁻ was an effective redox mediator,

decreasing the charge overpotentials as more additive was added to the system. As for the structural behaviour of ILCs, it is a very interesting property still underexplored in literature, raising a new perspective for the battery field. Dissolving [C₁₆mim][Br] in a solvent, the ILC tends to form aggregates, which become bigger as more ILC is added to the system, until they self-organise into structures with polar and apolar nano-domains. These structures affect the electrolyte properties, as deeply explained in section 4.1, and influence the electrochemical performance of the Li-O₂ battery, which could be improved depending on the concentration of the ILC used, as explained in section 4.2 of Chapter 4 (Results and Discussion). Even so, the system still faces some issues, especially related to the high viscosities of the ILC, and determining the proper concentration of the additive is essential for enhancing the cell operation. Further investigation will be necessary for complementing the main findings and it is important to highlight that the properties of the ILC could be explored for different solvents, other types of batteries, for quasi-solid and solid electrolytes.

Chapter 2

Literature Review and Fundamental Concepts

2.1. Historical Context – Development of Batteries

The development of batteries and the study of electrochemistry have been explored for centuries. However, the knowledge about batteries is not yet fully consolidated and new cell devices are still under investigation. The recently introduced Li-O₂ or Li-air batteries have been widely studied because theoretically they provide a lot more power and storage capacity than the currently used systems (YU; LIU; FENG, 2021), with ability to be used in electric vehicles (EVs), as well as for energy storage to couple with intermittent energy generation. However, the technology of Li-O₂ is still under development (BALAISH; KRAYTSBERG; EIN-ELI, 2014). To better understand how batteries have evolved through the years, the importance of electrochemistry and how studies led to the Li-O₂ cell, this section focuses on building a timeline from the first discoveries of electrochemistry, following with the creation of different cells until the concepts of the promising Li-O₂ cell.

Electrochemistry consists on the conversion of chemical energy into electrical energy and vice versa. It is extremely important for the everyday life. It is found in many industrial processes, as in electrolysis to separate chemical compounds, in the generation of electricity, and in batteries for electronic devices and electric vehicles. The first battery cells were developed in the late 18th and early 19th centuries thanks to the works of the Italian doctor and scientist Luigi Galvani and the Italian physicist Alessandro Volta (SCHUMM, 2019).

Galvani proposed that electricity could be stored in the muscles of living beings and that nerves could conduct electricity after an experiment in which he observed a frog leg being contracted when touched by different metals. Volta, in contrast, observed that zinc and silver are capable of producing electricity and created the first practical battery, by intercalating these materials and separating them by a porous membrane imbibed in a saline solution, this battery became known as “voltaic pile”. Later, both observations contributed to many other electrochemical works developed by several scientists, including the theoretical laws of electrochemistry elaborated by Faraday (SCROSATI, 2011).

In 1836, an English chemist, John F. Daniell, created a cell composed of copper ions soaked in a solution of copper-sulphate. Two years later, William R. Grove elaborated a cell containing a solution of nitric acid. In 1841, the German Robert W. Bunsen improved Grove’s

cell, by replacing the carbon electrode by platinum (BAGOTSKY, 2011). These cells mentioned above and all the other models developed until 1859 are batteries which cannot be reused after complete discharge, they are, then, disposable and are classified as primary batteries. The first storage (secondary) battery was built in 1859 by Gaston Planté in France, who created a rechargeable lead-acid battery and inspired other scientists to improve storage cells through the years (SCHUMM, 2019).

Lead-acid and nickel-cadmium secondary cells were the most commonly used rechargeable batteries until early 1980s. However, the increasing demand for rechargeable electronic devices were claiming for more efficient secondary batteries. Lead-acid and nickel cadmium had a limited energetic capacity and their aqueous electrolytes contributed to the battery's large size and weight. As an alternative, it was observed that lithium metal is a light material with superior theoretical capacity. However, previous works using lithium had only led to primary cells instead of secondary ones. Thus, many scientists devoted their studies to build a secondary lithium ion battery (LIB) (SCROSATI, 2011).

Three scientists stood out in the development of the rechargeable LIB. The British researcher M. Stanley Whittingham was the first to explain intercalation chemistry reactions in secondary batteries. He designed the first rechargeable battery in 1976, which was composed of TiS_2 and Li metal electrodes (WHITTINGHAM, 1976). However, due to the formation of Li dendrites, short-circuiting and risk of explosion, the battery could not be commercialized. Later in the 1979, The German scientist John B. Goodenough discovered that LiCoO_2 used as cathode material presents a high voltage and energy density (MIZUSHIMA *et al.*, 1980), which drew the attention of the Japanese Akira Yoshino. Yoshino, then, after several researches and trials, invented the current LIB, which is composed of a LiCoO_2 cathode, a carbonaceous material anode and a non-aqueous electrolyte (YOSHINO, 2012).

The design of the secondary LIB revolutionized science and awarded the 2019 Nobel Prize of Chemistry to the three scientists. Li-ion is the most sold battery in the world, being found in most of the portable electronic devices (MIRSKY, 2019). LIBs are also used in electric vehicles (EVs), but they have low energy density, being unable to provide enough energy to EVs travel long distances (LI; LU, 2017). Even when LIBs are associated in parallel to improve their capacity, it would imply high production and commercialization costs, large and heavy battery packages (GIRISHKUMAR *et al.*, 2010b). To improve capacity of EVs,

studies suggest the development and commercialization of Li-O₂ or Li-air batteries (LI; LU, 2017).

Littauer and Tsai (1976), introduced the first concepts of Li-air batteries, but the first practical rechargeable Li-O₂ cell was developed only in 1995 by Abraham and Jiang after they set up a system of a lithium metal electrode and a carbon composite electrode, both separated by an organic polymer electrolyte. In the carbon composite electrode, oxygen was used as the electro active material and was supplied from the environment. The cell showed good capacity, a large electrochemical window, good cyclability and stability. The cell design was totally solid, non-toxic components were utilized and this system was thus eco-friendly (ABRAHAM; JIANG, 1996). This discovery initiated the study of Li-O₂ batteries, especially in the last decade with the increasing interest of applying electrochemistry in the transport sector (Figure 1).

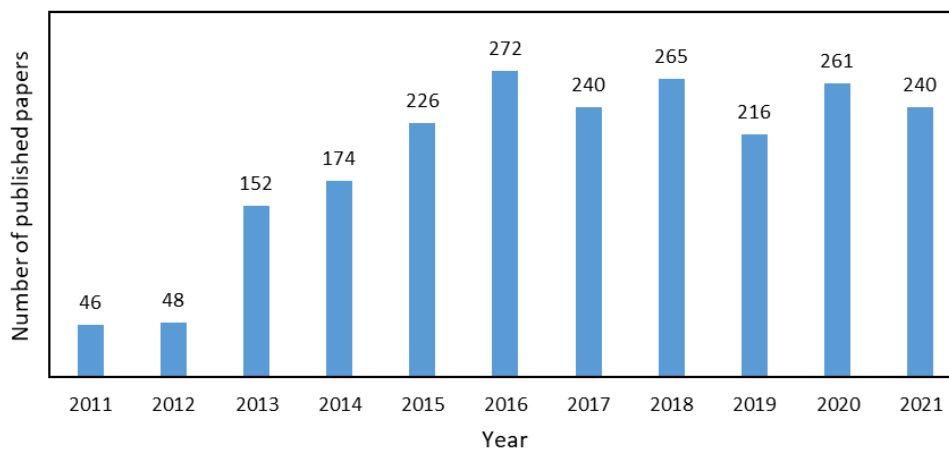


Figure 1. Number of papers published about Li-O₂ and Li-air batteries per year in the last decade. Graph based on Scopus data. Author, 2022.

The Li-O₂ cell is a promising battery configuration for use in EVs because they have the greatest practical energy density of ~1700 Wh/Kg (see Figure 2), which is close to gasoline (WANG; LI; & SUN, 2013). In addition, they are compact, more economic and lighter than other available batteries, forming a robust system (CHRISTENSEN *et al.*, 2011). However, to the fully development of Li-O₂ cells, it is necessary to overcome many challenges, especially in building an ideal electrolyte, which should be electrochemically stable, have high ionic conductivity and be compatible with all the cell components (LI; ZHANG; ZHOU, 2013).

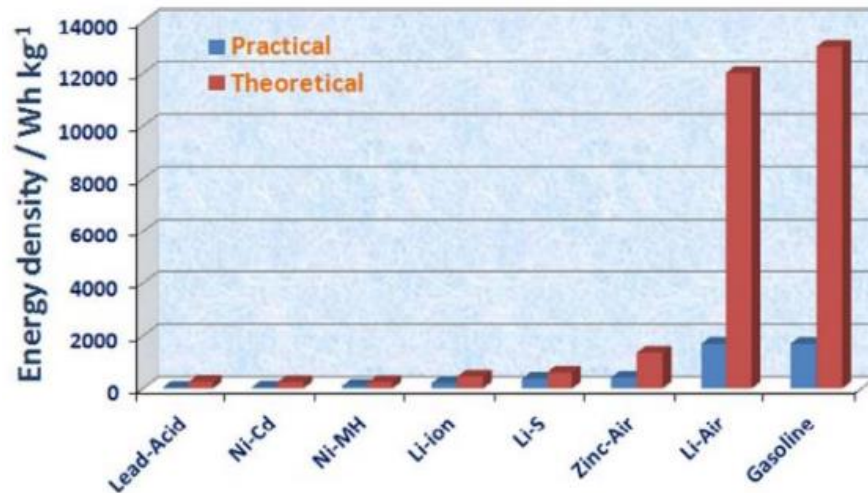


Figure 2. Comparison of the theoretical and practical energy density of various secondary batteries and gasoline. Adapted from WANG; LI; & SUN, 2013.

2.2. Configuration and Operation of Li-O₂ Batteries

The basic components of a battery cell are two electrodes, an electrolyte, and a separator membrane. The negative electrode is the anode and the positive electrode is the cathode. The electrolyte can be a solid or a liquid (aqueous, non-aqueous, mixed aqueous/aprotic) component that is responsible for conducting ions (TICIANELLI; GONZALEZ, 2005). The membrane separator is commonly used for liquid electrolytes because it aims to avoid electronic contact between the electrodes and thus prevents short-circuiting. In solid systems, the electrolyte assumes the membrane role and contributes to both the ionic conduction and to separate electronically the electrodes (ABRAHAM; JIANG, 1996).

The typical operation of a Li-O₂ battery is shown on Figure 3. The metallic lithium assumes the anode role, providing Li⁺ ions to the cell, whereas a porous carbon material is used as cathode to transport oxygen. In the discharge process, the anode is oxidized releasing Li⁺ ions ($Li \rightarrow Li^+ + e^-$), which are transferred to the cathode through the electrolyte (BRUCE *et al.*, 2012), whereas the cathode undergoes an oxygen reduction reaction (ORR). The products and by-products formed during discharge depend on the type of electrolyte, as shown in Table 1. An external circuit is used to transfer electrons in the same direction of the Li⁺ ions flow, generating electricity (TAN *et al.*, 2017).

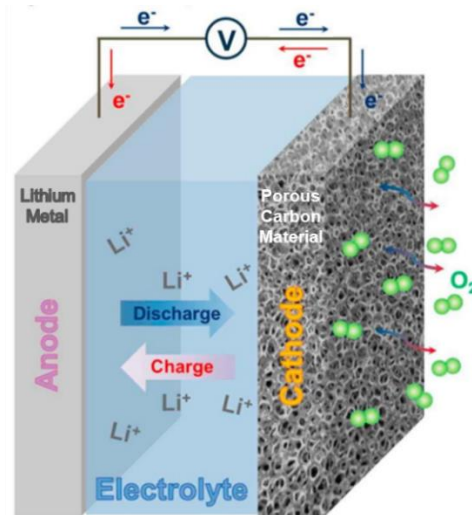


Figure 3. A typical discharge and recharge operation of an aprotic Li-O₂ battery. Adapted from TAN *et al.*, 2017.

The charging mode of a battery occurs in the opposite process of discharge. For reversible systems, the lithium electrode becomes the cathode, because lithium is now reduced and the oxygen electrode becomes the anode due to the oxygen evolution reaction (OER). In general, high charge overpotentials are necessary to decompose the discharge products, with Li⁺ ions flowing from the oxygen electrode back to the metallic lithium through the electrolyte, and the energy is stored in the cell device in the electrochemical form (TAN *et al.*, 2017). Ideally, discharge products should be decomposed under a potential lower than 4 V, because high overpotentials can degrade the electrolyte and damage the cathode (KUNDU *et al.*, 2015).

From Table 1, it is clear that for both aprotic and solid electrolytes the main discharge product is lithium peroxide, Li₂O₂. These configurations are excellent candidates for Li-O₂ cells because the main discharge product is decomposed to its original form ($Li_2O_2 \rightarrow O_2 + 2Li^+ + 2e^-$) when the battery is recharged. An alternative mechanism for formation of Li₂O₂ in aprotic systems is proposed by Bruce, with lithium superoxide (LiO₂) as an unstable intermediate. Also, in aprotic configuration, lithium oxide (Li₂O) is a discharge side product formed in smaller amount than Li₂O₂, it is harder to decompose and, hence, it hampers the cell rechargeability. Therefore, it may be conclude that Li₂O₂ is the most desirable reaction product (WANG; LI; & SUN, 2013).

Table 1. Most common discharge reactions observed for each cell configuration. Adapted from WANG; LI; & SUN, 2013.

Battery Configuration	Discharge Reactions
Aprotic / Non-Aqueous	$O_2 + 2Li^+ + 2e^- \rightarrow Li_2O_2$ (main product)
	$O_2 + 4Li^+ + 4e^- \rightarrow 2Li_2O$ (side product)
	$O_2 + e^- \rightarrow O_2^-$
	$O_2^- + Li^+ \rightarrow LiO_2$
	$2LiO_2 \rightarrow Li_2O_2 + O_2$ (alternative mechanism)
Aqueous	$O_2 + 4Li^+ + 4e^- \rightarrow 2Li_2O$
	$4Li + O_2 + 2H_2O \rightarrow 4LiOH$ (alkaline electrolyte)
	$4Li + O_2 + 4H^+ \rightarrow 4Li^+ + H_2O$ (acidic electrolyte)
Hybrid /Mixed	$4Li + O_2 + 2H_2O \rightarrow 4LiOH$ (alkaline electrolyte)
Aqueous-aprotic	$4Li + O_2 + 4H^+ \rightarrow 4Li^+ + H_2O$ (acidic electrolyte)
Solid Electrolyte	$O_2 + 2Li^+ + 2e^- \rightarrow Li_2O_2$

2.3. Lithium Anode

The use of lithium as electrode in metal-air cells is preferred over other materials because of its low cost and great specific capacity of ~3840 mAh/g in reactions with oxygen (EVOLVING ENERGY, 2014). Besides, it is the smallest, lightest, it has the greatest specific heat and is one of the most electropositive metals in periodic table (HELMENSTINE, 2019). However, the lithium metal is generally incompatible with the electrolyte in a battery, limiting its life cycle and compromising its safety. To avoid these issues, it is highly recommended the use of a protective layer on the anode surface to prevent its contact with the electrolyte (DATT BHATT *et al.*, 2014).

When a non-aqueous electrolyte is used, a kind of layer known as solid electrolyte interface (SEI) is formed, separating the anode from the electrolyte. This SEI can assume a protective function whether it presents good flexibility, cohesion and ionic conductivity, which would prevent decomposition of the lithium metal (BALAISH; KRAYTSBERG; & EIN-ELI, 2014). In solid systems, there is no formation of a natural SEI. Instead, an artificial SEI composed of a ceramic or polymeric material, compatible with the Li anode is used to provide its protection and avoid the cell short circuit. Ceramics are more expensive since they offer a more efficient protection. They are impermeable, thermally stable and block the

contaminants crossover (SUN, Yugang, 2013), while polymers are easier to fabricate and have more flexibility (TAN *et al.*, 2017).

When the oxygen for the cell is supplied by the atmospheric air (ambient air provides oxygen for Li-air cells, while in Li-O₂ cells pure oxygen is provided by an O₂ cylinder) (LAI *et al.*, 2020), all the other air components, such as nitrogen, oxygen, water, carbon dioxide and contaminants are also captured and can pass through the aqueous or non-aqueous electrolyte, reaching the anode electrode. Therefore, an efficient SEI also protects the lithium electrode from these contaminants, avoiding undesirable reactions, formation of side products and reduced cell life (KRAYTSBERG; EIN-ELI, 2011).

However, if the natural SEI is not mechanical stable and resistant to reactive medium, the multiple discharges and recharges of the Li-O₂ cell can imply on an excess of Li salts on the anode surface with an irregular current distribution, leading to formation of lithium “dendrites”. These dendrites have a branch form and their accumulation on the anode cause decomposition of the Li metal and the electrolyte (FOROOZAN; SHARIFI-ASL; SHAHBAZIAN-YASSAR, 2020). As consequence, the Coulombic efficiency of the cell is affected, electrochemical reactions are inhibited and an internal short circuit is caused between the electrodes. Figure 4 represents this phenomenon of dendrites growth and the cell damage. Artificial SEIs are the best alternative to suppress dendrites formation (BALAISH; KRAYTSBERG; & EIN-ELI, 2014).

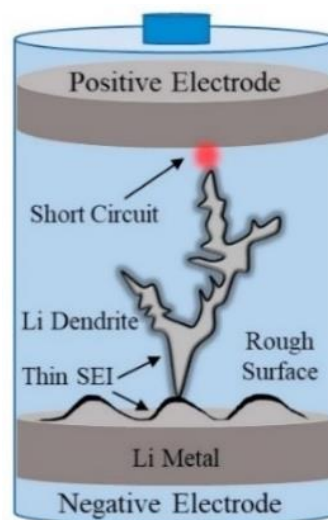


Figure 4. Short circuit caused by the growth of Li dendrites. Adapted from FOROOZAN *et al.*, 2020.

2.4. Oxygen Cathode

The development of a proper oxygen electrode is substantial for the best performance of the Li-O₂ or Li-air cell. The cathode has to meet a series of requirements, such as, electrochemical stability, long cycle life, rapid diffusion of oxygen and high ionic conductivity (LU *et al.*, 2014). Since the oxygen reduction reaction (ORR) is slower than the lithium oxidation (OLIVEIRA, 2018), the cathode is the main responsible for the discharge and charge potentials and provides the majority of the cell energy. In other words, the cathode influences the specific and power capacity of the battery (ZHANG; FOSTER; READ, 2010).

ORR and OER contribute to the cell energy loss. During ORR of solid and non-aqueous electrolytes (Table 1), it is possible to observe that Li⁺, O₂ and e⁻ participate in the electrochemical reactions, forming mainly Li₂O₂ as discharge products, and other side products. These products are insulating solids that are insoluble in aprotic electrolytes and are deposited on the cathode side (TAN *et al.*, 2017). Therefore, researchers suggest the importance of choosing a cathode material with large surface area in order to provide active sites to assist the electrochemical reactions, and mesoporous structure with adequate pore volume (from 2 to 50 nm) in order to store those insoluble products (LU *et al.*, 2014). Microporous and macroporous structures should be avoided, because the former is easily blocked by the discharge products, disrupting the discharge reactions, whereas the latter decreases the volumetric energy density as indicated by theoretical calculations (OLIVEIRA, 2018).

Carbons with various nanostructures have been widely employed as air cathode because of their singular morphology and defective structure. Besides storage of lithium oxides, carbon materials act as a conductor matrix, contributing with enough transference of electrons in the electrochemical reactions (DING *et al.*, 2014). Commonly materials cited in literature are carbon black (Super P, Ketjen Black, etc), carbon powder, graphene (Figure 5. a)), carbon fibres (Figure 5. b)), and carbon nanotubes (CNTs) (Figure 5. c)) (TAN *et al.*, 2017).

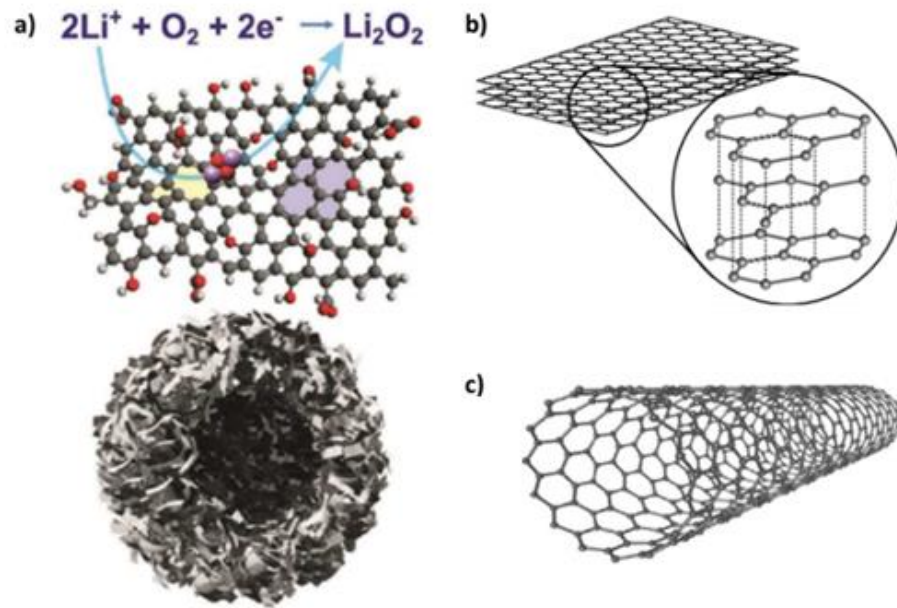


Figure 5. Schematic 3-D Structures of a) Graphene, b) Carbon Fibers and c) CNT. Adapted from TAN *et al.*, 2014; DAMBROT, 2016; & AQEL *et al.*, 2015, respectively.

Super P is a kind of carbon black that shows excellent performance in Li-O₂ batteries. JUNG *et al.* (2012), developed a Li-air cell with an improved capacity of 5,000 mAh/g and discharge potential of 2.7 V Li⁺/Li, using Gas Diffusion Layer (GDL)-Super P air-electrode and a TEGDME–LiCF₃SO₃ electrolyte. ZHANG *et al.* (2010), studied a different kind of carbon black, Ketjen Black (KB) in his research. The group found a cell with an energy of 362 Wh/Kg operating at ambient temperature and observed that the KB-based cathode suffered expansion and absorbed a large amount of electrolyte. The group concluded that the microstructures of KB carbon should be improved to reach a better specific energy.

Carbon powder and CNTs are also used in the development of Li-O₂ cells. CNTs, in especial, was proved to contribute to increase the diffusion capacity of soluble catalyts (redox mediators) when fabricated with an open and mesoporous structure (KWAK, Jin *et al.*, 2016). Also, a study carried out by TAN *et al.* (2014) employing both CNT and carbon powders at different rates indicated the best results for the proportion 1:1. The maximum gravimetric capacity was 779.14 mAh/g and the cell was cycled for 50 times. These authors found that CNT improved the cell capacity because it can provide efficient transport of oxygen and Li⁺. On the other hand, graphene materials have also been employed due to their impressive cell capacity. XIAO *et al.* (2011) investigated the use of graphene sheets as electrode for Li-air batteries, they found that the microporous channels and structure of

graphene offered an excellent oxygen diffusion, with an impressive cell capacity of 15,000 mAh/g.

As it can be seen above, each carbon material has its own particularity when applied to Li-O₂ systems. In general, the defective structure of carbon facilitates the ORR, acting as catalysts and, therefore, contributing to the discharge capacity. Even so, sometimes the use of soluble catalysts in the electrolyte is mandatory to perform ORR and, especially, OER due to the need of high overpotentials to decompose lithium oxides and charge the cell (LU *et al.*, 2014). Sections 2.7 and 2.8 will provide further information about overpotentials and the use of catalysts.

2.5. Electrolytes

It is known that four configurations are possible for Li-O₂: aqueous, non-aqueous (or aprotic), mixed aqueous/non-aqueous (hybrid) and all solid-state electrolytes. The *aqueous electrolyte* presents the configuration showed in Figure 6 a). The use of water as solvent is beneficial to the dissolution of the discharge products (Table 1), which avoid blockage of the cathode pores and the bulk expansion. The electrochemical reactions involved in this cell configuration occur between the lithium and oxygen electrodes, as well as with the aqueous electrolyte. Different discharge products are formed, depending on the chosen electrolyte medium (acidic or alkaline) and the pH of the solution (KOWALCZK; READ; SALOMON, 2007).

For basic aqueous systems, the discharge mode utilizes H₂O to react with lithium and oxygen, forming LiOH, a very corrosive compound (Reaction 2). This compound has a solubility of 12.8g/100 mL of H₂O at ambient temperature. When LiOH surpasses the solubility limit, it precipitates as LiOH.H₂O, which can block the pores of the oxygen electrode, and thus hinders the oxygen diffusion (LU *et al.*, 2014). Unlike basic solutions, the acidic aqueous electrolytes do not form insoluble by-products, and they reach higher discharge voltages (~4.27 V vs Li/Li⁺), leading to other electrochemical reactions (Table 1) (CAPSONI *et al.*, 2012). Even so, after long time of operation, acidic cells become an alkaline medium. Catalysts to improve ORR and OER are quite difficult to develop and these cells produce low specific capacities. Hence, basic solutions are preferred over acidic ones (LU *et al.*, 2014).

Since lithium is very reactive in water, forming the corrosive compound LiOH, a protection membrane selective of Li^+ must be used between the Li metal and the electrolyte of the aqueous cell. The development of this protective layer is a difficult task, ceramic and KOH based membranes have been tested, but they cannot totally avoid the water passage (LU *et al.*, 2014). Until now, the Ohara Corporation has produced the most attractive separators, $\text{Li}_2\text{O}-\text{Al}_2\text{O}_3-\text{TiO}_2-\text{P}_2\text{O}_5$ and $\text{Li}_2\text{O}-\text{Al}_2\text{O}_3-\text{Ge}_2\text{O}-\text{P}_2\text{O}_5$ membranes (FU, 1997a, b). These membranes have a NASICON structure, show great insulation of the metallic Li and are good conductors. However, they are expensive and incompatible with the lithium anode, requiring an additional conductive layer between the interface of the anode and the membrane to solve this issue (LU *et al.*, 2014).

The *aprotic* or *non-aqueous* electrolyte is currently the most studied battery configuration and is the focus of this project. Its advantages over other systems are the superior volumetric and gravimetric capacities, and the possibility of exploring many kinds of ionic conductor solvents as electrolytes (LU *et al.*, 2014). Its configuration (Figure 6 b)) is based on a Li anode imbibed in an electrolyte formed by a solution of Li salts (mainly LiTFSI, LiPF_6 , and LiClO_4) dissolved in an aprotic (organic and polar) solvent. The cathode is a meso-porous oxygen electrode (MARCINEK *et al.*, 2015). By choosing the right electrolyte components, a natural SEI, composed of organic and inorganic products, could be formed over the Li anode, conferring protection to this material from corrosion (VERMA; MAIRE; NOVÁK, 2010). The main discharge product is the Li_2O_2 produced via ORR. For the system reversibility, a high voltage is provided to decompose Li_2O_2 via OER and to recharge the cell (DATT BHATT *et al.*, 2014).

An ideal non-aqueous solvent should have a large electrochemical window, to guarantee the electrochemical stability and to avoid the cell degradation in the reactive medium. It should be compatible with all cell components, non-toxic to humans, non-flammable and eco-friendly (XU, 2004). Its viscosity should be as low as possible to facilitate a rapid ionic transport, high ionic conductivity and thus high energy to the cell. A high boiling point and low melting point are also essential properties to avoid electrolyte evaporation, phase change and degradation (MARCINEK *et al.*, 2015).

However, there is no aprotic electrolyte in literature with all those properties, being the main limitations related to safety issues since many aprotic systems are volatile and flammable (LAI *et al.*, 2020). Mixtures of organic carbonates (such as dimethyl, ethylene, and propylene carbonates) have been widely used as electrolytes in lithium-based cells due to their

wide electrochemical window, low volatility, and good compatibility to the Li anode. On the other hand, organic carbonates are unstable in the presence of very reactive species (such as LiO_2^- , O^{2-} , and O_2^{2-}), suffering from nucleophilic attack (BRUCE *et al.*, 2012). It means that these electrolytes are inadequate for Li- O_2 batteries, because they are easily degraded during discharge and form undesirable side products (DATT BHATT *et al.*, 2014). Instead, dimethyl sulfoxide (DMSO) and glyme-based solvents have been used in Li- O_2 cells, showing reasonable charge-discharge performance with formation of Li_2O_2 as the main discharge product (KITAURA; ZHOU, 2015). Even so, these electrolytes are also attacked during the cell operation, needing further improvement for the proper cell performance.

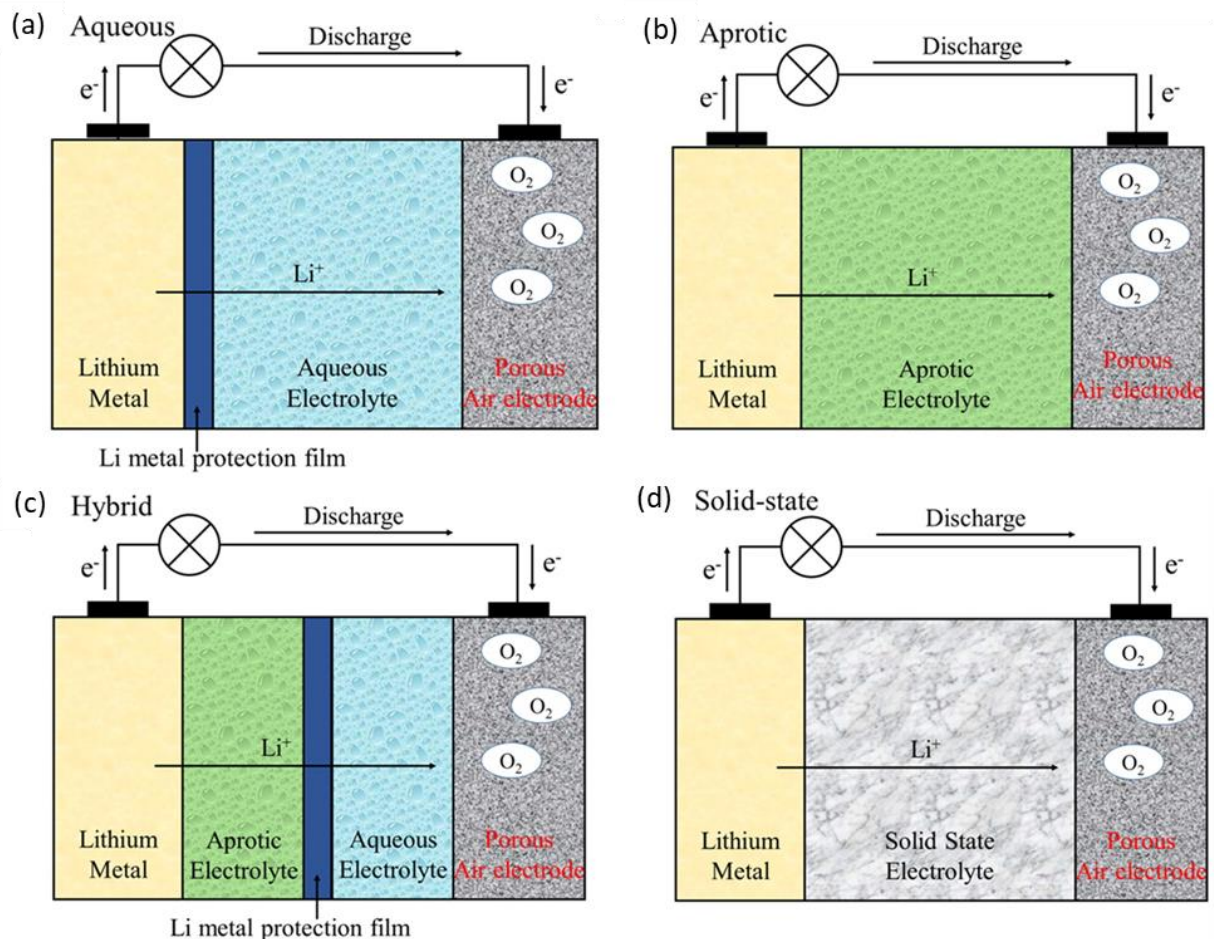


Figure 6. The four configurations of Li- O_2 Batteries. a) Aqueous, b) Aprotic or non-aqueous, c) Hybrid or mixed aqueous/aprotic, and d) Solid electrolytes. Adapted from LU *et al.*, 2014.

The electrolyte instabilities can be minimized by the use of additives, such as metal-oxides, noble and non-noble metals as catalysts (TAN *et al.*, 2017); redox mediators, which

are soluble catalysts that facilitate the cell cycling, reducing the charge and/or discharge overpotentials (PARK *et al.*, 2018); or ionic liquids, which are also a viable alternative because of their stability with oxygen intermediates, large potential window, hydrophobicity, low flammability and despicable vapour pressure (DATT BHATT *et al.*, 2014).

Hybrid (mixed aqueous/aprotic) battery configuration was proposed to solve limitations of the aqueous and non-aqueous systems. This architecture (Figure 6 c)) is based on the combination of both aqueous and non-aqueous electrolytes. It is formed by a Li anode soaked in the aprotic electrolyte and a protective SEI layer is formed on its surface. This side is separated from the aqueous electrolyte by a Li ion conductive solid membrane. In the aqueous side, the air cathode is wet by this aqueous electrolyte. Thus, the water cannot reach the Lithium metal and the anode will not suffer from corrosion (BALAISH; KRAYTSBERG; EIN-ELI, 2014). In discharge mode, O₂ enters the cathode and the ORR occurs, whereas the anode is oxidized with Li⁺ ions migrating from the aprotic to the aqueous electrolyte through the solid membrane (WANG; ZHOU, 2010).

Despite the benefits of this mixed aqueous electrolyte, many challenges need to be overcome. The protection of the lithium anode is primordial for the cell performance. However, it is very difficult to fully develop a good conductor solid separator that prevents water penetration. Ceramic separators with a NASICON-like structure are a fair alternative, demonstrating enough impermeability and conductivity (BALAISH; KRAYTSBERG; EIN-ELI, 2014). Another challenge is the corrosive compound LiOH as one of the products formed in the cathode side during discharge. Since its solubility in water is narrowed, this product precipitates and accumulates on the cell, limiting its life cycle. Furthermore, as well as other liquid electrolytes, hybrid configuration can also leak from the battery and cause safety issues (TAN *et al.*, 2017).

Solid electrolytes are an alternative to improve the cell durability and safety of the system. An all-solid-state battery (Figure 6 d)) replaces the liquid electrolytes for solid materials, which solves volatility issues, eliminating the possibility of leakages. It improves mechanical and thermal resistances, and reduces the battery size and weight, resulting in a more simplified and mechanically robust design with improved energy density (ZHAO *et al.*, 2019). Additionally, many solid electrolytes are compatible with the lithium metal, they do not suffer from dendrites formation, and can reach a voltage window over 5 V indicating they are not easily decomposed when an anodic current is applied (LI *et al.*, 2015).

Solid polymers and solid inorganic (ceramics) are the main types of all-solid-state electrolytes. The former is composed of polymers and lithium salts. Polymeric materials, like poly(ethylene glycol) (PEO), polyacrylonitrile (PAN), and poly(methyl methacrylate) (PMMA), are commonly used as solid matrices. As advantages, they are flexible materials and can endure the change in volume provided by the discharge and charge reactions. They have a simple fabrication process and are inexpensive, which facilitate their scalability. However, they have low ionic conductivity and are unstable under high potentials, suffering from nucleophilic attack when in the presence of O_2^- and Li_2O_2 (LAI *et al.*, 2020).

Solid inorganic materials generally have higher mechanical, electrochemical and thermal stabilities than polymers, and higher ionic conductivity (YANG, Min; HOU, 2012), but they have high costs, are brittle and unstable to volume variation due to temperature change (TAN *et al.*, 2017). Commonly used ceramics are oxysulfide and sulphide glasses, perovskites, garnet and the super-ionic conductor NASICON (YANG, Min; HOU, 2012). NASICON-like structures are the most attractive because they have the highest ionic conductivities, scalability, and are stable with moisture and air. However, their high interfacial resistance with the Li anode requires a conductive and protective layer between the anode and the electrolyte (LAI *et al.*, 2020).

To overcome the interfacial resistance and the low ionic conductivity of electrolytes in solid-state, more elaborated materials have been investigated. As instance, the combination of solid materials with non-aqueous solvents or/and ionic liquids can enhance the ionic conductivity of solid matrices (LAI *et al.*, 2020). ZHANG *et al.* (2010) developed a Li-air battery with a solid electrolyte composed of silica-PVDF-HFP as polymer, LiTFSI as lithium salt and the IL 1,2-dimethyl-3-propylimidazoliumbis(trifluoromethanesulfonyl)imide (PMMITFSI). The group found a battery with ionic conductivity of 1.83×10^{-3} S/cm at ambient temperature, reduced lithium degradation and stable interfacial resistance.

2.5.1. DMSO Solvent for Non-aqueous Electrolyte

Dimethyl sulfoxide (DMSO) is a universal organic solvent widely used for non-aqueous Li- O_2 batteries. Its low volatility of 189 °C guarantees that the electrolyte will not easily evaporate during cell operation, and its low viscosity of 1.95 cP contributes to the ionic transport. Other advantages are its good ionic conductivity of 2.11×10^{-3} S/cm, stability with

oxygen products, its ability to dissolve lithium salts formed during ORR and its high dissolution of O₂ gas compared to other organic solvents (XU *et al.*, 2012). DMSO was chosen as the solvent for the present study due to such advantages, further to its ability to dissolve ionic liquids and good acceptance with the imidazole group.

KHAN and ZHAO (2016) studied the ORR and OER of different ionic liquids mixed with DMSO for Li-O₂ cells. The authors used imidazolium ([BMIM][BF₄], [BMIM][PF₆] and [BMIM][NTf₂]), pyridinium ([BMPy][NTf₂]), and pyrrolidinium ([BMP][NTf₂]) electrolytes, all ILs had a fixed concentration of 3.5 M. Comparing with the individual use of ILs or DMSO, the mixture improved the solubility and diffusion coefficient of oxygen, as well as the cell cyclability. In addition, the electrolytes were stable under superoxide (O₂⁻) medium, with exception of [BMPy][NTf₂], whose cations reacted with O₂⁻.

DMSO is reasonably stable in superoxide mediums, however, it can react with unprotected lithium metal, and with oxide species, producing DMSO₂, Li₂SO₃, Li₂SO₄ and LiOH as undesirable side products. These side-reactions can accumulate and clog the air-cathode surface after multiple cycles (SHARON *et al.*, 2013). ROBERTS *et al.* (2014), proposed as alternative to avoid these undesirable reactions the use of electrolyte additives (0.3 M LiNO₃ and 0.14 M vinylene carbonate), which stabilized the SEI layer and improved the efficiency of a DMSO-based electrolyte from 25% to 82.5%.

ZENG and co-workers (2015) found that the addition of an imidazolium-based IL in DMSO solvent was capable to stabilize Li-O₂ cells. The authors prepared blended electrolytes: DMSO (80 wt%) – TEGDME (20 wt%), EMIMTFSI (20 wt%) – TEGDME (80 wt%) and DMSO (80 wt%) – EMIMTFSI (20 wt%). LiClO₄ was chosen as Li salt. The mixture of DMSO and EMIMTFSI presented the best stability. This IL improved the cell conductivity from 6.1 x 10⁻³ S/cm (pure DMSO) to 9.5 x 10⁻³ S/cm (EMIMTFSI and DMSO), enabled more than 65 cycles, decreased the recharge potential and, therefore, suppressed the DMSO decomposition (proved by X-ray diffraction and SEM analysis).

2.6. Ionic Liquids

2.6.1. General Properties of Ionic Liquids

Ionic liquids (ILs) are salts which have low melting points (lower than 100 °C) and similar features to common molten salts, such as large liquidus range and high electrochemical

stability (KAPER; SMARSLY, 2006). ILs are known since the 19th century and have aroused growing interest in the 1980s due to their great variety of applications, being used as green solvents, catalysts, in the fabrication of fuel cells, as electrolytes for batteries, among others (OLIVIER-BOURBIGOU; MAGNA; MORVAN, 2010). They are used as an alternative to volatile solvents because of their almost despicable vapour pressure so that they do not damage the environment through evaporation. In addition, they are able to dissolve a series of organic and inorganic compounds and some of them are well accepted in biphasic systems (SINGH, Geetanjali; KUMAR, 2008).

In general, ionic liquids are composed of a cation, which has an asymmetric organic structure, and an organic or inorganic anion. The most common cation groups are imidazolium, pyrrolidinium, pyridinium, among others (Figure 7). For the anionic side, halides, sulphates, alkyl groups, hexafluorophosphate, tetrafluoroborate, etc. are widely utilized. Different cations and anions can be combined in order to target a desirable application for ionic liquids, in other words, properties such as viscosity, density, conductivity, chemical or thermic stability are influenced by the intermolecular interactions of distinct cations and anions (SINGH, Geetanjali; KUMAR, 2008).

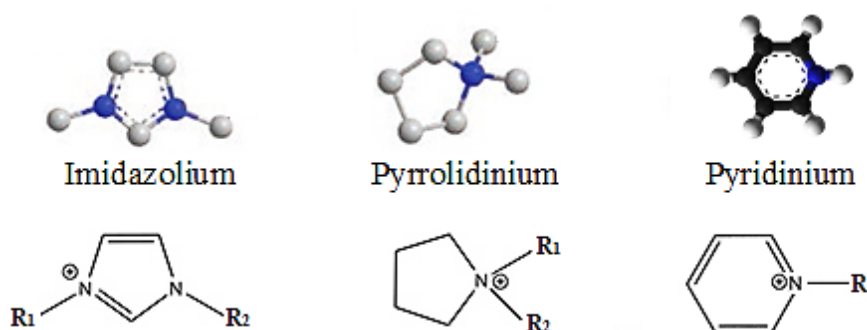


Figure 7. Common cationic groups of ionic liquids. Adapted from LI *et. al.*, 2018; & SUN *et. al.*, 2010.

Ionic liquids can be used in liquid, semi-solid and all-solid-state electrolytes (MAHMOOD, 2015). They have several properties that make them viable for use in Li-O₂ batteries, but the utilization of ILs in this cell is still in its infancy (LAI *et al.*, 2020). They are chemically and physically stable, and resistant to superoxide environments. In addition, they generally have high ionic conductivity (from 10⁻⁴ to 10⁻² S/cm), wide electrochemical window (many ILs are stable above 5 V), are capable of solvating compounds with a large polarity

range, have low volatility and non-flammability. However, they are combustible materials and cannot be near a heat source (ZHANG *et al.*, 2006).

Viscosity is one of the main challenges for ILs. They can be one to three times more viscous than regular solvents, due to Van der Waals forces and the hydrogen bonds, which could impair ion transport and diffusion, compromising the cell efficiency (FRÖBA; KREMER; LEIPERTZ, 2008). In most cases, viscosity is related to the size of ions, as bigger ions tend to present higher viscosities. It is also influenced by temperature because higher temperatures increase the kinetic energy, allowing greater mobility of ions and, therefore, decreasing the IL's viscosity. The possibility of various anions and cations combinations could result in less viscous ILs. Some groups, as ether, oligoether, imidazolium and anions as $[\text{NTf}_2]^-$ and $[\text{N}(\text{CN})_2]^-$ are found to be less viscous. When used as additives, such as in the combination of ILs in organic solvents, it is possible to produce a system with reasonable viscosity (PERRY *et al.*, 1995).

In this investigation, the focus will be on the imidazolium-group (Figure 7), which is formed by an imidazole ring with one of its nitrogens in a protonated (cationic) form. It shows promising performances in batteries and supercapacitors due to its high electrochemical (MERCK KGAA, 2020) and thermal stabilities (BENDER, 2014). In addition, molten imidazolium-based salts have lower viscosity than many other IL groups, contributing to the improved ionic conductivity (ARA *et al.*, 2014), and they can be used with varying chain lengths (LE MONG; KIM, 2019) and dissolved in different organic solvents (CHAGNES *et al.*, 2005).

2.6.2. Ionic Liquids Crystals

Ionic liquid crystals (ILCs) are a class of ionic liquids little explored in the energy storage field which possesses unique structural properties that could be interesting for application in electrolytes. ILCs receive this denomination because they have properties of ionic liquids joint to liquid crystals. It means that the ILC material has molecules with amphiphilic character, being composed of a hydrophilic (the “headgroup”) and a hydrophobic (the “tail”) part (Figure 8 a)), which give the material the ability to self-assemble, forming aggregates when dissolved in a solvent at a certain concentration (BENDER, 2014). These aggregates are known as micelles (Figure 8 b)), which become bigger as more ILCs are added to the solvent

and reorganise themselves into complex structures, affecting the properties of the solution, *i.e.* viscosity, superficial tension, conductivity, etc. (HILTROP, 1994).

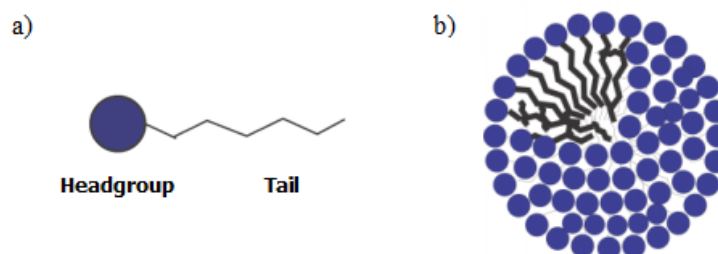


Figure 8. a) Representation of an amphiphilic molecule. b) Scheme of a spherical micellar arrangement. Adapted from PORT, 2018.

The structural property appears in ILs whose cationic group is connected to large alkyl chains, giving the material the ability of forming a crystalline mesophase, an intermediate phase between the liquid and the solid phases, which appears in a certain temperature range (DEVAKI; SASI, 2017) and which can be observed via polarizing optical microscopy (POM) (YUAN; YANG; *et al.*, 2019). The mesophase can also appear in electrolytes with ILCs and it has been reported that the formed structures can act like channels that enable the ionic transport and enhance the ionic conductivity, which is beneficial for the battery operation (DEVAKI; SASI, 2017). However, there is only a few papers reporting the ILC use in electrolytes, being found in supercapacitors, dye-sensitized solar cells (DSSC), and Li-ion batteries (DEVAKI; SASI, 2017), with no evidence of ILCs in Li-O₂ batteries.

YAMANAKA *et. al* (2005) developed DSSCs based on the IL [C₁₁MIM⁺][I⁻] and the ILC [C₁₂MIM⁺][I⁻] (the mesophase was formed in alkyl chains larger than C₁₁). Despite the ILC exhibited viscosity 2.5 times higher than the IL studied, [C₁₂MIM⁺][I⁻] presented superior diffusion coefficient and higher ionic conductivities. These observations were ascribed to the ability of ILC to form long-range conductive channels, which facilitated the ion transportation. On the other hand, YUAN *et al.* (2019) built a new imidazolium-based ILC salt used as a solvent-free electrolyte for Li-ion batteries. This group also explored the capacity of ILC to form fast ion-conductive channels, which enabled high ionic conductivity of 3.02 x 10⁻³ S/cm and wide electrochemical window at room-temperature.

Therefore, based on the studies of Yamanaka and Yuan, the use of imidazolium-based ILCs as electrolyte additive seems like a promising approach to improve the system stability and ionic conductivity. Furthermore, the lack of literature information about the ILC

application in Li-O₂ batteries rises the interest in investigating how this kind of additive affects the electrolyte properties and the cell performance. Thinking of that, this project proposes, for the first time, the use of an ionic liquid crystal as an additive in aprotic electrolytes, composed of DMSO/LiClO₄, for Li-O₂ batteries. The cationic imidazolium group with 16 carbons on the side of the alkyl chain, [C₁₆mim]⁺, was chosen for this study. As for the anionic group, the anion [Br]⁻ was chosen due to its redox mediator properties, which will be further explained in sections 2.7. *Cell Overpotential* and 2.8. *Redox Mediators*.

2.7. Cell Overpotential

Besides the choice of electrolyte, one of the biggest limitations of Li-O₂ is associated with the high cell overpotentials formed during ORR and OER. To better understand this challenge, it is important to first consider the Nernst equation, which determines the standard potential for formation/decomposition of Li₂O₂ to be $U_0 = 2.96$ V. This potential is the basis for discharge and charge reactions (GIRISHKUMAR *et al.*, 2010b), so ideally during the cell operation, in ORR a potential slightly lower than U_0 should be reached whereas in OER a voltage slightly higher than U_0 should be expected for a high energy efficiency. However, in practical operation of Li-O₂ batteries, these potentials are not easily reached (LAI *et al.*, 2020). For example, Figure 9 indicates a typical charge/discharge potential curve of aprotic electrolytes.

The initial cell potential is named open circuit voltage (OCV) or open circuit potential (OCP). When the battery is discharged, the working potential reaches its stability at potentials below U_0 . This difference between the discharge and standard potentials is known as the discharge overpotential, η_{dis} (see Figure 9). On the other hand, the cell voltage reaches its stability at potentials much greater than U_0 during the cell charge. This difference between charge potential and U_0 is the charge overpotential, η_{chg} . The difference between the discharge and charge overpotentials is the cell polarization and the efficiency of the cyclability can be calculated from the relation η_{dis}/η_{chg} , so usually Li-O₂ cells have low energy efficiency (GIRISHKUMAR *et al.*, 2010).

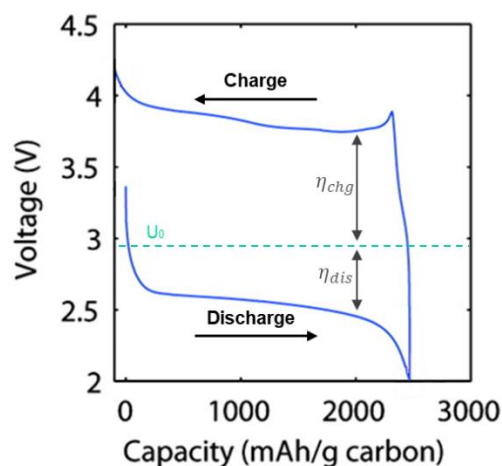


Figure 9. A typical charge/discharge cycle performed for a non-aqueous Li-O₂ battery.

Adapted from FREUNBERGER *et al.*, 2011.

From Figure 9, it is clear that discharge overpotentials are usually low and the charge overpotentials are much higher (KUNDU *et al.*, 2015). It is explained by the ORR, where Li₂O₂ and the side products are formed as an irregular film distributed on the cathode surface, causing its pore clogging. Besides, these side products are insulating, increasing the electrical resistance, causing slower transport of ions and oxygen, and high overpotentials are required during recharge (OER) to decompose these products (LIM *et al.*, 2016). High overpotentials can degrade the electrolyte, if it has a low electrochemical stability, and change the surface of the carbon cathode, forming the undesirable insoluble compound Li₂CO₃. This compound accumulates with Li₂O₂ over the cathode surface, increasing even more the charge overpotential, and hindering the cell cyclability (KUNDU *et al.*, 2015).

Reducing the charge overpotential would, therefore, enable a high energy efficiency and improve the cell operation. One way to overcome this hurdle is by the use of solid catalysts on the cathode side. Studies indicate that noble metals (such as Au, Pt, and Pd) are good candidates, because they substantially reduce overpotentials even when in small fractions. The use of MnO₂-based electrocatalysts is also a fair alternative due to its activity and low cost (KRAYTSBERG; EIN-ELI, 2011; OMINDE; YANG; QU, 2009). QIN *et al.* (2013) found an excellent catalytic capacity of α-MnO₂ nanorods in Li-O₂ cells. The catalyst improved the cell's performance by reducing its charge potential to 3.5 V, showed high cyclability and fine electrochemical activity.

Despite the benefits of solid catalysts, it was found that they can severely degrade the electrolyte (LIM *et al.*, 2016). In addition, they are unable to completely decompose the Li₂O₂

species because of their lack of contact with the entire lithium peroxide film located on the cathode surface. Therefore, only the contacting parts of the discharge product with the catalysts will be degraded during charge, as shown in Figure 10 a). As a better choice, the use of redox mediators (RMs) as soluble catalysts is increasing considerably and ensures a better reversibility of the system since they can spread homogeneously through the electrolyte (figure 10 b)) (PARK *et al.*, 2018).

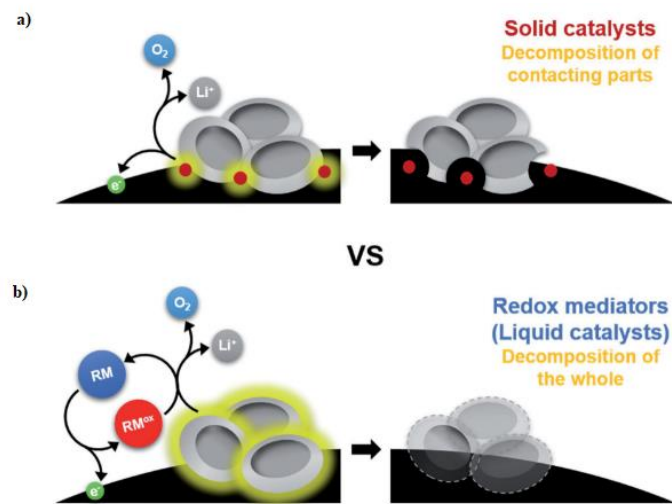


Figure 10. Decomposition of Li₂O₂ species during recharge of a Li-O₂ battery using a) solid catalysts and b) redox mediators (liquid catalysts). Adapted from PARK *et al.*, 2018.

2.8. Redox Mediators

The use of redox mediators (RMs) in Li-O₂ cells was first reported by Bruce and his group (2013) with the use of the RM tetrathiafulvalene (TTF) in an aprotic electrolyte. The presence of this RM provided rechargeability to the cell at a current density (1 mA/cm²) that was unlikely to be achieved without this RM. After that, many researchers dedicated their studies to develop other materials with redox properties for Li-air systems. As already mentioned in this work, RMs are catalysts that are easily diffused through the electrolyte, as they provide maximum contact with Li₂O₂ and other by-products, facilitating the OER (LIM *et al.*, 2016).

Many RMs are able to conduct the formation of Li₂O₂ as the only product in ORR, and oxidize this product in OER at a voltage range of 3 to 4 V vs Li (SHARON *et al.*, 2017). They provide a simpler path to decompose lithium peroxide, regardless of its size or structure, so that RMs boost the cell cyclability and efficiency (LIM *et al.*, 2016). Moreover, the redox

potential of a RM establishes the charge potential of the cell, so it is crucial to preselect the appropriate catalyst in order to optimize the charge reaction (PARK *et al.*, 2018).

To be classified as a RM, the catalyst should be completely soluble in the electrolyte and the redox reaction should be totally reversible. In addition, it should provide a charge potential lower than the cell's potential in the absence of this RM. The potential must be low enough to avoid degradation of any cell component, but it should be higher than the standard potential of Li_2O_2 ($U_0 = 2.96$ V). Finally, RMs should be resistant to oxidative medium (oxides formed during ORR/OER) and do not attack the lithium anode (PARK *et al.*, 2018).

Redox mediators are divided into three groups: organic, organometallic and halides. Each group has its pros and cons, but in this project, the focus is on halides, more specifically the anion Br^- . Their main advantage is that unlike the organic and organometallic mediators which react with discharge products and the lithium anode, halides are not reactive at potentials lower than 3.5 V. LiI and LiBr belong to the halide group and are commonly studied in literature. They form two redox couples: X^-/X_3^- or X_3^-/X_2 , but I_2 and Br_2 are both very corrosive so that their formation should be avoided. At potentials inferior to 4.2 V, I^-/I_3^- and $\text{Br}^-/\text{Br}_3^-$ are the only redox couple formed (PARK *et al.*, 2018).

Figure 11 illustrates the two-step mechanism for the OER of a Li- O_2 cell promoted by the anion Br^- . Firstly, the anion Br^- , which is soluble in aprotic solvents, is electrochemically oxidized close to the cathode surface, forming Br_3^- (step 1). Then, Br_3^- oxidizes the discharge product Li_2O_2 in a chemical process instead of electrochemical, releasing Li^+ ions, O_2 gas, and returning to its reduced form Br^- (step 2) (LAI *et al.*, 2020; PARK *et al.*, 2018).

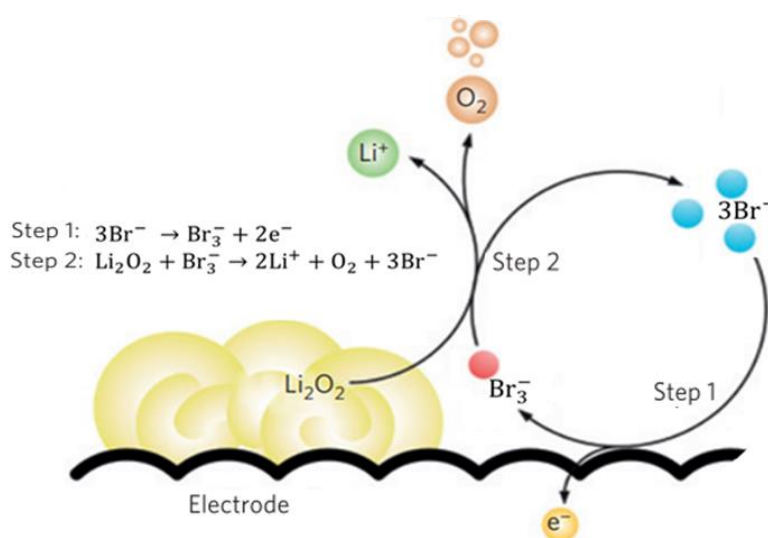


Figure 11. Reaction mechanism promoted by halide RM in a Li- O_2 cell. Adapted from LIM *et al.*, 2016.

Authors who investigated lithium halides as RMs found very interesting results. KWAK *et al.* (2016), studied the role of both LiI and LiBr mediators in Li-O₂ cells containing LiTFSI as Li salt and diglyme as solvent. They found better cyclability and catalytic effect for electrolytes with LiBr. The RM couple Br⁻/Br₃⁻ were both very effective, reducing the charge overpotential to values close to 3.5 V. In addition, cells containing LiBr were able to produce Li₂O₂ as the main discharge product even when H₂O was included into the battery cell. On the other hand for LiI it was observed that, when the cell system was completely sealed and its electrolyte was subjected to rigorous anhydrous processes, Li₂O₂ was formed as the only product in reduction reaction. Even the willful addition of H₂O into the cell resulted in formation of mainly Li₂O₂, and LiOH in small proportions.

Since this project investigates the joint function of RMs with ILs, studies including both additives in Li-O₂ cells were searched in literature. ZHENG *et. al* (2019) designed a cell with pyrrolidine group in the cationic side and Br⁻ as the redox counter-ion. The electrolyte was composed by a LiTFSI salt, TEGDME solvent, and N-methyl-N-propyl-pyrrolidine bromide (MPPBr) in different concentrations. The introduction of MPPBr into the cell facilitated the OER, and the redox couple Br⁻/Br₃⁻ reduced the charge overpotentials to ~3.6 V. In addition, the IL induced the formation of a stable SEI, which protected the Li anode and avoided the occurrence of side reactions. Finally, the presence of MPPBr increased considerably the cell cyclability and the best performances were found to concentration of 0.2 M MPPBr.

For the present work, the focus is on the ionic liquid crystal [C₁₆mim][Br] with redox mediator ability. The influence of this additive on the electrolyte properties are investigated, including how it affects the density, viscosity, ionic conductivity and electrochemical stabilities of the system. Besides, the RM function is evaluated and the influence of the structural character on the Li-O₂ cell operation.

2.9. Final Comments

Chapter 2 presented a general overview of the Li-O₂ battery, discussed about its components, the main advances in the electrochemical field and the main challenges for the cell full development, which are mostly related to the electrolyte instabilities. To suppress these instabilities, it was proposed the use of additives, such as ionic liquids, which can enhance the electrochemical and thermal stabilities of the electrolyte, and the use of redox mediators, which facilitate the cell operation by reducing the charge overpotentials. The combined use of both IL and RM materials was suggested to boost the cell performance.

Besides, ionic liquid crystals, a class of ILs with long alkyl chain, were also introduced in this chapter and proposed as possible additives for Li-O₂ cells. Despite the lack of literature evidence of the ILC use in Li-O₂ cells, this kind of material was reported in different energy storage devices, such as DSSCs and Li-ion batteries. It was showed that when ILCs are dissolved in a solvent, they have the ability to form organised structures that resemble channels for the ionic transport, enhancing the ionic conductivity of the system.

To summarize, based on the information provided by this chapter, this work focuses on the use of an ionic liquid crystal with redox mediator properties, [C₁₆mim][Br], as additive for aprotic DMSO/LiClO₄ electrolyte. It was investigated the effect of the ILC addition in the system, how it affects the electrolyte properties and the Li-O₂ battery performance.

Chapter 3

Methodology and Procedures

3.1. Preparation of Electrolytes

Considering the experimental tests, the electrolytes were prepared by dissolving different concentrations of the ionic liquid crystal 1-hexadecyl-3-methylimidazolium bromide, $[\text{C}_{16}\text{mim}]^+[\text{Br}]^-$ ($\text{C}_{16}\text{mimBr}$, or $[\text{C}_{16}\text{mim}][\text{Br}]$) (Figure 12) into DMSO/ LiClO_4 0.100 M electrolyte. The concentration range varied from 0.000 M ILC to 2.366 M ILC, which corresponds to the saturation limit of $[\text{C}_{16}\text{mim}][\text{Br}]$ into DMSO.

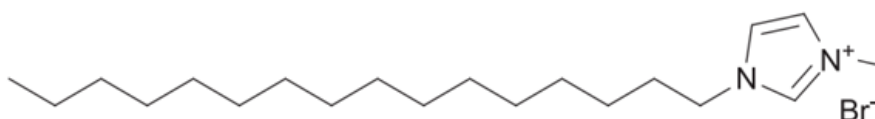


Figure 12. Chemical structure of the ionic liquid $\text{C}_{16}\text{mimBr}$. Adapted from KAPER & SMARSLY, 2006.

The use of the organic solvent DMSO and the salt LiClO_4 has been widely explored by our research group. The novelty of this project is the use of the ILC $[\text{C}_{16}\text{mim}][\text{Br}]$, which is a solid at ambient temperature, soluble in DMSO and other organic solvents. $[\text{C}_{16}\text{mim}][\text{Br}]$ can be used in sol-gel processes, for the manufacture of mesoporous polymers and metal oxides (such as hexagonal and cubic silica), as well as for the synthesis of surfactants and electrolytes (KAPER; SMARSLY, 2006). These processes are attributed to its ability to aggregate and form lyotropic (phase transitions occur with addition or removal of solvent) and thermotropic (phase transition with temperature change) liquid-crystalline phases (HILTROP, 1994). Because of these features, we believe that this ILC is a suitable candidate for our electrolytes.

3.2. Preparation of Catalytic Ink for the Cathode

The catalyst facilitates the oxygen reduction and oxygen evolution reactions by minimizing the activation barrier. For this step, a catalytic ink based on commercial carbon nanotube (CNT) as active material was synthesized for use with carbon paper cathode. For the substrate, discs of Toray carbon paper were cut ($D=16.5$ mm, $A=2.13$ cm²) and weighted by a

MX5 Mettler Toledo analytical balance. As for the catalytic ink preparation, it was based on the work of LI *et al.* (2018). An ultrasonic Sonicator (Eco-Sonics) was used for ~10 min to homogenise a mixture of 25 mg of commercial CNT (CNT CO. LTD), 4 mL of distilled H₂O, 1 mL of isopropanol (Synth > 99.5%), and 50 µL of Nafion® (Aldrich, 20wt%). Then, an aliquot of this solution (1 mL) was diluted in 400 µL of isopropanol by the ultrasonic sonicator for 5 min. The final product was a catalytic ink with low viscosity.

For the preparation of the cathode: With a micropipette, 28 µL of the catalytic ink was applied on each side (totalizing 56 µL) of the carbon paper disc. This ink volume was estimated for a CNT amount of 0.3 mg. During the applying process the electrode was dried in an oven at 100 °C, then left in a vacuum desiccator to remove any moisture. Then, the air electrode was transferred to an Argon glove box (MBRAUN-LABstar Workstation) to avoid interaction with water and oxygen (FRANCISCO, 2019).

3.3. Evaluation of the Electrolyte Properties

- **Ionic Conductivity:** We have seen that an electrolyte with high ionic conductivity is highly desirable for the proper cell operation. It was measured at ambient temperature by the digital conductivity meter Starter 3100C from OHAUS, which is a benchtop equipment that constitutes a four-pole linear electrode to prevent polarization and a temperature sensor.

- **Density and Viscosity:** A Stabinger SVM-3000 (Anton Paar) viscometer was used to determine the density and viscosity values of the electrolyte at various ILC concentrations. The measurements were conducted with and without LiClO₄, at a temperature range from 293.15 K to 353.15 K, with 10 K steps.

3.4. Electrochemical Tests

- **Li-O₂ Cell Assembly:** A homemade Swagelok cell design was used for the battery configuration, as indicated in Figure 13. It was used for the deep discharge and cycling tests to evaluate the cell performance. The cell consists of two stainless steel current collector plates, one being the anodic side and the other the cathodic. A thin lithium foil was used on the anodic side and the electrolyte was added. A fiberglass membrane was used to avoid the electrodes contact and thus prevent the cell short circuit. More electrolyte was added, totalizing 100 µL, which was enough to wet the fiberglass membrane. Then, the carbon

cathode was placed over the membrane, and finally, a stainless-steel current collector mesh and the spring were added to ensure the electric contact. The cell was hermetically sealed. All procedures for this assembly were performed inside an Argon filled glove box to avoid the lithium contact with H₂O or O₂ (CREMASCO, 2017).

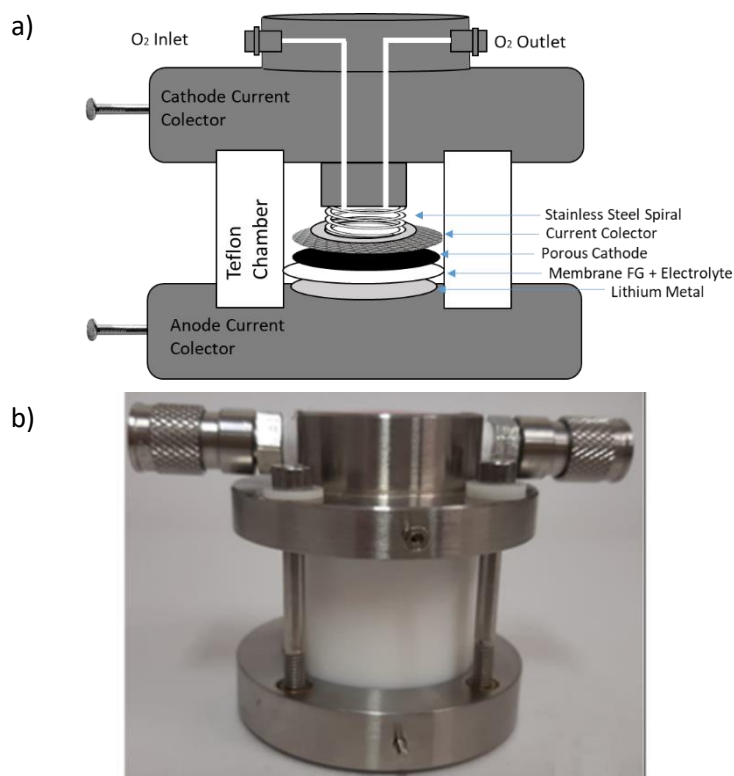


Figure 13. a) Li-O₂ Cell Assembly and b) Li-O₂ Cell fully sealed. Author, 2021.

- Electrochemical Stability and Assessment of the Bromide counter ion as mediator:

An electrolyte needs a high electrochemical stability to avoid decomposition under very reactive and oxidative mediums (ARA *et al.*, 2014). Thus, cyclic voltammetry (CV) tests were conducted at an argon atmosphere, using a homemade three-electrode cell setup with an Autolab potentiostat. A silver wire was the quasi-reference electrode, platinum was the counter, and the carbon glass was the working electrode. A scan rate of 50 mV/s was used, and a voltage range from 2.0 V to 6.5 V vs Li/Li⁺. Through CV tests, it was also possible to verify the redox property of the bromide anion. The redox peaks indicate the potentials for the oxidation and reduction of the [Br]⁻.

- Deep discharge: The deep discharge and the cycling test are important to understand the energetic performance during the cell operation. Deep discharge was conducted with

Chronopotentiometry (CP) technique using a potentiostat Multi Autolab/M204. For a closed system, an oxygen pressure of 3 bar was used, the applied current was 50 μA with a current density of 23 $\mu\text{A}/\text{cm}^2$ and no limiting time. The cut-off discharge potential was 2.2 V (JÚLIO, 2020).

After the deep tests, the gravimetric capacity was calculated, using equation 3. This information is important because it can be an indicative for the cell cyclability. It is common to expect a long cyclability for cells which present high discharge (gravimetric) capacities. Given the electric current in mA, the total operation time (h) and the mass (g) of active material (CNT) used at the cathode, the capacity was calculated from equation 3 (JÚLIO, 2020). The gravimetric capacity graphs as function of potential were plotted and analysed.

$$\text{Gravimetric capacity} \left(\frac{\text{mAh}}{\text{g}} \right) = \frac{\text{current (mA)} \times \text{time (h)}}{\text{Mass of active material (g)}} \quad (3)$$

- **Electrochemical Cycling Tests:** They are required to determine the cyclic performance of the battery. Using a potentiostat Multi Autolab/M204, limiting the oxygen pressure to 3 bar and the gravimetric capacity to 1000 mAh/g, cycling tests were performed at a current of 50 μA and cut-off potential of 2.2/4.5 V Li/Li⁺.

3.5. Chemical and Morphological Characterization

The electrolytes were characterised via Raman spectroscopy, while the carbon electrodes were characterized via Raman and FESEM techniques.

The *RAMAN Spectroscopy* technique is based on the incidence of a monochromatic laser at distinct wavelengths. This measurement was performed at a Renishaw Spectrometer equipment, using a laser with a 633 nm wavenumber. A scan range from 200 to 3200 cm^{-1} was used and a 1200 l/mm diffraction grating. The analysis was conducted using 10% laser power, 80 sec exposure time and 5 accumulations. Raman was used to identify the organic and inorganic compounds present on the carbon cathode after deep discharge and cycling tests, as well as the non-crystalline species and low-concentration products, such as Li₂O₂ (JÚLIO, 2020). Raman was also used in the electrolytes with different ILC concentrations to observe the Raman shifts and identify the chemical interactions between the [C₁₆mim][Br] molecules with the DMSO solvent.

Field emission scanning electron microscopy (FESEM) was used to observe the morphological changes of the cathode surface and the formed products. Images of the surface of the cathodes were obtained through a Thermoscientific Quattro S equipment with an Everhart Thornley Detector (ETD), which was set with a work distance (WD) of 10 mm, 10 kv beam power, 3.0 spot and varying magnifications.

3.6. Table of Nominal and Real Values

During the calculations of the experimental concentrations of ionic liquid crystal [C₁₆mim][Br], an error was committed, therefore we present below a table of Nominal and Real Values (Table 2). In the entire dissertation, the experimental concentrations of ILC must be read as in Table 2. All experimental conclusions and the correlation of theoretical and experimental data are preserved. An erratum is being written for the first paper, published in the Journal of Materials Chemistry A. The second paper, with writing in progress, will be corrected and will present the real values before being sent to the journal. A few experiments are still in progress due to the need of synchrotron facilities to answer some answers related to the cell performance. We regret any inconvenience that this mistake may have caused for the readers.

Table 2. Nominal and Real Values of ILC Concentration into DMSO/LiClO₄ 0.100 M

Molar Concentration of [C ₁₆ mim][Br]	
Nominal Values	Real Values
0.025 M	0.017 M
0.050 M	0.035 M
0.075 M	0.053 M
0.100 M	0.070 M
0.200 M	0.140 M
0.500 M	0.351 M
1.456 M	1.022 M
2.413 M	1.695 M
3.369 M	2.366 M

Chapter 4

Results and Discussion

This chapter presents and discusses the results obtained experimentally, including the evaluation of the electrolyte properties, characterization of the studied materials and electrochemical tests, as well as the simulation data obtained in a partnership with Dr. Tuanan C. Lourenço and Prof. Dr. Juarez L. F. da Silva from the Department of Chemistry from University of São Paulo, USP. This chapter is presented in journal publication format, being divided into three sections, as follows:

4.1. Investigation of the Electrolyte Properties – Title: Tuning Aprotic Solvent Properties with Long Alkyl Chain Ionic Liquid for Lithium-based Electrolytes – Paper published in the Journal of Materials Chemistry A

4.2. Investigation of the Ionic Liquid Crystal-Based Electrolyte in the Performance of Li-O₂ Batteries – Title: Multi-functional Imidazolium-Based Ionic Liquid Crystal with Redox Mediator Properties for Li-O₂ Batteries – Paper with writing in progress

4.3. General Discussion – This section discusses and correlates the results presented in both papers.

4.1. Investigation of the Electrolyte Properties

Tuning Aprotic Solvent Properties with Long Alkyl Chain Ionic Liquid for Lithium-based Electrolytes*

Tuanan C. Lourenço,^{*,†} Letícia M. S. Barros,^{*,‡} Chayene G. Anchieta,^{*,‡} Thayane C. M. Nepel,^{*,‡} Júlia P. O. Júlio,^{*,‡} Luis Gustavo Dias,^{*,¶} Rubens Maciel Filho,^{*,‡} Gustavo Doubek,^{*,‡} and Juarez L. F. Da Silva^{*,†}

†São Carlos Institute of Chemistry, University of São Paulo, P.O. Box 780, 13560-970, São Carlos, São Paulo, Brazil

‡School of Chemical Engineering, University of Campinas, Campinas 13083-852, Brazil

¶Chemistry Department, FFCLRP, University of São Paulo, 14040-901 Ribeirão Preto, SP, Brazil

E-mail: lourenco.tuanan@gmail.com; leticia.barros94@gmail.com; chayeneanchieta@gmail.com; thyanecarpanedo@gmail.com; julia_paula@outlook.com.br; lgdias@ffclrp.usp.br; rmaciel@unicamp.br; doubek@feq.unicamp.br; juarez_dasilva@iqsc.usp.br

Abstract

Lithium–metal batteries, such as Li–O₂, are some of the most promising candidates for high-performance energy storage applications, however, their performance is still limited by the electrolyte instability. To overcome this limitation it is necessary to develop improved electrolytes with good electrochemical stability and decent ionic transport. Here, we are the pioneers to investigate the influence of the imidazolium-based ionic liquid crystal (ILC) 1-hexadecyl-3-methylimidazole bromide [C₁₆mim][Br] as an additive for an aprotic electrolyte, dimethyl sulfoxide (DMSO) 0.100 M LiClO₄. Combining experimental and theoretical methods, we studied the influence of the [C₁₆mim][Br] addition on the electrolyte properties from a macroscopic up to an atomistic level. The unique structural features of the ILC were investigated and an enhancement in the electrolyte stability was shown due to its self-aggregation ability, which suggests fewer DMSO molecules available to react during the battery operation and consequent less electrolyte degradability. For the ionic transport perspective, the ILC addition leads to an ionic conductivity increase until 1.456 M concentration, after this point, a further ILC addition causes a small decrease in the conductivity due to the high viscosity and the decay in the ions self-diffusion coefficient. By combining Raman spectroscopy and molecular dynamics simulations, we confirmed that the [C₁₆mim][Br] interactions within the ions and molecules of this ternary system enabled the ILC to organize itself into large aggregates at high ILC concentrations. Besides DMSO, these ILC features can be reached in other aprotic and also aqueous electrolytes.

*** Paper published in the Journal of Materials Chemistry A**

1 Introduction

Lithium-based rechargeable batteries are a consolidated energy storage technology, in particular Li-ion batteries (LIB), which have been widely employed in electric and hybrid vehicles.¹ Lithium-metal batteries such as Li-S and Li-O₂ have also been increasingly studied due to their high energy storage capacity,² in which Li-O₂ stands out as an alternative to replace LIB due to its impressive theoretical energy density (3458 W h kg⁻¹), *i.e.*, ten times higher than the energy density of LIB.³

Despite the various benefits of lithium-metal based systems, a common limitation for all devices is the electrolyte stability and the battery safety. The use of aprotic solvents as lithium-based electrolytes is quite common in the battery field, mainly due to the high ionic transport and conductivity.⁴ However, some improvements are needed to reduce the drawbacks related to flammability, cell overpotential, safety issues, and chemical and electrochemical instabilities.⁵ To overcome some of these issues, it is quite attractive to use ionic liquids (ILs) as electrolyte additives;⁶ ILs are noted for their low vapor pressure, reasonable ionic conductivity, and high electrochemical and thermal stabilities.⁶⁻⁸

The application of ionic liquids as electrolytes and additives has been investigated in many energy storage devices such as supercapacitors, redox flow batteries, Li-ion, Li-S, and Li-O₂ batteries.^{7,8} However, their viscous nature compromises the battery performance due to the limited ionic conductivity and mass transport. To overcome this issue, the major part of IL-based electrolyte studies focus on ILs with low viscosity that in general are composed by small ionic structures, *e.g.*, short alkyl chains and low ionic volumes.⁹ Beyond that, the addition of organic electrolytes is also another approach to decrease the IL viscosity and improve the ionic conductivity due to the weakening of the ionic interactions in the liquid.^{7,10}

Although the ILs with short alkyl chains have low viscosity as an advantage, the ILs with long alkyl chains also present some interesting properties.¹¹⁻¹³ For example, when the IL has ions with large ionic structure in its composition, *e.g.*, large imidazolium, ammonium and phosphonium cations, it can assume a liquid crystal function, known as ionic liquid crystal (ILC), which is able to form aggregates and crystalline phases in the liquid medium and complex structures in the solvent.^{12,13} Yamanaka and co-workers have shown that the structural properties assigned to the crystalline phase are expected to suppress problems related to high viscosity,¹¹ but there is insufficient information about how these structures interact and affect the mixture properties and there is little literature evidence of ILCs used in aprotic ternary electrolytes for Li-metal based batteries.

Therefore, in this context, we propose an imidazolium-based ILC with a long alkyl chain, *i.e.*, hexadecyl, to tune a conventional aprotic electrolyte by seizing the self-organizing property and electrochemical stability of the ILC, and improving the ionic conductivity of the system, despite its high viscosity values.

As for the organic solvent used in the present work, we chose dimethyl sulfoxide (DMSO), because it is widely employed in electrolytes for Li–O₂ batteries, due to its low volatility (462 K),¹⁴ low viscosity (1.948 cP),¹⁵ and high donor number (DN = 29.8).^{5,16} The latter indicates that the Li⁺ ion solvation is facilitated by DMSO molecules, which also stabilizes the main and the intermediate (Li₂O₂ and LiO₂, respectively) discharge products formed during the Li–O₂ batteries operation.^{5,16}

Moreover, the high DN enables the formation of hydrogen bonds between DMSO molecules and some other solvents and salts in binary¹⁷ and ternary mixtures,¹⁸ which affect the physical properties of the electrolyte.¹⁷ Despite these great features, DMSO has an electrochemical window limited to 4.20 V,¹⁹ which means it can degrade during the electrochemical reactions in the Li–O₂ battery operation, forming undesirable and irreversible products, such as DMSO₂.²⁰ Fortunately, these side reactions can be diminished by the IL addition, due to the improvement of the electrolyte electrochemical window stability.²¹

The scientific community is involved in the development of electrolytes based on ionic liquids to improve battery performance and life cycle.^{7,22} Theoretical methods are a powerful tool to describe the electrolyte in an atomistic level of detail, providing information on the structure, solvation, and ionic transport in the systems.^{23,24} Many studies propose the use of classical molecular dynamics (MD) simulations to understand IL-based systems, in which it is possible to relate how the ionic structure impacts the electrolyte properties.²⁵ Beyond that, MD simulations have also been used as a tool to complement and improve the understanding of experimental measurements for electrolytes.^{26,27}

In summary, we performed an experimental–theoretical investigation of the effects of the addition of the ionic liquid crystal 1-hexadecyl-3-methylimidazolium bromide, [C₁₆mim][Br], on the physical, electrochemical, and structural properties of the dimethyl sulfoxide lithium perchlorate, DMSO/LiClO₄, 0.100 M electrolyte (Fig. 1). Furthermore, it should be noted that in addition to DMSO, the unique features of the investigated ILC could also be extended to different organic and aqueous solvents. Thus, we propose a new direction for the development of aprotic electrolytes for different electrical devices.

2 Methodology

To improve our understanding of the ILC ([C₁₆mim][Br]) in the aprotic electrolyte DMSO/LiClO₄ 0.100 M, we employed several experimental techniques combined with classical MD simulations and density functional theory calculations (DFT), which are described below.

2.1 Electrolyte Preparation

The chemical compounds 1-methylimidazole (Sigma Aldrich, 99%), 1-bromohexane (Sigma Aldrich, 98%) and ethyl acetate (Synth, 100%) were used in the synthesis of the solid ILC 1-hexadecyl-3-methylimidazole bromide [C₁₆mim][Br] by an optimized quaternization reaction.²⁸

Furthermore, the lithium salt, lithium perchlorate (LiClO_4 , 99.99%) and the organic solvent dimethyl sulfoxide (anhydrous, $\geq 99.9\%$) were purchased from Sigma-Aldrich. Therefore, the electrolytes were prepared by dissolving 0.100 M LiClO_4 and nine different concentrations of the synthesized $[\text{C}_{16}\text{mim}][\text{Br}]$ in DMSO solvent. The saturation point of 3.369 M $[\text{C}_{16}\text{mim}][\text{Br}]$ in DMSO at 298.15 K (0.9166 g $[\text{C}_{16}\text{mim}][\text{Br}]$ per mL^{-1} DMSO) was determined experimentally. On the basis of that, the saturation point was chosen as the highest concentration to avoid ionic liquid crystal precipitation. We characterized the $[\text{C}_{16}\text{mim}][\text{Br}]$ using ^{13}C MAS-NMR and the data is shown in Table S1.† The liquid crystal property of $[\text{C}_{16}\text{mim}][\text{Br}]$ was confirmed via polarized optical microscopy (POM) and via differential scanning calorimetry (DSC) with the data presented, respectively, in Fig. S1 and S2 in the ESI.†

2.2 Electrolyte Characterization

2.2.1 Physical Properties

For density, viscosity, and conductivity measurements, the DMSO solvent was used as purchased. Density and viscosity values were determined using the Stabinger SVM-3000 viscometer (Anton Paar) and the measurements were carried out with and without LiClO_4 , in a temperature range from 293.15 up to 353.15 K, with 10 K steps. Conductivity values were measured at ambient temperature (298.15 K) through the digital conductivity meter model Starter 3100C from OHAUS.

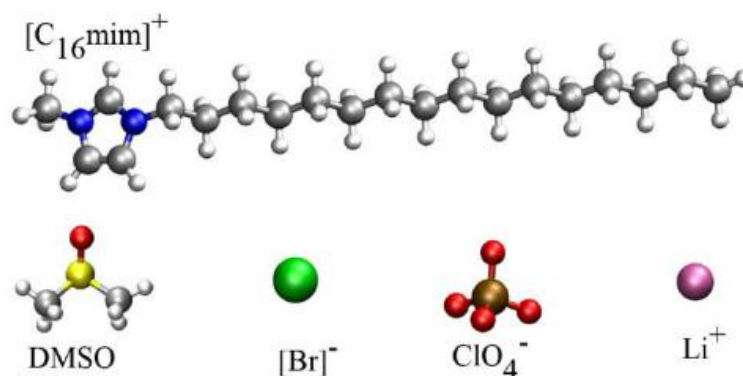


Fig. 1 Ions and molecule simulated in this work, 1-hexadecyl-3-methylimidazolium ($[\text{C}_{16}\text{mim}]^+$), dimethyl sulfoxide (DMSO), bromide ($[\text{Br}]^-$), perchlorate (ClO_4^-) and lithium-ion (Li^+).

2.2.2 Raman Spectroscopy

To obtain the spectra of the ternary mixtures, we used a Renishaw Raman spectrometer, which can help in the identification of the chemical interactions between the ILC molecules and the DMSO solvent by comparing the Raman shifts upon the addition of $[\text{C}_{16}\text{mim}][\text{Br}]$ into the electrolytes. The measurements were performed using a 633 nm He–Ne laser with 10% of power, diffraction grating of 1200 l mm^{-1} , a 50X zoom lens, 80 seconds of exposure time, 5 accumulations and a scan range from

200 to 3200 cm^{-1} . Electrolytes were prepared with 0.100 M LiClO_4 and concentrations of 0.000, 0.050, 0.500, 1.456 and 3.369 M $[\text{C}_{16}\text{mim}][\text{Br}]$ in DMSO. The reagent was dried with molecular sieves for 24 h before use and the solution preparation was performed inside an argon-filled glovebox with control of H_2O and O_2 contaminants.

2.2.3 Cyclic Voltammetry

Cyclic voltammetry was performed to determine the electrochemical stability of the electrolytes,¹⁰ which is a crucial information for a long-life cycling lithium battery. Using a three-electrode electrochemical setup with an Autolab potentiostat, a silver wire was applied as a quasi-reference electrode, platinum as a counter, and carbon glass as the working electrode. The experiment was carried out in an atmosphere of argon, with a scan rate of 50 mVs^{-1} and a voltage range from 2.00 up to 6.50 V *versus* Li/Li^+ . The DMSO solvent with 0.100 M LiClO_4 , as the supporting electrolyte, and ILC addition was used as electrolyte. The preparation of the solutions and the cell assembly were conducted using a glovebox with an argon atmosphere (MBRAUN-LABstar Workstation). The electrolyte solutions preparation and cell assembly were conducted using a glovebox with argon atmosphere (MBRAUN-LABstar Workstation). CV measurements at concentrations higher than 0.500 M ILC were not evaluated due to the high viscosity and high concentration of $[\text{Br}]^-$, leading to a huge $[\text{Br}_2]$ evolution.

2.3 Theoretical Calculations

2.3.1 Force Field Models

We performed classical MD simulations employing the GROMACS package, version 2020.5, and using a combination of OPLS-based force fields.²⁹ For the description of the $[\text{C}_{16}\text{mim}][\text{Br}]$ ILC and the DMSO molecules, we adopted the CL&P force field developed by Canongia Lopes and Pádua.³⁰ However, for the DMSO molecules, we employed the charges reported by Strader and Feller,³¹ while for the ClO_4^- ions we employed the parameters obtained by Acevedo et al.³² and the OPLS for the lithium-ion. Finally, we would like to highlight that all force fields are based on the OPLS force field and use the same potential form, combination, and exclusion rules, which ensure their compatibility.

The structure for DMSO molecule was obtained from the DLPGEN database, and the $[\text{C}_{16}\text{mim}]^+$ was built using the $[\text{C}_{18}\text{mim}]^+$ cation from the same database as starting point, and relaxed at HF/6-31G(d) level, as implemented in ORCA 4.0.1.³³ ClO_4^- was taken from the Acevedo github database.³⁴ All employed parameters are reported within the ESI† along with additional computational details.

2.3.2 Molecular Dynamics Simulations

As mentioned above, we employed electrolytes with $[\text{C}_{16}\text{mim}][\text{Br}]$ concentrations from 0.020 M up to 3.369 M for the experiments, however, it is a challenge to cover all those concentrations by

classical MD simulations as lower ILC concentrations can require more than 4000 DMSO molecules, *i.e.*, a huge computational cost. Thus, our MD simulations focused only on [C₁₆mim][Br] concentrations above 0.200 M. Table S9 in the ESI† shows the boxes compositions for all simulated systems. Furthermore, we are dealing with complex systems with different chemical species, and the [C₁₆mim]⁺ cations have a strong tendency to aggregate and form complex nanostructures,^{35,36} which could make the box equilibrium a difficult task. Then, to ensure the proper equilibrium of the MD boxes density, we adopted a multistep equilibrium approach based on annealing and compression/decompression steps.³⁷

Thus, the following sequential steps were employed for the classical MD simulations:

(1) All ions/molecules were packed randomly by the PACKMOL software³⁸ into boxes with initial volumes obtained from our experimental densities.

(2) The initial configurations were relaxed using the steepest descent algorithm followed by 500 ps of stochastic *NVT* simulations at 350 K.

(3) 10 ns of *NVT* simulations followed by 15 ns annealing *NPT* simulations in which the temperature was decreased/increased from 550 K to 400 K successive times at 1 bar.

(4) *NPT* simulations at 400 K and 1.5 bar for 20 ns.

(5) Then, the atomic charges of the ions were scaled by a factor of 0.8 to improve the dynamics of the systems, which is a usual protocol in IL simulations.³⁹

(6) Additional *NPT* simulations were carried out for 20 ns at 400 K and 1.0 bar, followed by 110 ns of *NVT* simulations at the same temperature that were used as production simulations, *e.g.*, in which all the properties were computed.

(7) To collect the systems densities in the temperature range from 383 K to 353 K we ran additional *NPT* simulations for 10 ns at each desired temperature.

We applied the smooth particle-mesh Ewald method⁴⁰ to handle coulombic interactions with a 1.6 nm cutoff, and the leap-frog algorithm to integrate motion equations with a 1.0 fs time step. Positions and energies were saved each 0.5 ps and 1.0 ps, respectively. The H-bonds were constrained by the LINCS algorithm⁴¹ as implemented in GROMACS package and defined in the CL&P force field. The Parrinello–Rahman barostat⁴² and the Nosé–Hoover thermostat⁴³ were used to control pressure and temperature with coupling times of 1.0 and 0.1 ps, respectively.

2.3.3 Density Functional Theory Calculations

To help in the assignment of the experimental Raman spectrum frequencies, we obtained the theoretical fundamental vibrational spectrum using DFT⁴⁴ calculations within the Perdew–Burke–Ernzerhof (PBE) formulation⁴⁵ for the exchange–correlation functional, as implemented in ORCA 4.0.1.³³ We employed the def2-TZVP basis set,⁴⁶ which yields accurate results for molecular systems.⁴⁷

For molecular systems, we randomly extracted an ionic/molecular cluster based on the Li^+ solvation shell from the MD trajectory using the TRAVIS package.⁴⁸ Then the Raman spectrum was obtained using two procedures, namely (i) directly from the frozen structure as obtained from the MD simulation and (ii) the equilibrium structure obtained by PBE optimization using the MD cluster as the starting configuration. A direct comparison of both schemes is reported within the ESI,[†] while the results obtained with the second approach will be discussed within the manuscript.

3 Results and Discussion

Experimental and theoretical frameworks were employed to obtain a deep macroscopic and atomistic understanding of the effects induced by the addition of $[\text{C}_{16}\text{mim}][\text{Br}]$ in the electrochemical, transport and structural properties of the aprotic electrolyte, DMSO/ LiClO_4 0.100 M. To reach our goals, our results will be presented and discussed step by step, where the most important findings will interconnect towards a single story summarized in the insights section.

3.1 Electrochemical Analysis

By performing cyclic voltammetry it is possible to understand the electrochemical behavior of an electrolyte in the battery operational voltage range. The electrochemical behavior provides information related to the redox properties of the electrolyte,^{49,50} which helps to distinguish the electrolyte applicability in different types of electrochemical devices. In the case of lithium-based batteries, a wide electrochemical stability means that the cell can operate for multiple cycles without significant changes in the potential profile, which prevents the electrolyte degradation and improves the battery cycle life, and is fundamental to produce commercial prototypes.²¹ Thus, we performed the cyclic voltammetry to characterize the electrolytes and investigate how the addition of the $[\text{C}_{16}\text{mim}][\text{Br}]$ ILC (0.000, 0.050, 0.500 M) affects the electrochemical stability of the DMSO/ LiClO_4 0.100 M system. The results are presented in Fig. 2. As stated in Section 2.2.3, we only evaluated the electrochemical stability for ILC concentrations lower than 0.500 M due to the high viscosity and the large evolution of Br_2 in those systems with higher concentrations.

We found that the $[\text{C}_{16}\text{mim}][\text{Br}]$ addition increases the electrolyte electrochemical stability in the range from 2.00 V to 6.50 V versus Li/Li^+ . When using only DMSO solvent with LiClO_4 0.100 M as the supporting electrolyte, we observe that the oxidation onset decreased 0.30 V after 10 cycles, indicating the degradation of DMSO. On the other hand, when using the ILC, even in the lower concentrations, 0.050 M and 0.025 M (ESI, Fig. S3[†]), the absence of the onset shift is noticed, pointing out the enhancement of the electrolyte stability due to the addition of the ILC.

The degradation of DMSO in potentials greater than 5.00 V is widely reported in the literature,^{19,51,52} which is attributed to the organic solvent molecules reaction with water traces present in the samples. Mozhzhukhina *et al.*⁵¹ indicated the beginning of DMSO degradation at 4.30 V over a

Pt electrode and the formation of dimethylsulfone. Using carbon glass as the working electrode, we verified the beginning of DMSO degradation at 4.50 V at the 10th cycle, in the absence of ILC. Therefore, we suggest that the addition of ILC reduces the DMSO availability to react with the water traces, which increases the electrolyte stability. DMSO strongly interacts with the [C₁₆mim]⁺ cation, specially by hydrogen bonds with the hydrogens in the imidazolium ring, thus decreasing the DMSO–water interactions.

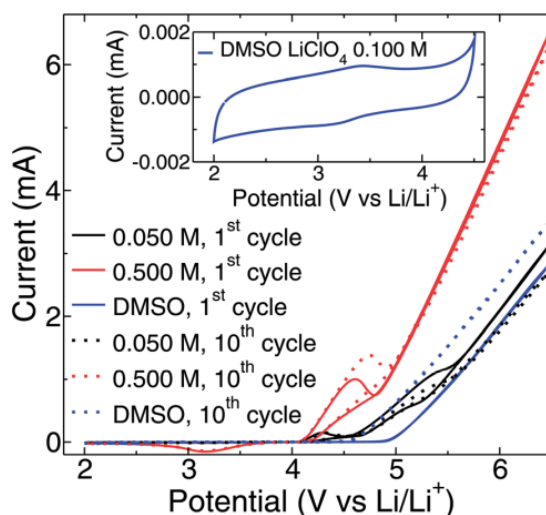
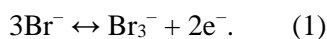
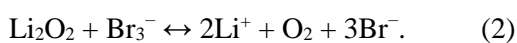


Fig. 2 Cyclic voltammetry on glass carbon working electrode performed at 50 mVs⁻¹ under argon atmosphere. The electrolyte was DMSO/LiClO₄ 0.100 M (blue line); adding 0.050 M [C₁₆mim][Br] (black line) and 0.500 M [C₁₆mim][Br] (red line). Inset: Cyclic voltammogram for DMSO/LiClO₄ 0.100 M recorded in the potential range of DMSO stability (2.00 V to 4.50 V vs. Li/Li⁺).

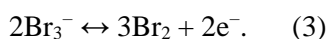
The [Br]⁻ anion of the studied ILC has redox properties, as pointed out in the redox peaks in Fig. 2. The [Br]⁻ anion oxidizes to Br₃⁻ at 4.00 V *versus* Li/Li⁺, as indicated by the equation below,



The Br₃⁻/Br⁻ reduction is verified at 3.70 V. These redox properties are very attractive for Li–O₂ cells applications because the Br₃⁻ formed electrochemically is reported as an efficient redox mediator,⁴⁹ which reacts chemically with the main discharge product, Li₂O₂, and releases Li⁺, O₂, and Br⁻ during the battery charge,¹⁶ as indicated by the equation below,



The chemical reaction with the mediator during the charge process of Li–O₂ cells favors the charge reaction, thus decreasing the overpotential and therefore improving the stability of the electrolyte and the cyclability of the battery.¹⁶ A second oxidation peak above 4.50 V is clearly observed in the diluted solution (0.050 M), which is assigned to the Br₃⁻ oxidation to Br₂ (eqn (3)),



The formation of the Br₂ product is also confirmed due to a color change in the solution, when using the concentration of 0.500 M (see the video in the ESI†). Comparable values of the redox potential are reported using InBr₃ as mediator, the [C₂mim][BF₄] ionic liquid and LiTFSI as a supporting electrolyte. Applying the MoS₂ nanoflakes catalyst on the working electrode, a slight shift to lower potential was observed, with peaks at 3.98 and 3.75 V due to the redox couple (Br⁻/Br₃⁻). However, the authors emphasized the challenge of detecting the redox peak (Br₃⁻/Br₂) due to the DMSO voltage window.⁵⁰ In the present paper, we observed that the decomposition of DMSO began near to 4.20 V, as can be visualized in the inset of Fig. 2.

The redox flow battery is another type of energy storage system that could be a promising application for this ternary system as a catholyte. IL and ILC combined with different solvents are capable of providing stable and long-life cycling efficiencies for flow batteries.⁵³ A high energy density could be achieved in this system due to the redox properties and the formation of Br₂.⁵⁴ Furthermore, the imidazolium group has been studied with different anions and alkyl chain sizes in redox flow batteries, however, a deep understanding is needed to guarantee the applicability of these materials.⁵⁵

3.2 Density

Fig. 3a shows the theoretical and experimental densities of the DMSO/LiClO₄ 0.100 M electrolyte as a function of temperature and ILC concentrations. As expected, for all systems, independent of the ILC concentration, the densities decrease linearly as the temperature increases, and the data can be fitted by a linear equation as follows,⁵⁶

$$\rho(T) = a + bT, \quad (4)$$

where a and b are the fitting parameters, while T is the temperature. The parameters obtained by the linear fitting of the experimental data are reported in Table S10 in the ESI.†

The neat [C₁₆mim][Br] is solid at temperatures lower than 333 K, so its simulation at high concentrations and low temperatures may be a challenge due to the limitations of the classical force field. Therefore, we performed several MD simulations for the systems in the ILC concentration range

from 0.200 up to 3.369 M at different temperatures to find the best temperature for our production simulations, *e.g.*, the temperature in the simulations in which all the properties are calculated.

For the systems with the lowest concentrations, 0.200 and 0.500 M of $[\text{C}_{16}\text{mim}][\text{Br}]$, it is possible to reach a proper equilibrium for the theoretical densities in the temperature range from 343 up to 400 K. However, when the ILC concentration increases, the electrolytes have a slow equilibrium rate, then it is not possible to reach a proper equilibrium for the density at temperatures lower than 363 K at the intermediate 1.456 M ILC concentration in the timescale used in our simulations. For the two highest ILC concentrations, 2.413 and 3.369 M, the equilibrium of the density is only reached at temperatures over 373 K. This effect is associated with the high viscosity of the $[\text{C}_{16}\text{mim}][\text{Br}]$ ILC and the well-known overestimation of the viscosity by the classical force fields, even with the 0.80 scaling charge approach.

Then, to ensure the equilibrium of the density and the convergence of the transport properties for all systems, we chose 400 K as our production temperature. We would like to highlight that high temperatures, ≥ 370 K, are usually employed in the MD simulations of ionic liquid based systems, to overcome the large viscosity of the ILs and improve the description of the dynamics of the ions in the simulations.^{25,26,32} With the use of high temperatures in the MD simulations is possible to speed up the diffusion of the ions and consequently achieve better convergence of the transport properties in smaller simulation times. Although 400 K is higher than the temperature used in the experimental measurements, it is still lower than the boiling point of DMSO, 462 K.¹⁴

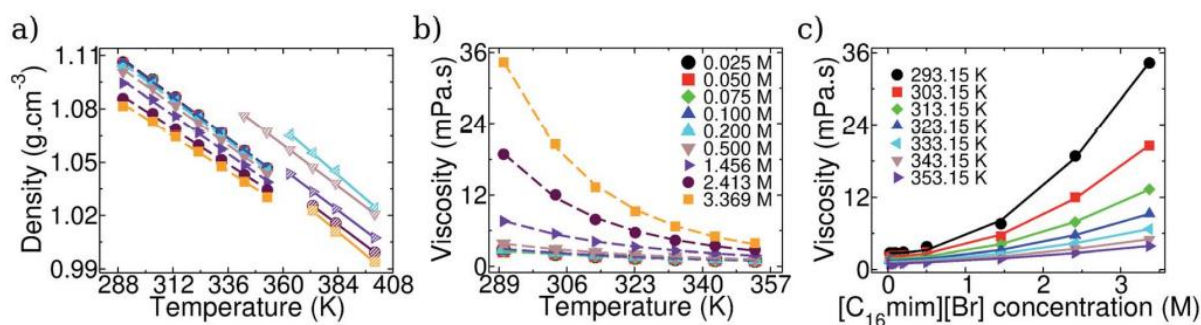


Fig. 3 (a) Densities and (b) viscosities for DMSO/LiClO₄ 0.100 M as function of temperature and (c) $[\text{C}_{16}\text{mim}][\text{Br}]$ concentration. The filled and hatched symbols are experimental and MD data, respectively. The dashed lines in the experimental densities and viscosities are the linear and the VTF fittings, while the straight lines are just guides to the eye.

The theoretical densities in Fig. 3a show deviations lower than 3.0% relative to the experimental values, that is, an acceptable rate for classical force fields.³² However, we highlight that the experimental data used for the force field validation was generated by the linear fitting showed above. Beyond the quantitative results, the theoretical densities also show a similar qualitative trend

compared to the experimental data, *e.g.*, the density decreasing upon the increase in temperature and addition of ILC.

3.3 Viscosity

As seen for the densities, the increase in temperature also leads to a decrease in experimental viscosity (η), Fig. 3b, which follows the typical electrolyte behavior,⁵⁶ *e.g.*, the convex curvature, and can be fitted using the Vogel–Tammann–Fulcher equation (VTF), as follows⁵⁷

$$\eta = \eta_0 \cdot \exp\left(\frac{k}{T-T_0}\right), \quad (5)$$

where η_0 , k and T_0 are fitting parameters and T is the temperature in kelvin. The VTF parameters are shown in ESI, Table S11.†

The addition of the ILC into the electrolyte leads to an increase in the viscosity, as seen for the lowest temperature, 293.15 K, in which the saturated 3.369 M system has a viscosity 10 times higher than the least concentrated one, 0.025 M. However, at the temperature of 353.15 K, we observe that the 3.369 M viscosity is only about 4 times higher than the 0.025 M. Therefore, the increase in the temperature, and consequently, the increase in the kinetic energy of the system, has a direct impact on the decrease in the electrolyte viscosity, which leads to a more “fluid” electrolyte at high temperatures.

The increase in the electrolyte viscosity upon ILC addition can be understood as a combination of different factors. First, the viscous nature of the ILC due to the strong electrostatic interactions among the ions,¹⁸ second, the tendency of the $[\text{C}_{16}\text{mim}]^+$ to form nanodomains in the liquid structure.⁵⁸ Since the positive charge in the $[\text{C}_{16}\text{mim}]^+$ cations is located in the aromatic ring, they tend to distribute themselves in a structure that resembles π – π interactions, with the cations forming a vertical stacking mediated by the anions, which leads to the formation of a polar nanodomain. On the other hand, when long alkyl chains are present in the imidazolium cations, like in $[\text{C}_{16}\text{mim}]^+$, the carbon and hydrogen atoms from the chains tend to establish strong intermolecular van der Waals interactions, resulting in the formation of nonpolar nanodomains in the liquid structure.⁵⁹

The formation of nanodomains directly affects the displacement of ions due to the increase in the interactions between the chemical species and due to the cage effects on the ions.⁶⁰ Beyond that, the large size of $[\text{C}_{16}\text{mim}]^+$ results in a large sterical hindrance, which leads to an increase in the diffusion activation energy and consequently to lower mobility and larger viscosity. Therefore, the increase in the viscosities seen in Fig. 3c can be understood as the joining of all these statements.

3.4 Ionic Conductivity

Fig. 4 shows the ionic conductivity obtained by both experimental and MD simulations together with the experimental viscosity of the DMSO/LiClO₄ 0.100 M electrolyte as a function of the [C₁₆mim][Br] concentration. The experimental measurements were conducted at 303 K, while the MD simulations were carried out at 400 K to improve the dynamics of the system and the convergence of transport properties, as stated above.^{25,32}

The ionic conductivities from the MD simulations were obtained using the Einstein-Helfand method, as follows,⁶¹

$$\sigma = \frac{1}{6Vk_B T} \lim_{t \rightarrow \infty} \frac{d}{dt} \langle \sum_i \sum_{j(j>i)} q_i q_j \Delta r_{ij}(t) \rangle, \quad \Delta r_{ij}(t) = [r_i(t) - r_i(0)] \cdot [r_j(t) - r_j(0)], \quad (6)$$

in which T is temperature, k_B the Boltzmann's constant, t is time and V the volume of the simulation box. q_i and q_j are the ionic charges and $\Delta r_{ij}(t)$ the collective mean square displacement, cMSD, for a given ij pair at time t . The ionic conductivities are obtained using a linear fitting in the linear part of the $\Delta r_{ij}(t)$, cMSD curve, which can be a "trick" task due to the accumulation of errors and the noisy behavior of the cMSD curve. Then, we computed the ionic conductivities as the average of four fittings in different time windows of $\Delta r_{ij}(t)$.

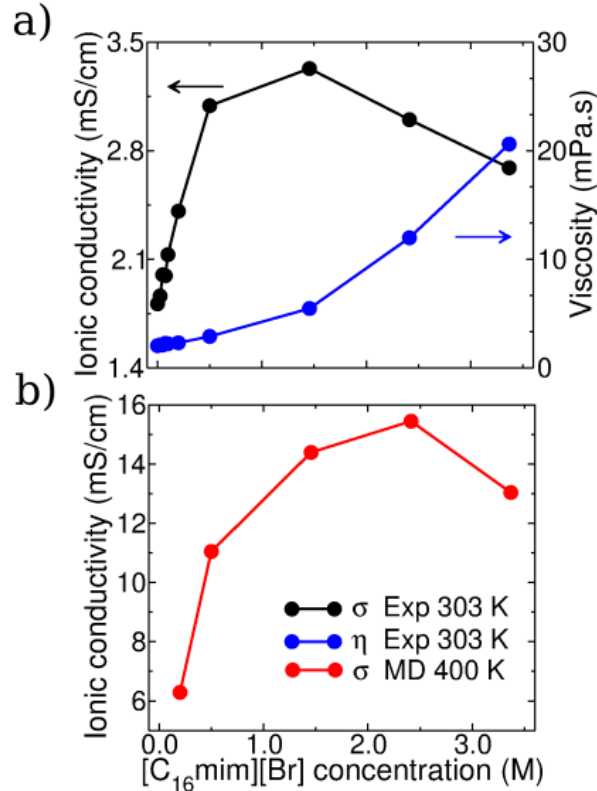


Fig. 4 Ionic conductivities and viscosities for the DMSO/LiClO₄ 0.100 M system as a function of the [C₁₆mim][Br] concentration. (a) Black and blue circles are, respectively, the experimental ionic conductivities and viscosity at 303 K. (b) The red circles are the MD ionic conductivity at 400 K.

As shown in Fig. 4a, the addition of the [C₁₆mim][Br] ILC to DMSO/LiClO₄ 0.100 M leads to a gradual increase in the experimental ionic conductivity until the 1.456 M concentration, in which we observe the highest ionic conductivity among the investigated systems in our work. However, after this point, the further addition of the ILC leads to a decrease in the ionic conductivity. Even so, the most concentrated systems, *e.g.*, 2.456 and 3.369 M, presented higher conductivities than the neat one (0.000 M), which shows that the addition of the [C₁₆mim][Br] to the DMSO/LiClO₄ electrolyte is beneficial to its conductivity.

We would like to highlight that although the 1.456 M concentration presented the highest ionic conductivity value in Fig. 4, we cannot ensure that this is the electrolyte composition that maximizes the ionic conductivity. To do this, a systematic investigation should be performed using the largest number of possible points between the 1.456 M and 2.456 M ILC concentrations. The same conclusion can be addressed to the point in which the ionic conductivity starts to decay. Hence, from Fig. 4a we can consider the region between 1.456 and 2.413 M ILC concentrations as the turning point for ionic conductivity.

Comparing the experimental ionic conductivity and viscosity trends in Fig. 4a, we see that the addition of the ILC leads to a constant rise in the viscosity which may be associated with the slowing down of the ionic transport. Therefore, the increase in the ionic conductivity until 1.456 M and its decay at higher concentrations, indicates that the viscosity only affects the ionic conductivity in the highest concentrations.

If we take into account the Nernst–Einstein equation, the conductivity of a system can be understood as the joining of the mobility and density of ions in the system. Thus, we can understand the ionic conductivity rise until 1.456 M, as the result of the increase in the number of charge carriers in the electrolyte. However, above the 1.456 M concentration, the strong interactions between the ions begin to hinder the ionic transport, leading to a small decrease in the ionic conductivity. Therefore, at high ILC concentrations, the low mobility of the ions, *i.e.*, high viscosity, plays a greater role in the electrolyte conductivity than the density/number of ions. However, we would like to highlight that the conductivity decreases only 10% from the 1.456 M to 2.413 M concentration, while the viscosity increases around 120% in the same range. Hence, the number of charge carriers is still important for ionic conductivity even at high concentrations, and this behavior needs further investigation.

Cummings and co-workers have conducted a series of studies focusing on the understanding of ionic liquid–solvent mixtures, using classical MD simulations and experimental measurements.^{39,62,63} They observed a similar behavior for the [C₄mim][Tf₂N] ionic conductivity with several organic solvents. The mixture presented optimal conductivity values in the IL mass fraction around 0.4–0.5, which they attributed to the mitigation of the ion pairing, *i.e.*, ionic dissociation due to the solvation of the ions by organic molecules. But, at high IL concentrations, the ions tend to interact strongly with their counterions, forming strong ion pairing, which leads to slow ionic transport and consequently, low ionic conductivity.³⁹ Then, to optimize the IL/organic solvent conductivity, it is necessary to find

the best ratio between charge carrier number and ionic transport in the system. For comparison, in our systems the optimal conductivity is reached at the ILC mass fraction of 0.265.

Although the ionic conductivities of the MD simulations, Fig. 4b, were conducted at higher temperatures than the experimental data, the qualitative trends are quite similar and the differences can be rationalized due to the effects of temperature. Unlike the experimental data, in the MD simulations the ionic conductivity reaches its maximum value at the 2.413 M concentration, which shows a shift of the optimum ILC concentration to higher values. Beyond that, the MD simulations show ionic conductivity values that are higher than those of the experimental data because of the high temperature used in the simulations.

As shown in Fig. 3b, at high temperatures the effect of ILC addition on the viscosity of the electrolyte is less pronounced, which can be attributed to the higher kinetic energy in the system, *e.g.*, faster ionic transport and lower ion pairing in the system. Then, we expect less influence of the viscosity on the ionic conductivity at higher temperatures, and consequently, a shift in the maximum ionic conductivity at higher ILC concentrations. However, the qualitative similarity between the MD and experimental data shows that the applied force field is able to reproduce the experimental behavior of the [C₁₆mim][Br] addition into the DMSO/LiClO₄ 0.100 M electrolyte. Therefore, we are able to use our MD simulations to understand the effects observed in the experimental measurements in Fig. 4.

3.5 Self-diffusion Coefficients

To improve our understanding of the transport of the ions and the DMSO molecules in the electrolytes, we computed the self-diffusion coefficients (D^*) for all species using the Einstein method and the MD data, *i.e.*,

$$D = \frac{1}{6} \lim_{t \rightarrow \infty} \frac{d}{dt} \langle \sum_{i=1}^N |r_i(t) - r_i(0)|^2 \rangle, \quad (7)$$

in which brackets are the ensemble average and r_i is the position vector for a The mean square displacements of ClO₄⁻, [C₁₆mim]⁺, and DMSO, were calculated using the Cl, CR (the carbon atom between nitrogens in the imidazolium ring), and S atoms as position vectors. The plots of the MSD curves and the time regions used for the D^* calculations are shown in the ESI, Section S3.5.†

Fig. 5 shows the self-diffusion coefficients for all species as function of the [C₁₆mim][Br] concentration at 400 K. Because of its molecular character, and consequently, weak electrostatic interactions, the DMSO molecule presents the highest self-diffusion coefficient in the system, followed by ClO₄⁻ > [Br]⁻ > Li⁺ > [C₁₆mim]⁺. For the ions, the diffusivity trend may be rationalized in terms of their size and charge density.

The larger size of the ClO_4^- anion compared to $[\text{Br}]^-$ leads to a lower charge density; therefore, we can expect weaker binding energies with the cations in the systems and consequently larger diffusivities than $[\text{Br}]^-$. On the other hand, the higher diffusivity of the bromide-ion compared to Li^+ may be explained in terms of the ion concentration in the mixture, which may result in a higher diffusion rate across different ionic environments. The long alkyl chains of the $[\text{C}_{16}\text{mim}]^+$ cation and its large sterical hindrance lead to the lowest transport among all ions in the electrolyte. Beyond that, strong van der Waals interactions between the alkyl chains also contribute to the low diffusivity of the cation.

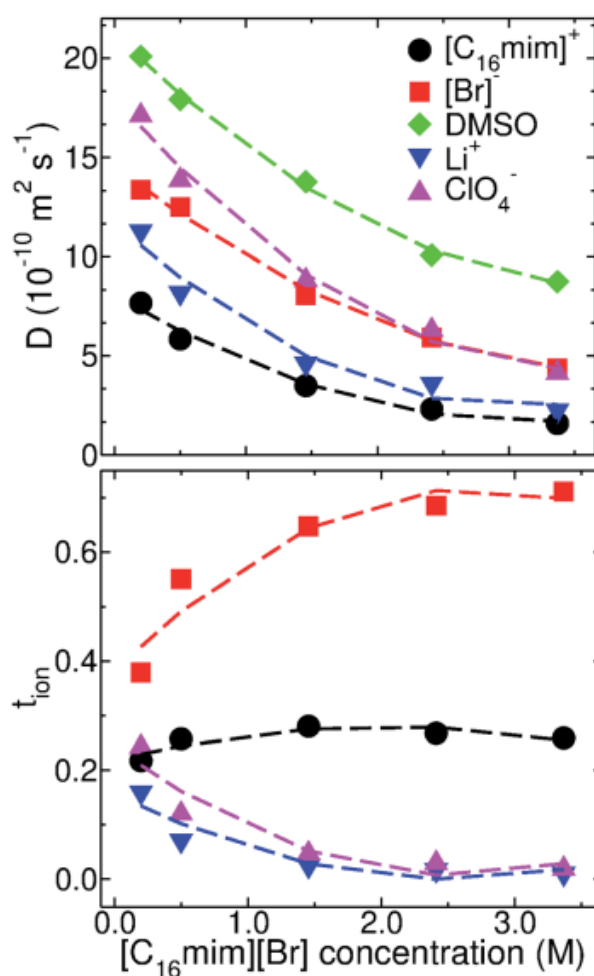


Fig. 5 Self-diffusion coefficients (D) and apparent transference numbers ($t_{\text{ion}}^{\text{app}}$) for all ions/molecules in the DMSO/ LiClO_4 0.100 M electrolyte as function of the $[\text{C}_{16}\text{mim}][\text{Br}]$ concentration at 400 K. The dashed lines are quadratic fittings.

The addition of the $[\text{C}_{16}\text{mim}][\text{Br}]$ ILC to the electrolyte leads to the decrease in the self-diffusion coefficients of all particles, which agrees with the expected trend from the viscosity, Fig. 3, and previous studies.³⁹ The decrease in the self-diffusion coefficients in Fig. 5 confirms that the increase in

the ionic conductivity for concentrations below 1.456 M is the result of the increase in the number/density of charge carriers in the systems.

3.6 Apparent Transference Number

To continue our characterization of the ionic transport in the electrolyte, we employed the Einstein approach, eqn (8), and the simulated self-diffusion coefficients to calculate the apparent transference numbers, $t_{\text{ion}}^{\text{app}}$, for all ions in the systems, using the equation below,

$$t_{\text{ion}}^{\text{app}} = \frac{D^{\text{ion}} N^{\text{ion}}}{\sum_{i=1}^5 D^{\text{ion}} N^{\text{ion}}}, \quad (8)$$

where D^{ion} and N^{ion} are the self-diffusion coefficients and the number of ions in the systems. Since $t_{\text{ion}}^{\text{app}}$ measures the contribution of each species to the ionic conductivity of the system, we do not consider the DMSO molecule due to its molecular character and negligible contribution to the ionic conductivity.

In the last years, there has been much debate about the approaches used to calculate the transference numbers in electrolytes, especially the disparities between them.^{64–66} For example, electrophoretic NMR measurements can deliver negative values for $t_{\text{Li}^+}^{\text{app}}$ in IL-based electrolytes, which is associated with the $\text{Li}_x[\text{anion}]_y^{x+y}$ coupled diffusion, *e.g.*, vehicular mechanism,^{64,67} while pulsed-field gradient NMR and the Bruce–Vincent methods, which do not take in account the ionic correlations, deliver positive values for Li^+ for similar systems.

Computationally, this comparison has been addressed by Molinari *et al.* using classical MD simulations,⁶⁵ in which they concluded that the addition of ionic correlations in the transference numbers calculations leads to negative values at low sodium-ion concentrations due to the strong $\text{Na}^+ - [\text{anion}]^-$ interactions. Hence, since we are using the Einstein approach, we discuss our data, Fig. 5, as individual contributions to the overall ionic diffusion in the systems, and we call our transference numbers as apparent transference numbers, $t_{\text{ion}}^{\text{app}}$.

Although the increase in the $[\text{C}_{16}\text{mim}][\text{Br}]$ concentrations leads to a slowdown of all ionic mobilities in the systems, for $t_{\text{ion}}^{\text{app}}$ the effect depends on the ion, Fig. 5. In the case of Li^+ and ClO_4^- , the $t_{\text{ion}}^{\text{app}}$ s drop when more ILC is added, which is related to the decrease in the D^{ion} s and also the reduction in the relative LiClO_4 concentrations. On the other hand, $t_{[\text{C}_{16}\text{mim}]^+}^{\text{app}}$ and $t_{[\text{Br}]^-}^{\text{app}}$ increase with the IL addition, which indicates that the $t_{\text{ion}}^{\text{app}}$ in those electrolytes is essentially dependent on the ion concentrations. Moreover, the high $t_{[\text{Br}]^-}^{\text{app}}$ and $D^{[\text{Br}]^-}$ values indicate a large $[\text{Br}]^-$ “availability” in the electrolyte, which may be correlated with the results shown for the cyclic voltammetry in Fig. 2, *e.g.*,

with more bromide-ion available in the electrolyte, more Br_3^- is formed and consequently improves the battery cyclability.

3.7 Radial Distribution Function

To analyze the Li^+ local environment, we computed the partial radial distribution functions for the $\text{Li}^+-\text{[Br]}^-$, $\text{Li}^+-\text{ClO}_4^-$ and Li^+-DMSO interactions as function of the ILC concentration, Fig. 6. The $\text{Li}^+-\text{[Br]}^-$ $g(r)$ presents only one intense and sharp peak at 0.25 nm, which indicates a strong interaction between the ions due to their large charge density. The $\text{Li}^+-\text{ClO}_4^-$ and Li^+-DMSO also present sharp peaks at 0.25 nm, but much less intense than $\text{Li}^+-\text{[Br]}^-$, indicating that the DMSO and ClO_4^- interactions with Li^+ are not as strong as $\text{Li}^+-\text{[Br]}^-$. Beyond that, $\text{Li}^+-\text{ClO}_4^-$ and Li^+-DMSO also have peaks at around 0.60 nm to 1.20 nm that are due to the secondary interactions between the lithium-ion and the species.

The increase in the ILC concentration decreases the peak intensity in the $\text{Li}^+ - \text{[Br]}^-$ $g(r)$ due to the increase in the number of bromide-ions in the electrolyte and in the lithium-ion solvation shell, which leads to multiple $\text{Li}^+-\text{[Br]}^-$ interactions. The peak at 0.25 nm in the $\text{Li}^+-\text{ClO}_4^-$ and Li^+-DMSO $g(r)$ also decreases when the ILC concentration increases, being almost negligible at concentrations higher than 1.456 M. At the same time, the secondary peaks at around 0.90 and 0.60 nm increase, which indicates that in ILC concentrations above 1.456 M, the Li^+ solvation shell is mainly occupied by bromide-ion interactions, while DMSO and ClO_4^- only establish secondary interactions with Li^+ .

Zhao and co-workers investigated the effect of the DMSO addition in different ionic liquids using MD simulations and DFT calculations,⁶⁸ in which they observed that the DMSO molecules are not able to break the cation-anion pair and can only establish secondary interactions with the ions, mainly by hydrogen-bonds with the cations. Similarly, the same effect can be seen in the Li^+-X $g(r)$ s in Fig. 6. Then, as in the work by Zhao *et al.*, in Fig. 6, the DMSO only acts as a cosolvent around the $\text{Li}^+-\text{[Br]}^-$ pairs.⁶⁸

The $[\text{Br}]^- - \text{DMSO}$, $\text{DMSO} - \text{ClO}_4^-$ and $\text{DMSO} - \text{DMSO}$ radial distribution functions have a similar behavior. The $g(r)$ s present the main peaks at 0.50 in the case of $[\text{Br}]^- - \text{DMSO}$ and 0.55 nm for $\text{DMSO} - \text{ClO}_4^-$ and $\text{DMSO} - \text{DMSO}$, while the secondary peaks are located at 0.92 ($[\text{Br}]^- - \text{DMSO}$), and 0.95 nm ($\text{DMSO} - \text{ClO}_4^-$ and $\text{DMSO} - \text{DMSO}$). The increase in the ILC content slightly affects the intensity of the peaks, which may suggest that the organic molecule always acts as a cosolvent of ionic aggregates independently of the ILC concentration, which is due to the molecular character of the DMSO molecule and its higher concentration in the systems.

As stated above, imidazolium cations with long alkyl chains, tend to form aggregates with polar and nonpolar nanodomains.⁶⁹ As shown by Shimizu and co-workers,⁶⁹ the CR atom in the imidazolium ring, *e.g.*, the carbon between the nitrogens, can be used as a reference to characterize the formation of the polar domains, while the last carbon atom in the alkyl chain, the CT atom, can be used to

characterize the nonpolar nanodomain in the aggregate. Then, to investigate and characterize this effect, we calculated $g(r)$ s for several $X\text{-CR}[\text{C}_{16}\text{mim}]^+$ and $X\text{-CT}[\text{C}_{16}\text{mim}]^+$ interactions, *i.e.* X denotes different atoms as $g(r)$ reference, Fig. 6.

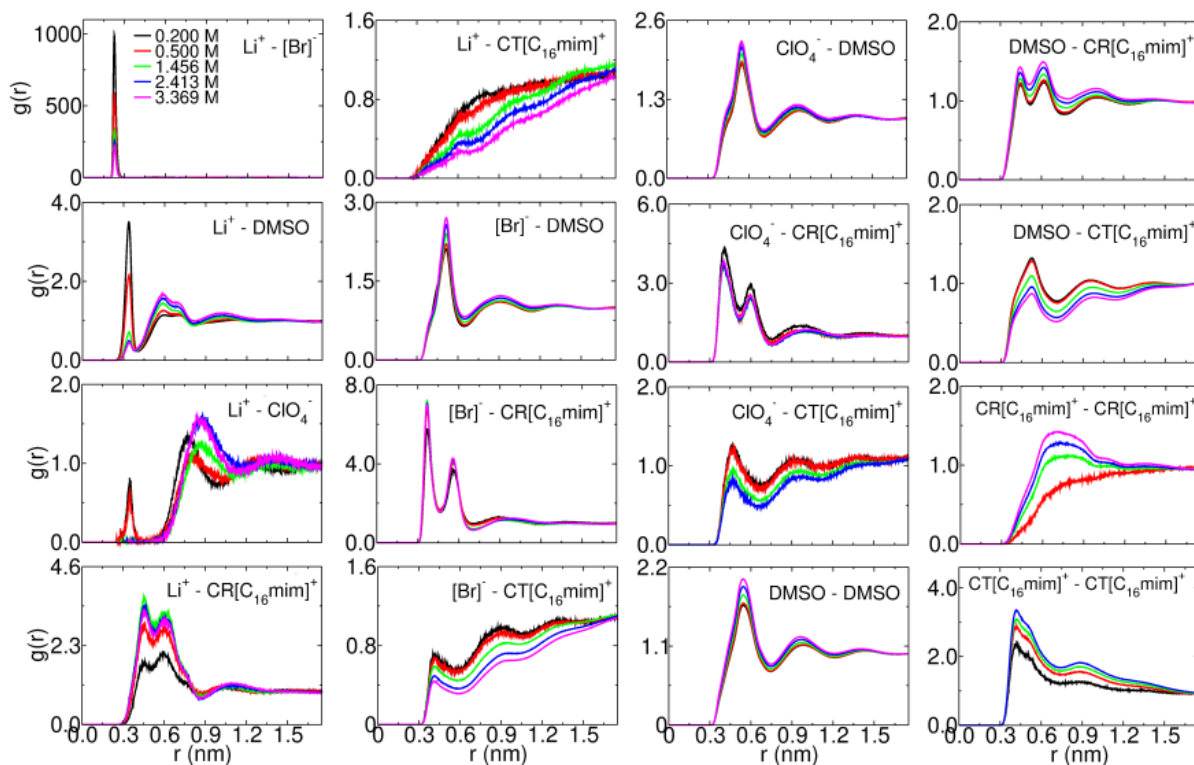


Fig. 6 Radial distribution functions ($g(r)$) for several atomic interactions as a function of the ionic liquid concentration. For the DMSO molecule and the ClO_4^- ion we used the center of mass for all the $g(r)$, while for the $[\text{C}_{16}\text{mim}]^+$ we used the CR atom, the geometric carbon in the imidazolium ring, and the CT atom, the last carbon atom in the alkyl chain, as references for the $g(r)$ calculations.

The $\text{CR}([\text{C}_{16}\text{mim}]^+)\text{-CR}([\text{C}_{16}\text{mim}]^+)$ and $\text{CT}([\text{C}_{16}\text{mim}]^+)\text{-CT}([\text{C}_{16}\text{mim}]^+)$ $g(r)$ s show that the addition of the ILC at concentrations higher than 1.456 M leads to the appearance of broad peaks at distances lower than 1.20 nm, which indicate the formation of polar and nonpolar nanodomains, and consequently, the aggregation of the $[\text{C}_{16}\text{mim}]^+$ cations in the systems. The $[\text{Br}]^-\text{-CR}([\text{C}_{16}\text{mim}]^+)$ and $\text{ClO}_4^-\text{-CR}([\text{C}_{16}\text{mim}]^+)$ $g(r)$ s show two peaks at distances lower than 0.60 nm, evidencing the strong and well-organized interaction between the ions and counterions, and consequently, the formation of polar domains in the aggregates with the anions interacting directly with the imidazolium ring. The presence of two well-defined peaks indicates that the cations and anions are well organized in layers along the liquid structure, evidencing the formation of a specific aggregate structure.

The high density of anions around the imidazolium rings also attracts the Li^+ to this region, as shown by the peaks at distances lower than 0.90 nm in the $\text{Li}^+\text{-CR}([\text{C}_{16}\text{mim}]^+)$ $g(r)$ s. At the same time, peaks with intensities lower than 1.00 at concentrations higher than 1.456 M in the $X\text{-CT}[\text{C}_{16}\text{mim}]^+$

$g(r)$ s indicate the low probability of those interactions in the systems, so we can assume that the nonpolar domains are mainly composed of the alkyl chains of the imidazolium cation.

The DMSO–[C₁₆mim]⁺ interactions show an interesting behavior with respect to the addition of ILC. At low [C₁₆mim][Br] concentrations, the DMSO–CT[C₁₆mim]⁺ $g(r)$ s present well-defined peaks at distances lower than 0.75 nm. However, when more ILC is added to the system, the main peak intensity decreases and reaches values lower than 1.00, indicating a lack of interactions at that distance. At the same time, the increase in the ILC concentration leads to the rise of the DMSO–CR [C₁₆mim]⁺ peaks at distances lower than 0.75 nm, indicating the enhancement of the interaction and the preferential distribution of DMSO molecules around the imidazolium rings. From these $g(r)$ s we can draw a simple picture: at low ILC concentrations the [C₁₆mim]⁺ cations are dispersed in the electrolyte, interacting with DMSO by the alkyl chain and the imidazolium ring. However, when the ILC concentration increases and the cations aggregate themselves, the DMSO molecules only occupy positions around the imidazolium ring, *e.g.* in the polar nanodomain, probably establishing hydrogen bonds with the acid hydrogens in the imidazolium ring.¹⁸

3.8 Combined Distribution Function

To characterize the aggregate structure, we calculated the combined distribution function (CDF) joining the CR([C₁₆mim]⁺) – CR([C₁₆mim]⁺) $g(r)$ and the angular distribution function for the angle between the normal vectors in the imidazolium ring plane, centered on the CR atoms, Fig. 7. We computed the CDFs using the TRAVIS⁴⁸ package and sampled the atomic positions every 5 ps in the MD trajectory. At 0.200 M concentration, the [C₁₆mim]⁺ cations do not show any specific organization in the electrolyte. Therefore, at low concentrations the [C₁₆mim]⁺ cations are dispersed in the liquid structure, without any aggregation or ordering among them in the system, as indicated in the $g(r)$ s in Fig. 6.

On the other hand, at the 3.369 M concentration, we can see a well-defined structure with two main populations at 300 pm and 0°/180°, and a secondary one at ≈700 pm and 90°. The populations at 0°/180° are due to the tendency of imidazolium cations to adopt a parallel orientation between the ring planes, resembling π – π stacking. This structure is quite similar to the one seen in ILCs,^{35,36} in which the [C_nmim]⁺ cations are distributed in the bulk structure in parallel stacking with all the imidazolium rings interacting with each other and mediated by the anions, forming the aforementioned polar nanodomains.

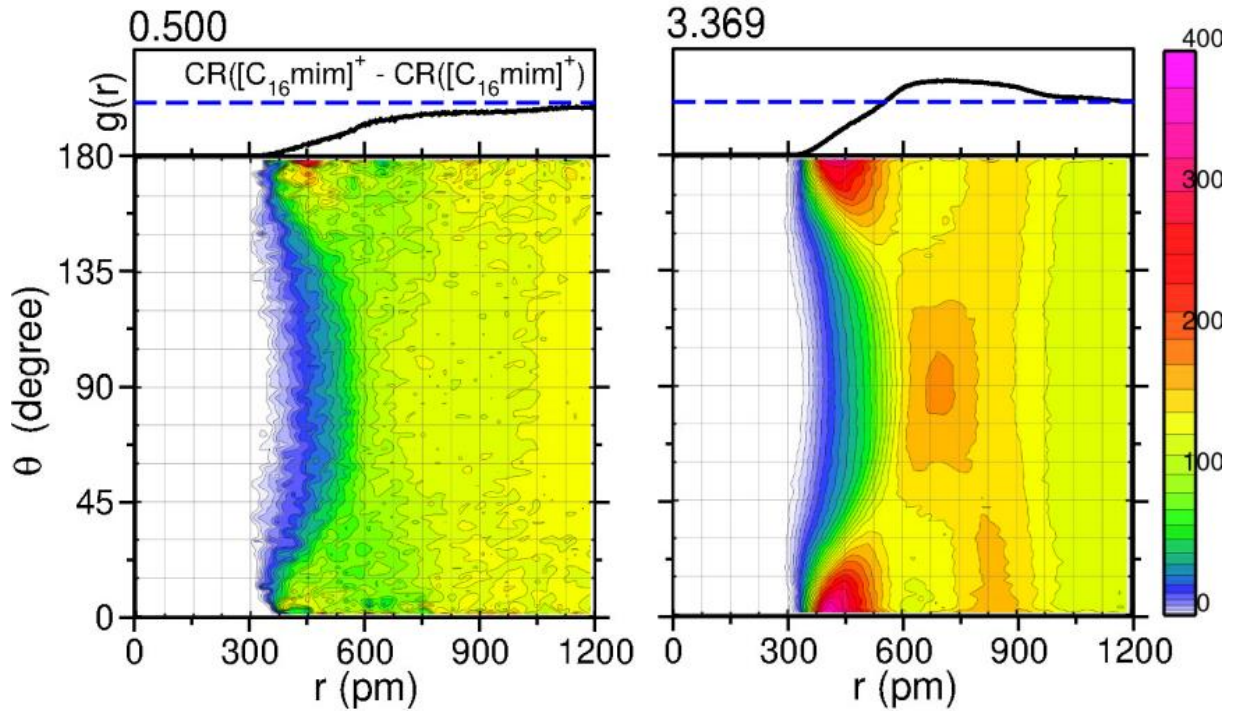


Figure 7: Combined distribution function (CDF) joining the $\text{CR}([\text{C}_{16}\text{mim}]^+) - \text{CR}([\text{C}_{16}\text{mim}]^+)$ $g(r)$ and the angular distribution function for the angle θ between the normal vectors in the imidazolium ring plane, in the 0.200 M and 3.369 M concentrations. The dashed blue lines in the $g(r)$ are the limit 1 in the $g(r)$ intensity.

The CDFs in Fig. 7 confirm the results from the $X - \text{CR}([\text{C}_{16}\text{mim}]^+) g(r)$, Fig. 6. The ILC addition leads to the aggregation of the ions in the systems (see Fig. S11† for the other ILC concentrations) and at high ILC concentrations, the ions are organized in nanostructures with polar and nonpolar nanodomains and beyond that, the organization of the imidazolium cations, *e.g.*, the planar stacking between the imidazolium rings, are similar to the structures seen in other ionic liquid crystals based on the imidazolium group.^{35,36}

3.9 Aggregates Size Analysis

To check the aggregates size and how they are distributed along the electrolyte structure, we computed the aggregate size distribution as a function of the ionic liquid crystal concentration. For this, we employed the AGGREGATES software⁷⁰ as follows:

$$P(n_a) = \frac{n \cdot \sum_{j=1}^C A_n(j)}{C \cdot I}, \quad (9)$$

where I and C are the total ions number in the system and the number of configurations in the trajectory, respectively. $A_n(j)$ gives the number of aggregates of size n for a configuration j . For the

aggregate cut-off, we used a 0.99 nm distance based on the first minimum in the $\text{CR}([\text{C}_{16}\text{mim}]^+) - \text{CR}([\text{C}_{16}\text{mim}]^+) g(r)$.

As expected, the $[\text{C}_{16}\text{mim}]^+$ aggregates size increases relative to the ILC concentration, Fig. 8, which is due to the rise in the number of ions in the system and the increase in the electrostatic interactions among them. At the same time, the probability to find large aggregates in the electrolyte also increases while the probability of small aggregates decreases. This reflects the tendency of the ILC to aggregate itself into organized structures, as indicated in Fig. 7.

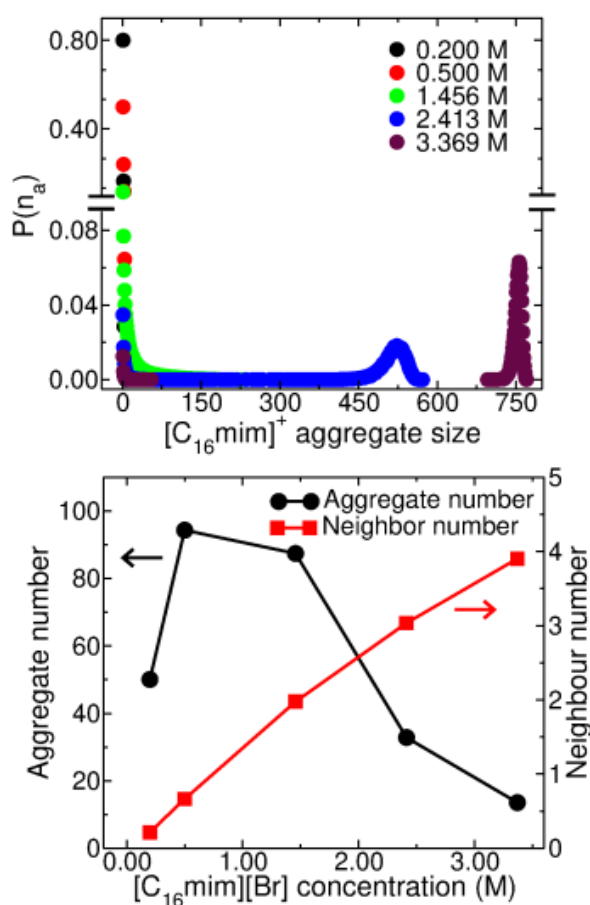


Fig. 8 Top panel: theoretical probability of distribution of $[\text{C}_{16}\text{mim}]^+$ aggregates size as function of the ILC concentration. Bottom panel: theoretical average number of aggregates (left axis) and average number of neighbors as a function of the ILC concentration. The aggregates were computed using a cutoff distance of 0.99 nm for the $([\text{C}_{16}\text{mim}]^+) - \text{CR}([\text{C}_{16}\text{mim}]^+)$ interaction.

For the 1.456 M concentration, we see a large probability for aggregates with sizes lower than 200 ions, which indicates that in this concentration the cations are more distributed as ionic pairs and small ionic clusters. However, when concentration increases, the systems show a higher probability for large aggregates, where for 3.369 M the aggregates with a size greater than 700 ions are more frequent than the lower ones. Hence, in this concentration we can expect that almost all $[\text{C}_{16}\text{mim}]^+$ are part of an

aggregate. We highlight that the increase in the probability of large aggregates occurs in the 2.413 M concentration, that is the same concentration in which the ionic conductivity starts to decay in the MD simulations, Fig. 4b.

Looking at the average number of aggregates in the systems in Fig. 8, we see that the number of aggregates decreases with ILC addition while the neighbor number increases, which reflect the increase in the probability to find larger aggregates, *i.e.*, the larger the aggregates, the lower their numbers in the system. Hence, our aggregates analysis confirms that the increase in the ILC concentration leads to the increase in the size of the aggregates and consequently the decrease in the number of aggregates in the electrolyte structure.

3.10 Structure Functions, $S(q)$

To obtain further insight into the nanostructure of the electrolytes and how [C₁₆mim][Br] affects it, we calculated the theoretical static structure factors ($S(q)$) using the TRAVIS package⁴⁸ as defined below,

$$S(q) = \frac{\sum_{i=1}^N \sum_{j=1}^N x_i x_j f_i(q) f_j(q) H_{ij}(q)}{(\sum_{i=1}^N x_i f_i(q))^2}, \quad H_{ij}(q) = 4\pi\rho_0 \int_0^{r_{max}} r^2 (g_{ij}(r) - 1) \frac{\sin qr}{qr} dr, \quad (10)$$

in which q and r are, respectively, the wave vector modulus and the distance, while i and j are different atomic species and N the total number of atoms in the simulation. x_i , x_j , $f_i(q)$ and $f_j(q)$, are the molar fractions and the scattering factors of the atoms i and j , respectively, and $g_{ij}(r)$ is the radial distribution function between them. r_{max} and ρ are the maximum distance used in the $g(r)$ and the number density of atoms in the box. In our calculations, we sampled the MD trajectory every 50 ps and did not use any atomic scattering factors.

Fig. 9 shows the theoretical structure factors for different concentrations of ILC. For concentrations lower than 0.500 M, the $S(q)$ s present a well-defined peak at $q \approx 13.0 \text{ nm}^{-1}$ and a small "peak shoulder" at $q \approx 22.0 \text{ nm}^{-1}$. However, when more ILC is added to the system, this "peak shoulder" shifts to higher q values $\approx 30.0 \text{ nm}^{-1}$ and a pre-peak raises at $q \approx 2.0 \text{ nm}^{-1}$. The shift of the peak at $q \approx 22.0 \text{ nm}^{-1}$ may be understood as changes in the local structure of the ions/molecules, *i.e.*, larger q values imply short distances in the real space, while the appearance of a pre-peak at lower values of q confirms the formation of nanodomains in the electrolyte.

The Canongia Lopes group has conducted a series of studies focusing on understanding the aggregation of imidazolium-based ILs and their nanostructures,^{37,69,71} in which they observed that the elongation of the alkyl chains in the imidazolium cations up to six carbons leads to the formation of a pre-peak at around $q \approx 2.0 \text{ nm}^{-1}$, which is related to the ion-ion interactions mediated by the alkyl chains, *e.g.*, the nonpolar nanodomains.

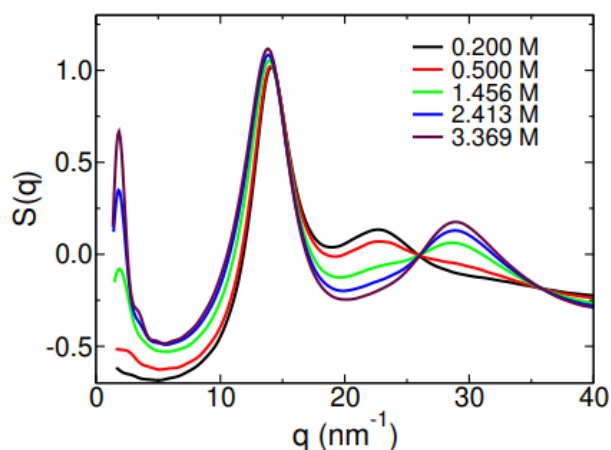


Figure 9: Theoretical structure function $S(q)$ for the DMSO/LiClO₄ 0.1 M electrolyte as function of the ILC concentration.

The presence of pre-peaks at concentrations higher than 1.456 M in Fig. 9 confirms the formation of the nonpolar nanodomains in the electrolyte. At the same time, the increase in the pre-peak intensity indicates the increase in the size of the non-polar nanodomain, which is in agreement with the increase in the size distribution of the aggregates shown in Fig. 8. We would like to highlight that the lack of resolution in the pre-peaks is due to the “small” size of the boxes used in our MD simulations. As shown by the Canongia Lopes group, boxes with 1600 IL pairs are required to obtain better resolution of this region.³⁷

In general, peaks at q values between 9 and 20 nm⁻¹ are related to the ionic interactions in the IL systems. So we can attribute the peak at $q \approx 15.0$ nm⁻¹ to direct interactions between cation–anion pairs, which do not change significantly with increasing ILC concentration, as indicated by Fig. 6. The peak at larger q values is associated with ionic interactions within the polar nanodomains.⁶⁹ However, unlike the Canongia Lopes group, in our $S(q)$ calculations, these peaks have significantly longer q values, which may be due to DMSO interactions within this region, as indicated by the DMSO–CR([C₁₆mim]⁺ g(r)s. Beyond that, the spacing layers between the aggregates are also defined by the third peak, which refers to the [C₁₆mim]⁺–[C₁₆mim]⁺ interaction, *i.e.*, the polar nanodomain. So the shift to q -values higher than 30 nm⁻¹ is associated with a crystalline stable structure behavior,⁷² which agrees with the high viscosity at higher concentrations and the structure characterization shown above.

3.11 Raman Spectroscopy

To obtain a deep atomistic understanding of the electrolyte structure, we performed experimental and theoretical Raman spectra analysis, as stated below. For the theoretical Raman of the DFT calculations, we used a molecular/ionic cluster extracted from the MD trajectory focusing on the Li⁺ chemical environment, as shown in Fig. 10. The orca_mapspc tool was used to obtain Raman spectra plots with a line width of 20; a comparison of different Gaussian line widths is shown in the ESI,

Section S3.7.† We used the theoretical Raman as a support and complement to identify the frequencies and contributions in each band in the experimental Raman spectra.

The enhancement of the ILC concentration results in different behaviors in the experimental Raman spectra, Fig. 10. The spectra of the neat electrolyte (0.000 M $[\text{C}_{16}\text{mim}][\text{Br}]$) shows bands related to strong dipole–dipole interactions, which are characteristic of pure DMSO,⁷³ even with LiClO_4 salt. The addition of $[\text{C}_{16}\text{mim}][\text{Br}]$ to the electrolyte enhances the intramolecular interaction strength. Small shifts to high wave-numbers (blue shift) were observed in the region of C–S stretching, bands located from 650 cm^{-1} to 720 cm^{-1} , as well as in the C–S–C and C–S=O bending regions, located from 280 up to 400 cm^{-1} .⁷⁴ These shifts confirm that the increase in ILC concentrations leads to the formation of a more cohesive system with strong molecular associations in agreement with what has been proposed above. The blue shift also indicates a stronger interaction in the solvation of Li^+ with the bromide anion.¹⁰

The bands located in the region of $\approx 670\text{ cm}^{-1}$ are related to the symmetric C–S stretching, while the $\approx 700\text{ cm}^{-1}$ regions are the antisymmetric,⁷⁵ as confirmed by the theoretical Raman, but in this case ≈ 628 and $\approx 654\text{ cm}^{-1}$, respectively. The peaks located in the theoretical Raman in the range from 260 up to 300 cm^{-1} and 317 cm^{-1} to 380 cm^{-1} are attributed to the C–S–C and C–S=O bending, respectively.

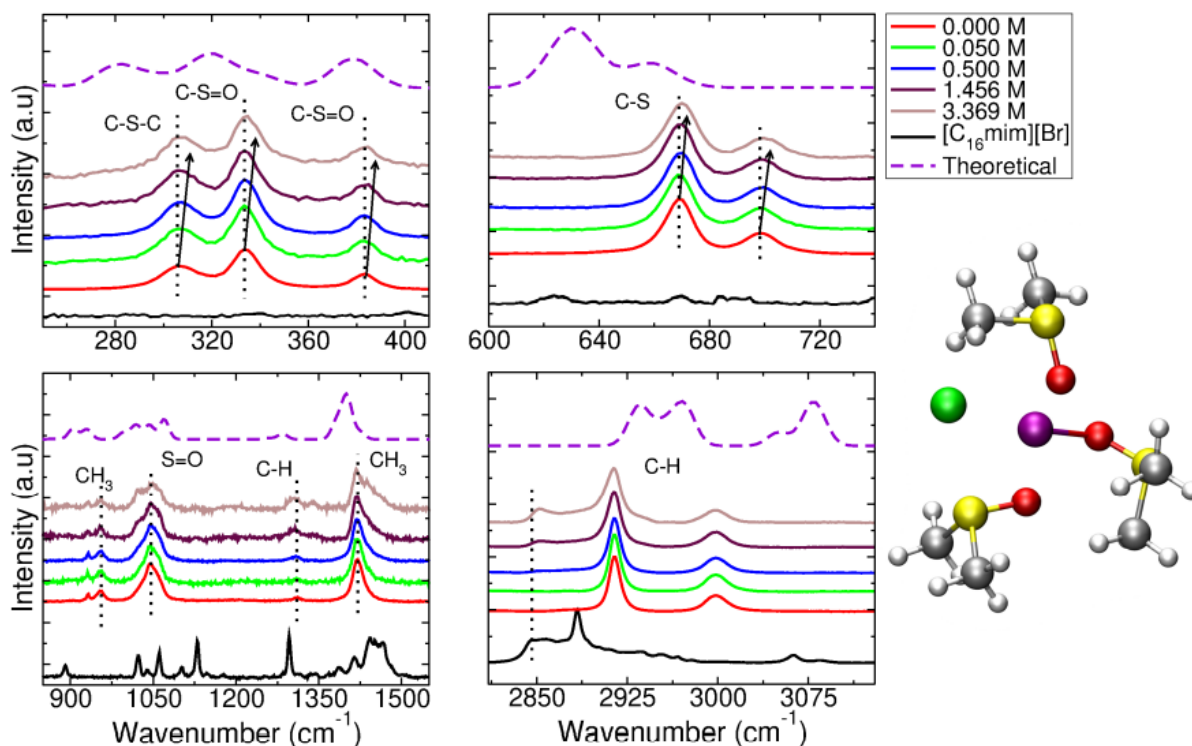


Fig. 10 Experimental and theoretical Raman spectra for the DMSO/ LiClO_4 0.100 M. Red, yellow, gray, white, purple, and green spheres indicate oxygen, sulfur, carbon, hydrogen, lithium-ion, and bromide atoms, respectively.

The bands located in the frequency range between 1020 and 1060 cm^{-1} for the experimental Raman spectra and between 994 and 1069 cm^{-1} for the theoretical one, are assigned to the S=O stretching and also the S–C–H bending.⁷⁴ Due to the high donor number (DN) of the DMSO molecule, it can form strong interactions with the $[\text{C}_{16}\text{mim}]^+$ cation, specially hydrogen bonds with the acid hydrogens in the imidazolium ring (S=O \cdots H–C), as previously reported by Takamuku *et al.*¹⁸ Hence, the small shoulder peak that arrives in the 1050 cm^{-1} region upon the $[\text{C}_{16}\text{mim}][\text{Br}]$ addition can be understood as changes in the DMSO solvation. In this region, the theoretical Raman presents three small peaks, which are due to the contribution of each individual DMSO molecule in the cluster used in the DFT calculation. Therefore, if a higher Gaussian width was used, those peaks would group themselves in only one peak, increasing the similarity with the experimental data. However, we opted to keep the Gaussian width as 30 cm^{-1} to keep the agreement in the range from 260 up to 390 cm^{-1} . See Fig. S13 in the ESI† for the Gaussian width test.

As stated above, the ILC tends to form aggregates which grow with increasing concentration and organize themselves into complex structures. This statement is shown by the disturbance in the DMSO solvation environment, as observed by the shifts of the S=O region, *e.g.*, from 1020 up to 1060 cm^{-1} . However, this can also be seen by the increase in the peak at 1130 cm^{-1} and the peak appearance at ≈ 2850 cm^{-1} when the ILC concentration is above 0.500 M. The increase at 1130 cm^{-1} is due to the coupling of the same peaks from the neat ILC and the DMSO electrolyte which are due to the H–C–H bending mode. On the other hand, the appearance of the peak in the 2850 cm^{-1} region is directly related to the greater amount of $[\text{C}_{16}\text{mim}^+]$ cations present in concentrated electrolytes, as can be compared to the black line of the pure $[\text{C}_{16}\text{mim}][\text{Br}]$ experimental Raman spectra.

The $[\text{C}_{16}\text{mim}][\text{Br}]$ addition also influences the symmetric C–H stretching as indicated by the small shift to lower wave number (red shift) and an enlargement in the band located at ≈ 2914 cm^{-1} . This phenomenon may occur due to van der Waals interactions between methyl groups of both, $[\text{C}_{16}\text{mim}][\text{Br}]$ and DMSO, or due to contributions to the band located at 2925 cm^{-1} from the neat $[\text{C}_{16}\text{mim}][\text{Br}]$. However, no change is observed in the asymmetrical C–H stretching at ≈ 2998 cm^{-1} . In the theoretical Raman, the symmetric C–H stretching region presents two bands at 2930 and 2963 cm^{-1} that are also due to the contribution of individual DMSO molecules, and hence could be grouped in the same band if a larger Gaussian width was used.

Additionally, the addition of ILC does not change the interaction of the bromide anion with DMSO, which is consistent with the discussion of the radial distribution functions shown in Fig. 6. The band located at ≈ 2998 cm^{-1} , related to the antisymmetric C–H vibrating mode, remains with the same intensity, and without shift. This behavior means that the bromide-rich environment in concentrated systems enhances the solvation of Li^+ due to an improvement in DN. These bands are not altered, because the amount of Li^+ species does not change (LiClO_4 concentration is fixed at 0.100 M), so the number of LiBr species formed in the electrolyte remains constant with ILC addition.⁷⁶

4 Insights into the ILC effect on the aprotic solvent properties

The effect of the ILC $[\text{C}_{16}\text{mim}][\text{Br}]$ addition on the ionic conductivity and viscosity is directly related to the aggregation of ions and the density of charge carriers in the system. The addition of the ILC to the electrolyte leads to an increase in the number of charge carriers and, consequently, to an increase in the ionic conductivity. At the same time, the increase in the number of charge carriers results in strong Coulomb interactions between them, and consequently the slowing down of the ions mobility and the viscosity increase. However, the limited ionic displacement only affects the ionic conductivity in concentrations higher than 1.456 and 2.413 M in the experimental and MD data, respectively.

As shown by our theoretical structural analysis, above the 1.456 M concentration, the $[\text{C}_{16}\text{mim}]^+$ cations tend to organize themselves in a well-defined structure with cation orientations that resemble the imidazolium ionic liquid crystals with polar and nonpolar nanodomains, as shown by the prepeak appearance in $S(q)$ s for concentrations higher than 1.456 M, Fig. 9. Beyond that, $[\text{Br}]^-$, ClO_4^- , and Li^+ also aggregate around the imidazolium ring; hence, the increase in the ILC concentration leads to the formation of ionic-rich environments in the electrolyte structure that hinders ionic transport.

Furthermore, the addition of the $[\text{C}_{16}\text{mim}][\text{Br}]$ ILC provides an increase in the stability of the electrolyte, as indicated by cyclic voltammetry, which can be related to the aggregation of ions and the DMSO- $[\text{C}_{16}\text{mim}]^+$ interactions. As shown by the DMSO-CR($[\text{C}_{16}\text{mim}]^+$) radial distribution functions and confirmed by the Raman spectra, Fig. 6 and 10, the DMSO molecules interact with the $[\text{C}_{16}\text{mim}]^+$ cations, which can decrease the interactions between DMSO and the water traces present in the experimental samples, avoiding degradation of DMSO and increasing the stability of the electrolyte. Just to highlight, the MD simulations do not have water, so, we cannot discuss this effect in the simulations. Furthermore, the ability of self-aggregation when increasing the ILC concentration does not affect the redox properties of bromide anion. The radial distribution functions explain this behavior, indicating the Li^+/Br^- interaction is not modified by the variation in the ILC concentration.

This study allows us to understand the ILC behavior when associated with an aprotic solvent medium. Considering that the DMSO solvent effect could be extended to other aprotic systems, this paper provides a new perspective of ILC usages and this behavior could also be achieved using aqueous electrolytes. It is interesting to notice that although the constant increase in the ILC concentration significantly increases the aggregates sizes and the viscosity, the ionic conductivities are not too much affected. Therefore, the nanostructure of the electrolyte may influence ionic transport. Further investigation and characterization of this phenomenon is then required to better understand the aggregation and structural behavior of ILCs in aprotic electrolytes.

5 Conclusion

In summary, imidazolium-based ionic liquid crystal [C₁₆mim][Br] was, for the first time, introduced as an additive in the aprotic DMSO/LiClO₄ 0.100 M electrolyte. We studied the physical, electrochemical, and structural properties of this ternary mixture using experimental and simulation approaches. With the addition of the ILC, the system becomes more cohesive, as indicated by the increase in the viscosity. At the same time, the increase in the number of charge carriers in the electrolyte also leads to ionic conductivity improvement until 1.456 M is reached.

After the 1.456 M concentration, the [C₁₆mim]⁺ cations tend to form aggregates in the system with a structure similar to an ionic liquid crystal that hinders ionic transport in the system and consequently decreases the overall ionic conductivity. Beyond that, the addition of ILC improved the stability of the electrolyte, in which it was possible to achieve 10 voltammetric cycles using the electrochemical window of 2.00 V to 6.50 V versus Li/Li⁺.

These features offer a new path of possibility for aprotic electrolytes and can also be explored in aqueous solvent. The combination between ionic liquid crystals and solvents is an interesting way to tune the electrolyte properties. In this context, our work suggests a new study direction for liquid electrolytes, which is a key step toward the improvement of different types of Li–metal batteries and the development of energy storage devices composed of organic solvents. Furthermore, recent studies have shown that IL-based electrolytes can form stable and robust solid electrolyte interphase (SEI) with lithium–metal anodes and consequently improve battery operation and performance.^{77–79} Hence, we are conducting a secondary study to investigate and characterize the effect of the [C₁₆mim][Br] addition in a lithium–metal battery device.

Author contributions

Tuanan C. Lourenço – DFT and MD simulations methodology, DFT and MD simulations formal analysis, investigation, DFT and MD simulations data curation, writing – original draft, visualization. Letícia M. S. Barros – experimental methodology, formal analysis of experimental data, investigation, experimental data curation, writing – original draft, visualization. Chayene G. Anchieta – conceptualization, experimental methodology, experimental data curation, formal analysis of experimental data, investigation, writing – original draft, visualization. Thayane C. M. Nepel – experimental methodology, formal analysis of experimental data, investigation, writing – original draft, visualization. Julia P. O. Júlio – formal analysis of experimental data, investigation. Luis Gustavo Dias – writing – review & editing. Rubens Maciel Filho – resources, funding acquisition. Gustavo Doubek – conceptualization, experimental methodology, resources, experimental data curation, writing – review & editing, visualization, supervision, funding acquisition. Juarez L. F. Da Silva – conceptualization, methodology for DFT and MD simulations, resources, data curation for DFT and MD simulations, writing – review & editing, visualization, supervision, project administration, funding acquisition.

Conflicts of interest

There are no conflicts of interest to declare.

Acknowledgement The authors gratefully acknowledge support from FAPESP (São Paulo Research Foundation, Grant Numbers 2017/11631-2, 2017/11958-1, 2018/21401-7 and 2019/23681-0), Shell and the strategic importance of the support given by ANP (Brazil's National Oil, Natural Gas and Biofuels Agency) through the R&D levy regulation and also to the University of São Paulo for providing the computational resources for the project execution. The authors acknowledge also the Laboratory of Advanced Scientific Computing (University of São Paulo) and the Department of Information Technology – Campus São Carlos, for hosting our cluster. The authors acknowledge also the National Laboratory for Scientific Computing (LNCC/MCTI, Brazil) for providing HPC resources of the SDumont supercomputer, which have contributed to the research results reported within this paper. URL: <https://sdumont.lncc.br>.

References

- 1 S. Wang, Q. Zeng, A. Wang, X. Liu, J. Chen, Z. Wang and L. Zhang, Constructing stable ordered ion channels for a solid electrolyte membrane with high ionic conductivity by combining the advantages of liquid crystal and ionic liquid, *J. Mater. Chem. A*, 2019, **7**, 1069–1075, DOI: [10.1039/c8ta09489f](https://doi.org/10.1039/c8ta09489f).
- 2 P. G. Bruce, S. A. Freunberger, L. J. Hardwick and J.-M. Tarascon, Li–O₂ and Li–S batteries with high energy storage, *Nat. Mater.*, 2012, **11**, 19–29, DOI: [10.1038/nmat3191](https://doi.org/10.1038/nmat3191).
- 3 I. Landa-Medrano, I. Lozano, N. Ortiz-Vitoriano, I. R. de Larramendi and T. Rojo, Redox mediators: a shuttle to efficacy in metal Li–O₂ batteries, *J. Mater. Chem. A*, 2019, **7**, 8746–8764, DOI: [10.1039/c8ta12487f](https://doi.org/10.1039/c8ta12487f).
- 4 P. Tan, H. Jiang, X. Zhu, L. An, C. Jung, M. Wu, L. Shi, W. Shyy and T. Zhao, Advances and challenges in lithium-air batteries, *Appl. Energy*, 2017, **204**, 780–806, DOI: [10.1016/j.apenergy.2017.07.054](https://doi.org/10.1016/j.apenergy.2017.07.054).
- 5 M. Christy, A. Arul, A. Zahoor, K. U. Moon, M. Y. Oh, A. M. Stephan and K. S. Nahm, Role of solvents on the oxygen reduction and evolution of rechargeable Li–O₂ battery, *J. Power Sources*, 2017, **342**, 825–835, DOI: [10.1016/j.jpowsour.2016.12.119](https://doi.org/10.1016/j.jpowsour.2016.12.119).
- 6 E. Jónsson, Ionic liquids as electrolytes for energy storage applications – A modelling perspective, *Energy Storage Mater.*, 2020, **25**, 827–835, DOI: [10.1016/j.ensm.2019.08.030](https://doi.org/10.1016/j.ensm.2019.08.030).
- 7 M. Watanabe, M. L. Thomas, S. Zhang, K. Ueno, T. Yasuda and K. Dokko, Application of Ionic Liquids to Energy Storage and Conversion Materials and Devices, *Chem. Rev.*, 2017, **117**, 7190–7239, DOI: [10.1021/acs.chemrev.6b00504](https://doi.org/10.1021/acs.chemrev.6b00504).

- 8 G. Yang, Y. Song, Q. Wang, L. Zhang and L. Deng, Review of ionic liquids containing, polymer/inorganic hybrid electrolytes for lithium metal batteries, *Mater. Des.*, 2020, **190**, 108563, DOI: [10.1016/j.matdes.2020.108563](https://doi.org/10.1016/j.matdes.2020.108563).
- 9 J. Lai, Y. Xing, N. Chen, L. Li, F. Wu and R. Chen, Electrolytes for Rechargeable Lithium–Air Batteries, *Angew. Chem., Int. Ed.*, 2020, **59**, 2974–2997, DOI: [10.1002/anie.201903459](https://doi.org/10.1002/anie.201903459).
- 10 U. Pal, F. Chen, D. Gyabang, T. Pathirana, B. Roy, R. Kerr, D. R. MacFarlane, M. Armand, P. C. Howlett and M. Forsyth, Enhanced ion transport in an ether aided super concentrated ionic liquid electrolyte for long-life practical lithium metal battery applications, *J. Mater. Chem. A*, 2020, **8**, 18826–18839, DOI: [10.1039/d0ta06344d](https://doi.org/10.1039/d0ta06344d).
- 11 N. Yamanaka, R. Kawano, W. Kubo, T. Kitamura, Y. Wada, M. Watanabe and S. Yanagida, Ionic liquid crystal as a hole transport layer of dye-sensitized solar cells, *Chem. Commun.*, 2005, 740–742, DOI: [10.1039/b417610c](https://doi.org/10.1039/b417610c).
- 12 S. J. Devaki and R. Sasi, Ionic Liquids/Ionic Liquid Crystals for Safe and Sustainable Energy Storage Systems, in Progress and Developments in Ionic Liquids, *InTech*, 2017, pp. 313–336, DOI: [10.5772/65888](https://doi.org/10.5772/65888).
- 13 A. Celeste, L. Silvestri, M. Agostini, M. Sadd, S. Palumbo, J. K. Panda, A. Matic, V. Pellegrini and S. Brutti, Enhancement of Functional Properties of Liquid Electrolytes for Lithium-Ion Batteries by Addition of Pyrrolidinium-Based Ionic Liquids with Long Alkyl-Chains, *Batteries Supercaps*, 2020, **3**, 1059–1068, DOI: [10.1002/batt.202000070](https://doi.org/10.1002/batt.202000070).
- 14 The Merck Index, The Royal Society of Chemistry, 2013. 15 D. Xu, Z.-l. Wang, J.-j. Xu, L.-l. Zhang and X.-b. Zhang, Novel DMSO-based electrolyte for high performance rechargeable Li–O₂ batteries, *Chem. Commun.*, 2012, **48**, 6948–6950, DOI: [10.1039/c2cc32844e](https://doi.org/10.1039/c2cc32844e).
- 16 L. F. Cremasco, C. G. Anchieta, T. C. M. Nepel, A. N. Miranda, B. P. Sousa, C. B. Rodella, R. M. Filho and G. Doubek, Operando Synchrotron XRD of Bromide Mediated Li–O₂ Battery, *ACS Appl. Mater. Interfaces*, 2021, **13**, 13123–13131, DOI: [10.1021/acsami.0c21791](https://doi.org/10.1021/acsami.0c21791).
- 17 B. Yang, X. Cao, C. Wang, S. Wang and C. Sun, Investigation of hydrogen bonding in water/DMSO binary mixtures by Raman spectroscopy, *Spectrochim. Acta, Part A*, 2020, 228, 117704, DOI: [10.1016/j.saa.2019.117704](https://doi.org/10.1016/j.saa.2019.117704).
- 18 T. Takamuku, T. Tokuda, T. Uchida, K. Sonoda, B. A. Marekha, A. Idrissi, O. Takahashi, Y. Horikawa, J. Matsumura, T. Tokushima, H. Sakurai, M. Kawano, K. Sadakane and H. Iwase, Hydrogen bonds of the imidazolium rings of ionic liquids with DMSO studied by NMR, soft X-ray spectroscopy, and SANS, *Phys. Chem. Chem. Phys.*, 2018, **20**, 12858–12869, DOI: [10.1039/c8cp00963e](https://doi.org/10.1039/c8cp00963e).
- 19 N. Mozhzhukhina, F. Marchini, W. R. Torres, A. Y. Tesio, L. P. Mendez De Leo, F. J. Williams and E. J. Calvo, Insights into dimethyl sulfoxide decomposition in Li–O₂ battery: Understanding carbon dioxide evolution, *Electrochem. Commun.*, 2017, **80**, 16–19, DOI: [10.1016/j.elecom.2017.05.004](https://doi.org/10.1016/j.elecom.2017.05.004).

- 20 D. Sharon, M. Afri, M. Noked, A. Garsuch, A. A. Frimer and D. Aurbach, Oxidation of Dimethyl Sulfoxide Solutions by Electrochemical Reduction of Oxygen, *J. Phys. Chem. Lett.*, 2013, **4**, 3115–3119, DOI: [10.1021/jz4017188](https://doi.org/10.1021/jz4017188).
- 21 A. R. Neale, R. Sharpe, S. R. Yeandel, C.-H. Yen, K. V. Luzyanin, P. Goddard, E. A. Petrucco and L. J. Hardwick, Design Parameters for Ionic Liquid–Molecular Solvent Blend Electrolytes to Enable Stable Li Metal Cycling Within Li–O₂ Batteries, *Adv. Funct. Mater.*, 2021, **31**, 2010627, DOI: [10.1002/adfm.202010627](https://doi.org/10.1002/adfm.202010627).
- 22 K. Karuppasamy, J. Theerthagiri, D. Vikraman, C.-J. Yim, S. Hussain, R. Sharma, T. Maiyalagan, J. Qin and H.-S. Kim, Ionic Liquid-Based Electrolytes for Energy Storage Devices: A Brief Review on Their Limits and Applications, *Polymers*, 2020, **12**, 918.
- 23 A. A. Franco, A. Rucci, D. Brandell, C. Frayret, M. Gaberscek, P. Jankowski and P. Johansson, Boosting Rechargeable Batteries R&D by Multiscale Modeling: Myth or Reality?, *Chem. Rev.*, 2019, **119**, 4569–4627, DOI: [10.1021/acs.chemrev.8b00239](https://doi.org/10.1021/acs.chemrev.8b00239).
- 24 J. Fiates, Y. Zhang, L. F. M. Franco, E. J. Maginn and G. Doubek, Impact of anion shape on Li⁺ solvation and on transport properties for lithium–air batteries: a molecular dynamics study, *Phys. Chem. Chem. Phys.*, 2020, **22**, 15842–15852, DOI: [10.1039/d0cp00853b](https://doi.org/10.1039/d0cp00853b).
- 25 D. Bedrov, J.-P. Piquemal, O. Borodin, A. D. MacKerell, B. Roux and C. Schröder, Molecular Dynamics Simulations of Ionic Liquids and Electrolytes Using Polarizable Force Fields, *Chem. Rev.*, 2019, **119**, 7940–7995, DOI: [10.1021/acs.chemrev.8b00763](https://doi.org/10.1021/acs.chemrev.8b00763).
- 26 Q. Huang, T. C. Lourenço, L. T. Costa, Y. Zhang, E. J. Maginn and B. Gurkan, Solvation Structure and Dynamics of Li⁺ in Ternary Ionic Liquid–Lithium Salt Electrolytes, *J. Phys. Chem. B*, 2019, **123**, 516–527, DOI: [10.1021/acs.jpcc.8b08859](https://doi.org/10.1021/acs.jpcc.8b08859).
- 27 Y. Zhang, N. H. C. Lewis, J. Mars, G. Wan, N. J. Weadock, C. J. Takacs, M. R. Lukatskaya, H.-G. Steinrück, M. F. Toney, A. Tokmakoff and E. Maginn, J. Water-in-Salt LiTFSI Aqueous Electrolytes. 1. Liquid Structure from Combined Molecular Dynamics Simulation and Experimental Studies, *J. Phys. Chem. B*, 2021, **125**, 4501–4513, DOI: [10.1021/acs.jpcc.1c02189](https://doi.org/10.1021/acs.jpcc.1c02189).
- 28 A. F. P. de Campos, A. R. O. Ferreira, L. L. da Silva, P. P. M. Neto and D. Cardoso, Synthesis and properties of hybrid silicas containing alkylammonium surfactants, *Catal. Today*, 2020, **344**, 41–51, DOI: [10.1016/j.cattod.2018.10.026](https://doi.org/10.1016/j.cattod.2018.10.026).
- 29 W. L. Jorgensen, D. S. Maxwell and J. Tirado-Rives, Development and Testing of the OPLS All-Atom Force Field on Conformational Energetics and Properties of Organic Liquids, *J. Am. Chem. Soc.*, 1996, **118**, 11225–11236, DOI: [10.1021/ja9621760](https://doi.org/10.1021/ja9621760).
- 30 J. N. Canongia Lopes and A. A. H. Pádua, CL&P: A generic and systematic force field for ionic liquids modeling, *Theor. Chem. Acc.*, 2012, **131**, 1129, DOI: [10.1007/s00214-012-1129-7](https://doi.org/10.1007/s00214-012-1129-7).
- 31 M. L. Strader and S. E. Feller, A Flexible All-Atom Model of Dimethyl Sulfoxide for Molecular Dynamics Simulations, *J. Phys. Chem. A*, 2002, **106**, 1074–1080, DOI: [10.1021/jp013658n](https://doi.org/10.1021/jp013658n).

- 32 B. Doherty, X. Zhong, S. Gathiaka, B. Li and O. Acevedo, Revisiting OPLS Force Field Parameters for Ionic Liquid Simulations, *J. Chem. Theory Comput.*, 2017, **13**, 6131–6135, DOI: [10.1021/acs.jctc.7b00520](https://doi.org/10.1021/acs.jctc.7b00520).
- 33 F. Neese, Software update: the ORCA program system, version 4.0, *Wiley Interdiscip. Rev.: Comput. Mol. Sci.*, 2018, **8**, e1327, DOI: [10.1002/wcms.1327](https://doi.org/10.1002/wcms.1327).
- 34 O. Acevedo, Ionic liquid force field parameters (OPLS-2009IL and OPLS-VSIL), <https://github.com/orlandoacevedo/IL>.
- 35 G. Saielli, A. Bagno and Y. Wang, Insights on the Isotropic to-Smectic A Transition in Ionic Liquid Crystals from Coarse-Grained Molecular Dynamics Simulations: The Role of Microphase Segregation, *J. Phys. Chem. B*, 2015, **119**, 3829–3836, DOI: [10.1021/jp5104565](https://doi.org/10.1021/jp5104565).
- 36 W. Cao, Y. Wang and G. Saielli, Metastable State during Melting and Solid–Solid Phase Transition of [C_nMim][NO₃] (n = 4–12) Ionic Liquids by Molecular Dynamics Simulation, *J. Phys. Chem. B*, 2018, **122**, 229–239, DOI: [10.1021/acs.jpcc.7b09073](https://doi.org/10.1021/acs.jpcc.7b09073).
- 37 A. A. Freitas, K. Shimizu and J. N. Canongia Lopes, Complex Structure of Ionic Liquids. Molecular Dynamics Studies with Different Cation–Anion Combinations, *J. Chem. Eng. Data*, 2014, **59**, 3120–3129, DOI: [10.1021/je500197x](https://doi.org/10.1021/je500197x).
- 38 L. Martínez, R. Andrade, E. G. Birgin and J. M. Martínez, PACKMOL: A package for building initial configurations for molecular dynamics simulations, *J. Comput. Chem.*, 2009, **30**, 2157–2164, DOI: [10.1002/jcc.21224](https://doi.org/10.1002/jcc.21224).
- 39 M. W. Thompson, R. Matsumoto, R. L. Sacci, N. C. Sanders and P. T. Cummings, Scalable Screening of Soft Matter: A Case Study of Mixtures of Ionic Liquids and Organic Solvents, *J. Phys. Chem. B*, 2019, **123**, 1340–1347, DOI: [10.1021/acs.jpcc.8b11527](https://doi.org/10.1021/acs.jpcc.8b11527).
- 40 M. J. Abraham and J. E. Gready, Optimization of parameters for molecular dynamics simulation using smooth particle-mesh Ewald in GROMACS 4.5, *J. Comput. Chem.*, 2011, **32**, 2031–2040, DOI: [10.1002/jcc.21773](https://doi.org/10.1002/jcc.21773).
- 41 B. Hess, H. Bekker, H. J. C. Berendsen and J. G. E. M. Fraaije, LINCS: A linear constraint solver for molecular simulations, *J. Comput. Chem.*, 1997, **18**, 1463–1472, DOI: [10.1002/\(SICI\)1096-987X\(199709\)18:123.0.CO;2-H](https://doi.org/10.1002/(SICI)1096-987X(199709)18:123.0.CO;2-H).
- 42 M. Parrinello and A. Rahman, Polymorphic transitions in single crystals: A new molecular dynamics method, *J. Appl. Phys.*, 1981, **52**, 7182–7190, DOI: [10.1063/1.328693](https://doi.org/10.1063/1.328693).
- 43 D. J. Evans and B. L. Holian, The Nose–Hoover thermostat, *J. Chem. Phys.*, 1985, **83**, 4069–4074, DOI: [10.1063/1.449071](https://doi.org/10.1063/1.449071).
- 44 J. Neugebauer, M. Reiher, C. Kind and B. A. Hess, Quantum chemical calculation of vibrational spectra of large molecules—Raman and IR spectra for Buckminsterfullerene, *J. Comput. Chem.*, 2002, **23**, 895–910, DOI: [10.1002/jcc.10089](https://doi.org/10.1002/jcc.10089).
- 45 J. P. Perdew, K. Burke and M. Ernzerhof, Generalized Gradient Approximation Made Simple, *Phys. Rev. Lett.*, 1996, **77**, 3865–3868, DOI: [10.1103/PhysRevLett.77.3865](https://doi.org/10.1103/PhysRevLett.77.3865).

- 46 F. Weigend and R. Ahlrichs, Balanced basis sets of split valence, triple zeta valence and quadruple zeta valence quality for H to Rn: Design and assessment of accuracy, *Phys. Chem. Chem. Phys.*, 2005, **7**, 3297, DOI: [10.1039/b508541a](https://doi.org/10.1039/b508541a).
- 47 E. Bodo, M. Bonomo and A. Mariani, Assessing the Structure of Protic Ionic Liquids Based on Triethylammonium and Organic Acid Anions, *J. Phys. Chem. B*, 2021, **125**, 2781–2792, DOI: [10.1021/acs.jpcc.1c00249](https://doi.org/10.1021/acs.jpcc.1c00249), PMID: 33719447.
- 48 M. Brehm and B. Kirchner, TRAVIS – A Free Analyzer and Visualizer for Monte Carlo and Molecular Dynamics Trajectories, *J. Chem. Inf. Model.*, 2011, **51**, 2007–2023, DOI: [10.1021/ci200217w](https://doi.org/10.1021/ci200217w).
- 49 W.-J. Kwak, D. Hirshberg, D. Sharon, M. Afri, A. A. Frimer, H.-G. Jung, D. Aurbach and Y.-K. Sun, Li–O₂ cells with LiBr as an electrolyte and a redox mediator, *Energy Environ. Sci.*, 2016, **9**, 2334–2345, DOI: [10.1039/c6ee00700g](https://doi.org/10.1039/c6ee00700g).
- 50 S. Rastegar, Z. Hemmat, C. Zhang, S. Plunkett, J. Wen, N. Dandu, T. Rojas, L. Majidi, S. N. Misal, A. T. Ngo, L. A. Curtiss and A. Salehi-Khojin, High-Rate Long Cycle-Life Li-Air Battery Aided by Bifunctional InX₃ (X = I and Br) Redox Mediators, *ACS Appl. Mater. Interfaces*, 2021, **13**, 4915–4922, DOI: [10.1021/acsami.0c15200](https://doi.org/10.1021/acsami.0c15200).
- 51 N. Mozhzhukhina, L. P. M. D. Leo and E. J. Calvo, Infrared Spectroscopy Studies on Stability of Dimethyl Sulfoxide for Application in a Li–Air Battery, *J. Phys. Chem. C*, 2013, **117**, 18375–18380, DOI: [10.1021/jp407221c](https://doi.org/10.1021/jp407221c).
- 52 T. C. M. Nepel, C. G. Anchieta, L. F. Cremasco, B. P. Sousa, A. N. Miranda, L. C. C. B. Oliveira, B. A. B. Francisco, J. P. d. O. Julio, F. C. B. Maia, R. O. Freitas, C. B. Rodella, R. M. Filho and G. Doubek, In Situ Infrared Micro and Nanospectroscopy for Discharge Chemical Composition Investigation of Non-Aqueous Lithium–Air Cells, *Adv. Energy Mater.*, 2021, **11**, 2101884, DOI: [10.1002/aenm.202101884](https://doi.org/10.1002/aenm.202101884).
- 53 Z. Chang, D. Henkensmeier and R. Chen, Shifting redox potential of nitroxyl radical by introducing an imidazolium substituent and its use in aqueous flow batteries, *J. Power Sources*, 2019, **418**, 11–16, DOI: [10.1016/j.jpowsour.2019.02.028](https://doi.org/10.1016/j.jpowsour.2019.02.028).
- 54 S. Das, S. Voskian, K. P. Rajczykowski, T. A. Hatton and M. Z. Bazant, Enabling a Stable High-Power LithiumBromine Flow Battery Using Task-Specific Ionic Liquids, *J. Electrochem. Soc.*, 2021, **168**, 070542, DOI: [10.1149/1945-7111/ac1396](https://doi.org/10.1149/1945-7111/ac1396).
- 55 B. R. Schrage, B. Zhang, S. C. Petrochko, Z. Zhao, A. FrkonjaKuczyn, A. Boika and C. J. Ziegler, Highly Soluble Imidazolium Ferrocene Bis(sulfonate) Salts for Redox Flow Battery Applications, *Inorg. Chem.*, 2021, **60**, 10764–10771, DOI: [10.1021/acs.inorgchem.1c01473](https://doi.org/10.1021/acs.inorgchem.1c01473).
- 56 L. G. Chagas, S. Jeong, I. Hasa and S. Passerini, Ionic Liquid-Based Electrolytes for Sodium-Ion Batteries: Tuning Properties to Enhance the Electrochemical Performance of Manganese-Based Layered Oxide Cathode, *ACS Appl. Mater. Interfaces*, 2019, **11**, 22278–22289, DOI: [10.1021/acsami.9b03813](https://doi.org/10.1021/acsami.9b03813).

- 57 L. S. Garca-Coln, L. F. del Castillo and P. Goldstein, Theoretical basis for the Vogel-Fulcher-Tammann equation, *Phys. Rev. B: Condens. Matter Mater. Phys.*, 1989, **40**, 7040–7044, DOI: [10.1103/physrevb.40.7040](https://doi.org/10.1103/physrevb.40.7040).
- 58 X. Wang, M. Sternberg, F. T. U. Kohler, B. U. Melcher, P. Wasserscheid and K. Meyer, Long-alkyl-chain-derivatized imidazolium salts and ionic liquid crystals with tailor-made properties, *RSC Adv.*, 2014, **4**, 12476–12481, DOI: [10.1039/c3ra47250g](https://doi.org/10.1039/c3ra47250g).
- 59 P. Bonhôte, A.-P. Dias, N. Papageorgiou, K. Kalyanasundaram and M. Grätzel, Hydrophobic, Highly Conductive Ambient-Temperature Molten Salts, *Inorg. Chem.*, 1996, **35**, 1168–1178, DOI: [10.1021/ic951325x](https://doi.org/10.1021/ic951325x).
- 60 J. C. Araque, J. J. Hettige and C. J. Margulis, Modern Room Temperature Ionic Liquids, a Simple Guide to Understanding Their Structure and How It May Relate to Dynamics, *J. Phys. Chem. B*, 2015, **119**, 12727–12740, DOI: [10.1021/acs.jpcc.5b05506](https://doi.org/10.1021/acs.jpcc.5b05506).
- 61 M. P. Allen, Computer simulation of liquids, Oxford University Press, Oxford, 2017.
- 62 R. Matsumoto, M. W. Thompson and P. T. Cummings, Ion Pairing Controls Physical Properties of Ionic Liquid-Solvent Mixtures, *J. Phys. Chem. B*, 2019, **123**, 9944–9955, DOI: [10.1021/acs.jpcc.9b08509](https://doi.org/10.1021/acs.jpcc.9b08509).
- 63 N. C. Osti, R. A. Matsumoto, M. W. Thompson, P. T. Cummings, M. Tyagi and E. Mamontov, Microscopic Dynamics in an Ionic Liquid Augmented with Organic Solvents, *J. Phys. Chem. C*, 2019, **123**, 19354–19361, DOI: [10.1021/acs.jpcc.9b05119](https://doi.org/10.1021/acs.jpcc.9b05119).
- 64 M. Brinkmötter, G. A. Giffin, A. Moretti, S. Jeong, S. Passerini and M. Schönhoff, Relevance of ion clusters for Li transport at elevated salt concentrations in [Pyr₁₂O₁][FTFSI] ionic liquid-based electrolytes, *Chem. Commun.*, 2018, **54**, 4278–4281, DOI: [10.1039/c8cc01416g](https://doi.org/10.1039/c8cc01416g).
- 65 N. Molinari, J. P. Mailoa, N. Craig, J. Christensen and B. Kozinsky, Transport anomalies emerging from strong correlation in ionic liquid electrolytes, *J. Power Sources*, 2019, **428**, 27–36, DOI: [10.1016/j.jpowsour.2019.04.085](https://doi.org/10.1016/j.jpowsour.2019.04.085).
- 66 D. B. Shah, H. Q. Nguyen, L. S. Grundy, K. R. Olson, S. J. Mecham, J. M. DeSimone and N. P. Balsara, Difference between approximate and rigorously measured transference numbers in Fluorinated electrolytes, *Phys. Chem. Chem. Phys.*, 2019, **21**, 7857–7866, DOI: [10.1039/c9cp00216b](https://doi.org/10.1039/c9cp00216b).
- 67 M. Gouverneur, F. Schmidt and M. Schönhoff, Negative effective Li transference numbers in Li salt/ionic liquid mixtures: does Li drift in the “Wrong” direction?, *Phys. Chem. Chem. Phys.*, 2018, **20**, 7470–7478, DOI: [10.1039/C7CP08580J](https://doi.org/10.1039/C7CP08580J).
- 68 Y. Zhao, J. Wang, H. Wang, Z. Li, X. Liu and S. Zhang, Is There Any Preferential Interaction of Ions of Ionic Liquids with DMSO and H₂O? A Comparative Study from MD Simulation, *J. Phys. Chem. B*, 2015, **119**, 6686–6695, DOI: [10.1021/acs.jpcc.5b01925](https://doi.org/10.1021/acs.jpcc.5b01925), PMID: 25970011.
- 69 K. Shimizu, C. E. S. Bernardes and J. N. Canongia Lopes, Structure and Aggregation in the 1-Alkyl-3-Methylimidazolium Bis(trifluoromethylsulfonyl)imide Ionic Liquid Homologous Series, *J. Phys. Chem. B*, 2014, **118**, 567–576, DOI: [10.1021/jp409987d](https://doi.org/10.1021/jp409987d).

- 70 C. E. S. Bernardes, AGGREGATES: Finding structures in simulation results of solutions, *J. Comput. Chem.*, 2017, **38**, 753–765, DOI: [10.1002/jcc.24735](https://doi.org/10.1002/jcc.24735).
- 71 C. E. S. Bernardes, K. Shimizu and J. N. Canongia Lopes, Comparative structural analyses in four ionic liquid systems: the two low-q peaks of IL structure factor functions, *Mol. Simul.*, 2018, **44**, 478–484, DOI: [10.1080/08927022.2017.1396329](https://doi.org/10.1080/08927022.2017.1396329).
- 72 F.-G. Wu, J.-S. Yu, S.-F. Sun, H.-Y. Sun, J.-J. Luo and Z.-W. Yu, Stepwise Ordering of Imidazolium-Based Cationic Surfactants during Cooling-Induced Crystallization, *Langmuir*, 2012, **28**, 7350–7359, DOI: [10.1021/la300739x](https://doi.org/10.1021/la300739x).
- 73 M. Śmiechowski, The influence of intermolecular correlations on the infrared spectrum of liquid dimethylsulfoxide, *Spectrochim. Acta, Part A*, 2021, **260**, 119869, DOI: [10.1016/j.saa.2021.119869](https://doi.org/10.1016/j.saa.2021.119869).
- 74 W. N. Martens, R. L. Frost, J. Kristof and J. T. Klopogge, Raman spectroscopy of dimethyl sulphoxide and deuterated dimethyl sulphoxide at 298 and 77 K, *J. Raman Spectrosc.*, 2002, **33**, 84–91, DOI: [10.1002/jrs.827](https://doi.org/10.1002/jrs.827).
- 75 Z. Wang, B. Huang, S. Wang, R. Xue, X. Huang and L. Chen, Vibrational spectroscopic study of the interaction between lithium perchlorate and dimethylsulfoxide, *Electrochim. Acta*, 1997, **42**, 2611–2617, DOI: [10.1016/s0013-4686\(96\)00440-9](https://doi.org/10.1016/s0013-4686(96)00440-9).
- 76 K. V. Ramana and S. Singh, Raman spectral studies of ion-molecular interactions of lithium bromide and lithium iodide with dimethyl sulphoxide, *J. Raman Spectrosc.*, 1989, **20**, 169–179, DOI: [10.1002/jrs.1250200308](https://doi.org/10.1002/jrs.1250200308).
- 77 G. M. A. Girard, M. Hilder, N. Dupre, D. Guyomard, D. Nucciarone, K. Whitbread, S. Zavorine, M. Moser, M. Forsyth, D. R. MacFarlane and P. C. Howlett, Spectroscopic Characterization of the SEI Layer Formed on Lithium Metal Electrodes in Phosphonium Bis(fluorosulfonyl)imide Ionic Liquid Electrolytes, *ACS Appl. Mater. Interfaces*, 2018, **10**, 6719–6729, DOI: [10.1021/acsami.7b18183](https://doi.org/10.1021/acsami.7b18183).
- 78 I. Yoon, S. Jung, D. P. Abraham, B. L. Lucht and P. R. Guduru, In Situ Measurement of the Plane-Strain Modulus of the Solid Electrolyte Interphase on Lithium-Metal Anodes in Ionic Liquid Electrolytes, *Nano Lett.*, 2018, **18**, 5752–5759, DOI: [10.1021/acs.nanolett.8b02363](https://doi.org/10.1021/acs.nanolett.8b02363).
- 79 N. Karimi, M. Zarrabeitia, A. Mariani, D. Gatti, A. Varzi and S. Passerini, Nonfluorinated Ionic Liquid Electrolytes for Lithium Metal Batteries: Ionic Conduction, Electrochemistry, and Interphase Formation, *Adv. Energy Mater.*, 2021, **11**, 2003521, DOI: [10.1002/aenm.202003521](https://doi.org/10.1002/aenm.202003521).

Appendix A – Supplementary Information

Electronic Supplementary Material: Tuning Aprotic Solvent Properties with Long Alkyl Chain Ionic Liquid for Lithium-based Electrolytes

Tuanan C. Lourenço,^{*,†} Letícia M. S. Barros,^{*,‡} Chayene G. Anchieta,^{*,‡} Thayane C. M. Nepel,^{*,‡} Júlia P. O. Júlio,^{*,‡} Luis Gustavo Dias,^{*,¶} Rubens Maciel Filho,^{*,‡} Gustavo Doubek,^{*,‡} and Juarez L. F. Da Silva^{*,†}

[†]São Carlos Institute of Chemistry, University of São Paulo, P.O. Box 780, 13560-970, São Carlos, São Paulo, Brazil

[‡]School of Chemical Engineering, University of Campinas, Campinas 13083-852, Brazil

[¶]Chemistry Department, FFCLRP, University of São Paulo, 14040-901 Ribeirão Preto, SP, Brazil

E-mail: lourenco.tuanan@gmail.com; leticia.barros94@gmail.com; chayeneanchieta@gmail.com; thyanecarpanedo@gmail.com; julia_paula@outlook.com.br; lgdias@ffclrp.usp.br; rmaciel@unicamp.br; doubek@feq.unicamp.br; juarez_dasilva@iqsc.usp.br

1 Introduction

Below, we summarize the additional information provided within the electronic supplementary material:

1. ¹H and ¹³C NMR characterization of the synthesized [C₁₆mim][Br], as well as POM and DSC characterization of the prepared electrolytes.

Table 1: ¹H and ¹³C NMR from [C₁₆mim][Br]

Core	¹ H Δ	¹³ C δ
	0.88 (t, ¹ H)	14.13
	1.29 (m, ⁹ H)	22.69
	1.88 (m, ¹ H)	26.29
	2.62 (s, ¹ H)	28.18
	3.41 (s, ¹ H)	28.77
	4.13 (s, ¹ H)	29.04
	4.32 (t, ¹ H)	29.55
	7.33 (s, ¹ H)	30.34
	7.45 (t, ¹ H)	31.93
	7.63 (d, ¹ H)	32.85
	10.13 (s, ¹ H)	34.12
		36.83
		50.17
		121.98
		123.80
		137.23

2. Force field parameters along with the atomic positions of the ionic/molecular structures and also the boxes compositions employed in the MD simulations.
3. Experimental cyclic voltammetry for the DMSO LiClO₄ 0.100 M electrolyte on a glass carbon electrode, the fitting parameters for the experimental densities as function of temperature and the plot for the experimental densities as function of the ionic liquid crystal concentration.
4. We show the Vogel–Tammann–Fulcher (VTF) parameters for the experimental viscosity in function of temperature, the collective mean square displacements (cMSD) and the mean square displacements (MSD) for all ions used to obtain the ionic conductivities and the self-diffusion coefficients from the MD simulations at 400 K, respectively.
5. Combined distribution function (CDF) joining the CR([C₁₆mim]⁺)–CR([C₁₆mim]⁺) g(r) and the angular distribution function for the angle θ between the normal vectors in the imidazolium ring plane, in the 0.500 M, 1.456 M and 2.413 M concentrations.
6. Finally, we show the comparison of the theoretical Raman from the density functional theory (DFT) calculations using the PBE relaxed structures and the frozen ones from the MD simulations and several Raman spectra for the PBE relaxed structures using different Gaussian width factors.

2 Methodology

2.1 Ionic Liquid Crystal Characterization

The [C₁₆mim][Br] synthesis was confirmed by elemental analysis (CHN) using a Perkin Elmer analyzer model 2400 and ¹³C MAS-NMR using a spectrometer, Bruker DPX-400 (400.13 MHz). Dimethyl sulfoxide (DMSO) was used as solvent during the NMR analysis which was conducted at 298.15 K. The spectral data confirmed that the structure was obtained successfully. The elemental analysis presented 20% of carbon, 48% of hydrogen and 1.14 of bromide. The results obtained by NMR spectras are summarized in Table 1. ¹³C-NMR (DMSO, δ ppm): 137.23, 123.80 and 121.98 (C–H imidazolium); 14.13 and 36.83 (NCH₃; CH₃ bonded to ring and CH₃ from alquil); peaks between 22.69 and 50.17 corresponding to CH₂ of alquil chain.

2.2 Liquid Cristal Behavior Characterization

The liquid crystal property of [C₁₆mim][Br] was confirmed via Polarized Optical Microscopy (POM), using an optical microscope by Leica DM LM with images captured at 303.15 K temperature and 50 X magnification, and via Differential Scanning Calorimetry (DSC), using an Exploratory Differential Calorimeter from Mettler under a N₂ atmosphere applying a cooling rate of 10 Kmin⁻¹. POM and DSC data are presented in Figures 1 and 2, respectively.

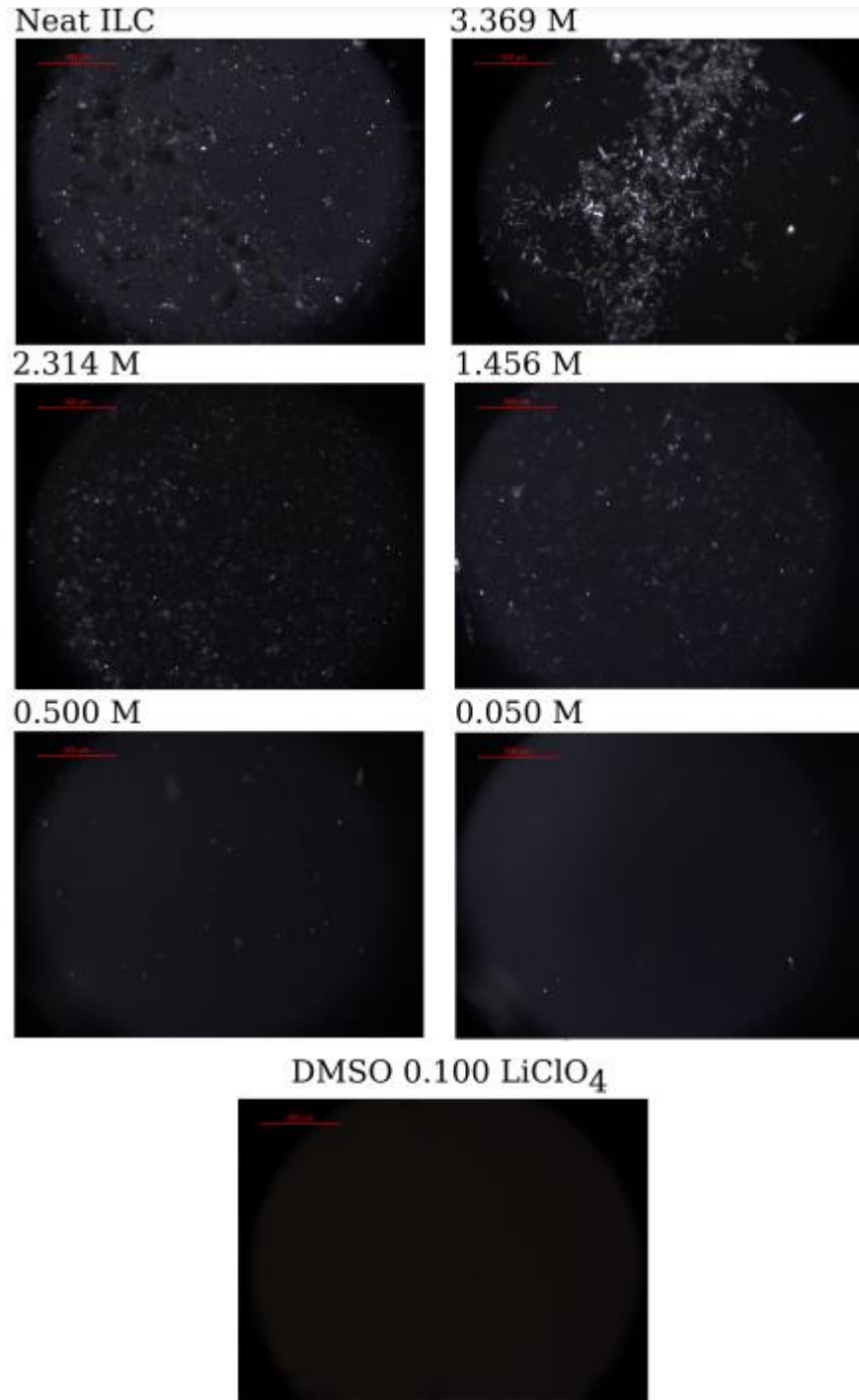


Figure 1: POM images at 303.15 K (magnification 50X) from pure $[C_{16}mim][Br]$, the electrolyte DMSO/LiClO₄ 0.100 M without ILC (0.000 M) and adding 0.050 M, 0.500 M, 1.456 M, 2.314 M and 3.369 M of $[C_{16}mim][Br]$.

Evaluating POM image at 303.15 K for the pure $[C_{16}mim][Br]$, we observe the optical anisotropy due to the liquid crystal behavior,¹ which can also be identified when the ILC is dissolved in the DMSO/LiClO₄ 0.100 M electrolyte. The mesophase formation can be clearly observed from a 0.500 M ILC concentration via POM.² It can also be noted an enhancement of the optical anisotropy and the

formation of nanodomains, as more ILC is added to the solution, in agreement to what is expected since we have a higher concentration of the liquid crystal species. The type of mesophase could not be determined through the POM analysis because the equipment magnification was limited to 50 times.

The DSC data also point out the liquid crystal character for the electrolyte solution when adding the ILC, as seen by the crystallization of the $[C_{16}mim][Br]$ material at a temperature higher than 273.15 K, i.e., 282.15 K, clearly identified from 1.456 M concentration, Figure 2.^{1,3} Kullmer *et al.* has observed a similar behavior of a hexadecyl ILC, which altered the crystallization properties when added to different solvents.¹ From Figure 2, it is verified the DMSO solvent solidification near 272.15 K for all ILC concentrations and the increase of ILC crystallization peak by the ILC addition with a little shift in the temperature is due to the DMSO-ILC interaction. The $LiClO_4$ was not identified due to its low concentration (0.100 M) electrolyte.

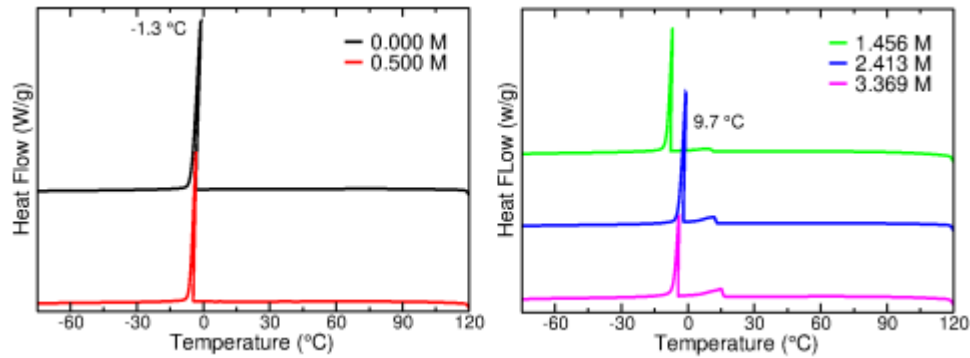


Figure 2: DSC curves of electrolytes for the DMSO/ $LiClO_4$ 0.100 M electrolyte without the ILC addition, 0.000 M, ILC (black curve) and adding 0.500 M ILC (red curve); 1.456 M ILC (green curve), 2.314 M ILC (blue curve) and 3.369 M ILC (magenta curve) during the cooling at $10\text{ }^\circ\text{C min}^{-1}$.

2 Theoretical Approach and Computational Details

2.1 Force field models

As stated in the manuscript, we carried out the MD simulations using the GROMACS package⁴ and a combination of several OPLS based force fields,⁵ which the potential energy at 0 K is described by the following equation,

$$U_{pot} = \sum_{i=1}^N \sum_{j>i}^N \left\{ 4\epsilon_{ij} \left[\left(\frac{\sigma_{ij}}{r_{ij}} \right)^{12} - \left(\frac{\sigma_{ij}}{r_{ij}} \right)^6 \right] + \frac{q_i q_j}{4\pi\epsilon_0 r_{ij}} \right\} + \sum_{bonds} \frac{k_{ir,j}}{2} (r_{ij} - r_{eq})^2 + \sum_{angle} \frac{k_{\theta,ijk}}{2} (\theta_{ijk} - \theta_{eq})^2 + \sum_{dihedrals} \frac{V_{n,ijkl}}{2} (1 + (-1)^n \cos(n\phi_{ijkl})),$$

where the Lennard–Jones terms are represented by ε_{ij} and σ_{ij} , while the atomic charges for the atoms i and j are indicated by q_i and q_j , respectively. The force constants for the intramolecular interactions, *e.g.*, bond stretching, angle bending, and dihedral torsion are represented by $k_{r,ij}$, $k_{\theta,ijk}$ and $k_{\phi,ijkl}$, respectively. The r_{ij} and θ_{ijk} terms are the atomic distances and the angle between i , j and k , respectively. ϕ is the dihedral angle.

For the 1-methyl,3-decahexylimidazolium bromide ([C₁₆mim][Br]) ionic liquid crystal we applied the CL&P force field developed by Canongia Lopes and Pádua, for the dimethyl sulfoxide (DMSO), we also adopted the CL&P force field with the charges set parametrized by Strader and Feller.⁶ The perchlorate ion (ClO₄⁻) was described by the force field parametrized by Acevedo and coworkers due to the availability of parameters,⁷ while the lithium-ion was taken directly from the OPLS database. The cross term parameters for the Lennard–Jones interactions, *e.g.* σ_{ij} and ε_{ij} , was generated by the geometric combination rule, while the 1–4 interactions were scaled down by a factor of 0.5.

The [C₁₆mim][Br] and DMSO structures and topologies inputs were built using the DLPGEN software,⁸ while the ClO₄⁻ was taken from the Acevedo group github database.⁹ In Tables 2, 4 and 3 we provide the force field parameters used in the MD simulations. In our simulations the partial charges of the ions were scaled by a factor of 0.8 as common used in ionic liquids molecular dynamics simulations.^{10–12} In Tables 5 to 8 we provide the *xyz* coordinates for the relaxed structures of the ions and DMSO molecules used in the simulations and their respective atomic charges.

Table 2: Parameters employed for the force-fields: bonds (k_r^a , r_o^a) and angles (k_θ^a , θ_o^a), hydrogen bonds (X-H) are constrained by LINCS algorithm. Units are $k_r^a = \text{kJ mol}^{-1}\text{nm}^{-2}$, $r_o^a = \text{nm}$, $k_\theta^a = \text{kJ mol}^{-1}\text{rad}^{-2}$, and θ_o^a are degrees.

Bonds	k_r^a	r_o^a	Angles	k_θ^a	θ_o^a
C_R-N_A	399200.00	0.1315	$N_A-C_R-N_A$	585.000	109.800
C_W-N_A	357400.00	0.1378	$C_R-N_A-C_W$	585.000	108.000
C_W-C_W	435100.00	0.1341	$C_1-N_A-C_R$	585.000	126.400
C_1-N_A	282000.00	0.1466	$C_1-N_A-C_W$	585.000	125.600
C_1-C_2	224300.00	0.1529	$N_A-C_1-C_2$	418.000	112.700
C_2-C_S	224300.00	0.1529	$C_1-C_2-C_S$	488.000	112.700
C_S-C_S	224300.00	0.1529	$C_2-C_S-C_S$	488.000	112.700
C_S-C_E	224300.00	0.1529	$C_S-C_S-C_S$	488.000	112.700
$Cl-O_C$	633959.68	0.1506	$C_S-C_S-C_E$	488.000	112.700
S_Z-O_{SZ}	585800.00	0.1530	$H_1-C_1-N_A$	314.000	110.700
$C_{SZ}-S_Z$	284500.00	0.1790	$H_{C_R}-C_R-N_A$	293.000	125.100
C_R-H_R	—	0.1080	$H_{C_W}-C_W-N_A$	293.000	122.000
C_E-H_C	—	0.1080	$H_{C_W}-C_W-C_W$	293.900	130.000
C_1-H_1	—	0.1080	$H_1-C_1-H_1$	276.000	107.800
C_2-H_C	—	0.1080	$H_1-C_1-C_2$	314.000	110.700
C_S-H_C	—	0.1080	$H_C-C_E-H_C$	276.000	107.800
$C_{SZ}-H_C$	—	0.1090	$C_1-C_2-H_C$	314.000	110.700
—	—	—	$H_C-C_2-H_C$	276.000	107.800
—	—	—	$H_C-C_2-C_S$	314.000	110.700
—	—	—	$H_C-C_S-H_C$	276.000	107.800
—	—	—	$H_C-C_S-C_S$	314.000	110.700
—	—	—	$H_C-C_S-C_E$	314.000	110.700
—	—	—	O_C-Cl-O_C	1739.707	109.500
—	—	—	$C_{SZ}-SZ-C_{SZ}$	519.000	96.000
—	—	—	$C_{SZ}-SZ-O_{SZ}$	619.000	107.000
—	—	—	$H_C-C_{SZ}-H_C$	276.000	107.800
—	—	—	$H_C-C_{SZ}-SZ$	293.000	109.500

Table 3: Parameters employed for the proper and improper dihedrals in the force-fields. Units are $V_n = \text{kJ mol}^{-1}$.

Dihedral	V_1	V_2	V_3	V_4
$C_R-N_A-C_W-C_W$	0.0000	12.5500	0.0000	0.0000
$C_R-N_A-C_1-C_2$	-5.2690	0.0000	0.0000	0.0000
$C_R-N_A-C_1-H_1$	0.0000	0.0000	0.0000	0.0000
$C_R-N_A-C_W-H_W$	0.0000	12.5500	0.0000	0.0000
$H_R-C_R-N_A-C_W$	0.0000	19.4600	0.0000	0.0000
$H_R-C_R-N_A-C_1$	0.0000	19.4600	0.0000	0.0000
$H_W-C_W-N_A-C_1$	0.0000	12.5500	0.0000	0.0000
$H_W-C_W-C_W-H_W$	0.0000	44.9800	0.0000	0.0000
$N_A-C_1-C_2-C_S$	-7.4800	3.1640	-1.2030	0.0000
$N_A-C_1-C_2-H_C$	0.0000	0.0000	0.0000	0.0000
$H_1-C_1-C_2-H_C$	0.0000	0.0000	1.3305	0.0000
$C_2-C_S-C_S-C_S$	7.2800	-0.6569	1.1673	0.0000
$C_2-C_S-C_S-H_C$	0.0000	0.0000	1.5313	0.0000
$C_S-C_S-C_S-C_S$	7.2800	-0.6569	1.1673	0.0000

Continued on next page

$C_S - C_S - C_S - H_C$	0.0000	0.0000	1.5313	0.0000
$H_C - C_S - C_S - H_C$	0.0000	0.0000	1.3305	0.0000
$C_S - C_S - C_S - C_T$	7.2800	-0.6569	1.1673	0.0000
$H_C - C_S - C_S - C_T$	0.0000	0.0000	1.3305	0.0000
$C_S - C_S - C_T - H_C$	0.0000	0.0000	1.5313	0.0000
$C_W - C_W - N_A - C_1$	0.0000	12.5500	0.0000	0.0000
$C_W - N_A - C_1 - C_2$	-7.1540	6.1060	0.7940	0.0000
$C_W - N_A - C_1 - H_1$	0.0000	0.0000	0.5190	0.0000
$C_W - N_A - C_R - N_A$	0.0000	19.4600	0.0000	0.0000
$H_C - C_2 - C_S - H_C$	0.0000	0.0000	1.3305	0.0000
$H_C - C_{SZ} - S_Z - C_{SZ}$	0.0000	0.0000	0.0000	0.0000
$H_C - C_{SZ} - S_Z - O_{SZ}$	0.0000	0.0000	0.0000	0.0000
$C_R - N_A - C_W - C_1$	180.0000	8.3700	2.0000	—
$C_R - N_A - C_1 - C_W$	180.0000	8.3700	2.0000	—
$N_A - C_R - N_A - H_R$	180.0000	9.2000	2.0000	—
$N_A - C_R - H_R - N_A$	180.0000	9.2000	2.0000	—
$N_A - C_W - C_W - H_W$	180.0000	9.2000	2.0000	—
$N_A - C_W - H_W - C_W$	180.0000	9.2000	2.0000	—

Table 4: Lennard–Jones parameters employed for force-fields. Units are $\sigma = \text{nm}^{-1}$ and $\epsilon = \text{kJ mol}^{-1}$.

Atom type	σ	ϵ
N _A	0.32500	0.71128
C _R	0.35500	0.29288
C _W	0.35500	0.29288
C ₁	0.35000	0.27614
H _R	0.24200	0.12552
H _W	0.24200	0.12552
H ₁	0.25000	0.12552
C ₂	0.35000	0.27614
C _S	0.35000	0.27614
H _C	0.25000	0.12552
C _T	0.35000	0.27614
Br ⁻	0.39700	0.86000
S _Z	0.35600	1.65268
C _{SZ}	0.35000	0.27614
O _{SZ}	0.29300	1.17152
Cl	0.35000	0.49283
O _C	0.29000	0.87864
Li ⁺	0.21260	0.07647

Table 5: Atom type, atomic positions (\AA) and atomic charges (e) for 1-hexadecyl-3-methylimidazole, $[\text{C}_{16}\text{mim}]^+$. The atomic charges were scaled down by a 0.8 factor.

Atom type	x	y	z	atomic charge
N_A	-0.043	0.177	-0.044	0.120
C_R	0.073	0.339	1.257	-0.088
N_A	1.189	-0.213	1.678	0.120
C_W	1.829	-0.759	0.587	-0.104
C_W	1.061	-0.518	-0.486	-0.104
C_I	-1.151	0.644	-0.881	-0.136
H_R	-0.636	0.841	1.879	0.168
C_I	1.690	-0.216	3.068	-0.136
H_W	2.763	-1.270	0.675	0.168
H_W	1.193	-0.776	-1.514	0.168
H_I	-1.621	-0.204	-1.358	0.104

Continued on next page

H ₁	-1.871	1.151	-0.258	0.104
H ₁	-0.773	1.328	-1.626	0.104
C ₂	2.815	0.794	3.278	0.008
H ₁	0.844	-0.001	3.705	0.104
H ₁	2.014	-1.225	3.282	0.104
C _S	3.324	0.773	4.723	-0.096
H _C	3.632	0.573	2.597	0.048
H _C	2.453	1.787	3.025	0.048
H _C	2.499	0.988	5.399	0.048
H _C	3.672	-0.228	4.968	0.048
C _S	4.453	1.778	4.962	-0.096
H _C	5.275	1.562	4.283	0.048
H _C	4.103	2.777	4.713	0.048
C _S	4.967	1.763	6.403	-0.096
H _C	5.314	0.762	6.650	0.048
H _C	4.143	1.978	7.080	0.048
C _S	6.096	2.766	6.646	-0.096
H _C	6.920	2.551	5.966	0.048
H _C	5.748	3.767	6.396	0.048
C _S	6.612	2.753	8.086	-0.096
H _C	6.959	1.752	8.334	0.048
H _C	5.788	2.967	8.764	0.048
C _S	7.741	3.756	8.330	-0.096
H _C	8.565	3.542	7.651	0.048
H _C	7.394	4.757	8.081	0.048
C _S	8.258	3.744	9.770	-0.096
H _C	8.605	2.742	10.019	0.048
H _C	7.434	3.958	10.449	0.048

Continued on next page

C _S	9.387	4.746	10.015	-0.096
H _C	10.211	4.532	9.336	0.048
H _C	9.040	5.747	9.766	0.048
C _S	9.904	4.734	11.455	-0.096
H _C	10.251	3.733	11.704	0.048
H _C	9.080	4.948	12.134	0.048
C _S	11.034	5.736	11.700	-0.096
H _C	11.857	5.522	11.020	0.048
H _C	10.686	6.737	11.451	0.048
C _S	11.550	5.724	13.140	-0.096
H _C	11.898	4.723	13.389	0.048
H _C	10.726	5.938	13.819	0.048
C _S	12.680	6.726	13.385	-0.096
H _C	13.504	6.513	12.706	0.048
H _C	12.333	7.728	13.136	0.048
C _S	13.197	6.715	14.824	-0.096
H _C	13.546	5.715	15.074	0.048
H _C	12.375	6.930	15.504	0.048
C _T	14.325	7.719	15.061	-0.144
H _C	15.177	7.510	14.420	0.048
H _C	13.998	8.734	14.853	0.048
H _C	14.670	7.687	16.090	0.048

Table 6: Atom type, atomic positions (Å) and atomic charges (e) for 1dimethylsulfoxide, DMSO.

Atom type	<i>x</i>	<i>y</i>	<i>z</i>	atomic charge
S _Z	5.288	1.974	5.999	0.359151
C _{SZ}	6.726	2.889	6.534	-0.498374

Continued on next page

H _C	6.794	3.703	6.029	0.187137
H _C	7.514	2.359	6.393	0.187137
H _C	6.645	3.098	7.467	0.187137
C _{SZ}	5.359	0.642	7.178	-0.498374
H _C	5.328	1.000	8.069	0.187137
H _C	6.175	0.152	7.059	0.187137
H _C	4.611	0.055	7.043	0.187137
O _{SZ}	4.081	2.802	6.425	-0.485225

Table 7: Atom type, atomic positions (Å) and atomic charges (e) for perchlorate, ClO₄⁻

Atom type	x	y	z	atomic charge
Cl	-0.218	-0.096	0.000	0.9408
O _C	-1.668	-0.096	-0.000	-0.4352
O _C	0.265	0.588	1.184	-0.4352
O _C	0.265	-1.463	-0.000	-0.4352
O _C	0.265	0.588	-1.184	-0.4352

Table 8: Atom type, atomic positions (Å) and atomic charges (e) for bromide-ion and lithium-ion.

Atom type	x	y	z	atomic charge
Br ⁻	0.000	0.000	0.000	-0.800
Li ⁺	0.000	0.000	0.000	0.800

2.3.2 Molecular Dynamic Simulation Details

As stated in the manuscript, the MD simulations were carried out employing the GROMACS package version 2019.3,⁴ while the MD boxes were built using PACKMOL software and its volume guesser function to define the initial volumes.¹³ Table 9 shows the composition and the total number of atoms in each simulation box.

Table 9: Ionic liquid crystal concentrations, number of ions/molecules and total number of atoms in each simulated box.

ILC Concentration (M)	[C ₁₆ mim] ⁺	[Br] ⁻	Li ⁺	ClO ₄ ⁻	DMSO	Atoms
0.200	56	56	28	28	3944	43080
0.500	137	137	27	27	3863	47286
1.456	375	375	25	25	3625	59650
2.413	585	585	24	24	3415	70564
3.369	772	772	22	22	3228	80276

3 Results and Discussion

3.1 Electrochemical Analysis

3.2 Density

Table 10 shows the a and b parameters for the linear fitting, $\rho(T) = a + bT$, for the experimental density as function of the temperature for the DMSO/LiClO₄ 0.1 M electrolyte in the ILC concentration range from 0.025 M to 3.369 M.

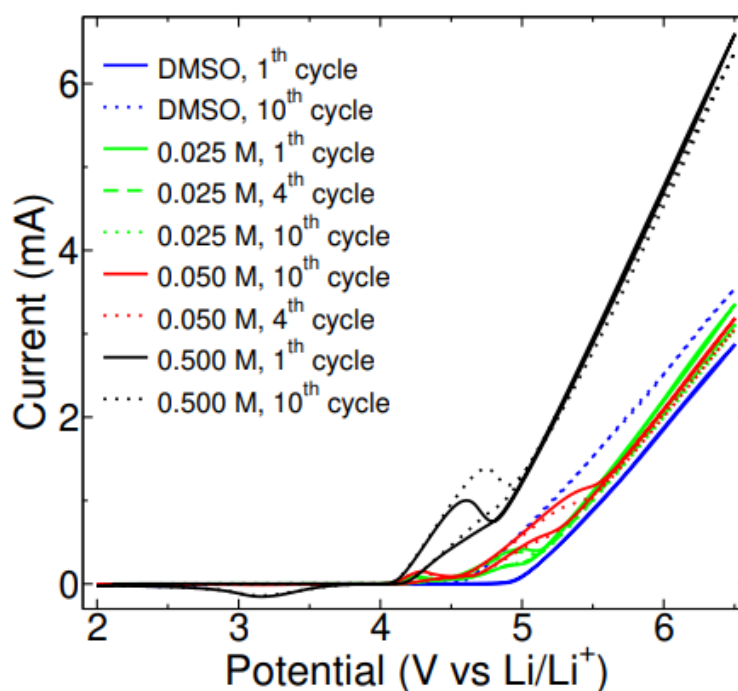


Figure 3: Cyclic voltammetry on glass carbon working electrode performed at 50 mVs^{-1} under argon atmosphere. The electrolyte was LiClO₄ 0.1 M in DMSO (blue line); adding 0.025 M [C₁₆mim][Br] (green line), 0.050 M [C₁₆mim][Br] (red line) and 0.500 M [C₁₆mim][Br] (black line).

Table 10: Linear fitting parameters a and b for the experimental density as function of the temperature for the DMSO/LiClO₄ 0.1 M as function of the ILC concentration.

ILC Concentration (M)	a	b
0.025	1.3866	-0.00096094
0.050	1.3846	-0.00095495
0.075	1.3850	-0.00095729
0.100	1.3825	-0.00094893
0.200	1.3784	-0.00094147
0.500	1.3699	-0.00092276
1.456	1.3551	-0.00089358
2.413	1.3270	-0.00082754
3.369	1.3212	-0.00082205

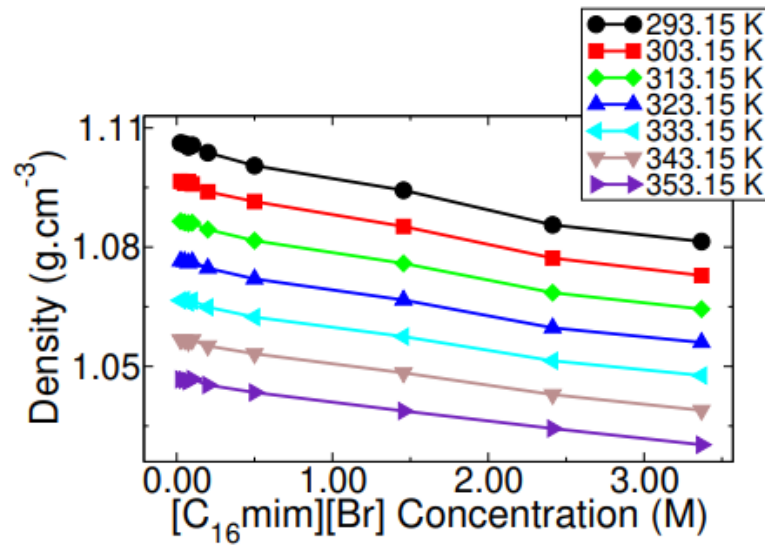


Figure 4: Experimental densities for DMSO/LiClO₄ 0.10 M in the temperature range from 293.15 K to 353.15 K as a function of [C₁₆mim][Br] concentration.

3.3 Viscosity

Table 11 shows the η_0 , k and T_0 parameters for the Vogel–Tammann–Fulcher (VTF) equation¹⁴ fitted for the experimental viscosity as a function of temperature for the DMSO/LiClO₄ 0.1 M electrolyte in the ILC concentration range from 0.025 M to 3.369 M.

Table 11: Vogel–Tammann–Fulcher parameters η_0 , k and T_0 for the experimental viscosity as a function of the temperature for the DMSO/LiClO₄ 0.10 M as function of the ILC concentration

ILC Concentration (M)	η_0	k	T_0
0.025	3.15651×10^{-2}	923.334	83.2557
0.050	2.78085×10^{-4}	4840.860	-239.8840
0.075	1.66863×10^{-4}	5092.700	-234.2190
0.100	5.03559×10^{-4}	4097.090	-186.0670
0.200	1.64733×10^{-3}	2992.300	-110.6790
0.500	1.41953×10^{-2}	1370.240	44.6675
1.456	2.81528×10^{-3}	2204.180	11.2720
2.413	1.63121×10^{-3}	2176.950	57.6182
3.369	5.87918×10^{-5}	4091.390	-17.9295

3.4 Ionic Conductivity

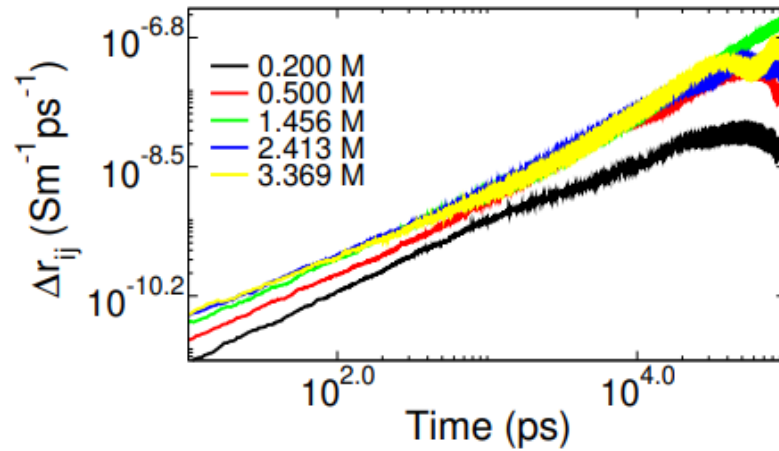


Figure 5: Collective mean square displacement (cMSD) from the MD simulations for DMSO/LiClO₄ 0.10 M as a function of the [C₁₆mim][Br] concentration at 400 K.

Table 12: Individual ionic conductivities, σ_x , (mS cm⁻¹), and the time regions, Δ_{tx} , (ps) for the linear fittings in the collective mean square displacement for DMSO/LiClO₄ 0.1 M and all [C₁₆mim][Br] concentrations at 400 K.

System	σ_1	Δ_{t1}	σ_2	Δ_{t2}	σ_3	Δ_{t3}	σ_{av}
0.200 M	6.86	80/260	4.93	674/1938	6.23	186/1024	6.00
0.500 M	10.43	80/300	11.50	180/950	12.03	517/2270	11.32
1.456 M	16.48	80/400	14.67	200/750	12.15	500/2500	14.35
2.413 M	15.07	105/375	15.29	400/1500	15.45	470/3000	15.27
3.369 M	14.17	80/315	12.97	170/900	11.96	550/2240	13.04

3.5 Self-diffusion Coefficients

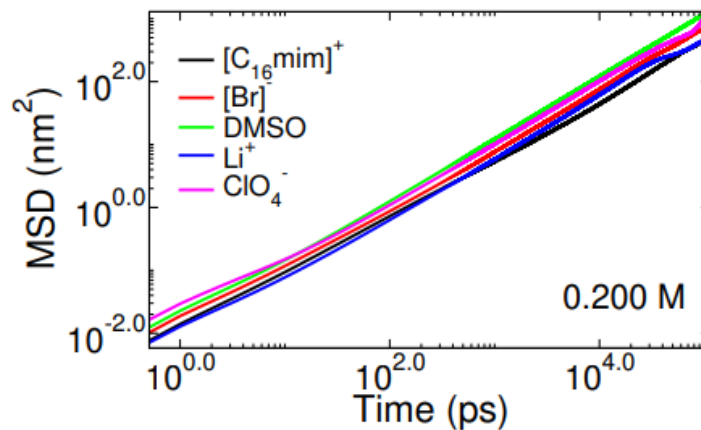


Figure 6: Mean square displacement (MSD) from the MD simulations for DMSO/LiClO₄ 0.10 M in the 0.200 M [C₁₆mim][Br] concentration at 400 K.

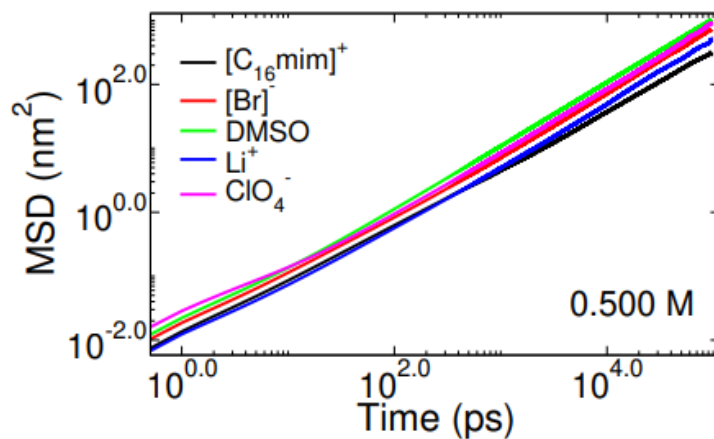


Figure 7: Mean square displacement (MSD) from the MD simulations for DMSO/LiClO₄ 0.10 M in the 0.500 M [C₁₆mim][Br] concentration at 400 K.

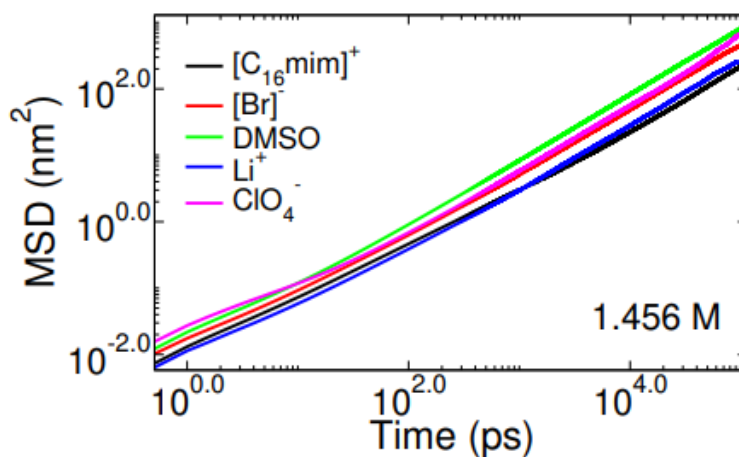


Figure 8: Mean square displacement (MSD) from the MD simulations for DMSO/LiClO₄ 0.10 M in the 1.456 M [C₁₆mim][Br] concentration at 400 K.

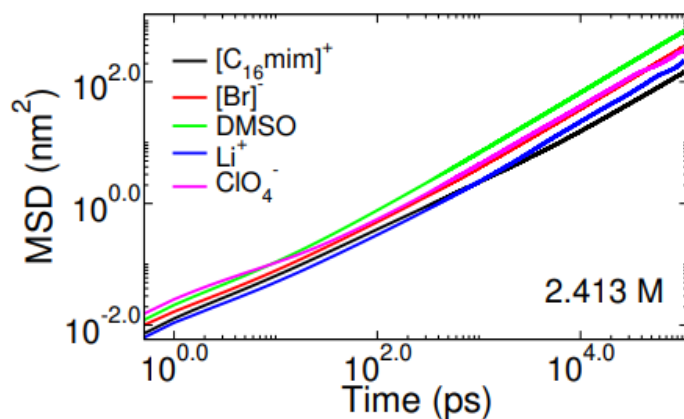


Figure 9: Mean square displacement (MSD) from the MD simulations for DMSO/LiClO₄ 0.10 M in the 2.413 M [C₁₆mim][Br] concentration at 400 K.

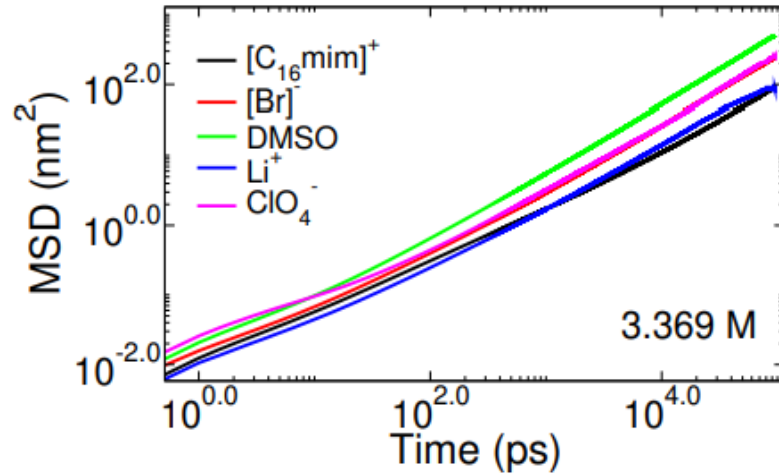


Figure 10: Mean square displacement (MSD) from the MD simulations for DMSO/LiClO₄ 0.10 M in the 3.369 M [C₁₆mim][Br] concentration at 400 K.

Table 13: Self-diffusion coefficients (D), the time regions (t_1 and t_2) for the linear fittings in the mean square displacement and transference numbers (t_{ion}) for DMSO/LiClO₄ 0.1 M in the 0.200 M [C₁₆mim][Br] concentration at 400 K.

0.200 M	$D (1 \times 10^{-10} \text{ m}^2 \text{ s}^{-1})$	t_1 (ps)	t_2 (ps)	t_{ion}
[C ₁₆ mim] ⁺	7.672 17	10000	21000	0.21769
[Br] ⁻	13.367 67	5600	21000	0.37930
DMSO	20.10000	6100	22700	—
Li ⁺	11.279 67	5300	21300	0.16003
ClO ₄ ⁻	17.125 00	3900	12000	0.24296

Table 14: Self-diffusion coefficients (D), the time regions (t_1 and t_2) for the linear fittings in the mean square displacement and transference numbers (t_{ion}) for DMSO/LiClO₄ 0.1 M in the 0.500 M [C₁₆mim][Br] concentration at 400 K.

0.500 M	$D (1 \times 10^{-10} \text{ m}^2 \text{ s}^{-1})$	t_1 (ps)	t_2 (ps)	t_{ion}
[C ₁₆ mim] ⁺	5.84900	6000	21000	0.25765
[Br] ⁻	12.506 50	7000	21000	0.55093
DMSO	17.933 33	8000	22000	—
Li ⁺	8.179 50	2500	9600	0.07101
ClO ₄ ⁻	13.868 33	5000	21000	0.12040

Table 15: Self-diffusion coefficients (D), the time regions (t_1 and t_2) for the linear fittings in the mean square displacement and transference numbers (t_{ion}) for DMSO/LiClO₄ 0.1 M in the 1.456 M [C₁₆mim][Br] concentration at 400 K.

1.456 M	$D (1 \times 10^{-10} \text{ m}^2 \text{ s}^{-1})$	t_1 (ps)	t_2 (ps)	t_{ion}
$[\text{C}_{16}\text{mim}]^+$	3.49283	7000	16000	0.28066
$[\text{Br}]^-$	8.05583	6500	22000	0.64733
DMSO	13.77783	6000	22000	—
Li^+	4.62483	6000	22000	0.02477
ClO_4^-	8.81450	6000	22000	0.04722

Table 16: Self-diffusion coefficients (D), the time regions (t_1 and t_2) for the linear fittings in the mean square displacement and transference numbers (t_{ion}) for DMSO/ LiClO_4 0.1 M in the 2.413 M $[\text{C}_{16}\text{mim}][\text{Br}]$ concentration at 400 K.

2.413 M	$D (1 \times 10^{-10} \text{ m}^2 \text{ s}^{-1})$	t_1 (ps)	t_2 (ps)	t_{ion}
$[\text{C}_{16}\text{mim}]^+$	2.31817	9000	24000	0.26796
$[\text{Br}]^-$	5.92617	6000	21000	0.68503
DMSO	10.07833	6000	22000	—
Li^+	3.60867	7000	15000	0.01711
ClO_4^-	6.30183	7000	22000	0.02988

Table 17: Self-diffusion coefficients (D), the time regions (t_1 and t_2) for the linear fittings in the mean square displacement and transference numbers (t_{ion}) for all ions/molecules for DMSO/ LiClO_4 0.1 M in the 3.369 M $[\text{C}_{16}\text{mim}][\text{Br}]$ concentration at 400 K.

3.369 M	$D (1 \times 10^{-10} \text{ m}^2 \text{ s}^{-1})$	t_1 (ps)	t_2 (ps)	t_{ion}
$[\text{C}_{16}\text{mim}]^+$	1.59595	5700	21700	0.25929
$[\text{Br}]^-$	4.37717	6000	22000	0.71116
DMSO	8.74883	9000	24000	—
Li^+	2.24483	5700	16000	0.01039
ClO_4^-	4.13583	5000	15000	0.01914

3.6 Combined Distribution Function

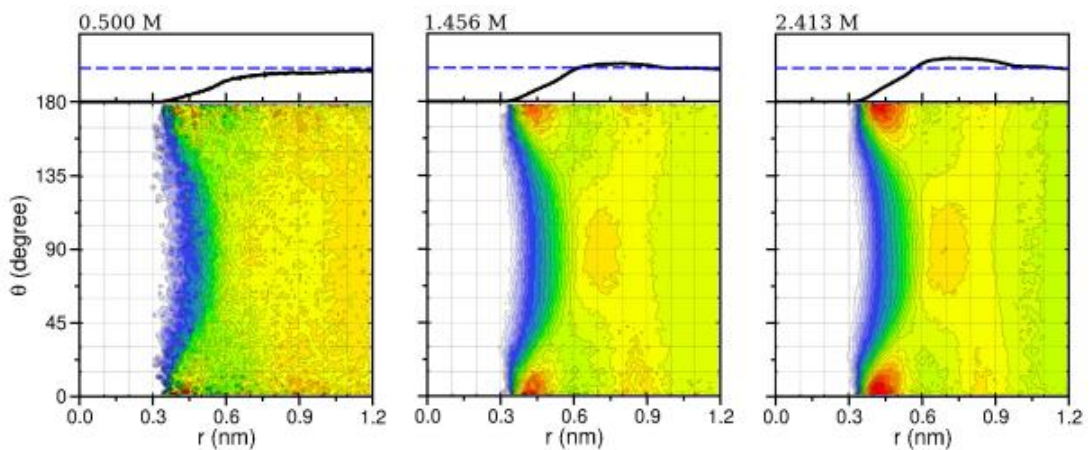


Figure 11: Combined distribution function (CDF) joining the CR([C₁₆mim]⁺)–CR([C₁₆mim]⁺) $g(r)$ and the angular distribution function for the angle θ between the normal vectors in the imidazolium ring plane, in the 0.500 M, 1.456 M and 2.143 M concentrations. The dashed blue lines in the $g(r)$ are the limit 1 in the $g(r)$ intensity.

3.7 Raman Spectroscopy

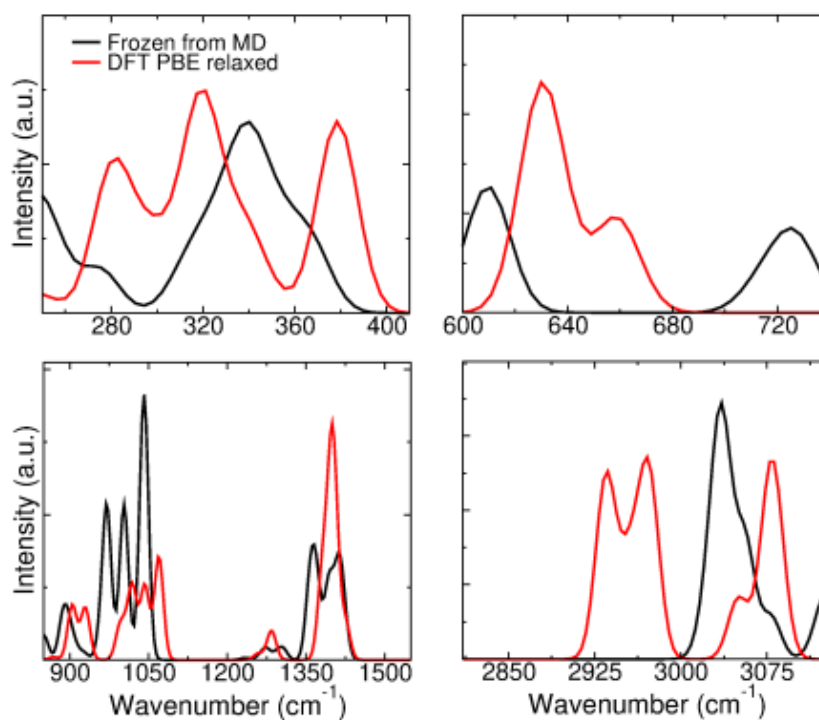


Figure 12: Theoretical Raman spectra obtained by orca_mapspc tool with a Gaussian width factor of 20 using the PBE relaxed structures from the DFT calculations and the frozen structures from the MD trajectories.

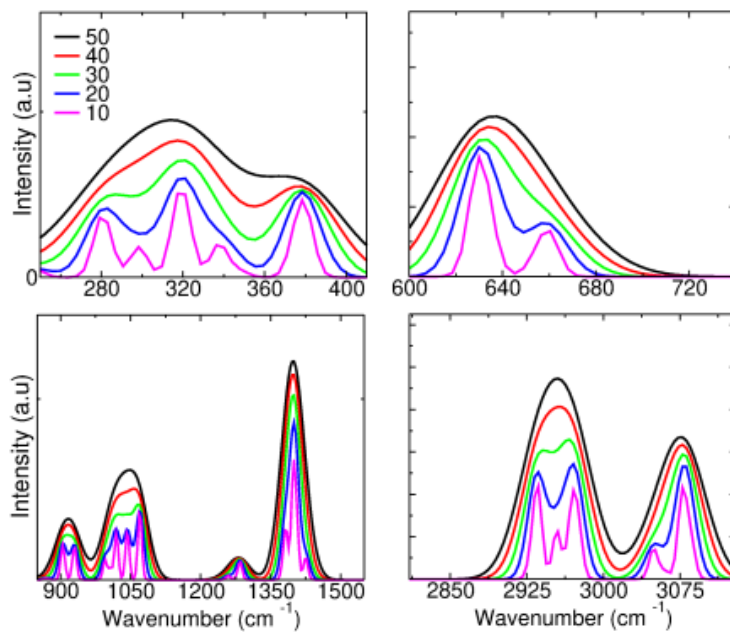


Figure 13: Theoretical Raman spectra for the PBE relaxed structures with different Gaussian width factors for the spectra plots obtained by orca_mapspc tool.

Table 18: Atomic coordinates (\AA) for the molecular cluster (frozen structure from the MD simulation) used in the theoretical Raman spectra.

Element	x	y	z
Li	0.000	0.000	0.000
H	-0.800	1.720	2.990
H	2.680	4.080	2.730
H	3.270	2.880	1.390
H	2.700	2.370	3.000
O	0.990	1.740	0.660
S	0.980	2.830	1.720

Continued on next page

C	-4.410	0.900	0.530
C	-2.480	2.620	-0.010
H	-4.940	0.380	1.320
H	-4.330	0.230	-0.330
H	-1.560	3.140	0.260
H	-2.390	2.310	-1.050
S	-2.800	1.290	1.120
S	-0.180	-0.360	-3.140
H	-0.690	-2.500	-2.190
O	-0.770	0.340	-1.900
H	-1.830	-2.030	-3.560
H	-0.610	1.180	-4.870
H	-1.150	-0.450	-5.340
H	-3.310	3.320	0.110
O	-1.940	0.140	0.600
H	0.170	2.780	3.910
H	0.810	1.170	3.390
C	-1.170	0.300	-4.550
C	0.240	2.050	3.100
H	-0.160	-2.600	-3.780
H	-4.930	1.830	0.280
C	2.610	3.120	2.220
Br	1.220	-1.710	0.530
C	-0.820	-2.010	-3.150
H	-2.160	0.640	-4.240

References

- 1 Kullmer, C. N. P.; Ta, D.; Chen, C. Y.; Cieker, C. J.; Annunziata, O.; Dzyuba, S. V. Hexadecyl-Containing Organic Salts as Novel Organogelators for Ionic, Eutectic, and Molecular Liquids. *ACS Omega* **2019**, 4, 9400–9406, DOI: [10.1021/acsomega.9b00038](https://doi.org/10.1021/acsomega.9b00038).
- 2 Binnemans, K. Ionic Liquid Crystals. *Chemical Reviews* **2005**, 105, 4148–4204, DOI: [10.1021/cr0400919](https://doi.org/10.1021/cr0400919).
- 3 Bousrez, G.; Renier, O.; Adranno, B.; Smetana, V.; Mudring, A.-V. Ionic Liquid-Based Dye-Sensitized Solar Cells—Insights into Electrolyte and Redox Mediator Design. *ACS Sustain. Chem. Eng.* **2021**, 9, 8107–8114, DOI: [10.1021/acssuschemeng.1c01057](https://doi.org/10.1021/acssuschemeng.1c01057).

- 4 Abraham, M. J.; Murtola, T.; Schulz, R.; Páll, S.; Smith, J. C.; Hess, B.; Lindahl, E. GROMACS: High performance molecular simulations through multi-level parallelism from laptops to supercomputers. *SoftwareX* **2015**, 1-2, 19–25, DOI: [10.1016/j.softx.2015.06.001](https://doi.org/10.1016/j.softx.2015.06.001).
- 5 Jorgensen, W. L.; Maxwell, D. S.; Tirado-Rives, J. Development and Testing of the OPLS All-Atom Force Field on Conformational Energetics and Properties of Organic Liquids. *J. Am. Chem. Soc.* **1996**, 118, 11225–11236, DOI: [10.1021/ja9621760](https://doi.org/10.1021/ja9621760).
- 6 Strader, M. L.; Feller, S. E. A Flexible All-Atom Model of Dimethyl Sulfoxide for Molecular Dynamics Simulations. *J. Phys. Chem. A* **2002**, 106, 1074–1080, DOI: [10.1021/jp013658n](https://doi.org/10.1021/jp013658n).
- 7 Doherty, B.; Zhong, X.; Gathiaka, S.; Li, B.; Acevedo, O. Revisiting OPLS Force Field Parameters for Ionic Liquid Simulations. *J. Chem. Theo. Comput.* **2017**, 13, 6131–6135, DOI: [10.1021/acs.jctc.7b00520](https://doi.org/10.1021/acs.jctc.7b00520).
- 8 Bernardes, C. E. S.; Joseph, A. Evaluation of the OPLS-AA Force Field for the Study of Structural and Energetic Aspects of Molecular Organic Crystals. *J. Phys. Chem. A* **2015**, 119, 3023–3034, DOI: [10.1021/jp512349r](https://doi.org/10.1021/jp512349r).
- 9 Acevedo, O. Ionic liquid force field parameters (OPLS-2009IL and OPLS-VSIL). <https://github.com/orlandoacevedo/IL>.
- 10 Vicent-Luna, J. M.; Azaceta, E.; Hamad, S.; Ortiz-Roldán, J. M.; Tena-Zaera, R.; Calero, S.; Anta, J. A. Molecular Dynamics Analysis of Charge Transport in Ionic-Liquid Electrolytes Containing Added Salt with Mono, Di, and Trivalent Metal Cations. *ChemPhysChem* **2018**, 19, 1665–1673, DOI: [10.1002/cphc.201701326](https://doi.org/10.1002/cphc.201701326).
- 11 Thompson, M. W.; Matsumoto, R.; Sacci, R. L.; Sanders, N. C.; Cummings, P. T. Scalable Screening of Soft Matter: A Case Study of Mixtures of Ionic Liquids and Organic Solvents. *J. Phys. Chem. B* **2019**, 123, 1340–1347, DOI: [10.1021/acs.jpcc.8b11527](https://doi.org/10.1021/acs.jpcc.8b11527).
- 12 Matsumoto, R.; Thompson, M. W.; Cummings, P. T. Ion Pairing Controls Physical Properties of Ionic Liquid-Solvent Mixtures. *J. Phys. Chem. B* **2019**, 123, 9944–9955, DOI: [10.1021/acs.jpcc.9b08509](https://doi.org/10.1021/acs.jpcc.9b08509).
- 13 Martínez, L.; Andrade, R.; Birgin, E. G.; Martínez, J. M. PACKMOL: A package for building initial configurations for molecular dynamics simulations. *J. Comp. Chem.* **2009**, 30, 2157–2164, DOI: [10.1002/jcc.21224](https://doi.org/10.1002/jcc.21224).
- 14 Garca-Coln, L. S.; del Castillo, L. F.; Goldstein, P. Theoretical basis for the Vogel-Fulcher-Tammann equation. *Phys. Rev. B* **1989**, 40, 7040–7044, DOI: [10.1103/physrevb.40.7040](https://doi.org/10.1103/physrevb.40.7040).

4.2. Investigation of the Ionic Liquid Crystal-Based Electrolyte in the Performance of Li-O₂ Batteries

Multi-functional Imidazolium-Based Ionic Liquid Crystal with Redox Mediator Properties for Li-O₂ Batteries *

Letícia M. S. Barros,[†] Chayene G. Anchieta,[†] Thayane C. M. Nepel,[†] Tuanan C. Lourenço,[‡] Júlia P. O. Júlio,[†] Juarez L. F. Da Silva,[‡] Gustavo Doubek,[†] and Rubens Maciel Filho[†]

[†]*School of Chemical Engineering, University of Campinas, Campinas 13083-852, Brazil*

[‡]*São Carlos Institute of Chemistry, University of São Paulo, P.O. Box 780, 13560-970, São Carlos, São Paulo, Brazil*

E-mail: leticia.barros94@gmail.com; chayeneanchieta@gmail.com; thayanecarpanedo@gmail.com; lourenco.tuanan@gmail.com; bruno.aurelio@hotmail.com; julia_paula@outlook.com.br; juarez_dasilva@iqsc.usp.br; doubek@feq.unicamp.br; rmaciel@unicamp.br;

Abstract

The promising technology of Li-O₂ batteries, which have a great energy density, still faces some challenges related to electrolyte stability. To suppress electrochemical issues, the use of additives, such as ionic liquids and redox mediators, have been proposed to enhance the cell performance. In this sense, we propose, for the first time, the use of a multi-functional ionic liquid crystal (ILC), [C₁₆mim][Br], which combines structural organisation properties, due to the long alkyl chain connected to the imidazolium ring, as well as, redox mediator function, due to the [Br]⁻ anion, as additive for aprotic electrolyte. Different concentrations of the proposed additive were investigated and the optimum composition defined. We found an efficient reduction in the charge overpotentials as more ILC was dissolved in the electrolyte, because more [Br]⁻ was available to react with the Li₂O₂ discharge product, even so, higher compositions of [C₁₆mim][Br] did not guarantee a better cycling performance, which was strongly affected by the structural property and the viscosity of the system. At a certain concentration, organised structures are formed, enhancing the ionic and molecular transport and improving the cell cyclability, however, this effect competes with the high viscosity and the great number of species present in the system. This study raises a new perspective in the batteries field and could be explored for different devices.

Keywords: Li-O₂ batteries, ionic liquid, ionic liquid crystal, redox mediator.

* Paper with writing in progress

1 Introduction

Li-O₂ batteries are an interesting technology that could contribute to attend the global demand of energy due to their impressive specific capacity. However, there is still many challenges that need to be overcome for the complete development of this device.^{1,2} Non-aqueous electrolytes, generally based in DMSO and glyme-based solvents, are the most studied for this kind of technology, because of their superior ionic transport and conductivity compared to solid electrolytes.³ However, their instability is a major issue, since they have a limited electrochemical window and can suffer from electrochemical and chemical attack during the battery operation.^{2,4} During discharge, Li₂O₂ is the main product expected to be formed electrochemically, through a reaction between Li⁺ with the oxygen reduced from an oxygen reduction reaction (ORR) process. This discharge product is reversible and oxidizes to its original form during the cell charge, in which oxygen evolves through an oxygen evolution reaction (OER) mechanism. According to Nernst equation, the standard potential for Li₂O₂ formation/decomposition is at 2.96 V Li/Li⁺.⁵ However, this process is not ideal, so different potentials are reached during the practical cell operation, especially at recharge, which high overpotentials are necessary for Li₂O₂ decomposition.³ These high overpotentials cause the solvent attack,⁶ poisoning the electrolyte and leading to the formation of side products, which degrade the unprotected lithium anode and block the cathode's pores, causing the cathode passivation and a poor cell performance.⁷

Much effort has been devoted in the scientific field to suppress the electrolyte issues, especially through the use of additives, which could improve the system operation and guarantee a longer cycle life. The application of ionic liquids (ILs) and redox mediators (RMs) are two pragmatic examples that could contribute to the electrolyte stability. ILs are salts basically composed by ions, which have singular features that are attractive for electrolytes use, such as almost negligible vapour pressure, which minimize leakage issues, wide thermal, electrochemical, and chemical stabilities. Different cationic groups, such as imidazolium,⁸ pyrrolidinium,⁹ piperidinium,¹⁰ etc., have been explored in the battery field. They can be used in mixtures with organic solvents to boost the cell performance and different properties can be obtained for varying the cationic groups and the size of their alkyl chain side.

As for redox mediators, they are soluble catalysts that are employed in non-aqueous systems to enhance the cell cyclability. During the cell charge, RMs are the first specie to oxidize, providing electrons to the cathode side, reaching their oxidation mode. Then, the oxidized RMs react with the discharge specie Li₂O₂, providing its chemical oxidation, while RMs return to their reduced form.^{11, 18} It is important to note that redox potentials of RMs are higher than the theoretical standard potential (2.96 V Li/Li⁺) for Li₂O₂ formation/degradation, but lower than the potentials reached in the practical cell rechargeability. It means that using RMs allow the reduction in the charge overpotentials, because the cell OER occurs at potentials close to redox potentials of RMs, with a consequent decrease in

parallel reactions and formation of undesirable products. So RMs prolong the battery cycling lifetime.^{6, 11, 13}

In view of the various benefits associated with IL and RMs use for Li-O₂ cell stability, arises the proposal for combining the properties of both additives into non-aqueous electrolytes, thus, different authors have found interesting results for the simultaneous use of both materials. Rastegar *et al.*,¹⁴ found a synergy when adding InBr₃ or InI₃ RMs into DMSO/[EMIM][BF₄]/LiTFSI electrolyte. This hybrid system delivered impressive cyclability of 600 and 450 cycles for InBr₃ and InI₃, respectively, when operated at a current density of 1 A g⁻¹. The bromide and iodide halides offered effective redox properties, reducing the charge overpotentials to values close to 3.5 V Li/Li⁺ and maintaining a stable charge plateau for the first 150 cycles in the case of InBr₃. In addition, it was found that the specie In³⁺ reacted with the lithium anode, creating a protective solid electrolyte interface (SEI) layer that avoided its corrosion. Li and co-workers also observed a synergy between RMs and ILs,¹⁵ by adding different concentrations of DMPII, 1,2-dimethyl-3-propylimidazolium iodide, into TEGDME/LiTFSI electrolyte. DMPII is an ionic liquid whose anionic side, the iodide anion, acts as redox mediator. The system showed a stable reversibility, with charge potentials close to 3.6 V and a long cyclability of 438 cycles for a capacity limited to 500 mAh g⁻¹ and a current density of 200 mA g⁻¹.

In this aspect of combining IL with RM properties to boost the Li-O₂ cell stability, we propose, for the first time, the use of a long alkyl chain imidazolium-based IL additive with redox properties for a DMSO-based electrolyte. The material selected, [C₁₆mim][Br] is a solid at ambient temperature, which possesses properties of ionic liquids with liquid crystals, due to the 16 carbons in the alkyl chain connected to the imidazolium cation, so it receives the denomination of ionic liquid crystal (ILC).¹⁶ ILCs have the ability of forming organized structures when dissolved in a solvent at a certain concentration.^{17,18} We have showed elsewhere that this effect enhances the ionic conductivity, because nanochannels are created for the ionic transport. In addition, the bromide anion was used as RM to reduce the charge overpotentials and enhance the cell cyclability. Therefore, different concentrations of this multi-functional ILC were tested into the performance of Li-O₂ batteries. We confirmed the RM effect of the proposed material and evaluated how the concentration affected the specific discharge capacity. We determined the optimum ILC concentration, and proved that this material could retard the cell failure, even so, we could not prevent the system attack, as observed from the products formed through the carbon cathode characterization. We also found that despite the mentioned properties, some difficulty was faced for the cell cyclability at intermediate and high concentrations, which were discussed through the text. This study introduces a new perspective suggesting the use of long alkyl chain electrolytes in aprotic systems, however, deeper investigation is still necessary, associated with more advanced techniques.

2 Methodology

2.1 Materials

The ionic liquid crystal (ILC) 1-hexadecyl-3-methylimidazolium bromide, $[\text{C}_{16}\text{mim}][\text{Br}]$, was synthesised via a quaternization route, using for the compounds: 1-bromohexane ($\text{CH}_3(\text{CH}_2)_5\text{Br}$, 98 %) and 1-methylimidazole ($\text{C}_4\text{H}_6\text{N}_2$, $\geq 99\%$), purchased from Sigma Aldrich, and ethyl Acetate ($\text{CH}_3\text{COOC}_2\text{H}_5$, 100 %), purchased from Synth. A yield of 85% was obtained. Dimethyl sulfoxide (DMSO anhydrous, $\geq 99.9\%$) and Lithium perchlorate (LiClO_4 , 99.99 %) were used for the electrolyte preparation and were purchased from Sigma-Aldrich. Toray carbon paper 060, commercial carbon nanotube (CNT CO. LTD), isopropanol ($\text{C}_3\text{H}_8\text{O}$, $> 99.5\%$ from Synth), NafionTM (20 wt%, Sigma Aldrich), Lithium discs (99.99%, Tob Machine) and glass fiber (GF50/A, HNM).

2.2 Electrolyte and Cathode Preparation

After the $[\text{C}_{16}\text{mim}][\text{Br}]$ synthesis, the material was left in a vacuum desiccator at 0.5 bar for 24 h to remove water remains before being transferred to a glovebox with Argon atmosphere (MBRAUN-LABstar Workstation). To avoid the presence of contaminants (such as water and O_2), the electrolyte preparation was performed inside the glovebox. Molecular sieves were used to dry the DMSO for 24h. The electrolyte was prepared dissolving different molar concentrations of $[\text{C}_{16}\text{mim}][\text{Br}]$ ILC additive into DMSO/ LiClO_4 0.100 M electrolyte. The electrolyte compositions are presented in Table 1 and the molecular structure of the materials used in the electrolyte are illustrated in Figure 1. The minimum ILC concentration of 0.05 M was chosen based on the concentration of LiBr generally used as redox mediator (RM) in aprotic systems^{13, 19, 20} while the maximum 3.369 M ILC was based on the $[\text{C}_{16}\text{mim}][\text{Br}]$ saturation into DMSO, determined experimentally. Neat electrolyte (0 M $[\text{C}_{16}\text{mim}][\text{Br}]$) was also prepared for comparing the results.

Table 1. Composition of Electrolytes used in this Study.

Electrolyte Composition	Abbreviation
DMSO / LiClO_4 0.100 M	0 M ILC
DMSO / LiClO_4 0.100 M / $[\text{C}_{16}\text{mim}][\text{Br}]$ 0.050 M	0.050 M ILC
DMSO / LiClO_4 0.100 M / $[\text{C}_{16}\text{mim}][\text{Br}]$ 0.500 M	0.500 M ILC
DMSO / LiClO_4 0.100 M / $[\text{C}_{16}\text{mim}][\text{Br}]$ 1.456 M	1.456 M ILC
DMSO / LiClO_4 0.100 M / $[\text{C}_{16}\text{mim}][\text{Br}]$ 3.369 M	3.369 M ILC

As for the cathode preparation, discs of carbon paper were cut with a 16 mm diameter and used as substrate, it was coated with a CNT-based catalytic ink. The methodology for the catalyst preparation

was reported elsewhere. Briefly, 25 mg of CNT, 4 mL of distilled water, 1 mL of isopropanol and 70 μL of NafionTM were homogenised by an ultrasonic Sonicator (Eco-Sonics), then a 1 mL aliquot of this mixture was diluted into 400 μL of isopropanol with the Sonicator support. In each side of the carbon paper substrate, 28 μL of the resulting ink was applied, then the electrodes were dried in a vacuum desiccator for 24 h. Then, they were weighted by an analytical balance and the active material mass was calculated, varying from 0.3 to 0.4 mg for each cathode. The prepared electrodes were transferred to the Argon-filled glovebox.

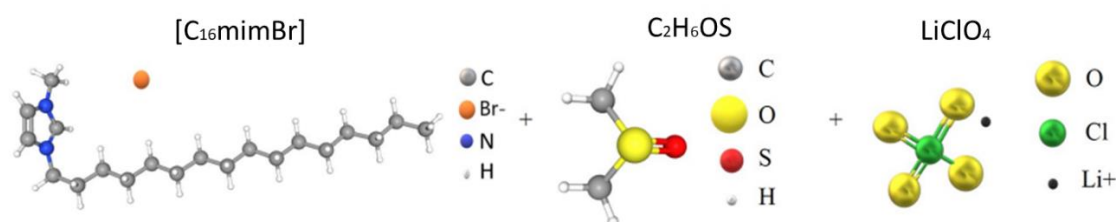


Figure 1. Molecular structure of compounds used for the electrolyte preparation, $[\text{C}_{16}\text{mim}][\text{Br}]$, DMSO ($\text{C}_2\text{H}_6\text{OS}$) and LiClO_4 , respectively.

2.3 Cell Assembly and Electrochemical Tests

Deep Discharge tests were conducted to evaluate the specific discharge capacity of the Li-O₂ battery. The cell assembly was performed inside the argon-filled glovebox using a homemade Swagelok cell configuration. Discs of lithium metal were used as the anode and the carbon paper coated with CNT was the cathode. A glassfiber membrane wetted with 100 μL electrolyte was placed between the electrodes to avoid their contact. After cell assembling, it was left inside the glovebox for three days for stabilization, then removed for the experiments. Chronopotentiometry technique was applied using a potentiostat Multi Autolab/M204. The batteries worked with O₂ at a pressure of 3 bar in a closed system. The applied current was 50 μA and the cut-off discharge potential was set at 2.2 V. After these tests, the gravimetric capacity of each cell was calculated from equation 1, in which, the applied current was considered in mA, the total operation time in hours, and the mass of the active material (the CNT ink) in grams.

$$\text{Gravimetric capacity} \left(\frac{\text{mAh}}{\text{g}} \right) = \frac{\text{current (mA)} \times \text{time (h)}}{\text{Mass of active material (g)}} \quad (1)$$

Cyclic voltammetry (CV) tests were performed under argon inert atmosphere to validate the redox function of $[\text{C}_{16}\text{mim}][\text{Br}]$ ILC, property attributed to the bromide anion. A homemade three-electrode cell constituted by a platinum counter electrode, a silver wire as quasi-reference and a carbon glass

with a CNT ink as working electrode, was used in these tests. The cell was assembled inside the argon-filled glovebox. Thirty-two millilitres of DMSO were used for each concentration with 0.100 M LiClO₄ supporting electrolyte. Neat electrolyte (0 M ILC) was used as a blank reference, a second electrolyte with 0.500 M ILC was prepared, in which 0.500 M is the maximum ILC concentration that can be used in the three-electrode cell without reaching the overload mode, and in the last condition 0.500 M LiBr was used to compare its redox peaks to those of [C₁₆mim][Br]. A 50 mV/s scan rate was applied in a potentiostat Multi Autolab/M204 for a voltage window from 2 to 5 V vs Li/Li⁺. For the cycling tests, the cell assembly was similar to that explained for deep tests. Also using the Multi Autolab/M204 potentiostat, a O₂ pressure of 3 bar and 50 μA current, the cut-off potential was set at 2.2 V/4.5 and a fixed capacity of 1000 mAh/g was used.

2.4 Characterization

After the electrochemical tests, the cathodes were removed from the battery and characterised through Raman and Scanning Electron Microscopy (FESEM) techniques. For the Raman analysis, a Renishaw Spectrometer equipment was used with a 633 nm wavenumber, 1200 l/mm diffraction grating in a scan range from 200 to 1700 cm⁻¹. The analysis was conducted using 10% laser power, 80 sec exposure time and 5 accumulations. Different chemical species and molecular interactions were identified based on the characteristic peaks of each material. As for the FESEM measurements, images of the surface of the cathodes were obtained through a Thermoscientific Quattro S equipment with an Everhart Thornley Detector (ETD), which was set with a work distance (WD) of 10 mm, 10 kv beam power, 3.0 spot and varying magnifications.

3 Results and Discussion

[C₁₆mim][Br] material was chosen as additive for the aprotic electrolyte DMSO/LiClO₄ 0.100 M due to its multi-functional features of ionic liquid crystal, which has the properties of conventional ionic liquids combined to the capability of forming well-organised structures, attributed to the long alkyl chain of the imidazolium cation [C₁₆mim]⁺, as well as the redox mediator (RM) effect, due to the anion [Br]⁻. Therefore, different concentrations of the synthesised material were tested into the aprotic electrolyte, varying from 0.05 M, corresponding to the amount of the RM LiBr generally used in aprotic systems found in literature,^{13, 19, 20} up to 3.369 M, which is the saturation point of the ILC into the DMSO solvent at ambient temperature. It is important to note that this is the first study of an ILC with redox properties as additive for aprotic electrolytes in Li-O₂ batteries.

3.1 Electrochemical Performance

First, deep discharge tests were performed varying the $[C_{16}mim][Br]$ concentration to evaluate the influence of the ILC addition into the battery discharge capacity (mAh/g), which was determined according to equation 1 and the graph plotted in Figure 2 a). We observe that, in general, the specific capacity was not improved with the ILC addition, except for 0.050 M ILC, which presented a better capacity when compared to the neat electrolyte (0 M ILC). Increasing the concentration to 0.500 M ILC, the capacity value decayed considerably, which may be associated to the structural function of the ILC studied (Figure 2 c) We reported elsewhere a study of the electrochemical, transport and structural properties of the proposed electrolyte at varying ILC concentrations and found that due to the crystal liquid features of the $[C_{16}mim]^+$ cation, it interacts with the DMSO molecules, forming aggregates, which grow and form structures at a minimum ILC concentration. However, at 0.500 M ILC, a large number of aggregates with undefined structures are present in the system (Figure 2 c)), which could affect the electrochemical performance of the Li-O₂ battery. From Figure 2 a), we can observe that this great number of aggregates hamper the cell discharge potentials, reaching values lower than 2.7 V Li/Li⁺, which means that the electrolyte is more prone to form undesirable side reactions at 0.500 M ILC, limiting the cell capacity. Deep repetitions for 0.050, 0.500 and 3.369 M ILC are shown in the supporting information, SI 1.

Increasing the concentration to 1.456 M ILC, the discharge capacity raises again, because the aggregates become bigger and organise themselves into well-defined structures, charge confinement, as proposed in Figure 1 c), which enhances a better ionic transport than 0.500 M ILC. Despite the 1.456 M ILC concentration delivered a lower capacity than 0 M ILC (14,855 mAh/g vs 18,772 mAh/g, respectively), the total time that the cell with 1.456 M ILC took to discharge was slightly lower than the cell with 0 M ILC (125 h and 135 h, respectively), and the considerable difference in the capacity values is due to the variation in the mass of active material CNT between the cathodes used for each composition.

At 3.369 M ILC the molecular arrangement is also well-defined, but the lowest capacity is reached because there is less free DMSO molecules available in the system, the electrolyte viscosity is considerably increased while the ionic conductivity decreases in this composition, resulting in higher charge transport resistance²¹ and competing with the crystal liquid function. In addition, the electrolyte is saturated, which means that a small variation in temperature during the cell operation could lead to the ILC precipitation and accumulation at the electrodes, as explained later in the characterization section.

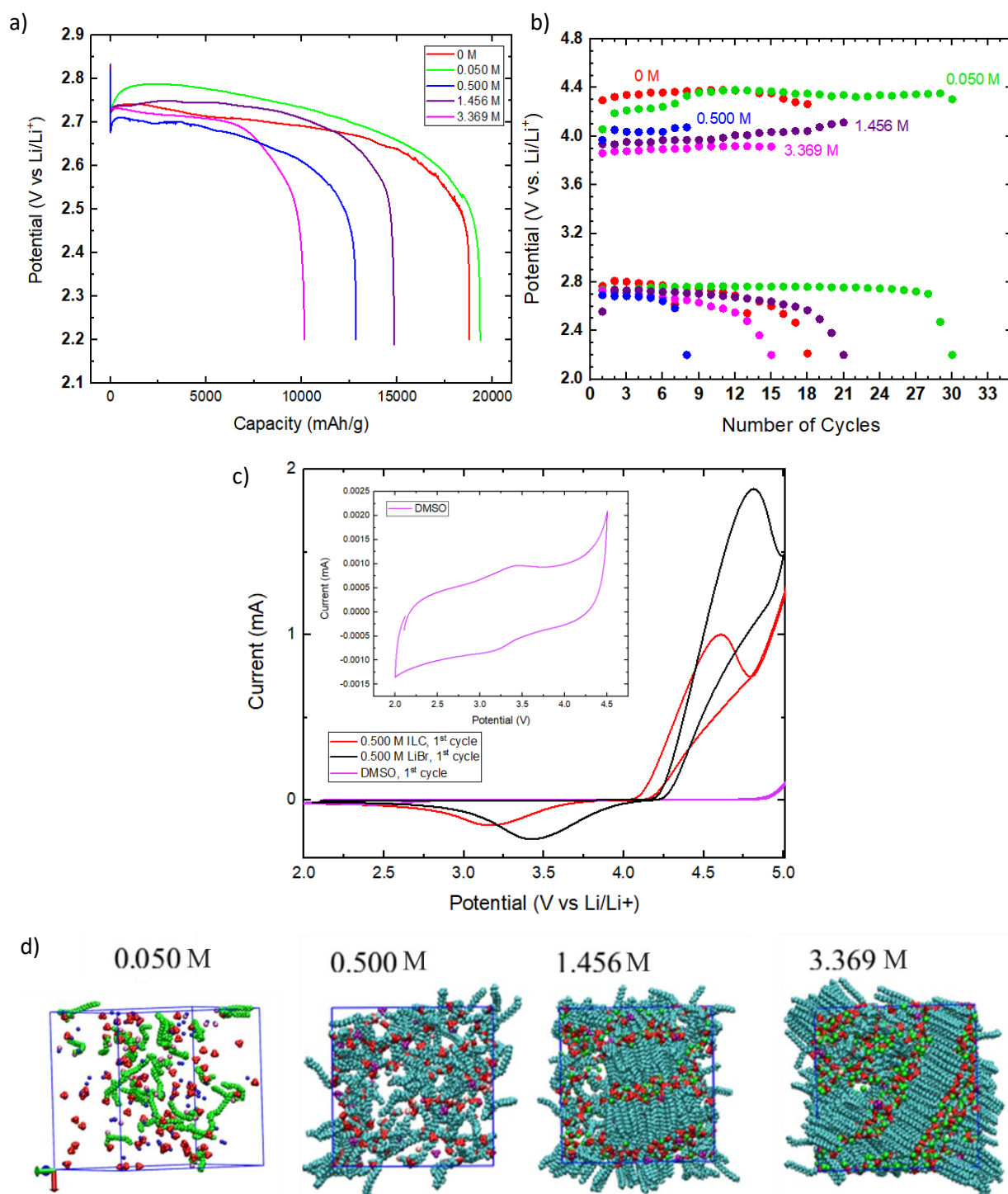
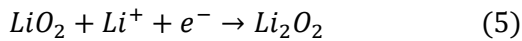
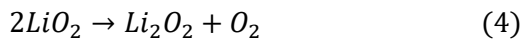
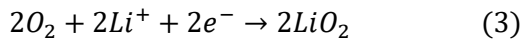
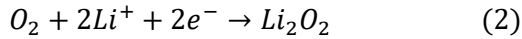


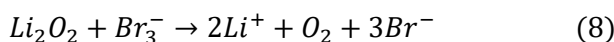
Figure 2. a) Specific discharge capacity and b) cycling profiles of Li-O₂ batteries using DMSO/LiClO₄ 0.100 M systems with different concentrations of the [C₁₆mim][Br] additive, varying from neat (0 M ILC) to saturated (3.369 M ILC) electrolytes at a current density of 23 $\mu\text{A}/\text{cm}^2$. c) Cyclic Voltammetry (50 mV/s) tests of DMSO/0.100 M LiClO₄ (lilac), 0.500 M LiBr/DMSO/0.100 M LiClO₄ (black) and 0.500 M ILC/DMSO/0.100 M LiClO₄ (red) under an argon atmosphere. Inset: CV of DMSO/0.100 M LiClO₄ in the potential window of DMSO from 2 to 4.5 V Li/Li⁺. d) Ionic and Molecular arrangement of the [C₁₆mim][Br] into the electrolyte with varying concentrations. Green, red, blue and pink are [C₁₆mim]⁺, [ClO₄]⁻, Li⁺ and [Br]⁻, respectively.

As for Figure 2 b), it shows the cycling tests of Li-O₂ batteries with different compositions of the [C₁₆mim][Br] additive. These tests were conducted to evaluate the additive effect into the cell lifetime. Traditionally, the main product Li₂O₂ is electrochemically formed during discharge, in the oxygen reduction reaction (ORR), according to the possible mechanisms presented in equations 2 to 5. This product is reversible and decomposed during the cell charge, in the oxygen evolution reaction (OER).²²



However, during the cell recharge, high overpotentials, usually close to 4.5 V Li/Li⁺, are necessary for the Li₂O₂ degradation, which could decompose the electrodes and electrolyte, causing the formation of side products until the cell death.^{12, 14} In the case of DMSO solvent, its degradation is reported to initiate at potentials over 4.2 V Li/Li⁺ (see inset Figure 2 c)).²³ Therefore, the use of the [C₁₆mim][Br] ILC is also important because it can act in the cell reversibility due to its redox mediator function, attributed to the [Br]⁻ anion.

Before interpreting the cycling results, it is important to validate the redox ability of the [C₁₆mim][Br] additive, which was showed in Figure 2 c) through CV tests in an inert atmosphere. In literature, RMs are used to reduce the charge and/or discharge overpotentials, enhancing the electrode and electrolyte stability and prolonging the battery operation time. In the case of [Br]⁻, it acts in the cell charge, forming electrochemically two reversible redox couples Br⁻/Br₃⁻ and Br₃⁻/Br₂, as indicated in equations 6 and 7, respectively. During the operation of Li-O₂ cells, it is important to note that the first Br⁻/Br₃⁻ redox couple is more desirable, since the Br₂ specie formed from the Br₃⁻ oxidation is highly reactive, degrading the electrolyte and electrodes, which compromise the cell cyclability. The species [Br₃]⁻ formed in the cell charge, eq. 6, oxidizes chemically the discharge product Li₂O₂ to Li⁺ and O₂, while [Br₃]⁻ is reduced back to [Br]⁻ (eq. 8).²⁴ Therefore, this process facilitates the Li₂O₂ reversibility and decreases the Li-O₂ cell charge overpotentials, because the lithium peroxide is oxidized at potential values close to the redox potentials of RMs,¹¹ reducing the system attack and prolonging the cell cyclability.



As expected from Figure 2 c), the DMSO/LiClO₄ 0.100 M electrolyte does not have redox properties, as indicated by the absence of any redox peak in the range from 2 to 5 V vs Li/Li⁺. For the other electrolytes (DMSO/ LiClO₄ 0.100 M /[C₁₆mim][Br] 0.500 M and DMSO/LiClO₄ 0.100 M/LiBr 0.500 M), the presence of redox peaks is evident, confirming that the [Br]⁻ anion present in the ILC has a RM effect which could be comparable to LiBr.²⁴ Besides, a small displacement was observed between the oxidation/reduction peaks of LiBr and [C₁₆mim][Br], probably associated with the change from Li⁺ to [C₁₆mim]⁺ cation, which affect the solvation properties of the system²⁵ and due to the strong molecular interaction of [C₁₆mim]⁺ with the DMSO solvent. In addition, we observe a higher ohmic drop for the electrolyte with LiBr, which is assigned to the higher number of ionic species in the ILC-based electrolyte and its consequent superior ionic conductivity and lower ohmic resistance.²⁶ However, this observation can only be confirmed by electrochemical impedance spectroscopy (EIS) measurements, which will be necessary to determine the resistance of both systems and correct this ohmic drop.²⁷

While the oxidation of [Br]⁻ to [Br₃]⁻ takes place at ~4.2 V vs. Li/Li⁺ for [C₁₆mim][Br] and the reduction occurs at ~3.2 V vs. Li/ Li⁺, the same [Br₃]⁻ specie is formed at ~4.1 V vs. Li/Li⁺ and reduced at ~3.4 V vs. Li/ Li⁺ when LiBr is used. The undesirable corrosive specie Br₂ was observed to be formed at potentials higher than 4.4 V for both [C₁₆mim][Br] and LiBr, indicating an advantage to the electrolyte systems since it is not easily formed during the cycling potential window. Therefore, CV tests confirmed the redox property of [C₁₆mim][Br] in an argon atmosphere, but CV under O₂ atmosphere will still be necessary for complement with the cycling tests (Figure 2 b)).

From Figure 2. b), we can see the cycling tests of Li-O₂ cell with different ILC concentrations. We observe that the neat 0 M ILC system reaches a charging potential over 4.2 V since the 1st cycle, which is the value for initiating the DMSO degradation, as indicated in the inset Figure 2 c).²³ On the other hand, even with a small addition of [C₁₆mim][Br], such as in the 0.05 M ILC concentration, the charging overpotentials were efficiently reduced to values lower than 4.2 V. Therefore, this graph evidences the effect of the redox mediator [Br]⁻ on the cell reversibility by reducing the charging overpotentials, which become lower as more ILC is added to the system. Increasing the amount of ILC means that there is more [Br]⁻ available to degrade the discharge product Li₂O₂ at lower charge overpotentials. Even so, for ILC concentrations higher than 0.500 M, the overpotential decrease becomes more discreet. This could be explained by the addition of ohmic resistance due the conductivity decrease with the ILC concentration enhancement, besides, the mass transport is compromised because of the viscosity increase. It is important to highlight that at concentrations above 1.456 M ILC, the conductivity decreases and the viscosity enhancement are more pronounced.

Despite it is common to associate the number of cycles to the discharge capacity of the battery, expecting longer cyclability for systems that present superior capacity,⁶ comparing Figures 2 a) and b), our cycling results showed a small difference in the tendency observed for deep tests. For deep analysis, the electrolyte concentrations which had the highest gravimetric discharge capacities were, as

follows: 0.050 M ILC > 0 M ILC > 1.456 M ILC > 0.050 M ILC > 3.369 M ILC. So, it could be expected lower cycling performances for high and intermediate ILC concentrations. However, the best cycling results were found for the following concentrations: 0.050 M ILC > 1.456 M ILC > 0 M ILC > 3.369 M ILC > 0.500 M ILC. Despite there is no obvious relationship between deep and cycling results and no obvious tendency for both tests, evaluating a cell performance is more complex than the simple association of these two results.

Knipping and co-workers²⁸ studied the use of ionic liquids with different group and structures into the performance of Li-O₂ cells, and found that the cell specific capacity is enhanced by the proper lithium solvation, ionic conductivity and viscosity, but other factors could affect the cyclability, such as the electrolyte stability window and its attack.

For the deep results, in fact the discharge capacity decreased for ILC concentrations higher than 1.456 M because there was a significant increase in viscosity, as shown in our previous study, since ionic liquids have a viscous nature, which reduces the ionic transport, associated to great accumulation of products on the carbon fibres, insulating them and impeding the charge transfer, as explained later in the characterization section. In addition, at intermediate 0.500 M ILC composition, the discharge capacity is limited by the great number of aggregates in the system. As for the cyclability, we suggest that the cell cycling was associated with the combination of the RM effect with the molecular and ionic organisation of the system. Compared to the neat electrolyte, the 0.050 M ILC presents the RM effect well pronounced with the efficient decrease in the charge overpotentials, combined with the ability of conventional ionic liquids of enhancing the electrochemical stability. This means that the cell could operate longer, even with the increase in the charge potentials observed over the cycles, which increased as a consequence of the small amount of Br⁻ available to oxidize and react with Li₂O₂ in the charge, causing the accumulation of non-decomposed products. At this concentration, the structural effect of [C₁₆mim]⁺ is practically negligible, because there is just the formation of small clusters in the electrolyte, as indicated by the molecular arrangement in the boxes of figure 2 d). It is important to note that the crystal liquid effect, assigned to the 16 carbons in the alkyl chain of the imidazolium ring, is more apparent from a certain ILC concentration, because by increasing its concentration, the [C₁₆mim]⁺ cation tend to self-organize forming complex structures with polar and non-polar nanodomains. A better explanation about these structures and how they affect the electrolyte properties were published by our research group elsewhere. For 0.500 M ILC concentration, there is excess of [Br]⁻ anions, which explains the considerable decrease in the charge overpotentials, however, as we can observe from figure 2 d), the amount of [C₁₆mim]⁺ cations also increases, forming bigger agglomerates with the DMSO molecules, which have undefined structures at this concentration, causing a disorder in the electrolyte. This disorder is evidenced by the low discharge potential (< 2.7 V) and the rapid decay in the discharge capacity during the cycling test.

Increasing the ILC concentration to 1.456 M, we observe that the battery performance is considerably improved, because besides the decrease in the charge overpotentials due to excess [Br]⁻,

we also have the structural effect, in which the aggregates become bigger and reorganise themselves into structures that resemble a lamellar Smectic phase (figure 2 d)). This structure works as ionic channels, enhancing the ionic conductivity and thus the cell's cyclability.

Increasing even more the ILC content until its saturation in the DMSO solvent *i.e.*, 3.369 M ILC, the lamellar structure is also observed, but the electrolyte viscosity is so high, that it competes with the ionic transport, affecting the cell cyclability and reducing its performance. In addition, since the $[\text{C}_{16}\text{mim}][\text{Br}]$ dissolved in the electrolyte is at its saturation, there is a great number of ionic species, which precipitate over the cathode during the cycles, insulating the carbon fibres more rapidly, as shown in the FESEM images, causing the decay in discharge potential until the cell death. Therefore, the best ILC concentration was observed for 0.050 M ILC, followed by the 1.456 M ILC.

3.2 Interpretation of the Cycling Profiles

As the 0.050 M and 1.456 M ILC concentration presented the best cycling performance, both graphs were plotted in Figure 3 a) and b), in order to analyse the potential change during the cell cyclability. The cycling profile of 0.500 and 3.369 M ILC compositions are available at SI 2. For Figure 3 a), it is observed that the variation in the charge potentials of 0.05 M ILC is much more pronounced than the discharge variation, but when the cell reaches its cycling limit, a rapid decay in the discharge to ~ 2.47 V is observed in the 29th cycle, losing 80% of its capacity in the 30th cycle and leading to the cell failure. In the first cycle of Fig. 3 a), a two-step oxidation is observed, with the charging potential initiating at 3.8 V vs Li/Li^+ , then rising to ~ 4.05 V vs Li/Li^+ , which was maintained for most of the charging process, indicating the Li_2O_2 oxidation at a potential close to the potential of $[\text{Br}]^-$ oxidation to $[\text{Br}_3]^-$,¹¹ in agreement with the CV tests. Then, in the final of the first charging process, the potential returns to 3.8 V because enough Li_2O_2 was decomposed to its original Li^+ and O_2 form, so at this potential $[\text{Br}_3]^-$ reduces back to $[\text{Br}]^-$, also in analogy to the CV data. These results point out that the $[\text{C}_{16}\text{mim}]^+$ cation does not affect the redox properties of the electrolyte, in agreement with Zheng *et al.*,²⁴ who investigated the use of an ionic liquid with redox properties, $[\text{MPP}]^+[\text{Br}]^-$, into TEGDME/LiTFSI electrolyte. The author confirmed the redox ability of the additive due to the bromide anion, obtaining lower charging potentials and longer cyclability.

CREMASCO *et al.*²⁰ investigated the reaction mechanism involved in the application of LiBr redox mediator into DMSO/ LiClO_4 electrolyte. Similarly, we also propose that the insulating product Li_2O_2 formed in the first discharge path is evenly distributed to the surface of the carbon electrode due to its available pore sites. For the first five cycles, charging overpotentials are lower than 4.2 V. However, due to the low concentration of $[\text{Br}]^-$ species (0.05 M ILC) dissolved in the electrolyte and due to the accumulation of discharge products that reduce the availability of vacant sites for the $[\text{Br}]^-$ oxidation to $[\text{Br}_3]^-$, the decomposition of Li_2O_2 becomes more difficult, thus higher potentials are necessary to decompose Li_2O_2 and enable the OER. Therefore, at a certain point, the charging

potentials raise to values over 4.4 V, as observed in the 8th cycle, indicating that the corrosive Br₂ species could appear, in analogy with the CV data, but further investigation is necessary. This accumulation of species could also explain the charge shifts observed over the cycles. Besides, parallel reactions can occur during the cell cyclability, leading to the formation of side products, which accumulate in the system, also causing the shifts of the discharge and charge stretches, covering the carbon fibres and clogging its pores, until a point that the concentration of products is so high that the carbon pores become totally blocked by products, impeding the charge flow³ and thus ceasing the cell operation after the 29th cycle. It is also important to note that despite some ionic liquid groups improve the anode stability by forming at its surface a stable solid electrolyte interface (SEI) layer, no stable SEI was observed for the proposed [C₁₆mim][Br] additive, as evidenced by the lithium corrosion after cell cycling (inset Figure 3 a)). Many authors attribute the SEI formation to the selection of the right Li salt^{6, 29, 30} and/or to the synergy between ILs and Li salts,^{15, 31, 32} therefore, if another salt, like LiTFSI, LiFSI, LiNO₃, etc., was added to the system, it is possible that a stable SEI would be formed.

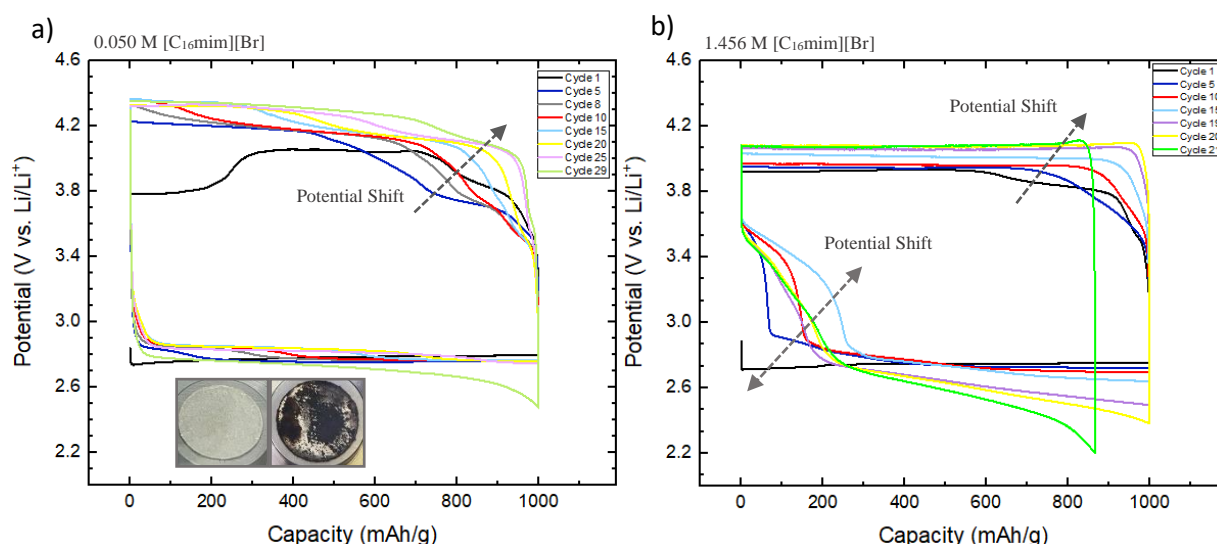


Figure 3. Cycling performance for DMSO/LiClO₄ 0.100 M electrolyte with a) 0.050 M and b) 1.456 M concentration of [C₁₆mim][Br] additive, at a current of 50 μ A and a fixed capacity of 1000 mAh/g. Inset arrows indicate the direction of the potential shift and inset figures a) show the lithium anode before and after cycling at 0.050 M ILC.

As for the 1.456 M ILC concentration (Fig. 3 b)), we have already proposed that at this composition the structural effect enhances the cell cyclability due to the formation of ionic channels that enable the ionic transport and conductivity. In addition, the great amount of [Br]⁻ diminishes considerably the charging potential, which is maintained lower than 4.2 V Li/Li⁺ over the cycles, despite of the small charge shift observed from \sim 3.9 V in the 1st cycle to \sim 4.1 V in the last. This means that it is possible that the corrosive Br₂ was not formed at 1.456 M ILC concentration and it could be

confirmed by the absence of a second charge plateau over the cycles. On the other hand, plateaus are observed during the cell discharge, as consequence to the excess $[\text{Br}_3]^-$ species which could not be totally reduced to $[\text{Br}]^-$ in the cell charge, so part of $[\text{Br}_3]^-$ was reduced during discharge.¹⁴ In addition, the great amount of $[\text{C}_{16}\text{mim}][\text{Br}]$ also impacts in the cell performance, because the system becomes much more viscous and there is a great number of species dissolved in the DMSO solvent, which compete with the structural effect. As the cell cycles, parallel reactions occur, leading to the increasing accumulation of products, and raising even more the electrolyte viscosity. This effect causes the blockage of the cathode pores, leading to a more rapid decay in the discharge potential and the consequent raise in the charge potentials, as an attempt to decompose the discharge products. In the 21st cycle, the cell reaches the cut-off discharge potential because the cathode is completely covered by product, which causes its passivation and interrupts the charge transfer. Therefore, the small addition of 0.050 M ILC is more beneficial for the overall performance of the battery, but both 0.050 M and 1.456 M ILC are better than the conventional DMSO/LiClO₄ 0.100 M electrolyte due to the unique features of $[\text{C}_{16}\text{mim}][\text{Br}]$ mentioned above.

3.3 Characterization of the Cathodes

After deep and cycling tests, the carbon electrodes were characterized via Raman and FESEM techniques. During the Li-O₂ battery operation, the main product Li₂O₂ is expected to be formed electrochemically during the cell discharge through different possible mechanisms (equations 2 to 5) and are reversible during recharge.²² However, side products can also be formed during the cell operation. Therefore, the employment of Raman Spectroscopy can serve as a basis for understanding the possible routes involved in the electrochemical tests and to identify the species formed during reactions, while FESEM is important to observe the products formed and the morphological changes in the cathode surface.³³

The characteristic bands of carbon materials are well known in literature³⁴ and were observed through Raman in our virgin cathodes (carbon paper with CNT ink, see SI 3), even so, they were not considered for the characterization of the cathodes after the electrochemical tests because we focused on the formation of products. Figure 4 a) and b) show the products formed after deep and cycling tests, respectively. It is important to note that we can barely observe the products formed for the saturated 3.369 M ILC composition (Figure 4 a) and b)), since the ILC precipitated and covered the cathodes during the cell operation, as showed later at the FESEM images. The Raman peaks correspondent to the ILC (see SI 4) are observed in both graphs for concentrations above 0.500 M ILC, because at 0.050 M ILC the amount of $[\text{C}_{16}\text{mim}][\text{Br}]$ is so small that it can barely be detected by the Raman beam. In addition, the amount of the salt LiClO₄ is also small, 0.100 M, so it can also be barely seen by the laser beam in regions close to $\sim 930\text{ cm}^{-1}$.³⁵

The pink region, ~ 250 and ~ 790 cm^{-1} correspond to the coupled vibration of Li-O₂ and the O-O stretch, respectively,^{33, 36} which are attributed to the Lithium peroxide (Li₂O₂), which can be formed directly through the electrochemical reaction between the Li⁺ cation and the O₂ specie, as indicated by equation 2,³⁷ or through other alternative mechanisms, in which the Li⁺ and the O₂ compounds form initially the intermediate LiO₂, which later reacts according to equation 3 to form Li₂O₂, or LiO₂ reacts with Li⁺, forming Li₂O₂ according to equation 4.³⁸ Despite these alternative mechanisms, no intermediate specie was observed in the Raman analysis for deep tests, so the mechanism presented in equation 2 is the one that best fits the formation of the Li₂O₂ in the deep discharge for all electrolyte compositions.

Despite the difference in the peak intensity observed for each electrolyte concentration, the Li₂O₂ product was observed for all systems in Figure 4 a) and the Li₂O₂ peaks were most intense at 1.456 M ILC, because the laser beam passed over a region rich in discharge products. We highlight that different regions of the 1.456 M ILC cathode were analysed via Raman and this high concentration of Li₂O₂ was not observed for the other measurements (Raman repetitions for deep and cycling data available at Figures SI 5 and 6), indicating that the products are not evenly distributed over the cathode, as confirmed by FESEM images (Figure 5). Besides, the peak intensity of Raman spectroscopy are related to the polarization of the products surface and their morphology,³³ which could explain the intensity variation with different concentrations of [C₁₆mim][Br]. Comparing to the cycling tests, the superoxide intermediate LiO₂ specie was observed besides the Li₂O₂ product, for 0.050 M and 3.369 M ILC at a wavenumber close to 1140 cm^{-1} , corresponding to the O-O bonding.³³ This side product is formed due to the incomplete oxidation of Li₂O₂ during cell charge and it is soluble in high donor number (DN) solvents, such as the case of DMSO.³⁹

The asterisks in the Figure 4 are assigned to the remains of the DMSO solvent, at ~ 675 and ~ 708 cm^{-1} , corresponding to the C-S symmetric and antisymmetric ligands, respectively,^{35, 40, 41} which are the most intense peaks of pure DMSO (see SI 7). DMSO was observed in deep tests for 0, 0.500 and 1.456 M ILC concentrations and also identified at a Raman measurement repetition for the 3.369 M ILC concentration, as indicated in the SI 5 figure. DMSO was identified in all cathodes used in cycling tests for different ILC concentrations.³⁸ The peaks at ~ 1083 cm^{-1} are assigned to the interaction of the DMSO molecule with the Li⁺ from LiClO₄.³⁵ The zones in green are attributed to the formation of the side product DMSO₂, which arises from the nucleophilic attack of Li₂O₂ to the DMSO solvent during discharge.^{38, 42} Note that DMSO₂ was formed in the presence of the ILC for both graphs and that [Br]⁻ is a nucleophile, so it is also possible that [C₁₆mim][Br] had an effect at the DMSO degradation. The characteristic bands of DMSO₂ were found at ~ 295 and ~ 460 cm^{-1} , corresponding to the scissoring bend of SC₂, ~ 700 and ~ 1405 cm^{-1} , corresponding to the symmetric stretching of SC₂, while the CH₃ in-plane rocking or bending is found at 1013 cm^{-1} and the CH₃ in-plane scissoring or bend is found at 1460 cm^{-1} .⁴³

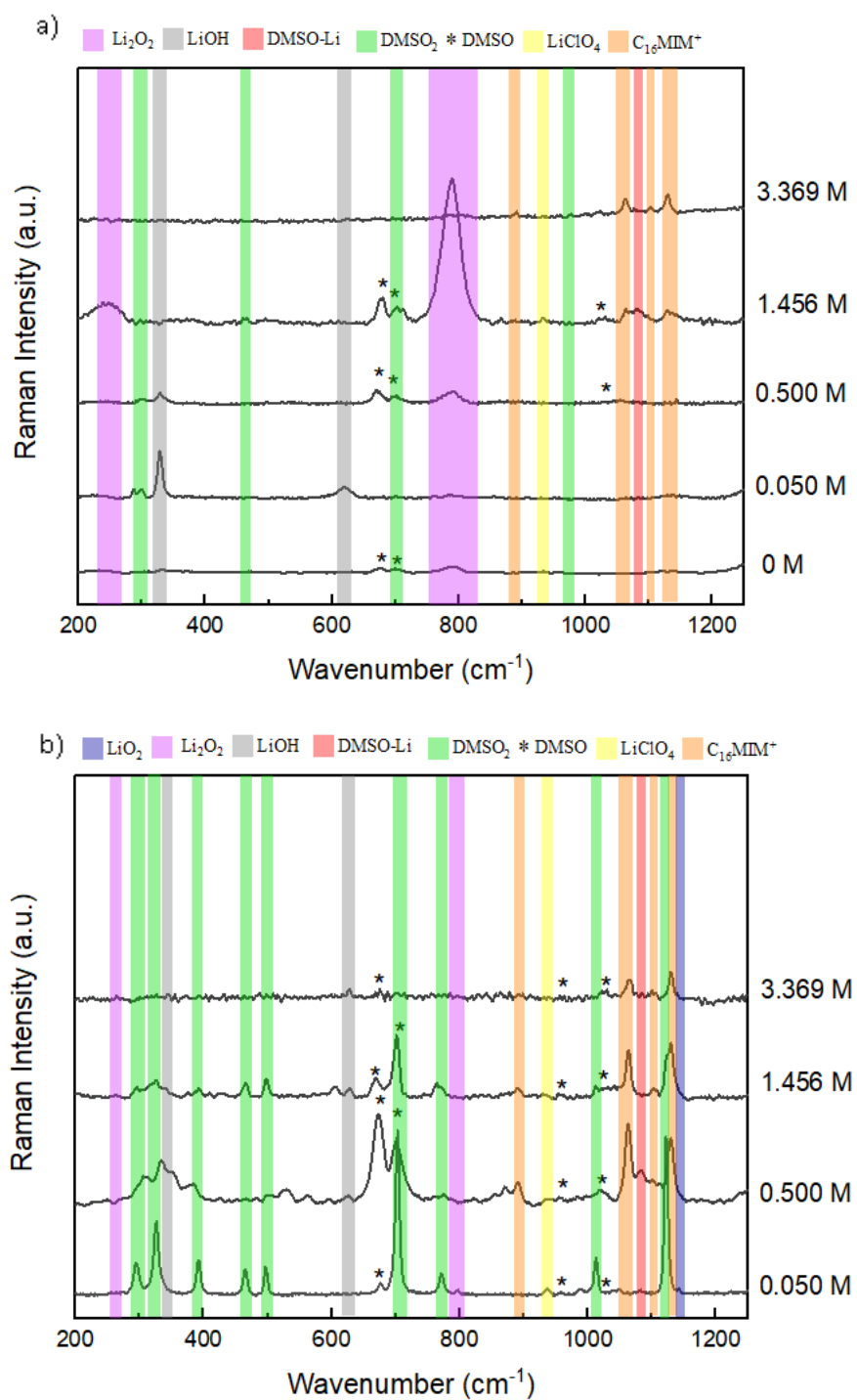


Figure 4. Raman Spectroscopy of the cathodes after use in a) deep discharge and b) cycling tests at different [C₁₆mim][Br] concentrations in DMSO/LiClO₄ 0.100 M systems.

The side product lithium hydroxide, LiOH, was only found at 0.05 M and 0.500 M ILC for deep tests and at concentrations from 0.500 M ILC for cycling tests, and for repetition of Raman measurement for 3.369 M deep and cycling (SI 5 and 6) This product arises from the reaction between

Li_2O_2 and DMSO.^{20, 38} The peaks of LiOH appear around ~ 327 and 618 cm^{-1} , which correspond to the translational vibration of the cation Li^+ and anion OH^- layers.⁴⁴

As for the FESEM technique, it was used to analyse the surface of the cathodes after deep discharge and cycling tests, being indicated in Figures 5 and 6, respectively. Different magnitudes were chosen because image quality varied with the ILC concentrations. From Figure 5, we observe the product distribution over the cathodes and the product shape with the variation in the ILC concentration. In the top left, we see the fibres of the pure carbon paper electrodes with some roughness due to the CNT ink deposition. Note that after discharge, the carbon fibres of all cathodes were covered with a layer of product, which become thicker as we raised the ILC concentration. For 0 and 0.050 M ILC the product was randomly distributed over the cathodes.

Increasing the concentration to 0.500 M ILC, a thicker layer of product was formed. For 1.456 M ILC concentration, toroidal shape particles⁴⁵ are formed, but at 3.369 M ILC concentration, we observe a tremendous change in the carbon fibres, which became totally rough due to the complete product covering. It is important to note that the ILC $[\text{C}_{16}\text{mim}][\text{Br}]$ is a solid at ambient temperature and was dissolved at its saturation point at 3.369 M concentration, so besides the formation of Li_2O_2 over the cathode, the ILC material also precipitated at the carbon surface, forming big agglomerates which deposited at the carbon's fibres as observed at the bottom right of the FESEM images. This great accumulation of products explains the low discharge capacity of the saturated electrolyte, because a layer of products was quickly formed over the fibres, causing an electrical passivation and the rapid decay in the cell potential.⁴⁶

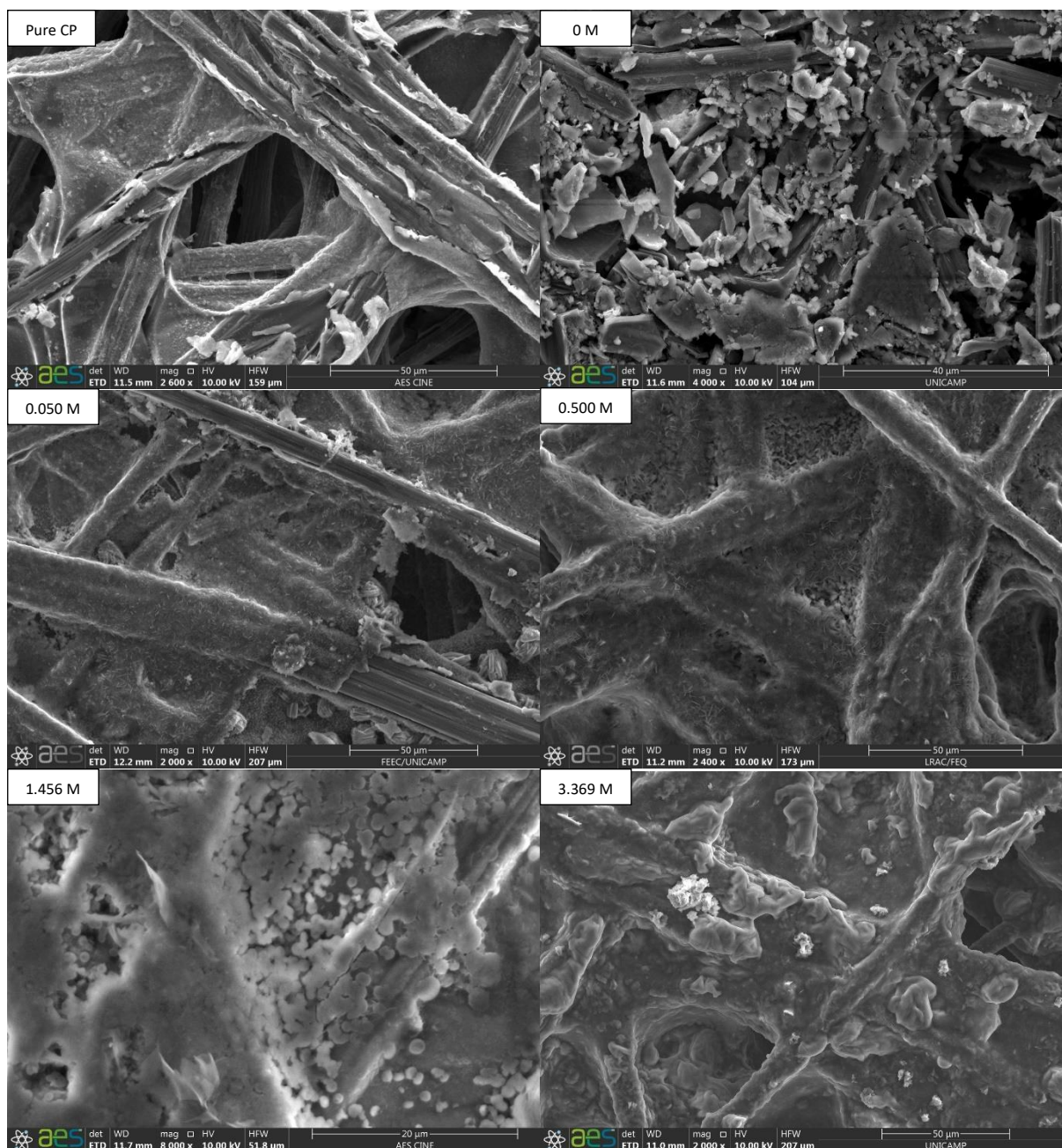


Figure 5. FESEM images at different magnitudes for the carbon paper/CNT cathodes after use in deep discharge tests at different $[C_{16}mim][Br]$ concentrations in DMSO/LiClO₄ 0.100 M systems.

As for the products formed during cycling, we can also see from SEM images of Figure 6 the change in the carbon surface when ILC is added to the electrolyte compared to pristine cathode in Figure 5. For the lowest concentration of 0.050 M ILC, we can observe a relatively small concentration of Li₂O₂ species, which were randomly distributed over the cathode, with no significant change in the carbon fibre structure. However, when more ILC is added to the electrolyte, the carbon fibres become clearly covered by products. In addition, the products morphology is totally different when cycling results are compared to the deep data at the same

concentrations, except for 3.369 M in which a great concentration of agglomerates was observed for both tests. Therefore, the cell failure has also a great association with the great accumulation of products after long battery operation.

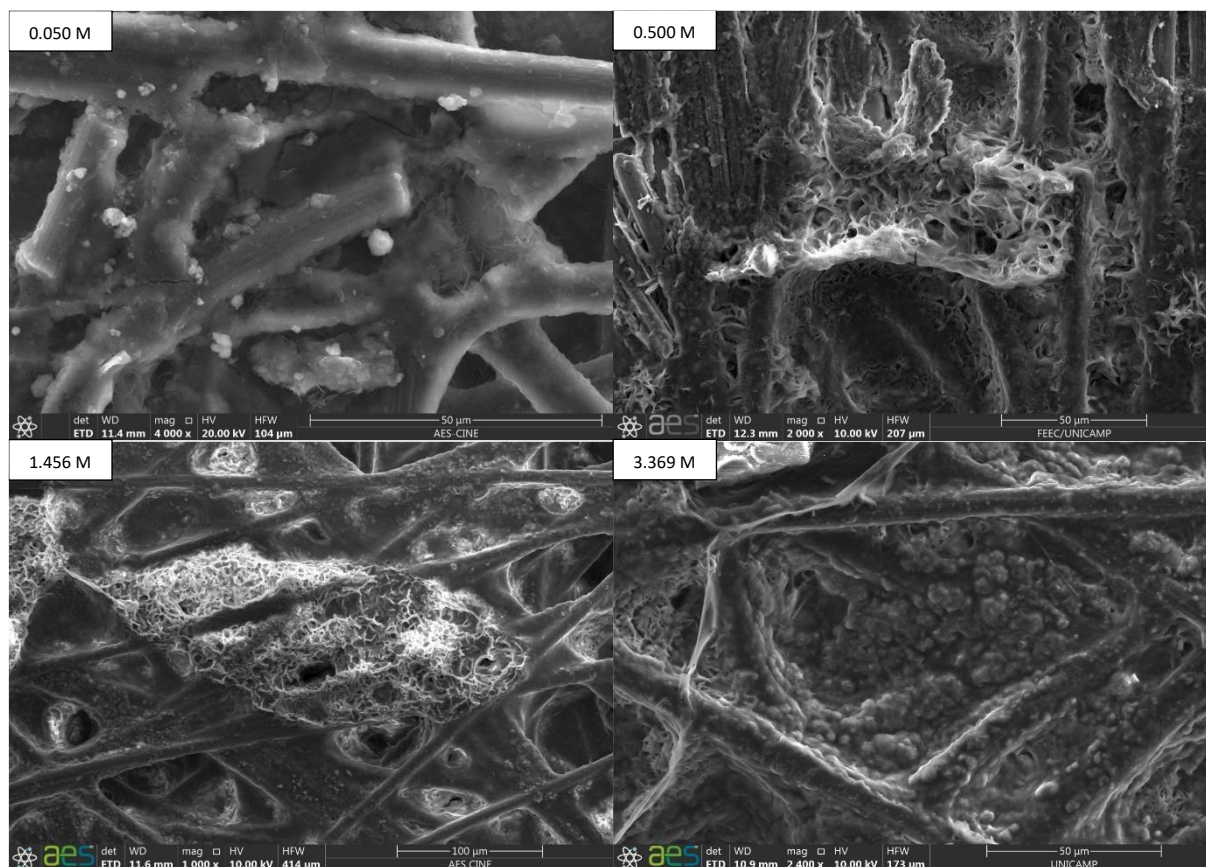


Figure 6. FESEM images at different magnitudes for the carbon paper/CNT cathodes after cycling tests at a fixed capacity of 1000 mAh/g using different $[C_{16}mim][Br]$ concentrations in DMSO/LiClO₄ 0.100 M systems.

4 Conclusion

A multifunctional ionic liquid crystal additive, $[C_{16}mim][Br]$, which combines the properties of conventional ionic liquids with structural and redox mediator properties, was first introduced into aprotic electrolyte DMSO/LiClO₄ for Li-O₂ batteries. The redox function was confirmed through CV at an inert atmosphere, with the first redox couple $[Br]^-/[Br_3]^-$ being formed close to 4.2 V vs. Li/Li⁺, while the corrosive $[Br_2]$ specie is only formed at potentials over 4.4 V Li/Li⁺, which is beneficial for the system cycling lifetime. This additive was tested in Li-O₂ cells at various concentrations to investigate how it affects the electrochemical performance of the battery.

The decrease in the charge overpotentials was clearly associated with the amount of ILC in the system, because as more ILC is dissolved in the electrolyte, more $[Br]^-$ is available to react with the

discharge product Li_2O_2 . However, poor electrochemical efficiency was reached for intermediate 0.500 M ILC composition, because at this concentration, the ILC tends to form a great number of aggregates randomly distributed in the electrolyte. As for the highest ILC concentration of 3.369 M IL, the cell efficiency is limited to the high viscosity of the system and slow dynamics, hampering the ionic transport.

The optimum concentration was found for the most diluted 0.050 M ILC, because it is less viscous, enabling the ionic and molecular mobility, joining to an efficient RM property. At 1.456 M ILC, the second better performance is achieved, with a long cell operation due to the combination of the redox property with the structural effect of ILC well pronounced, leading to the formation of molecular channels that enhance the ionic transport, however, this effect competes with the high viscosities and the great number of species in the system, which deposit on the cathode over time, causing its passivation. In summary, introducing multifunctional additives to electrolytes is an important approach to solve some issues associated with the solvent stability, but there are some inconveniences that need to be overcome. Deeper investigations are necessary to better understand the structural effect associated to other characterization techniques.

Acknowledgement The authors gratefully acknowledge support from FAPESP (São Paulo Research Foundation, Grant Numbers 2017/11631-2, 2017/11958-1, 2018/21401-7 and 2019/23681-0), Shell and the strategic importance of the support given by ANP (Brazil's National Oil, Natural Gas and Biofuels Agency) through the R&D levy regulation and also to the University of Campinas for providing resources for the experiments and University of São Paulo for providing the computational resources for the project execution. The authors acknowledge the Laboratory of Advanced Energy Storage (AES) and the Faculty of Chemical Engineering of University of Campinas. The authors acknowledge also the Laboratory of Advanced Scientific Computing (University of São Paulo) and the Department of Information Technology - Campus São Carlos, for hosting our cluster. The authors acknowledge also the National Laboratory for Scientific Computing (LNCC/MCTI, Brazil) for providing HPC resources of the SDumont supercomputer, which have contributed to the research results reported within this paper. URL: <http://sdumont.lncc.br>

Supporting Information Available

Repetition of deep data for 0.050, 0.500 and 3.369 M ILC concentrations, cycling performance of 0.500 and 3.369 M ILC, Raman of virgin carbon electrodes with CNT ink, Raman of pure $[\text{C}_{16}\text{mim}][\text{Br}]$, Raman repetition of cathodes after deep and cycling tests, Raman of Pure DMSO, FESEM images of pure $[\text{C}_{16}\text{mim}][\text{Br}]$.

References

- (1) Kraysberg, A.; Ein-Eli, Y. Review on Li-Air Batteries - Opportunities, Limitations and Perspective. *Journal of Power Sources*. Elsevier B.V. **2011**, pp 886–893. <https://doi.org/10.1016/j.jpowsour.2010.09.031>.
- (2) Balaish, M.; Kraysberg, A.; Ein-Eli, Y. A Critical Review on Lithium-Air Battery Electrolytes. *Phys. Chem. Chem. Phys.* **2014**, 16 (7), 2801–2822. <https://doi.org/10.1039/c3cp54165g>.
- (3) Lai, J.; Xing, Y.; Chen, N.; Li, L.; Wu, F.; Chen, R. Electrolytes for Rechargeable Lithium–Air Batteries. *Angew. Chemie Int. Ed.* **2020**, 59 (8), 2974–2997. <https://doi.org/10.1002/anie.201903459>.
- (4) Sharon, D.; Hirshberg, D.; Afri, M.; Frimer, A. A.; Aurbach, D. The Importance of Solvent Selection in Li-O₂ Cells. *Chem. Commun.* **2017**, 53 (22), 3269–3272. <https://doi.org/10.1039/c6cc09086a>.
- (5) Girishkumar, G.; McCloskey, B.; Luntz, A. C.; Swanson, S.; Wilcke, W. Lithium-Air Battery: Promise and Challenges. *J. Phys. Chem. Lett.* **2010**, 1 (14), 2193–2203. <https://doi.org/10.1021/jz1005384>.
- (6) Ahmadiparidari, A.; Fuladi, S.; Majidi, L.; Plunkett, S.; Sarnello, E.; Gholivand, H.; Hemmat, Z.; Rastegar, S.; Misal, S. N.; Jimenez, N.; Redfern, P. C.; Wen, J.; Li, T.; Ngo, A. T.; Khalili-Araghi, F.; Curtiss, L. A.; Salehi-Khojin, A. Enhancing the Performance of Lithium Oxygen Batteries through Combining Redox Mediating Salts with a Lithium Protecting Salt. *J. Power Sources* **2021**, 491 (229506), 1–10. <https://doi.org/10.1016/j.jpowsour.2021.229506>.
- (7) Ara, M.; Meng, T.; Nazri, G.-A.; Salley, S. O.; Ng, K. Y. S. Ternary Imidazolium-Pyrrolidinium-Based Ionic Liquid Electrolytes for Rechargeable Li-O₂ Batteries. *J. Electrochem. Soc.* **2014**, 161, 1969–1975. <https://doi.org/10.1149/2.0031414jes>.
- (8) Zeng, J.; Francia, C.; Amici, J.; Bodoardo, S.; Penazzi, N. A Highly Reversible Li-O₂ Battery Utilizing a Mixed Electrolyte and a Cathode Incorporating Co₃O₄. *R. Soc. Chem.* **2015**, 5, 83056–83064. <https://doi.org/10.1039/c5ra13483h>.
- (9) Neale, A. R.; Sharpe, R.; Yeandel, S. R.; Yen, C. H.; Luzyanin, K. V.; Goddard, P.; Petrucco, E. A.; Hardwick, L. J. Design Parameters for Ionic Liquid–Molecular Solvent Blend Electrolytes to Enable Stable Li Metal Cycling Within Li–O₂ Batteries. *Adv. Funct. Mater.* **2021**, 31 (27). <https://doi.org/10.1002/ADFM.202010627>.
- (10) León, A.; Fiedler, A.; Blum, M.; Yang, W.; Bä, M.; Scheiba, F.; Ehrenberg, H.; Heske, C.; Weinhardt, L. Electrolyte Stability and Discharge Products of an Ionic-Liquid-Based Li–O₂ Battery Revealed by Soft X-Ray Emission Spectroscopy. *J. Phys. Chem.* **2019**, 123, 30827–30832. <https://doi.org/10.1021/acs.jpcc.9b08777>.
- (11) Park, J.-B.; Lee, S. H.; Jung, H.-G.; Aurbach, D.; Sun, Y.-K. Redox Mediators for Li-O₂ Batteries: Status and Perspectives. *Adv. Mater.* **2018**, 30 (1), 1704162. <https://doi.org/10.1002/adma.201704162>.
- (12) Kwak, W.-J.; Kim, H.; Jung, H.-G.; Aurbach, D.; Sun, Y.-K. Review-A Comparative Evaluation of Redox Mediators for Li-O₂ Batteries: A Critical Review. *J. Electrochem. Soc.* **2018**, 165 (10), 2274–2293. <https://doi.org/10.1149/2.0901810jes>.

- (13) Kwak, J.; Hirshberg, D.; Sharon, D.; Afri, M.; Frimer, A. A.; Jung, H.-G.; Aurbach, D.; Sun, Y.-K. Li-O₂ Cells with LiBr as an Electrolyte and a Redox Mediator. *Energy Environ. Sci. Environ. Sci* **2016**, *9*, 2334–2345. <https://doi.org/10.1039/c6ee00700g>.
- (14) Rastegar, S.; Hemmat, Z.; Zhang, C.; Plunkett, S.; Wen, J.; Dandu, N.; Rojas, T.; Majidi, L.; Misal, S. N.; Ngo, A. T.; Curtiss, L. A.; Salehi-Khojin, A. High-Rate Long Cycle-Life Li-Air Battery Aided by Bifunctional InX₃(X = i and Br) Redox Mediators. *ACS Appl. Mater. Interfaces* **2021**, *13* (4), 4915–4922. <https://doi.org/10.1021/acsami.0c15200>.
- (15) Li, D.; Zhu, C.; Zhang, M.; Wang, Y.; Kang, Z.; Liu, Y.; Liu, J.; Liu, J.; Xie, H. 1,2-Dimethyl-3-Propylimidazolium Iodide as a Multiple-Functional Redox Mediator for Li-O₂ Batteries: In Situ Generation of a “Self-Defensed” SEI Layer on Li Anode. *Chem. Eng. J.* **2021**, 408. <https://doi.org/10.1016/j.cej.2020.127335>.
- (16) Kaper, H.; Smarsly, B. Templating and Phase Behaviour of the Long Chain Ionic Liquid C 16mimCl. *Zeitschrift fur Phys. Chemie* **2006**, *220* (10–11), 1455–1471. <https://doi.org/10.1524/zpch.2006.220.10.1455>.
- (17) Yamanaka, N.; Kawano, R.; Kubo, W.; Kitamura, T.; Wada, Y.; Watanabe, M.; Yanagida, S. Ionic Liquid Crystal as a Hole Transport Layer of Dye-Sensitized Solar Cells. *Chem. Commun.* **2005**, No. 6, 740. <https://doi.org/10.1039/b417610c>.
- (18) Yuan, F.; Yang, L.; Zou, X.; Dong, S.; Chi, S.; Xie, J.; Xing, H.; Bian, L.; Bao, L.; Wang, J. Flexible All-Solid-State Electrolytes with Ordered Fast Li-Ion-Conductive Nano-Pathways for Rechargeable Lithium Batteries. *J. Power Sources* **2019**, 444. <https://doi.org/10.1016/j.jpowsour.2019.227305>.
- (19) Xin, X.; Ito, K.; Kubo, Y. Highly Efficient Br⁻/NO₃ Dual-Anion Electrolyte for Suppressing Charging Instabilities of Li–O₂ Batteries. **2017**. <https://doi.org/10.1021/acsami.7b05692>.
- (20) Cremasco, L. F.; Anchieta, C. G.; Nepel, T. C. M.; Miranda, A. N.; Sousa, B. P.; Rodella, C. B.; Filho, R. M.; Doubek, G. Operando Synchrotron XRD of Bromide Mediated Li–O₂ Battery. *ACS Appl. Mater. Interfaces* **2021**, *13*, 13123–13131. <https://doi.org/10.1021/acsami.0c21791>.
- (21) Lu, H.; Chen, Z.; Yuan, Y.; Du, H.; Wang, J.; Liu, X.; Hou, Z.; Zhang, K.; Fang, J.; Qu, Y. A Rational Balance Design of Hybrid Electrolyte Based on Ionic Liquid and Fluorinated Ether in Lithium Sulfur Batteries. *J. Electrochem. Soc.* **2019**, *12* (166), 2453–2458. <https://doi.org/10.1149/2.0321912jes>.
- (22) Pan, J.; Li, H.; Sun, H.; Zhang, Y.; Wang, L.; Liao, M.; Sun, X.; Peng, H. A Lithium–Air Battery Stably Working at High Temperature with High Rate Performance. *Adv. Sci. News* **2018**, *14* (1703454). <https://doi.org/10.1002/sml.201703454>.
- (23) Mozhzhukhina, N.; Marchini, F.; Torres, W. R.; Tesio, A. Y.; Mendez De Leo, L. P.; Williams, F. J.; Calvo, E. J. Insights into Dimethyl Sulfoxide Decomposition in Li-O₂ Battery: Understanding Carbon Dioxide Evolution. *Electrochem. commun.* **2017**, *80*, 16–19. <https://doi.org/10.1016/J.ELECOM.2017.05.004>.

- (24) Zheng, C.; Ding, W.; Wang, C. N-Methyl-N-Propyl Pyrrolidine Bromide (MPPBr) as a Bi-Functional Redox Mediator for Rechargeable Li-O₂ Batteries †. *J. Mater. Chem. A* **2019**, *7*, 6180–6186. <https://doi.org/10.1039/c8ta11849c>.
- (25) Torriero, A. A. J.; Howlett, P. C. Ionic Liquid Effects on the Redox Potential of Ferrocene. *Electrochem. commun.* **2012**, *16* (1), 84–87. <https://doi.org/10.1016/j.elecom.2011.12.006>.
- (26) Chen, J. Y.; Hsieh, C. L.; Hsu, N. Y.; Chou, Y. S.; Chen, Y. S. Determining the Limiting Current Density of Vanadium Redox Flow Batteries. *Energies* **2014**, *7* (9), 5863–5873. <https://doi.org/10.3390/EN7095863>.
- (27) Roy, S.; Marzorati, S.; Schievano, A.; Pant, D. Microbial Fuel Cells. *Encycl. Sustain. Technol.* **2017**, 245–259. <https://doi.org/10.1016/B978-0-12-409548-9.10122-8>.
- (28) Knipping, E.; Aucher, C.; Guirado, G.; Aubouy, L. Room Temperature Ionic Liquids versus Organic Solvents as Lithium–Oxygen Battery Electrolytes. *New J. Chem.* **2018**, *42* (6), 4693–4699. <https://doi.org/10.1039/C8NJ00449H>.
- (29) Yoo, E.; Zhou, H. Enhanced Cycle Stability of Rechargeable Li–O₂ Batteries by the Synergy Effect of a LiF Protective Layer on the Li and DMTFA Additive. *ACS Appl. Mater. Interfaces* **2017**, *9*, 16. <https://doi.org/10.1021/acsami.7b05466>.
- (30) Zhang, J.; Sun, B.; Zhao, Y.; Tkacheva, A.; Liu, Z.; Kang, Y.; Guo, X.; Mcdonagh, A. M.; Shanmukaraj, D.; Wang, C.; Rojo, T.; Armand, M.; Peng, Z.; Wang, G. A Versatile Functionalized Ionic Liquid to Boost the Solution-Mediated Performances of Lithium–Oxygen Batteries. *Nat. Commun.* **2019**, 1–10. <https://doi.org/10.1038/s41467-019-08422-8>.
- (31) Singh, N.; Arthur, T. S.; Jones, M.; Tutusaus, O.; Takechi, K.; Matsunaga, T.; Kerr, R.; Howlett, P. C.; Forsyth, M.; Mizuno, F. Artificial SEI Transplantation: A Pathway to Enabling Lithium Metal Cycling in Water-Containing Electrolytes. *Appl. Energy Mater.* **2019**, *2*, 8912–8918. <https://doi.org/10.1021/acsaem.9b01937>.
- (32) Zhu, C.; Sun, Q.; Xie, J.; Jin, Y.; Wang, K.; Chen, Z.; Tu, J.; Cao, G.; Zhao, X. Ionic Liquid/Ether-Plasticized Quasi-Solid-State Electrolytes for Long-Life Lithium–Oxygen Cells. *New J. Chem.* **2018**, *42* (24), 19521–19527. <https://doi.org/10.1039/C8NJ03389G>.
- (33) Gittleston, F. S.; Yao, K. P. C.; Kwabi, D. G.; Sayed, S. Y.; Ryu, W.; Shao-Horn, Y.; Taylor, A. D. Raman Spectroscopy in Lithium–Oxygen Battery Systems. *ChemElectroChem* **2015**, *2*, 1446–1457.
- (34) Dettlaff, A.; Sawczak, M.; Klugmann-Radziemska, E.; Czyłkowski, D.; Miotk, R.; Wilamowska-Zawłocka, M. High-Performance Method of Carbon Nanotubes Modification by Microwave Plasma for Thin Composite Films Preparation †. *R. Soc. Chem. Adv.* **2017**, *7*, 31940–31949. <https://doi.org/10.1039/c7ra04707j>.
- (35) Wang, Z.; Huang, B.; Wang, S.; Xue, R.; Huang, X.; Chen, L. Vibrational Spectroscopic Study of the Interaction between Lithium Perchlorate and Dimethylsulfoxide. *Electrochim. Acta* **1997**, *42* (17), 2611–2617. [https://doi.org/10.1016/S0013-4686\(96\)00440-9](https://doi.org/10.1016/S0013-4686(96)00440-9).

- (36) Yang, J.; Zhai, D.; Wang, H.-H.; Lau, K. C.; Schlueter, J. A.; Du, P.; Myers, D. J.; Sun, Y.-K.; Curtiss, L. A.; Amine, K. Evidence for Lithium Superoxide-like Species in the Discharge Product of a Li-O₂ Battery †. *J. C. Soc.* **2013**, 15, 3764. <https://doi.org/10.1039/c3cp00069a>.
- (37) Wang, J.; Li, Y.; Sun, X. Challenges and Opportunities of Nanostructured Materials for Aprotic Rechargeable Lithium-Air Batteries. *Nano Energy* **2013**, 2, 443–467. <https://doi.org/10.1016/j.nanoen.2012.11.014>.
- (38) Sharon, D.; Afri, M.; Noked, M.; Garsuch, A.; Frimer, A. A.; Aurbach, D. Oxidation of Dimethyl Sulfoxide Solutions by Electrochemical Reduction of Oxygen. *J. Phys. Chem. Lett.* **2013**, 4 (18), 3115–3119. <https://doi.org/10.1021/jz4017188>.
- (39) Wang, Y.; Lai, N. C.; Lu, Y. R.; Zhou, Y.; Dong, C. L.; Lu, Y. C. A Solvent-Controlled Oxidation Mechanism of Li₂O₂ in Lithium-Oxygen Batteries. *Joule* **2018**, 2 (11), 2364–2380. <https://doi.org/10.1016/J.JOULE.2018.07.021>.
- (40) Martens, W. N.; Frost, R. L.; Kristof, J.; Theo Klopogge, J. Raman Spectroscopy of Dimethyl Sulphoxide and Deuterated Dimethyl Sulphoxide at 298 and 77 K. *J. Raman Spectrosc.* **2002**, 33 (2), 84–91. <https://doi.org/10.1002/JRS.827>.
- (41) Selvarajan, A. RAMAN SPECTRUM OF DIMETHYL SULFOXIDE (DMSO) AND THE INFLUENCE OF SOLVENTS. *Proc. Indian Acad. Sci. - Sect. A* **1966**, 64, 44–50.
- (42) Aurbach, D.; McCloskey, B. D.; Nazar, L. F.; Bruce, P. G. Advances in Understanding Mechanisms Underpinning Lithium–Air Batteries. *Nat. Energy* **2016**, 1 (9), 1–11. <https://doi.org/10.1038/nenergy.2016.128>.
- (43) Yang, C. C.; Hsu, H. Y. Raman Spectroscopic Study of a New Type of Room Temperature ZnCl₂-DMSO₂ Molten Salts. *Zeitschrift fur Naturforsch. - Sect. A J. Phys. Sci.* **2010**, 65 (8–9), 745–748. <https://doi.org/10.1515/ZNA-2010-8-917/MACHINEREADEABLECITATION/RIS>.
- (44) Harbach, F.; Fischer, F. RAMAN SPECTRA OF LITHIUM HYDROXIDE SINGLE CRYSTALS. *J. Phys. Chem. Solids* **1975**, 36, 601–603.
- (45) Wang, L.; Zhang, Y.; Liu, Z.; Guo, L.; Peng, Z. Understanding Oxygen Electrochemistry in Aprotic LiO₂ Batteries. *Green Energy Environ.* **2017**, 2, 186–203.
- (46) Aetukuri, N. B.; McCloskey, B. D.; Garcíá, J. M.; Krupp, L. E.; Viswanathan, V.; Luntz, A. C. Solvating Additives Drive Solution-Mediated Electrochemistry and Enhance Toroid Growth in Non-Aqueous Li–O₂ Batteries. *Nat. Chem.* **2014**, 7 (1), 50–56. <https://doi.org/10.1038/nchem.2132>.

Appendix B – Supplementary Information

Multi-functional Imidazolium- Based Ionic Liquid Crystal with Redox Mediator Properties for Li-O₂ Batteries

Letícia M. S. Barros,[†] Chayene G. Anchieta,[†] Thayane C. M. Nepel,[†] Tuanan C. Lourenço,[‡] Júlia P. O. Júlio,[†] Juarez L. F. Da Silva,[‡] Gustavo Doubek,[†] and Rubens Maciel Filho[†]

[†]*School of Chemical Engineering, University of Campinas, Campinas 13083-852, Brazil*

[‡]*São Carlos Institute of Chemistry, University of São Paulo, P.O. Box 780, 13560-970, São Carlos, São Paulo, Brazil*

E-mail: leticia.barros94@gmail.com; chayeneanchieta@gmail.com; thyanecarpanedo@gmail.com; lourenco.tuanan@gmail.com; bruno.aurelio@hotmail.com; julia_paula@outlook.com.br; juarez_dasilva@iqsc.usp.br; doubek@feq.unicamp.br; rmaciel@unicamp.br;

Here, we are providing additional data concerning Raman spectroscopy characterizations of virgin carbon paper/CNT electrode, pure [C₁₆mim][Br] ILC and Pure DMSO. These data are complementary to the results discussed in this paper.

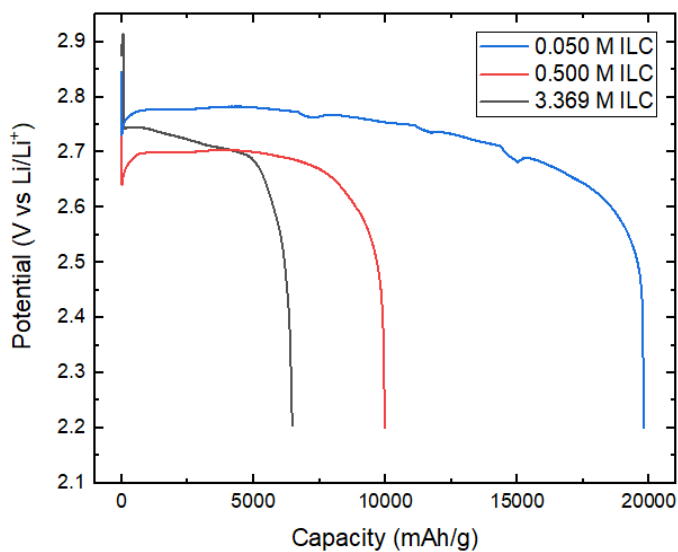


Figure SI 1. Specific Discharge Capacity of 0.050, 0.500 and 3.369 M ILC electrolytes into Li-O₂ batteries.

Figure SI 1 shows the repetition data for the deep tests at different ILC concentrations. For 0.050 M ILC, a discharge capacity of ~19,780 mAh/g was achieved, while for 0.500 M ILC the discharge capacity was close to 9,980 mAh/g, and ~6,465 mAh/g for 3.369 M ILC.

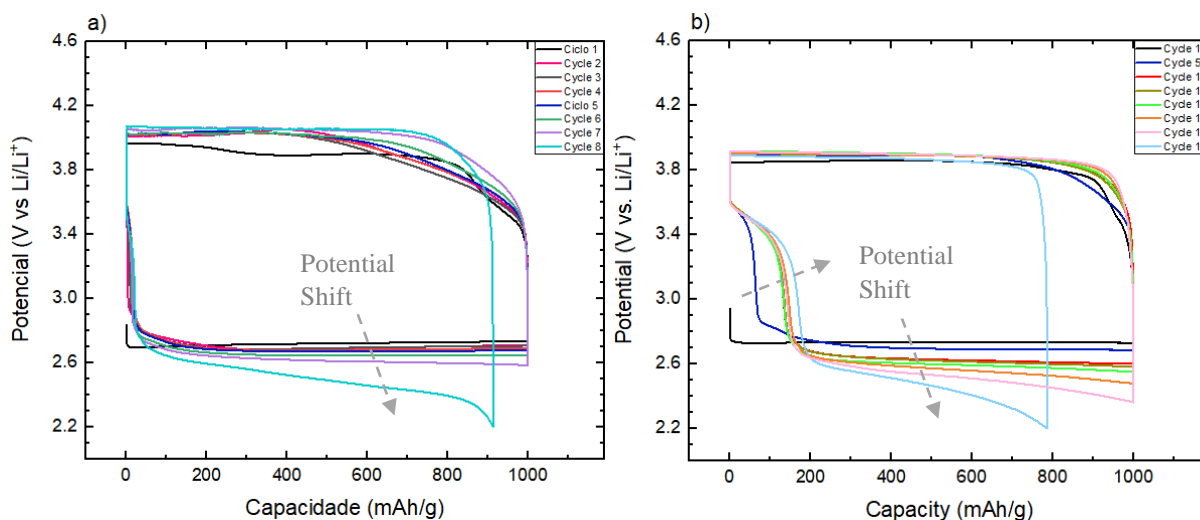


Figure SI 2. Cycling profiles of Li-O₂ batteries with a) 0.500 M ILC and b) 3.369 M ILC.

Figure SI 2 shows the cycling profiles of Li-O₂ batteries with 0.500 M [C₁₆mim][Br] and 3.369 M [C₁₆mim][Br] concentrations, respectively. The poor cycling performance for 0.500 M ILC composition is attributed to the high number of aggregates in the system, as shown in Figure 2 d), which implies in a low discharge potential with a rapid decay during the cell cycling. The low charge overpotentials are due to the presence of the [Br]⁻ anion RM. As for 3.369 M ILC, the charging potentials are maintained at values lower than 4.0 V, because of the great availability of the [Br]⁻

anion for the system. This great amount of $[\text{Br}]^-$ implies in excess $[\text{Br}_3]^-$ species, which were not totally reduced back to $[\text{Br}]^-$ during the Li_2O_2 decomposition in the charging path, so the discharge plateau is assigned to the reduction of the $[\text{Br}_3]^-$ anion. At 3.369 M ILC well-defined structures that resemble a smectic phase are formed, which enhance the ionic transport. Even so, the system is very viscous and is saturated, which compete with the structural effect and cause the rapid decay in the discharge potentials.

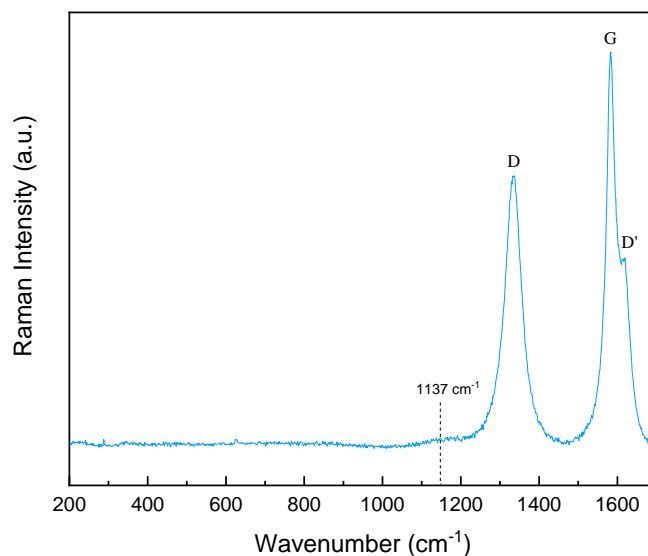


Figure SI 3. Raman spectra of virgin carbon paper electrode with CNT ink.

The characteristic bands of the carbon paper and CNT are well known in literature and are indicated in Figure SI 3. Band-G, at 1583 cm^{-1} , is attributed to the graphite material. Bands D and D' represent the disorder in the carbon's network symmetry, being found at 1335 cm^{-1} and 1619 cm^{-1} , respectively.¹ A small band was identified at 1137 cm^{-1} .

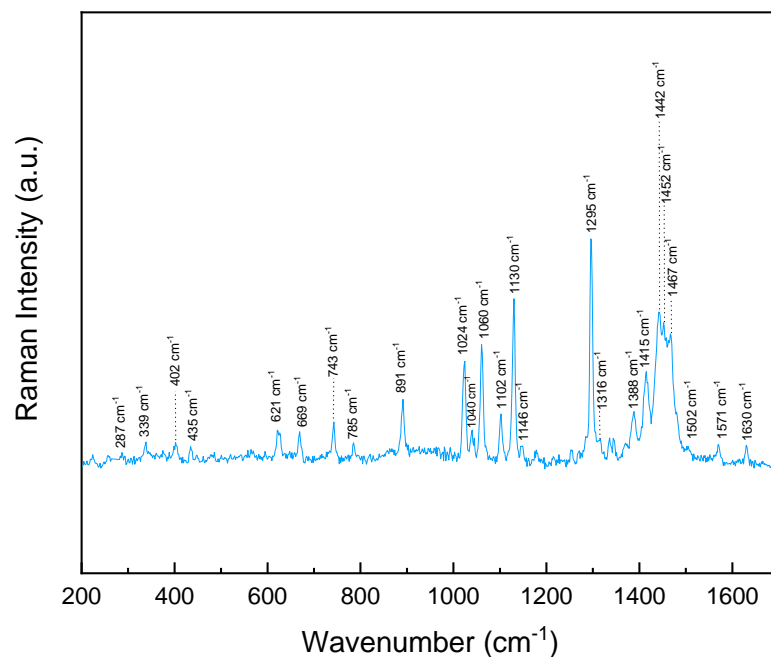


Figure SI 4. Raman spectra of pure [C₁₆mim][Br].

Figure SI 4 indicates the characteristic peaks of the [C₁₆mim][Br] additive, which were characterized via Raman Spectroscopy.

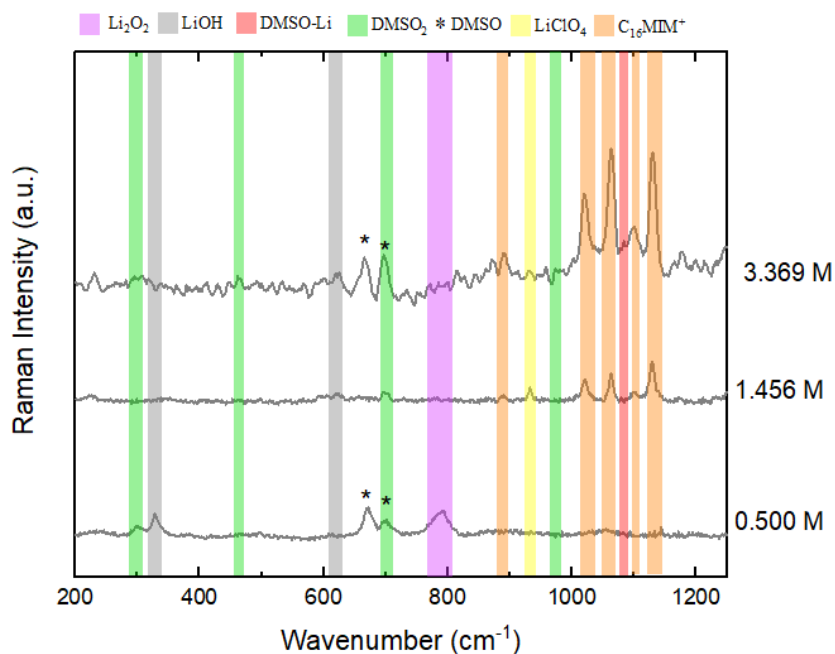


Figure SI 5. Repetition of the Raman Spectroscopy of the cathodes after deep discharge tests at different [C₁₆mim][Br] concentrations in DMSO/LiClO₄ 0.100 M systems.

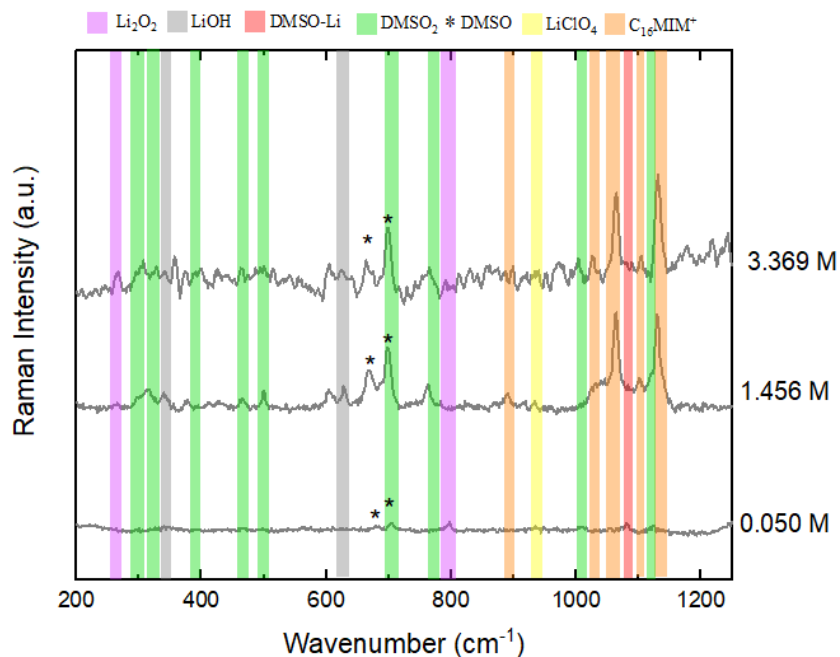


Figure SI 6. Repetition of the Raman Spectroscopy of the cathodes after cycling tests at different $[\text{C}_{16}\text{mim}][\text{Br}]$ concentrations in DMSO/LiClO₄ 0.100 M systems.

Figures SI 5 and 6 show the repetition of the Raman spectroscopy for deep and cycling tests, respectively. Deep discharge product Li_2O_2 can only be identified at repetition of the 0.500 M ILC concentration, confirming that the strong Li_2O_2 peak observed for 1.456 M ILC in Figure 4 was due to a region rich in discharge product. Peaks for $[\text{C}_{16}\text{mim}]^+$ were identified for concentrations above 1.456 M for both deep and cycling tests. Side products LiOH and DMSO_2 were observed from the measurements, which originate from the DMSO composition.

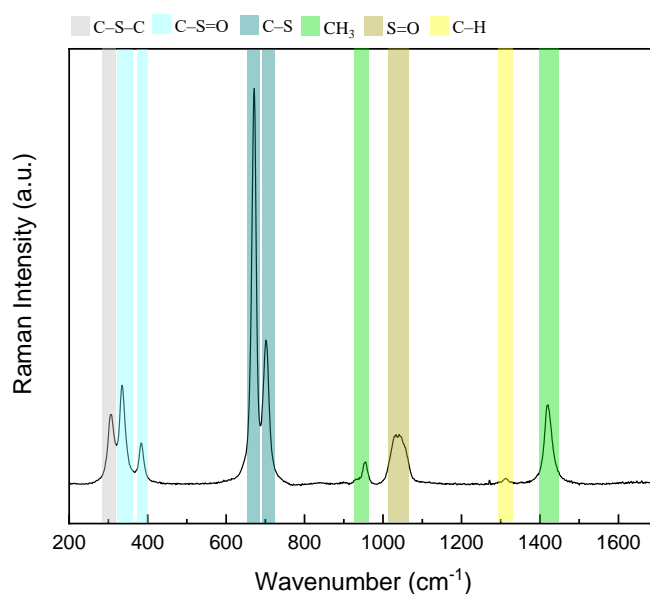


Figure SI 7. Raman spectra of pure DMSO.

Figure SI 7 shows the Raman spectra of the pure DMSO. The peak observed at 307 cm^{-1} corresponds to the C–S–C stretching; at 335 and 384 cm^{-1} we see the bands for C–S=O out of plane and in plane, respectively; the highest bands at 672 and 701 cm^{-1} indicate the C–S symmetric and antisymmetric ligands, respectively; the 955 cm^{-1} peak is attributed to the CH_3 vibration, while the 1029 and 1041 cm^{-1} peaks correspond to the S=O symmetric and antisymmetric stretching.² At 1311 cm^{-1} the C–H symmetric deformation is observed and at 1421 cm^{-1} we see the asymmetric deformation of CH_3 .³

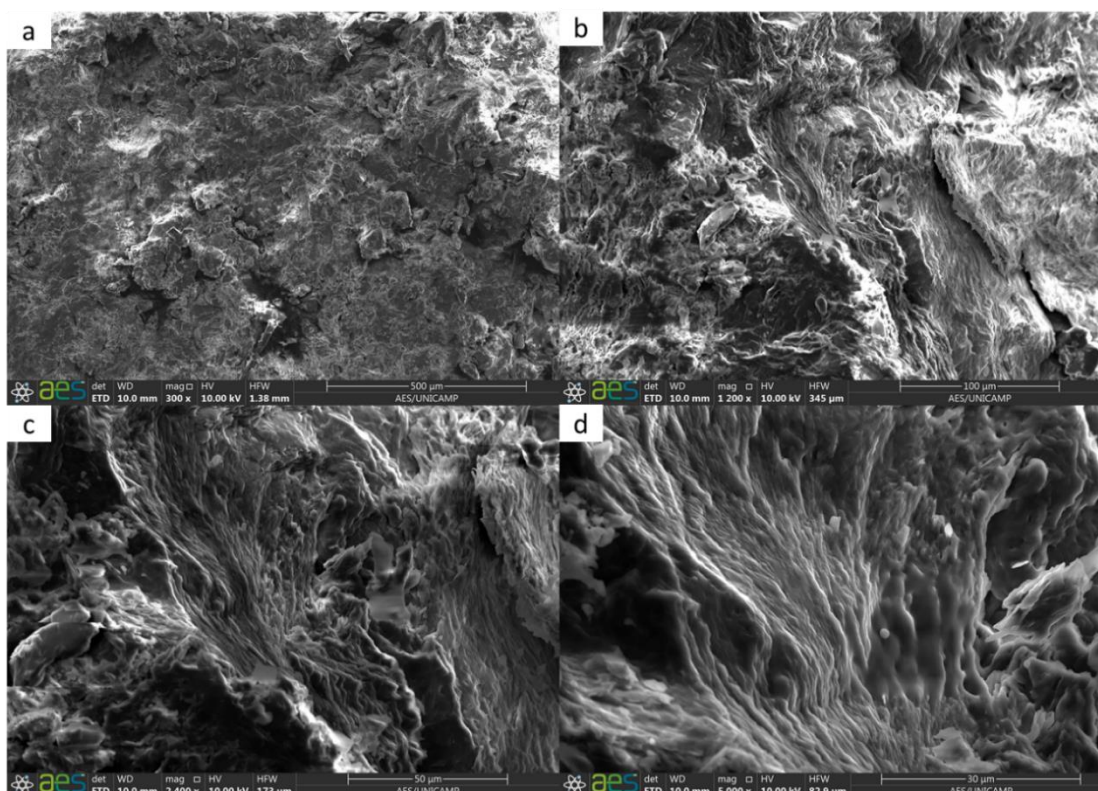


Figure SI 8. FESEM images of pure $[\text{C}_{16}\text{mim}][\text{Br}]$ at different magnifications. Author, 2021

The FESEM images of Figure SI 8 were produced from different zoom and magnifications. Despite the crystalline nature of the pure $[\text{C}_{16}\text{mim}][\text{Br}]$, we observe undefined form of this material. The possible explanation is the high viscosity of the ILC, which hinders the microscopic analysis.

References

(1) Dettlaff, A.; Sawczak, M.; Klugmann-Radziemska, E.; Czyrkowski, D.; Miotk, R.; Wilamowska-Zawłocka, M. High-Performance Method of Carbon Nanotubes Modification by Microwave Plasma for Thin Composite Films Preparation †. *R. Soc. Chem. Adv.* **2017**, *7*, 31940–31949. <https://doi.org/10.1039/c7ra04707j>.

(2) Martens, W. N.; Frost, R. L.; Kristof, J.; Theo Kloprogge, J. Raman Spectroscopy of Dimethyl Sulphoxide and Deuterated Dimethyl Sulphoxide at 298 and 77 K. *J. Raman Spectrosc.* **2002**, *33* (2), 84–91. <https://doi.org/10.1002/JRS.827>.

(3) Selvarajan, A. RAMAN SPECTRUM OF DIMETHYL SULFOXIDE (DMSO) AND THE INFLUENCE OF SOLVENTS. *Proc. Indian Acad. Sci. - Sect. A* **1966**, *64*, 44–50.

4.3. General Discussion

We have discussed in Chapter 2 (Literature Review and Fundamental Concepts) the principles of electrochemistry and the importance of developing electrochemical devices as clean alternatives for attending the increasing demand for energy. We cited different devices and highlighted Li-O₂ battery as one of the most promising technologies due to its superior energy capacity. However, many challenges need to be overcome for its future commercialization, especially in the development of electrochemically, chemically and thermally stable electrolytes, with adequate ionic conductivity and low volatility. Therefore, focusing on solving some of those issues, this work proposed the use of an ionic liquid crystal (ILC), 1-hexadecyl-3-methylimidazole bromide [C₁₆mim][Br], as additive for non-aqueous electrolytes. This material can be considered a multi-functional additive, because it has properties of ionic liquids, liquid crystals and redox mediators, which could be interesting for application in batteries field. In addition, it is important to note that the use of ILC materials with redox properties had never been applied in Li-O₂ cells, so this project could be a guide to develop other studies in the future, exploring other materials with similar properties.

In section 4.1, we deeply investigated the electrochemical, transport and structural properties of [C₁₆mim][Br] into aprotic DMSO/LiClO₄ electrolyte. Combining experiments with MD simulations, the latter developed through a partnership with the group of Professor Juarez L. F. Da Silva, we could conduct a macroscopic and atomistic study of the proposed system. Varying compositions of ILC were tested into the electrolyte, limiting its concentration to 3.369 M, which is the saturation point of [C₁₆mim][Br] into DMSO at ambient temperature. Through CV tests, we could confirm the ILC ability to improve the electrochemical stability of DMSO/LiClO₄ system, observed for a wide electrochemical window from 2 to 6.5 V vs Li/Li⁺. In addition, the CV tests showed the redox peaks of the [Br]⁻ anion, which oxidizes to Br₃⁻ at potentials close to 4.0 V vs Li/Li⁺ for diluted 0.050 M ILC concentration, and a second oxidation peak was seen at potentials over 4.5 V, which indicates the formation of Br₂, a very corrosive specie that should be avoided in the electrolyte. On the other hand, the [Br]⁻ anion is a very important redox mediator (RM) for Li-O₂ batteries, because its oxidized form Br₃⁻ acts in the cell charge, facilitating the discharge product Li₂O₂ degradation and reducing the charge overpotentials.

As for the physical and transport properties of the proposed electrolyte, also discussed in section 4.1, we found that the system's viscosity raises with the ILC addition, which was an

expected behaviour due to the large structure of the imidazolium cation. Even so, high viscosity values did not have an important effect on the electrolyte ionic conductivity, which surprisingly raised until 1.456 M concentration, as observed experimentally at 303 K, and until 2.413 M concentration, as showed through MD simulations at 400 K. For higher ILC concentrations (> 1.456 M ILC for exp. and > 2.413 M ILC for MD), the viscosity effect is more pronounced, and the conductivity starts to decay. Therefore, the conductivity raise was mainly associated to the increase in the number of charge carriers. The ILC addition shows strong intermolecular interactions, with $[\text{C}_{16}\text{mim}]^+$ cations forming polar and nonpolar nanodomains, which resemble a Smectic phase conformation for concentrated systems. The strong molecular and ionic interactions were confirmed by experimental and simulated Raman Spectroscopy, as well as by simulated Radial distribution functions $g(r)$ and theoretical structure function $S(q)$. Besides, the electrolyte density decreases within the ILC addition, which indicates a more cohesive system, due to strong coulombic interactions between $[\text{C}_{16}\text{mim}][\text{Br}]$ ions and DMSO molecules, which also explains the increase in viscosity and the consequent decrease in the self-diffusion coefficient.

In summary, the study conducted in section 4.1 was important to validate that $[\text{C}_{16}\text{mim}][\text{Br}]$ additive has potential to be applied into electrolytes for Li-O₂ batteries. Also, because of the unique properties of the studied material, we believe that $[\text{C}_{16}\text{mim}][\text{Br}]$ use could be extended to other solvents besides DMSO, and be applied into other Li-metal devices, or even supercapacitors. Furthermore, some authors have showed that ILCs could be applied into quasi-solid and solid electrolytes for dye-sensitized solar cells and Li-ion batteries, so we believe that the structural properties of $[\text{C}_{16}\text{mim}][\text{Br}]$ could also be seized for these kind of systems. Even so, further investigation is necessary, especially the use of more advanced characterization techniques to better comprehend the structural effect and the practical application of this material in different electronic devices.

The work presented in section 4.1 was a guide for the study developed in section 4.2, which showed the practical application of the electrolyte into Li-O₂ batteries. The cell performance was evaluated by varying the ILC composition into DMSO/LiClO₄ 0.100 M system. We observed that the variation in the ILC concentration impacts the cell discharge capacity. At low 0.050 M ILC concentration, the discharge capacity was enhanced, however, for higher concentrations, the capacity values were observed to decay. At 0.500 M ILC a significant decrease in the discharge capacity was seen, because at this composition the ILC forms large aggregates which hinder the cell operation, implying in a rapid potential decay.

Increasing the concentration to 1.456 M, the cell discharge capacity increases again, but the deep discharge lasts slightly less than the cell operating with neat (0 M ILC) electrolyte (125 h and 135 h, respectively). While for the saturated concentration at 3.369 M ILC, the cell presented the lowest capacity, operating for only 67 h. This observation can be correlated to the findings of the study presented in section 4.1. Despite the increase in the ionic conductivity due to the high density of charge carriers and the structural effect, the system become more viscous, especially at the highest concentration, which impacts in the ionic transport, reducing the ionic mobility and causing an increase in the charge transfer resistance. In addition, for the most concentrated system, part of the ILC precipitated and accumulated over the carbon fibres, as observed through FESEM images, causing the cathode passivation and reducing, therefore, the discharge capacity.

As for the cycling performance, it was noted that the charge overpotentials decreased as more ILC was added to the electrolyte, because of the increase in the availability of $[\text{Br}]^-$ species which formed more Br_3^- to react with the Li_2O_2 discharge product. The redox potentials were evidenced by CV tests at an inert atmosphere, which were also conducted for this study. Even so, this redox effect did not guarantee longer cyclability for higher ILC concentrations, because the structural behaviour of the long alkyl chain connected to the imidazolium cation appeared to have a major effect at the cyclability.

The optimum composition was found for diluted 0.050 M ILC, which enhanced the cell cyclability due to the ionic liquid function of improving the electrolyte electrochemical stability, as discussed in section 4.1 through CV tests, and due to the efficient redox property of $[\text{Br}]^-$ anion, which effectively reduced the charge overpotentials, retarding the electrolyte attack and the cell death. At this concentration, the structural effect is less pronounced because only small clusters are formed in the system. In addition, the 1.456 M ILC composition also enhanced the cell cyclability and provided the second-best operation performance. For 1.456 M ILC, a different effect was observed. Despite the high viscosities in the system, a good cyclability was obtained, because the system combined the efficient reduction in the charge overpotentials with the electrochemical stability of ionic liquids and the structural effect of liquid crystals. In this case, the system presents a high molecular and ionic organization, with the well-defined structures, which serve as ionic channels for the ionic conductivity and transport. This phenomenon was also discussed in section 4.1 and was important to understand the results found for the cell operation in section 4.2.

As for the highest 3.369 M ILC concentration, the structural effect was maintained, however the viscosity is so high that the system becomes very resistive, therefore, we observe a decrease in the cell performance. In addition, as the system was saturated with ILC, part of this material precipitated, accumulating over the carbon electrodes, totally changing their morphology, as seen in the FESEM tests, blocking the cathode pores and causing its passivation, until the cell death. We highlight that after the electrochemical tests, all cathodes were characterized via FESEM and Raman Spectroscopy. We observed that despite the use of redox mediator, side products were found in the system, which could be expected because Li_2O_2 products accumulate over time, and eventually react with DMSO, producing DMSO_2 and LiOH .

In summary, the study presented in section 4.2 is complementary to that presented in section 4.1. We could confirm the ILC ability to enhance the electrolyte stability and cyclability. The redox mediator effect combined with structural properties contributed to the battery operation. Even so, the most diluted composition was the optimum concentration. However, the use of the proposed system still faces many challenges. Depending on the concentration of $[\text{C}_{16}\text{mim}][\text{Br}]$, it could retard the electrolyte attack, but could not avoid its decomposition over time. In addition, the high viscosities and low charge transference impact in the cell performance. Even so, we recognise the importance of this study into introducing an unexplored material in the batteries field. We also believe in the potential of ILCs to be applied into other battery devices and its use in different solvents, for semi-solid and solid electrolytes. Besides, the system needs further refinement for more promising and concrete results, as well as additional electrochemical tests and characterizations to complement the main findings.

Chapter 5

Conclusions

This project proposed the use of a multi-functional ionic liquid crystal (ILC), [C₁₆mim][Br], as additive for Li-O₂ batteries. The material combined wide electrochemical window, structural and redox mediator functions which were explored to attend the main issues associated to the electrolyte instabilities. Different concentrations of [C₁₆mim][Br] were tested for electrolytes composed by DMSO/LiClO₄. We studied the electrochemical, transport and structural properties of the systems, evaluating their potential as electrolytes for Li-metal cells and investigated their influence on the performance of practical Li-O₂ batteries.

We found that the ILC addition improved the electrolyte conductivity, despite the high viscosity values. These findings are associated to the number of charge carriers and the liquid crystal behaviour of [C₁₆mim][Br], which provides strong molecular and ionic interactions in the DMSO-based system. Increasing the ILC concentration, polar and nonpolar nanodomains are created, forming organised structures at ILC compositions over 1.456 M. These structures act as channels for the ionic transport. In addition, we validated that the bromide anion from [C₁₆mim][Br] material has redox mediator properties, as observed through CV studied at an inert atmosphere. CV tests also showed that ILC addition improved the electrolyte stability.

Testing the electrolyte in practical Li-O₂ batteries, the optimum concentration was found at 0.050 M ILC, followed by 1.456 M. In the diluted system, the structural effect is less evident since small clusters are formed, even so, the cation [C₁₆mim]⁺ provided the electrochemical stability while the anion [Br]⁻ acted in the cell charge. As for the 1.456 M ILC concentration, the structural character seems to have a major effect in the cell performance, contributing to its cyclability despite high viscosities of the electrolyte. On the other hand, rising the concentration to 3.369 M ILC, high viscosities suppress the structural behaviour, causing the rapid decay in the discharge capacity and cyclability. Therefore, the proper concentration of [C₁₆mim][Br] could enhance the cell performance and reduce the charge overpotentials, but the appearance of side products and the cathode passivation could not be avoided.

Finally, we conclude that this study was important to investigate an underexplored field for electrolyte applications: the use of ionic liquid crystals and the impact of the structural effect on electrolytes. In fact, [C₁₆mim][Br] has interesting properties for application in Li-O₂ batteries and could be extended to other electronic devices. Even so, complementary studies and a refinement in the system are necessary for improving the battery performance.

Chapter 6

Future Work and Perspectives

The present work introduced the use of ionic liquid crystals with redox properties into Li-O₂ batteries. The structural effect was important to create ionic channels and enhance the ionic conductivity. The combination of ILC can be extended to other solvents and can be an interesting approach for enhancing the conductivity of semi-solid and solid electrolytes in the future. This kind of material has the potential to be explored for different electronic devices, such as li-metal batteries, supercapacitors or solar cells. Further study of the structural effect is necessary, including characterization techniques, such as small angle X-ray scattering (SAXS), X-ray photon correlation spectroscopy (XPCS), and laser conoscopy measurements.

As for the redox mediator effect, it is necessary further experimental tests to define if [C₁₆mim][Br] is better than LiBr redox mediator. In this sense, cycling tests and cyclic voltammetry at O₂ ambient should be performed for DMSO/LiClO₄ electrolyte using [C₁₆mim][Br] and LiBr at the same concentrations, to guarantee the same availability of [Br]⁻ anions and for comparison. In addition, electrochemical impedance spectroscopy (EIS) at OCP will be necessary to determine the ohmic resistance of both systems. Other complementary tests, including determining the system interfacial resistance, the transference number of Li ions and experimental ionic diffusivity will be necessary.

Chapter 7

Scientific Production

Patent Request*: Instituto Nacional da Propriedade Industrial, INPI (Appendix C)

Process Number: BR 10 2021 016975 3

Title: Eletrólito, baterias que compreendem um líquido iônico cristalino como aditivo em eletrólito e o uso do líquido iônico cristalino em baterias

Authors: Chayene Gonçalves Anchieta, Letícia Maria Sampaio Barros, Gustavo Doubek, Thayane Carpanedo de Moraes Nepel, Rubens Maciel Filho

* This patente was licensed by Shell.

Paper Published at the Journal of Materials Chemistry A (Section 4.1)

Title: Tuning Aprotic Solvent Properties with Long Alkyl Chain Ionic Liquid for Lithium-based Electrolytes

Authors: Tuanan C. Lourenço, Letícia M. S. Barros, Chayene G. Anchieta, Thayane C. M. Nepel, Júlia P. O. Júlio, Luis Gustavo Dias, Rubens Maciel Filho, Gustavo Doubek, and Juarez L. F. Da Silva

Paper with Writing in Progress

Title: Multi-functional Imidazolium-Based Ionic Liquid Crystal with Redox Mediator Properties for Li-O₂ Batteries

Authors: Letícia M. S. Barros, Chayene G. Anchieta, Thayane C. M. Nepel, Tuanan C. Lourenço, Bruno A. B. Francisco, Júlia P. O. Júlio, Juarez L. F. Da Silva, Gustavo Doubek, and Rubens Maciel Filho

Appendix C – Patent Request



26/08/2021 870210078971
20:01
29409161927522527

Pedido nacional de Invenção, Modelo de Utilidade, Certificado de Adição de Invenção e entrada na fase nacional do PCT

Número do Processo: BR 10 2021 016975 3

Dados do Depositante (71)

Depositante 1 de 1

Nome ou Razão Social: UNIVERSIDADE ESTADUAL DE CAMPINAS - UNICAMP

Tipo de Pessoa: Pessoa Jurídica

CPF/CNPJ: 46068425000133

Nacionalidade: Brasileira

Qualificação Jurídica: Instituição de Ensino e Pesquisa

Endereço: Cidade Universitária Zeferino Vaz

Cidade: Campinas

Estado: SP

CEP: 13084-971

País: Brasil

Telefone:

Fax:

Email: patentes@inova.unicamp.br

PETICIONAMENTO ELETRÔNICO

Esta solicitação foi enviada pelo sistema Peticionamento Eletrônico em 26/08/2021 às 20:01, Petição 870210078971

Dados do Pedido**Natureza Patente:** 10 - Patente de Invenção (PI)**Título da Invenção ou Modelo de Utilidade (54):** ELETRÓLITO, BATERIAS QUE COMPREENDEM UM LÍQUIDO IÔNICO CRISTALINO COMO ADITIVO EM ELETRÓLITO E O USO DO LÍQUIDO IÔNICO CRISTALINO EM BATERIAS**Resumo:** A presente invenção se refere a um líquido iônico como aditivo de eletrólito de alta condutividade com atuação catalítica, a baterias que compreendem o uso do líquido iônico cristalino, e o uso do líquido iônico cristalino em baterias Li-O2 utilizando células com a configuração Swagelok (célula vedada ou célula auto vedante). Comparando o líquido iônico da presente invenção com outros líquidos iônicos nota-se vantagens como uma ampla janela de potencial, alta eficiência energética de baterias Li-O2 em termos de horas de operação, alta ciclabilidade das baterias Li-O2 e propriedades estruturais que facilitam o transporte dos íons de lítio e solvatação. O líquido iônico pode ser aplicado em baterias de Li-O2, Li-ar e Li-ion e outras configurações de baterias, além de supercapacitores.**Figura a publicar:** 1**Dados do Procurador****Procurador:****Nome ou Razão Social:** Raquel Moutinho Barbosa**Numero OAB:****Numero API:****CPF/CNPJ:** 30579878856**Endereço:** Rua Roxo Moreira, 1831**Cidade:** Campinas**Estado:** SP**CEP:** 13083-591**Telefone:** 1935212620**Fax:****Email:** raquel.barbosa@inova.unicamp.br**PETICIONAMENTO ELETRÔNICO**

Esta solicitação foi enviada pelo sistema Petição Eletrônica em 26/08/2021 às 20:01, Petição 870210078971

Petição 870210078971, de 26/08/2021, pág. 2/40

Dados do Inventor (72)**Inventor 1 de 5****Nome:** CHAYENE GONÇALVES ANCHIETA**CPF:** 01071623001**Nacionalidade:** Brasileira**Qualificação Física:** Pesquisador**Endereço:** Rua Izabel Negrão Bertotti, 101 apto 111**Cidade:** Campinas**Estado:** SP**CEP:** 13087-508**País:** BRASIL**Telefone:****Fax:****Email:** cganchi@unicamp.br

Inventor 2 de 5**Nome:** LETÍCIA MARIA SAMPAIO BARROS**CPF:** 08376512471**Nacionalidade:** Brasileira**Qualificação Física:** Estudante de Pós Graduação**Endereço:** rua Gilberto Pattaro, 150**Cidade:** Campinas**Estado:** SP**CEP:** 13084-375**País:** BRASIL**Telefone:****Fax:****Email:** leticia.barros94@gmail.com**Inventor 3 de 5****PETICIONAMENTO
ELETRÔNICO**

Esta solicitação foi enviada pelo sistema Peticionamento Eletrônico em 26/08/2021 às 20:01. Petição 870210078971

Petição 870210078971, de 26/08/2021, pág. 3/40

Nome: GUSTAVO DOUBEK**CPF:** 04807296973**Nacionalidade:** Brasileira**Qualificação Física:** Professor do ensino superior**Endereço:** Avenida Albert Einstein, 500**Cidade:** Campinas**Estado:** SP**CEP:** 13083-852**País:** BRASIL**Telefone:****Fax:****Email:** doubek@unicamp.br**Inventor 4 de 5****Nome:** THAYANE CARPANEDO DE MORAIS NEPEL**CPF:** 10584629702**Nacionalidade:** Brasileira**Qualificação Física:** Estudante de Pós Graduação**Endereço:** Avenida Albert Einstein, 500**Cidade:** Campinas**Estado:** SP**CEP:** 13083-852**País:** BRASIL**Telefone:****Fax:****Email:** thayanecarpanedo@gmail.com**Inventor 5 de 5****PETICIONAMENTO
ELETRÔNICO**

Esta solicitação foi enviada pelo sistema Peticionamento Eletrônico em 26/08/2021 às 20:01. Petição 870210078971

Petição 870210078971, de 26/08/2021, pág. 4/40

Nome: RUBENS MACIEL FILHO
CPF: 04605671870
Nacionalidade: Brasileira
Qualificação Física: Professor do ensino superior
Endereço: Rua Albert Einstein, 500
Cidade: Campinas
Estado: SP
CEP: 13083-552
País: BRASIL
Telefone:
Fax:
Email: maciел@unicamp.br

Documentos anexados

Tipo Anexo	Nome
Relatório Descritivo	1638_RELATORIO_DESCRITIVO_260821.pdf
Reivindicação	1638_REIVINDICACOES_260821.pdf
Desenho	1638_FIGURAS_260821.pdf
Resumo	1638_RESUMO_260821.pdf
Comprovante de pagamento de GRU 200	1638_NOVO DEPOSITO DE PI_161220_8_GRU_200_161220_2527_PAGO. pdf
Procuração	INPI_PROCURAÇÃO_290621_1380261.pdf

Acesso ao Patrimônio Genético

Declaração Negativa de Acesso - Declaro que o objeto do presente pedido de patente de invenção não foi obtido em decorrência de acesso à amostra de componente do Patrimônio Genético Brasileiro, o acesso foi realizado antes de 30 de junho de 2000, ou não se aplica.

Declaração de veracidade

Declaro, sob as penas da lei, que todas as informações acima prestadas são completas e verdadeiras.

PETICIONAMENTO ELETRÔNICO

Esta solicitação foi enviada pelo sistema Petição Eletrônica em 26/08/2021 às 20:01, Petição 870210078971

References

- ABRAHAM, K. M.; JIANG, Z. A Polymer Electrolyte-Based Rechargeable Lithium/Oxygen Battery. **J. Electrochem. Soc.**, vol. 143, no. 1, p. 1–5, 1996. .
- AETUKURI, N. B.; MCCLOSKEY, B. D.; GARCÍA, J. M.; KRUPP, L. E.; VISWANATHAN, V.; LUNTZ, A. C. Solvating additives drive solution-mediated electrochemistry and enhance toroid growth in non-aqueous Li–O₂ batteries. **Nature Chemistry** **2014 7:1**, vol. 7, no. 1, p. 50–56, 15 Dec. 2014. DOI 10.1038/nchem.2132. Available at: <https://www.nature.com/articles/nchem.2132>. Accessed on: 10 Jan. 2022.
- AHMADIPARIDARI, A.; FULADI, S.; MAJIDI, L.; PLUNKETT, S.; SARNELLO, E.; GHOLIVAND, H.; HEMMAT, Z.; RASTEGAR, S.; MISAL, S. N.; JIMENEZ, N.; REDFERN, P. C.; WEN, J.; LI, T.; NGO, A. T.; KHALILI-ARAGHI, F.; CURTISS, L. A.; SALEHI-KHOJIN, A. Enhancing the performance of lithium oxygen batteries through combining redox mediating salts with a lithium protecting salt. **Journal of Power Sources**, vol. 491, no. 229506, p. 1–10, 15 Apr. 2021. DOI 10.1016/j.jpowsour.2021.229506. Available at: <https://doi.org/10.1016/j.jpowsour.2021.229506>. Accessed on: 15 Apr. 2021.
- AQEL, A.; EL-NOUR, K. M. M. A.; AMMAR, R. A. A.; AL-WARTHAN, A. Carbon nanotubes, science and technology part (I) structure, synthesis and characterisation. **Arabian Journal of Chemistry**, vol. 5, p. 1–23, 2015. .
- ARA, M.; MENG, T.; NAZRI, G.-A.; SALLEY, S. O.; NG, K. Y. S. Ternary Imidazolium-Pyrrolidinium-Based Ionic Liquid Electrolytes for Rechargeable Li–O₂ Batteries. **Journal of Electrochemical Society**, vol. 161, p. 1969–1975, 2014. <https://doi.org/10.1149/2.0031414jes>.
- AURBACH, D.; MCCLOSKEY, B. D.; NAZAR, L. F.; BRUCE, P. G. Advances in understanding mechanisms underpinning lithium–air batteries. **Nature Energy** **2016 1:9**, vol. 1, no. 9, p. 1–11, 8 Sep. 2016. DOI 10.1038/nenergy.2016.128. Available at: <https://www.nature.com/articles/nenergy2016128>. Accessed on: 10 Jan. 2022.
- BAGOTSKY, V. S. Fuel cells, batteries, and the development of electrochemistry. **Journal of Solid State Electrochem**, vol. 15, p. 1559–1562, 4 Jan. 2011. <https://doi.org/10.1007/s10008-010-1281-8>.
- BALAISH, M.; KRAYTSBERG, A.; EIN-ELI, Y. A critical review on lithium–air battery electrolytes. **Physical Chemistry Chemical Physics**, vol. 16, no. 7, p. 2801–2822, 2014. DOI

10.1039/c3cp54165g. Available at: www.rsc.org/pccp. Accessed on: 17 Mar. 2020.

BENDER, C. R. **Efeito dos ânions de líquidos iônicos dicatiônicos na formação de agregados em solução**. 2014. 1–175 f. Federal University of Santa Maria, 2014.

BRUCE, P. G.; FREUNBERGER, S. A.; HARDWICK, L. J.; TARASCON, J. M. Li-O₂ and Li-S batteries with high energy storage. **Nature Materials**, vol. 11, no. 1, p. 19–29, 2012. <https://doi.org/10.1038/nmat3191>.

CAPSONI, D.; BINI, M.; FERRARI, S.; QUARTARONE, E.; MUSTARELLI, P. Recent advances in the development of Li-air batteries. **Journal of Power Sources**, vol. 220, p. 253–263, 2012. <https://doi.org/https://doi.org/10.1016/j.jpowsour.2012.07.123>.

CHAGNES, A.; DIAW, M.; CARRÉ, B.; WILLMANN, P.; LEMORDANT, D. Imidazolium-organic solvent mixtures as electrolytes for lithium batteries. **Journal of Power Sources**, vol. 145, no. 1, p. 82–88, 4 Jul. 2005. <https://doi.org/10.1016/j.jpowsour.2004.12.035>.

CHEN, Y.; FREUNBERGER, S. A.; PENG, Z.; FONTAINE, O.; BRUCE, P. G. Charging a Li-O₂ battery using a redox mediator. **nature chemistry**, vol. 5, p. 489–494, 2013. DOI 10.1038/NCHEM.1646. Available at: www.nature.com/naturechemistry. Accessed on: 13 Aug. 2020.

CHRISTENSEN, J.; ALBERTUS, P.; SANCHEZ-CARRERA, R. S.; LOHMANN, T.; KOZINSKY, B.; LIEDTKE, R.; AHMED, J.; KOJIC, A. A Critical Review of Li/Air Batteries. **Journal of The Electrochemical Society**, vol. 159, no. 2, p. R1–R30, 2011. <https://doi.org/10.1149/2.086202jes>.

CREMASCO, L. F. **DESENVOLVIMENTO DE SISTEMAS CATALÍTICOS E ELETRODOS PARA BATERIAS DE LÍTIO-AR**. [S. l.: s. n.], 2017. Available at: www.tcpdf.org. Accessed on: 3 May 2020.

CREMASCO, L. F.; ANCHIETA, C. G.; NEPEL, T. C. M.; MIRANDA, A. N.; SOUSA, B. P.; RODELLA, C. B.; FILHO, R. M.; DOUBEK, G. Operando Synchrotron XRD of Bromide Mediated Li–O₂ Battery. **ACS Appl. Mater. Interfaces**, vol. 13, p. 13123–13131, 2021. DOI 10.1021/acsami.0c21791. Available at: <https://dx.doi.org/10.1021/acsami.0c21791>. Accessed on: 11 Apr. 2021.

DAMBROT, S. M. Chemistry Helps Athlete Keep Moving. **ChemMatters**, , p. 11, 2016. Available at: www.acs.org/chemmatters.

DATT BHATT, M.; GEANEY, H.; NOLAN, M.; O'DWYER, C. Key scientific challenges in current rechargeable non-aqueous Li-O₂ batteries: experiment and theory. **Phys. Chem. Chem. Phys.**, vol. 16, p. 12093, 2014. DOI 10.1039/c4cp01309c. Available at:

www.rsc.org/pccp. Accessed on: 12 May 2020.

www.rsc.org/pccp. Accessed on: 12 May 2020.

DENG, D. Li-ion batteries: Basics, progress, and challenges. **Energy Science and Engineering**, vol. 3, no. 5, p. 385–418, 1 Sep. 2015. DOI 10.1002/ese3.95. Available at:

http://doi.wiley.com/10.1002/ese3.95. Accessed on: 6 Mar. 2020.

http://doi.wiley.com/10.1002/ese3.95. Accessed on: 6 Mar. 2020.

DETTLAFF, A.; SAWCZAK, M.; KLUGMANN-RADZIEMSKA, E.; CZYLKOWSKI, D.;

MIOTK, R.; WILAMOWSKA-ZAWŁOCKA, M. High-performance method of carbon

nanotubes modification by microwave plasma for thin composite films preparation †. **The**

Royal Society of Chemistry Advances, vol. 7, p. 31940–31949, 2017.

https://doi.org/10.1039/c7ra04707j.

DEVAKI, S. J.; SASI, R. Ionic Liquids/Ionic Liquid Crystals for Safe and Sustainable Energy Storage Systems. **Intech**. [S. l.: s. n.], 2017. p. 24. DOI http://dx.doi.org/10.5772/65888.

Available at: https://www.intechopen.com/books/advanced-biometric-technologies/liveness-detection-in-biometrics.

DING, N.; CHIEN, S. W.; HOR, T. S. A.; LUM, R.; ZONG, Y.; LIU, Z. Influence of carbon pore size on the discharge capacity of Li-O₂ batteries. **Journal of Materials Chemistry A**,

vol. 2, no. 31, p. 12433–12441, 21 Aug. 2014. https://doi.org/10.1039/c4ta01745e.

ETACHERI, V.; MAROM, R.; ELAZARI, R.; SALITRA, G.; AURBACH, D. Challenges in the development of advanced Li-ion batteries: a review. **Energy & Environmental Science**,

vol. 4, p. 3243–3262, 2011. DOI 10.1039/c1ee01598b. Available at: www.rsc.org/ees.

Accessed on: 6 Mar. 2020.

EVOLVING ENERGY. Lithium – air Battery Overview. 2014. **Evolving Energy Pty Ltd.** .

FOROOZAN, T.; SHARIFI-ASL, S.; SHAHBAZIAN-YASSAR, R. Mechanistic

understanding of Li dendrites growth by in- situ/operando imaging techniques. **Journal of Power Sources**, vol. 461, no. 228135, p. 1–23, 15 Jun. 2020.

https://doi.org/10.1016/j.jpowsour.2020.228135.

FRANCISCO, B. A. B. ANÁLISE DAS VARIÁVEIS QUE AFETAM A OPERAÇÃO E FUNCIONAMENTO DE UMA BATERIA LÍTIO-OXIGÊNIO. Campinas: [s. n.], 2019.

Available at:

https://drive.google.com/drive/u/0/folders/1Qd_p7hFjBDm6VGcOtzaNQYXIUe-1zxze.

Accessed on: 14 Sep. 2020.

FREUNBERGER, S. A.; CHEN, Y.; PENG, Z.; GRIFFIN, J. M.; HARDWICK, L. J.; BARDÉ, F.; NOVÁK, P.; BRUCE, P. G. Reactions in the rechargeable lithium-O₂ battery with alkyl carbonate electrolytes. **Journal of the American Chemical Society**, vol. 133, no. 20, p. 8040–8047, 25 May 2011. <https://doi.org/10.1021/ja2021747>.

FRÖBA, A. P.; KREMER, H.; LEIPERTZ, A. Density, Refractive Index, Interfacial Tension, and Viscosity of Ionic Liquids [EMIM][EtSO₄], [EMIM][NTf₂], [EMIM][N(CN)₂], and [OMA][NTf₂] in Dependence on Temperature at Atmospheric Pressure. **J. Phys. Chem. B**, vol. 112, no. 39, p. 12420–12430, 2008. DOI 10.1021/jp804319a. Available at: <https://pubs.acs.org/sharingguidelines>. Accessed on: 19 Mar. 2020.

FU, J. Fast Li⁺ ion conducting glass-ceramics in the system Li₂O–Al₂O₃–GeO₂–P₂O₅. **Solid State Ionics**, vol. 104, p. 191–194, 1997a. .

FU, J. Superionic conductivity of glass-ceramics in the system Li₂O–Al₂O₃–TiO₂–P₂O₅. **Solid State Ionics**, vol. 96, p. 195–200, 1997b. Available at: <https://reader.elsevier.com/reader/sd/pii/S0167273897000180?token=17F146E78EDB90C1F0FE323F5B4517D14DE7426E4D74A96892A63A03DED46127BDAA363505A38130F9A09BA0376AD306>. Accessed on: 24 Apr. 2020.

GIRISHKUMAR, G.; MCCLOSKEY, B.; LUNTZ, A. C.; SWANSON, S.; WILCKE, W. Lithium-air battery: Promise and challenges. **Journal of Physical Chemistry Letters**, vol. 1, no. 14, p. 2193–2203, 2010a. DOI 10.1021/jz1005384. Available at: <https://pubs.acs.org/sharingguidelines>. Accessed on: 16 Mar. 2020.

GIRISHKUMAR, G.; MCCLOSKEY, B.; LUNTZ, A. C.; SWANSON, S.; WILCKE, W. Lithium-Air Battery: Promise and Challenges. **The Journal of Physical Chemistry Letters**, vol. 1, p. 2193–2203, 2010b. DOI 10.1021/jz1005384. Available at: <https://pubs.acs.org/sharingguidelines>. Accessed on: 16 Mar. 2020.

GITTLESON, F. S.; YAO, K. P. C.; KWABI, D. G.; SAYED, S. Y.; RYU, W.; SHAO-HORN, Y.; TAYLOR, A. D. Raman Spectroscopy in Lithium–Oxygen Battery Systems. **ChemElectroChem**, vol. 2, p. 1446–1457, 2015. Available at: https://scholar.cu.edu.eg/?q=sysayed/files/gittleston_et_al-2015-chemelectrochem.pdf. Accessed on: 30 Dec. 2021.

- HARBACH, F.; FISCHER, F. RAMAN SPECTRA OF LITHIUM HYDROXIDE SINGLE CRYSTALS. **J. Phys. Chem. Solids**, vol. 36, p. 601–603, 1975. Available at: <https://reader.elsevier.com/reader/sd/pii/0022369775901493?token=9C37C30621AA69AB330823C0CE340639C8DACF37A254B00FCA0B2AB0002A69A319EC44A5094E32FB8C138969BDF91C99&originRegion=us-east-1&originCreation=20220109231444>. Accessed on: 9 Jan. 2022.
- HARJANI, J. R.; SINGER, R. D.; GARCIA, M. T.; SCAMMELLS, P. J. Biodegradable pyridinium ionic liquids: design, synthesis and evaluation. **Green Chemistry**, vol. 11, p. 83–90, 2009. DOI 10.1039/b811814k. Available at: www.rsc.org/greenchem. Accessed on: 25 Mar. 2020.
- HELMENSTINE, A. M. Lithium Facts: Li or Element 3. 14 Aug. 2019. **ThoughtCo**. Available at: <https://www.thoughtco.com/lithium-facts-li-or-element-3-606554>. Accessed on: 9 Jul. 2020.
- HILTROP, K. Lyotropic Liquid Crystals. **Liquid Crystal**. [S. l.]: Topics in Physical Chemistry, 1994. vol. 3, p. 143–171.
- INTERNATIONAL ENERGY AGENCY. Global EV Outlook 2019 – Analysis - IEA. 2019a. Available at: <https://www.iea.org/reports/global-ev-outlook-2019>. Accessed on: 16 Mar. 2020.
- INTERNATIONAL ENERGY AGENCY. World Energy Outlook 2019 – Analysis - IEA. 2019b. Available at: <https://www.iea.org/reports/world-energy-outlook-2019>. Accessed on: 15 Mar. 2020.
- JÚLIO, J. de P. O. **Avaliação dos Produtos de Descarga e Desempenho das Baterias de Lítio-Oxigênio em Sistemas Aberto e Fechado**. 2020. UNICAMP, Campinas, 2020. Available at: https://drive.google.com/drive/u/0/folders/1x54gCtWz-Xvn0yA8E6p8luF92P28TH5_. Accessed on: 6 May 2020.
- JUNG, H. G.; HASSOUN, J.; PARK, J. B.; SUN, Y. K.; SCROSATI, B. An improved high-performance lithium-air battery. **Nature Chemistry**, vol. 4, no. 7, p. 579–585, 10 Jul. 2012. <https://doi.org/10.1038/nchem.1376>.
- KAPER, H.; SMARSLY, B. Templating and phase behaviour of the long chain ionic liquid C₁₆mimCl. **Zeitschrift fur Physikalische Chemie**, vol. 220, no. 10–11, p. 1455–1471, 2006. <https://doi.org/10.1524/zpch.2006.220.10.1455>.

KHAN, A.; ZHAO, C. Oxygen Reduction Reactions in Aprotic Ionic Liquids Based Mixed Electrolytes for High Performance of Li–O₂ Batteries. **ACS Sustainable Chemistry & Engineering**, vol. 4, p. 506–513, 2016. DOI 10.1021/acssuschemeng.5b00890. Available at: <https://pubs.acs.org/sharingguidelines>. Accessed on: 9 Aug. 2020.

KITAURA, H.; ZHOU, H. All-solid-state lithium-oxygen battery with high safety in wide ambient temperature range OPEN. **Scientific Reports**, , p. 1–8, 2015. DOI 10.1038/srep13271. Available at: www.nature.com/scientificreports/. Accessed on: 21 Jun. 2020.

KNIPPING, E.; AUCHER, C.; GUIRADO, G.; AUBOUY, L. Room temperature ionic liquids versus organic solvents as lithium–oxygen battery electrolytes. **New Journal of Chemistry**, vol. 42, no. 6, p. 4693–4699, 12 Mar. 2018. DOI 10.1039/C8NJ00449H. Available at: <https://pubs.rsc.org/en/content/articlehtml/2018/nj/c8nj00449h>. Accessed on: 9 Jan. 2022.

KOWALCZK, I.; READ, J.; SALOMON, M. Li-air batteries: A classic example of limitations owing to solubilities. **Pure and Applied Chemistry**, vol. 79, no. 5, p. 851–860, 2007. .

KRAYTSBERG, A.; EIN-ELI, Y. Review on Li-air batteries - Opportunities, limitations and perspective. **Journal of Power Sources**, vol. 196, no. 3, p. 886–893, 1 Feb. 2011. <https://doi.org/10.1016/j.jpowsour.2010.09.031>.

KUNDU, D.; BLACK, R.; ADAMS, B.; NAZAR, L. F. A Highly Active Low Voltage Redox Mediator for Enhanced Rechargeability of Lithium–Oxygen Batteries. **ACS Central Science**, vol. 1, p. 510–515, 2015. DOI 10.1021/acscentsci.5b00267. Available at: <http://pubs.acs.org/journal/acscii>. Accessed on: 22 May 2020.

KWAK, J.; HIRSHBERG, D.; SHARON, D.; AFRI, M.; FRIMER, A. A.; JUNG, H.-G.; AURBACH, D.; SUN, Y.-K. Li-O₂ cells with LiBr as an electrolyte and a redox mediator. **Energy & Environmental Science Environ. Sci**, vol. 9, p. 2334–2345, 2016. DOI 10.1039/c6ee00700g. Available at: www.rsc.org/ees. Accessed on: 3 May 2020.

KWAK, W.-J.; KIM, H.; JUNG, H.-G.; AURBACH, D.; SUN, Y.-K. Review-A Comparative Evaluation of Redox Mediators for Li-O₂ Batteries: A Critical Review. **Journal of The Electrochemical Society**, vol. 165, no. 10, p. 2274–2293, 2018. <https://doi.org/10.1149/2.0901810jes>.

LAI, J.; XING, Y.; CHEN, N.; LI, L.; WU, F.; CHEN, R. Electrolytes for Rechargeable Lithium–Air Batteries. **Angewandte Chemie International Edition**, vol. 59, no. 8, p. 2974–2997, 17 Feb. 2020. DOI 10.1002/anie.201903459. Available at:

<https://onlinelibrary.wiley.com/doi/abs/10.1002/anie.201903459>. Accessed on: 10 Jul. 2020.

LE MONG, A.; KIM, D. Solid electrolyte membranes prepared from poly(arylene ether ketone)-g-polyimidazolium copolymer intergrated with ionic liquid for lithium secondary battery. **Journal of Power Sources**, vol. 422, no. December 2018, p. 57–64, 15 May 2019. DOI 10.1016/j.jpowsour.2019.03.038. Available at:

<https://doi.org/10.1016/j.jpowsour.2019.03.038>. Accessed on: 17 Feb. 2020.

LI, D.; ZHU, C.; ZHANG, M.; WANG, Y.; KANG, Z.; LIU, Y.; LIU, J.; LIU, J.; XIE, H. 1,2-dimethyl-3-propylimidazolium iodide as a multiple-functional redox mediator for Li-O₂ batteries: In situ generation of a “self-defensed” SEI layer on Li anode. **Chemical Engineering Journal**, vol. 408, 15 Mar. 2021. DOI 10.1016/j.cej.2020.127335. Available at: <https://doi.org/10.1016/j.cej.2020.127335>. Accessed on: 26 Mar. 2021.

LI, F.; ZHANG, T.; ZHOU, H. Challenges of non-aqueous Li-O₂ batteries: Electrolytes, catalysts, and anodes. **Energy and Environmental Science**, vol. 6, no. 4, p. 1125–1141, 20 Mar. 2013. <https://doi.org/10.1039/c3ee00053b>.

LI, J.; MA, C.; CHI, M.; LIANG, C.; DUDNEY, N. J. Solid Electrolyte: the Key for High-Voltage Lithium Batteries. **Advanced Energy Materials**, vol. 5, no. 4, p. 1401408, 1 Feb. 2015. DOI 10.1002/aenm.201401408. Available at:

<http://doi.wiley.com/10.1002/aenm.201401408>. Accessed on: 28 Apr. 2020.

LI, Y.; LU, J. Metal-Air Batteries: Will They Be the Future Electrochemical Energy Storage Device of Choice? **ACS Energy Letters**, vol. 2, no. 6, p. 1370–1377, 9 Jun. 2017. DOI 10.1021/acsenenergylett.7b00119. Available at: <http://pubs.acs.org/journal/aelccp>. Accessed on: 11 Sep. 2020.

LIM, H.-D.; LEE, B.; ZHENG, Y.; HONG, J.; KIM, J.; GWON, H.; KO, Y.; LEE, M.; CHO, K.; KANG, K. Rational design of redox mediators for advanced Li-O₂ batteries. **Nature Energy**, vol. 66, p. 1–10, 2016. DOI 10.1038/NENERGY.2016.66. Available at: www.nature.com/natureenergy. Accessed on: 11 Aug. 2020.

LIN, M.-C.; CHEN, H.; DAI, H. Ionic Liquids Based Electrolytes for Rechargeable Batteries. **Material Matters**, vol. 13.1, 2018. <https://doi.org/10.1002/0471762512.ch6>.

LITTAUER, E. L.; TSAI, K. C. Anodic Behavior of Lithium in Aqueous Electrolytes. **J. Electrochem. Soc.**, vol. 123, no. 7, p. 964–969, 1976. .

LU, J.; LI, L.; PARK, J. B.; SUN, Y. K.; WU, F.; AMINE, K. Aprotic and aqueous Li-O₂ batteries. **Chemical Reviews**, vol. 114, no. 11, p. 5611–5640, 2014.
<https://doi.org/10.1021/cr400573b>.

MAHMOOD, A. Recent research progress on quasi-solid-state electrolytes for dye-sensitized solar cells. **Journal of Energy Chemistry**, vol. 24, no. 6, p. 686–692, 1 Nov. 2015.
<https://doi.org/10.1016/j.jechem.2015.10.018>.

MARCINEK, M.; SYZDEK, J.; MARCZEWSKI, M.; PISZCZ, M.; NIEDZICKI, L.; KALITA, M.; PLEWA-MARCZEWSKA, A.; BITNER, A.; WIECZOREK, P.; TRZECIAK, T.; KASPRZYK, M.; ŁĘŻAK, P.; ZUKOWSKA, Z.; ZALEWSKA, A.; WIECZOREK, W. Electrolytes for Li-ion transport - Review. **Solid State Ionics**, vol. 276, p. 107–126, 1 Aug. 2015. <https://doi.org/10.1016/j.ssi.2015.02.006>.

MARTENS, W. N.; FROST, R. L.; KRISTOF, J.; THEO KLOPROGGE, J. Raman spectroscopy of dimethyl sulphoxide and deuterated dimethyl sulphoxide at 298 and 77 K. **Journal of Raman Spectroscopy**, vol. 33, no. 2, p. 84–91, 2002.
<https://doi.org/10.1002/JRS.827>.

MERCK KGAA. Imidazolium Ionic Liquids. 2020. **Sigma-Aldrich**. Available at: <https://www.sigmaaldrich.com/chemistry/chemistry-products.html?TablePage=16255914>. Accessed on: 8 Aug. 2020.

MIRSKY, S. Lithium-Ion Battery Creators Win Chemistry Nobel Prize - Scientific American. 9 Oct. 2019. **Chemistry Science Talk**. Available at: <https://www.scientificamerican.com/podcast/episode/lithium-ion-battery-creators-win-chemistry-nobel-prize/>. Accessed on: 1 Apr. 2020.

MIZUSHIMA, K.; JONES, P. C.; WISEMAN, P. J.; GOODENOUGH, J. B. Li_xCoO₂ (0 < x < 1): A new cathode material for batteries of high energy density. **Materials Research Bulletin**, vol. 15, no. 6, p. 783–789, Jun. 1980. DOI 10.1016/0025-5408(80)90012-4. Available at: <https://linkinghub.elsevier.com/retrieve/pii/0025540880900124>. Accessed on: 1 Apr. 2020.

MOZHUKHINA, N.; MARCHINI, F.; TORRES, W. R.; TESIO, A. Y.; MENDEZ DE LEO, L. P.; WILLIAMS, F. J.; CALVO, E. J. Insights into dimethyl sulfoxide decomposition

in Li-O₂ battery: Understanding carbon dioxide evolution. **Electrochemistry Communications**, vol. 80, p. 16–19, 1 Jul. 2017. <https://doi.org/10.1016/J.ELECOM.2017.05.004>.

OLIVEIRA, L. C. C. B. **Avaliação de parâmetros para a criação de eletrodos de MnO₂ sobre espuma de Ni aplicados a baterias de Li-O₂**. 2018. [s.n.], Campinas, 2018. Available at: www.tcpdf.org. Accessed on: 8 May 2020.

OLIVIER-BOURBIGOU, H.; MAGNA, L.; MORVAN, D. Ionic liquids and catalysis: Recent progress from knowledge to applications. **Applied Catalysis A: General**, vol. 373, no. 1–2, p. 1–56, 2010. <https://doi.org/10.1016/j.apcata.2009.10.008>.

OMINDE, N.; YANG, X.-Q.; QU, D. **The investigation of oxygen reduction mechanism on activated carbon electrodes loaded with MnO₂ catalyst**. [S. l.: s. n.], 2009.

PAN, J.; LI, H.; SUN, H.; ZHANG, Y.; WANG, L.; LIAO, M.; SUN, X.; PENG, H. A Lithium–Air Battery Stably Working at High Temperature with High Rate Performance. **Advanced Science News**, vol. 14, no. 1703454, 8 Feb. 2018. <https://doi.org/10.1002/sml.201703454>.

PARK, J.-B.; LEE, S. H.; JUNG, H.-G.; AURBACH, D.; SUN, Y.-K. Redox Mediators for Li-O₂ Batteries: Status and Perspectives. **Advanced Materials**, vol. 30, no. 1, p. 1704162, 4 Jan. 2018. DOI 10.1002/adma.201704162. Available at: <http://doi.wiley.com/10.1002/adma.201704162>. Accessed on: 22 May 2020.

PERRY, R. L.; JONES, K. M.; SCOTT, W. D.; LIAO, Q.; HUSSEY, C. L. Densities, Viscosities, and Conductivities of Mixtures of Selected Organic Cosolvents with the Lewis Basic Aluminum Chloride + 1-Methyl-3-ethylimidazolium Chloride Molten Salt. **Journal of Chemical and Engineering Data**, vol. 40, no. 3, p. 615–619, 1995. Available at: <https://pubs.acs.org/sharingguidelines>. Accessed on: 24 Mar. 2020.

PORT, V. C. **Síntese e caracterização de novos cristais líquidos derivados do centro 1,3,5-triazina**. Fklorianópolis: [s. n.], Nov. 2018.

QIN, Y.; LU, J.; DU, P.; CHEN, Z.; REN, Y.; WU, T.; MILLER, J. T.; WEN, J.; MILLER, D. J.; ZHANG, Z.; AMINE, K. In situ fabrication of porous-carbon-supported α -MnO₂ nanorods at room temperature: application for rechargeable Li-O₂ batteries † ‡. **Energy & Environmental Science**, vol. 6, p. 519–531, 2013. DOI 10.1039/c2ee23621d. Available at: www.rsc.org/ees. Accessed on: 30 Apr. 2020.

RASTEGAR, S.; HEMMAT, Z.; ZHANG, C.; PLUNKETT, S.; WEN, J.; DANDU, N.; ROJAS, T.; MAJIDI, L.; MISAL, S. N.; NGO, A. T.; CURTISS, L. A.; SALEHI-KHOJIN, A. High-Rate Long Cycle-Life Li-Air Battery Aided by Bifunctional InX₃(X = i and Br) Redox Mediators. **ACS Applied Materials and Interfaces**, vol. 13, no. 4, p. 4915–4922, 2021. <https://doi.org/10.1021/acsami.0c15200>.

ROBERTS, M.; YOUNESI, R.; RICHARDSON, W.; LIU, J.; GUSTAFSSON, T.; ZHU, J.; EDSTRÖM, K. Increased Cycling Efficiency of Lithium Anodes in Dimethyl Sulfoxide Electrolytes For Use in Li-O₂ Batteries. **ECS Electrochemistry Letters**, vol. 3, no. 6, p. 62–65, 2014. <https://doi.org/10.1149/2.007406eel>.

SALVUCCI, R.; TATTINI, J. **DTU International Energy Report 2019 - Transforming Urban Mobility**. Kongens Lyngby: [s. n.], 2019. Available at: <https://www.researchgate.net/publication/336529607>. Accessed on: 15 Mar. 2020.

SCHUMM, B. Battery. 28 Feb. 2019. **Encyclopædia Britannica, inc.** Available at: <https://www.britannica.com/technology/battery-electronics/Development-of-batteries>. Accessed on: 1 Apr. 2020.

SCROSATI, B. History of lithium batteries. **Journal of Solid State Electrochem**, vol. 15, p. 1623–1630, 4 May 2011. <https://doi.org/10.1007/s10008-011-1386-8>.

SELVARAJAN, A. RAMAN SPECTRUM OF DIMETHYL SULFOXIDE (DMSO) AND THE INFLUENCE OF SOLVENTS. **Proceedings of the Indian Academy of Sciences - Section A**, vol. 64, p. 44–50, 1966. .

SHARON, D.; AFRI, M.; NOKED, M.; GARSUCH, A.; FRIMER, A. A.; AURBACH, D. Oxidation of dimethyl sulfoxide solutions by electrochemical reduction of oxygen. **Journal of Physical Chemistry Letters**, vol. 4, no. 18, p. 3115–3119, 19 Sep. 2013. <https://doi.org/10.1021/jz4017188>.

SHARON, D.; HIRSHBERG, D.; AFRI, M.; FRIMER, A. A.; AURBACH, D. The importance of solvent selection in Li-O₂ cells. **Chemical Communications**, vol. 53, no. 22, p. 3269–3272, 14 Mar. 2017. <https://doi.org/10.1039/c6cc09086a>.

SIMONETTI, E.; CAREWSKA, M.; MARESCA, G.; DE FRANCESCO, M.; APPETECCHI, G. B. Highly Conductive, Ionic Liquid-Based Polymer Electrolytes. **Journal of The Electrochemical Society**, vol. 164, no. 1, p. A6213–A6219, 2017. <https://doi.org/10.1149/2.0331701jes>.

SINGH, G.; KUMAR, A. Ionic liquids: Physico-chemical, solvent properties and their applications in chemical processes. **Indian Journal of Chemistry - Section A Inorganic, Physical, Theoretical and Analytical Chemistry**, vol. 47, no. 4, p. 495–503, 2008. .

SINGH, N.; ARTHUR, T. S.; JONES, M.; TUTUSAUS, O.; TAKECHI, K.; MATSUNAGA, T.; KERR, R.; HOWLETT, P. C.; FORSYTH, M.; MIZUNO, F. Artificial SEI Transplantation: A Pathway to Enabling Lithium Metal Cycling in Water-Containing Electrolytes. **Applied Energy Materials**, vol. 2, p. 8912–8918, 2019. DOI 10.1021/acsaem.9b01937. Available at: <https://pubs.acs.org/sharingguidelines>. Accessed on: 31 Aug. 2020.

SOLAR IMPULSE FOUNDATION. Solutions to the energy crisis: how to achieve sustainable energy? 2019. Available at: <https://solarimpulse.com/energy-crisis-solutions>. Accessed on: 15 Mar. 2020.

SUN, P.; ARMSTRONG, D. W. Ionic liquids in analytical chemistry. **Analytica Chimica Acta**, vol. 661, no. 1, p. 1–16, 2010. <https://doi.org/10.1016/j.aca.2009.12.007>.

SUN, Y. Lithium ion conducting membranes for lithium-air batteries. **Nano Energy**, vol. 2, no. 5, p. 801–816, 1 Sep. 2013. <https://doi.org/10.1016/j.nanoen.2013.02.003>.

TAN, P.; JIANG, H. R.; ZHU, X. B.; AN, L.; JUNG, C. Y.; WU, M. C.; SHI, L.; SHYY, W.; ZHAO, T. S. Advances and challenges in lithium-air batteries. **Applied Energy**, vol. 204, p. 780–806, 2017. DOI 10.1016/j.apenergy.2017.07.054. Available at: <http://dx.doi.org/10.1016/j.apenergy.2017.07.054>. Accessed on: 26 Apr. 2020.

TAN, P.; SHYY, W.; WEI, Z. H.; AN, L.; ZHAO, T. S. A carbon powder-nanotube composite cathode for non-aqueous lithium-air batteries. **Electrochimica Acta**, vol. 147, p. 1–8, 20 Nov. 2014. <https://doi.org/10.1016/j.electacta.2014.09.074>.

TICIANELLI, EDSON ANTONIO; RAFAEL GONZALEZ, E. **Eletroquímica: princípios e aplicações**. 2nd ed. São Paulo: edusp, 2005.

VERMA, P.; MAIRE, P.; NOVÁK, P. A review of the features and analyses of the solid electrolyte interphase in Li-ion batteries. **Electrochimica Acta**, vol. 55, no. 22, p. 6332–6341, 1 Sep. 2010. <https://doi.org/10.1016/j.electacta.2010.05.072>.

WANG, C.; XIE, Z.; ZHOU, Z. Lithium-air batteries: Challenges coexist with opportunities. **APL Materials**, vol. 7, no. 4, 1 Apr. 2019. <https://doi.org/10.1063/1.5091444>.

WANG, J.; LI, Y.; SUN, X. Challenges and opportunities of nanostructured materials for aprotic rechargeable lithium-air batteries. **Nano Energy**, vol. 2, p. 443–467, 2013.

<https://doi.org/10.1016/j.nanoen.2012.11.014>.

WANG, L.; ZHANG, Y.; LIU, Z.; GUO, L.; PENG, Z. Understanding oxygen electrochemistry in aprotic LiO₂ batteries. **Green Energy & Environment**, vol. 2, p. 186–203, 2017. Available at:

<https://reader.elsevier.com/reader/sd/pii/S2468025717301061?token=092031C461E7AB564886860B112892B2BC9F7EB0D0FA6193A0EF20D5C9D5AB9856EEC08FF6ACA9BE5BF0D5B0D79D8535&originRegion=us-east-1&originCreation=20220110093519>. Accessed on: 10 Jan. 2022.

WANG, Yonggang; ZHOU, H. A lithium-air battery with a potential to continuously reduce O₂ from air for delivering energy. **Journal of Power Sources**, vol. 195, p. 358–361, 2010. .

WANG, Yu; LAI, N. C.; LU, Y. R.; ZHOU, Y.; DONG, C. L.; LU, Y. C. A Solvent-Controlled Oxidation Mechanism of Li₂O₂ in Lithium-Oxygen Batteries. **Joule**, vol. 2, no. 11, p. 2364–2380, 21 Nov. 2018. <https://doi.org/10.1016/J.JOULE.2018.07.021>.

WANG, Z.; HUANG, B.; WANG, S.; XUE, R.; HUANG, X.; CHEN, L. Vibrational spectroscopic study of the interaction between lithium perchlorate and dimethylsulfoxide.

Electrochimica Acta, vol. 42, no. 17, p. 2611–2617, 1 Jan. 1997.

[https://doi.org/10.1016/S0013-4686\(96\)00440-9](https://doi.org/10.1016/S0013-4686(96)00440-9).

WHITTINGHAM, M. S. Electrical Energy Storage and Intercalation Chemistry. **Science**, vol. 192, p. 1126–1127, 1976. DOI 10.1126/science.192.4244.1126. Available at:

<http://science.sciencemag.org/>. Accessed on: 1 Apr. 2020.

XIAO, J.; MEI, D.; LI, X.; XU, W.; WANG, D.; GRAFF, G. L.; BENNETT, W. D.; NIE, Z.; SARAF, L. V.; AKSAY, I. A.; LIU, J.; ZHANG, J. G. Hierarchically porous graphene as a lithium-air battery electrode. **Nano Letters**, vol. 11, no. 11, p. 5071–5078, 9 Nov. 2011.

<https://doi.org/10.1021/nl203332e>.

XU, D.; WANG, Z. L.; XU, J. J.; ZHANG, L. L.; ZHANG, X. B. Novel DMSO-based electrolyte for high performance rechargeable Li-O₂ batteries. **Chemical Communications**, vol. 48, no. 55, p. 6948–6950, 14 Jun. 2012. <https://doi.org/10.1039/c2cc32844e>.

XU, K. Nonaqueous liquid electrolytes for lithium-based rechargeable batteries. **Chemical Reviews**, vol. 104, no. 10, p. 4303–4417, Oct. 2004. <https://doi.org/10.1021/cr030203g>.

YAMANAKA, N.; KAWANO, R.; KUBO, W.; KITAMURA, T.; WADA, Y.; WATANABE, M.; YANAGIDA, S. Ionic liquid crystal as a hole transport layer of dye-sensitized solar cells. **Chemical Communications**, no. 6, p. 740, 2005. DOI 10.1039/b417610c. Available at: <http://xlink.rsc.org/?DOI=b417610c>.

YANG, C. C.; HSU, H. Y. Raman Spectroscopic Study of a New Type of Room Temperature ZnCl₂-DMSO₂ Molten Salts. **Zeitschrift fur Naturforschung - Section A Journal of Physical Sciences**, vol. 65, no. 8–9, p. 745–748, 1 Sep. 2010. DOI 10.1515/ZNA-2010-8-917/MACHINEREADEABLECITATION/RIS. Available at: <https://www.degruyter.com/document/doi/10.1515/zna-2010-8-917/html>. Accessed on: 22 Dec. 2021.

YANG, J.; ZHAI, D.; WANG, H.-H.; LAU, K. C.; SCHLUETER, J. A.; DU, P.; MYERS, D. J.; SUN, Y.-K.; CURTISS, L. A.; AMINE, K. Evidence for lithium superoxide-like species in the discharge product of a Li-O₂ battery †. **This journal is c the Owner Societies**, vol. 15, p. 3764, 2013. DOI 10.1039/c3cp00069a. Available at: www.rsc.org/pccp. Accessed on: 30 Dec. 2021.

YANG, M.; HOU, J. Membranes in Lithium Ion Batteries. , p. 367–383, 2012. <https://doi.org/10.3390/membranes2030367>.

YAO, P.; YU, H.; DING, Z.; LIU, Y.; LU, J.; LAVORGNA, M.; WU, J.; LIU, X. Review on Polymer-Based Composite Electrolytes for Lithium Batteries. **Frontiers in Chemistry**, vol. 7, 8 Aug. 2019. <https://doi.org/10.3389/fchem.2019.00522>.

YOO, E.; ZHOU, H. Enhanced Cycle Stability of Rechargeable Li–O₂ Batteries by the Synergy Effect of a LiF Protective Layer on the Li and DMTFA Additive. **ACS Appl. Mater. Interfaces**, vol. 9, p. 16, 2017. DOI 10.1021/acsami.7b05466. Available at: www.acsami.org. Accessed on: 11 Jan. 2022.

YOSHINO, A. The Birth of the Lithium-Ion Battery. **Angewandte Chemie International Edition**, vol. 51, no. 24, p. 5798–5800, 11 Jun. 2012. DOI 10.1002/anie.201105006. Available at: <http://doi.wiley.com/10.1002/anie.201105006>. Accessed on: 1 Apr. 2020.

YU, H.; LIU, D.; FENG, X. Mini Review: Recent Advances on Flexible Rechargeable Li–Air Batteries. **Energy Fuels**, vol. 35, p. 4751–4761, 2021. Available at: <https://pubs.acs.org/doi/pdf/10.1021/acs.energyfuels.1c00201>. Accessed on: 6 Feb. 2022.

YUAN, F.; CHI, S.; DONG, S.; ZOU, X.; LV, S.; BAO, L.; WANG, J. Ionic liquid crystal

with fast ion-conductive tunnels for potential application in solvent-free Li-ion batteries.

Electrochimica Acta, vol. 294, p. 249–259, 20 Jan. 2019. DOI

10.1016/j.electacta.2018.10.079. Available at: <https://doi.org/10.1016/j.electacta.2018.10.079>.

Accessed on: 17 Sep. 2020.

YUAN, F.; YANG, L.; ZOU, X.; DONG, S.; CHI, S.; XIE, J.; XING, H.; BIAN, L.; BAO, L.;

WANG, J. Flexible all-solid-state electrolytes with ordered fast Li-ion-conductive nano-

pathways for rechargeable lithium batteries. **Journal of Power Sources**, vol. 444, 31 Dec.

2019. <https://doi.org/10.1016/j.jpowsour.2019.227305>.

ZENG, J.; FRANCIÀ, C.; AMICI, J.; BODOARDO, S.; PENAZZI, N. A highly reversible

Li-O₂ battery utilizing a mixed electrolyte and a cathode incorporating Co₃O₄. **The Royal**

Society of Chemistry, vol. 5, p. 83056–83064, 2015. DOI 10.1039/c5ra13483h. Available at:

www.rsc.org/advances. Accessed on: 4 Sep. 2020.

ZHANG, D.; LI, R.; HUANG, T.; YU, A. Novel composite polymer electrolyte for lithium air batteries. **Journal of Power Sources**, vol. 195, p. 1202–1206, 2010. Available at:

<https://reader.elsevier.com/reader/sd/pii/S0378775309014517?token=11108589DAB1D019FEB41AF01529D91FB910A00A526B1C18D81749EFFEBD272EA8D93E988422B38E673482FB1DA53330>. Accessed on: 31 Jul. 2020.

ZHANG, J. G.; WANG, D.; XU, W.; XIAO, J.; WILLIFORD, R. E. Ambient operation of Li/Air batteries. **Journal of Power Sources**, vol. 195, no. 13, p. 4332–4337, 1 Jul. 2010.

<https://doi.org/10.1016/j.jpowsour.2010.01.022>.

ZHANG, J.; SUN, B.; ZHAO, Y.; TKACHEVA, A.; LIU, Z.; KANG, Y.; GUO, X.;

MCDONAGH, A. M.; SHANMUKARAJ, D.; WANG, C.; ROJO, T.; ARMAND, M.; PENG,

Z.; WANG, G. A versatile functionalized ionic liquid to boost the solution-mediated

performances of lithium–oxygen batteries. **Nature Communications**, , p. 1–10, 2019. DOI

10.1038/s41467-019-08422-8. Available at: <https://doi.org/10.1038/s41467-019-08422-8>.

Accessed on: 22 May 2020.

ZHANG, S. S.; FOSTER, D.; READ, J. Discharge characteristic of a non-aqueous electrolyte Li/O₂ battery. **Journal of Power Sources**, vol. 195, p. 1235–1240, 2010. .

ZHANG, S.; SUN, N.; HE, X.; LU, X.; ZHANG, X. Physical Properties of Ionic Liquids:

Database and Evaluation. **Journal of Physical and Chemical Reference Data**, vol. 35, p.

1475–1517, 2006. DOI 10.1063/1.2204959. Available at:

<https://doi.org/10.1063/1.3373178><https://doi.org/10.1063/1.4975450>. Accessed on: 19 Mar. 2020.

ZHAO, W.; YI, J.; HE, P.; ZHOU, H. Solid-State Electrolytes for Lithium-Ion Batteries: Fundamentals, Challenges and Perspectives. **Electrochemical Energy Reviews**, vol. 2, p. 574–605, 2019. DOI 10.1007/s41918-019-00048-0. Available at: <https://doi.org/10.1007/s41918-019-00048-0>. Accessed on: 9 Jul. 2020.

ZHENG, C.; DING, W.; WANG, C. N-Methyl-N-propyl pyrrolidine bromide (MPPBr) as a bi-functional redox mediator for rechargeable Li-O₂ batteries †. **Journal of Materials Chemistry A**, vol. 7, p. 6180–6186, 2019. <https://doi.org/10.1039/c8ta11849c>.

ZHOU, D.; TKACHEVA, A.; TANG, X.; SUN, B.; SHANMUKARAJ, D.; LI, P.; ZHANG, F.; ARMAND, M.; WANG, G. Stable Conversion Chemistry-Based Lithium Metal Batteries Enabled by Hierarchical Multifunctional Polymer Electrolytes with Near-Single Ion Conduction. **Angewandte Chemie International Edition**, vol. 58, p. 6001–6006, 2019. DOI 10.1002/ange.201901582. Available at: <https://doi.org/10.1002/anie.201901582>. Accessed on: 17 Feb. 2020.

ZHU, C.; SUN, Q.; XIE, J.; JIN, Y.; WANG, K.; CHEN, Z.; TU, J.; CAO, G.; ZHAO, X. Ionic liquid/ether-plasticized quasi-solid-state electrolytes for long-life lithium–oxygen cells. **New Journal of Chemistry**, vol. 42, no. 24, p. 19521–19527, 3 Dec. 2018. DOI 10.1039/C8NJ03389G. Available at: <https://pubs.rsc.org/en/content/articlehtml/2018/nj/c8nj03389g>. Accessed on: 11 Jan. 2022.